# Investigation of the effect of compositional variations on the flotability of pyrite in a gold ore

*by*
Omeshan Naidoo

Thesis presented in partial fulfilment
of the requirements for the Degree

*of*

MASTER OF ENGINEERING
(EXTRACTIVE METALLURGICAL ENGINEERING)

in the Faculty of Engineering
at Stellenbosch University

The financial assistance of the National Research Foundation (NRF) towards this research is hereby acknowledged. Opinions expressed and conclusions arrived at, are those of the author and are not necessarily to be attributed to the NRF.

*Supervisor*
Dr. Margreth Tadie

*Co-Supervisor*
Dr. Bjorn Von Der Heyden

March 2020

## DECLARATION

By submitting this thesis electronically, I declare that the entirety of the work contained therein is my own, original work, that I am the sole author thereof (save to the extent explicitly otherwise stated), that reproduction and publication thereof by Stellenbosch University will not infringe any third party rights and that I have not previously in its entirety or in part submitted it for obtaining any qualification.

Date: *March 2020*

## PLAGIARISM DECLARATION

1. Plagiarism is the use of ideas, material and other intellectual property of another's work and to present is as my own.

2. I agree that plagiarism is a punishable offence because it constitutes theft.

3. I also understand that direct translations are plagiarism.

4. Accordingly all quotations and contributions from any source whatsoever (including the internet) have been cited fully. I understand that the reproduction of text without quotation marks (even when the source is cited) is plagiarism.

5. I declare that the work contained in this assignment, except where otherwise stated, is my original work and that I have not previously (in its entirety or in part) submitted it for grading in this module/assignment or another module/assignment.

Initials and surname: O. Naidoo

Date: March 2020

## ABSTRACT

Gold is associated with pyrite, arsenopyrite and arsenian pyrite in refractory gold ores. Due to the presence of arsenic or other compositional variations in the pyrite, the semiconductor properties are expected to differ from that of bulk pyrite. Semiconducting properties play a role in the attachment of a flotation collector to the mineral surface, an improvement in recovery in froth flotation may be possible if the compositional variations of pyrite can be related to the optimisation of collector reagent suites in froth flotation.

The project aim was to relate the variation in pyrite composition to its impact on recovery in a flotation system and the effectiveness of reagent suites in overcoming the challenges presented by compositional variations in valuable mineral recovery.

Batch flotation of a refractory ore from the Barberton Greenstone Belt in South Africa, using SIBX, PAX and SIBDTP as collectors is investigated as a case study for this phenomenon. Two different “pure” pyrite samples were floated in a micro-flotation cell to fundamentally study the differences in flotation of different pyrite samples.

Pyrite in the case study ore had, among others, compositional variation of differing amounts of arsenic within the pyrite. Gold in the case study ore was associated with pyrite containing high arsenic content. SIBX and PAX in batch flotation achieved a pyrite recovery of 30.63% and 38.25% respectively, while SIBDTP recovered 27%. SIBDTP only recovered 20.97% of gold compared to 70.97% by SIBX and 73.89% by PAX. SIBDTP recovered less gold because SIDTP was shown to selectively recover pyrite with no arsenic or a low weight percentage arsenic, compared to SIBX and PAX which selectively recovered pyrite with a higher weight percentage arsenic. Compositional variations in pyrite thus impacted the recovery of the pyrite in the batch flotation system via the selective attachments of different collectors to pyrite with different compositional variations.

Pyrite samples for microflotation showed trace amounts of copper and lead (Pyrite 1) and cobalt (Pyrite 2). Pyrite 1 and Pyrite 2 differences extended to zeta potential measurements, where Pyrite 2 showed a zeta potential of approximately 10 mV lower across the pH range than Pyrite 1. Even though variations were present, no trends of differences were seen between the two pyrite samples in micro-flotation recovery.

When SIBDTP and the Xanthates were mixed, an increased recovery of pyrite was seen over single collectors alone. Collector mixtures of 75% SIBX and 25% SIBDTP (mass basis) in batch flotation recovered the most pyrite (69.92%) at the highest pyrite grade (6.4%) with the most gold recovered (100%) at the highest gold grade (50.6g/ton). A recovery increase of up to 5.88% of pyrite after 20 minutes of microflotation was observed with 25% SIBDTP and 75% xanthate. The result of increased recovery of pyrite in batch flotation and in micro-flotation with 75% xanthate and 25% SIBDTP lead to the conclusion of collector mixtures are beneficial to the recovery of pyrite when applied in the correct ratio and can overcome the mineralogical barrier posed by varying compositions.

## OPSOMMING

Goud word geassosieer met piriet, arsenopiriet en arseniese piriet in vuurvaste gouderts. As gevolg van die teenwoordigheid van arseniese of ander komposisionele variasies in die piriet, word dit verwag dat die halfgeleiereienskappe sal verskil van die van die grootmaat piriet. Halfgeleidingseienskappe speel ’n rol in die aanhegting van ’n flottasieversamelaar aan die mineraaloppervlak. ’n Verbetering in herwinning van skuimflottasie kan moontlik wees as die komposisionele variasies van piriet verwant is aan die optimering van versamelaarreagentsuites in skuimflottasie.

Die projek het beoog om die variasies in pirietkomposisies in verband te bring met sy impak op herwinning in ’n flottasiestelsel en die doeltreffendheid van reagentsuites om die uitdagings voorgestel deur komposisionele variasies in waardevolle mineraalherwinning te oorkom.

Lotflottasie van ’n vuurvaste erts uit die Barberton Greenstone Belt in Suid-Afrika, wat SIBX, PAX en SIBDTP as versamelaars gebruik het, is as ’n gevallestudie vir hierdie fenomeen ondersoek. Twee verskillende “suiwer” pirietsteekproewe is in ’n mikroflottasiesel gedryf om die verskille in flottasie van verskillende pirietsteekproewe fundementeel te bestudeer.

Piriet in die gevallestudie-erts het onder andere komposisionele variasies van verskillende hoeveelhede arseen binne die piriet gehad. Goud in die gevallestudie-erts is geassosieer met piriet wat hoë arseen inhoud bevat het. SIBX en PAX in lotflottasie het ’n pirietherwinning van 30.63% en 38.25% onderskeidelik bereik terwyl SIBDTP 27% herwin het. SIBDT het slegs 20.87% goud herwin, in vergelyking met 70.97% deur SIBX en 73.89% deur PAX. SIBDTP het minder goud herwin want dis gewys dat SIBDTP piriet selektief herwin met geen arseen of ’n lae gewigspersentasie arseen, in vergelyking met SIBX en PAX wat piriet selektief herwin het met ’n hoër persentasie arseen. Komposisionele variasies in piriet het dus die herwinning van die piriet in die lotflottasiestelsel via die selektiewe aanhegtings van verskillende versamelaars aan piriet met verskillende komposisionele variasies beïnvloed.

Pirietsteekproewe vir mikro-flottasie het baie klein hoeveelhede koper en lood (Piriet 1) en kobalt (Piriet 2) aangetoon. Piriet 1- en Piriet 2-verskille het gestrek na zeta-potensiaalafmetings, waar Piriet 2 ’n zeta-potensiaal van ongeveer 10 mV laer oor die pH-bestek aangeteken het as Piriet 1. Selfs al was variasies teenwoordig, is geen tendense van verskille gesien tussen die twee pirietsteekproewe in mikroflottasie nie.

Toe SIBDTP en die xanate gemeng is, is ’n verhoging van herwinning van piriet gesien oor slegs enkelversamelaars. Versamelaarmengsels van 75% SIBX en 25% SIBDTP (massa basis) in lotflottasie het die meeste piriet (69.92%) herwin by die hoogste pirietgraad (6.4%) met die meeste goud herwin

(100%) by die hoogste goudgraad (50.6 g/ton). ’n Herwinningsverhoging van tot 5.88% van piriet na 20 minute van mikroflottasie is waargeneem met 25% SIBDTP en 75% xanaat. Die resultaat van verhoogde herwinning van piriet in lotflottasie en in mikroflottasie met 75% xanaat en 25% SIBDTP het tot die gevolgtrekking gelei dat versamelaarmengsels voordelig is vir die herwinning van piriet as dit in die korrekte ratio toegepas word en kan die mineralogie versperring oorkom wat deur variërende komposisies gestel word.

## ACKNOWLEDGEMENTS

*This section is dedicated to thanking those that have made this project and thesis possible, from people that contributed directly to the document or to support the author in other methods during the duration of the project*.

I would like to thank my parents, Sasheeta and Suthamen Naidoo. Not only did they help fund living expenses and provide for me financially, but they provided emotional support in the most stressful times. They kept me motivated to close out the project.

Thanks has to be made to my supervisor, Dr Margareth Tadie. Since my final year in undergraduate, she has been guiding and supporting me through my journey as an academic.

I would like to thank Mareli Grobbelaar-Moolman and Riana Rossouw of SU CAF, and Madelaine Frazenberg of the SU EM unit for assisting me through all analysis problems and coming up with solutions.

Thanks has to go to Michael Gooden, for all he has done and for being a close friend through the project.

Thank you to Hendri Jooste, who always looked out for me, was there when I needed a friend.

I would like to thank everybody who made me smile over the course of the project, contributing to my happiness over the project duration. Special mention has to be made of the quiz night group at Courtyard Cafe and the staff of the establishment.

To everybody on Summoner's Rift, to Moe and his chat, I say thank you for keeping me company during early hours of the mornings while working on the project data and writing.

To the Maties Underwater Club and the members of the Legacy of Alveera, for providing completely different worlds to explore and passions to follow.

To Florian Kovats and Benjamin Myburgh, for always being there when needed and for working on cars and other projects together. To Matthew Turner, for the late-night trips to McDonalds to get food to fuel late night working.

To Alice, Ashe and Risky, for being safe spaces and never failing to put a smile on my face, even at the worst of times.

I would additionally like to thank the NRF for funding that helped me pay for rent and living costs.

## TABLE OF CONTENTS

# NOMENCLATURE

## Abbreviations

| | |
|---|---|
| BET | Brunauer-Emmett-Teller |
| BSE | Back Scattered Electrons |
| CIC | Carbon In Columns |
| CIL | Carbon In Leach |
| CIP | Carbon In Pulp |
| CAF | Central Analytical Facilities |
| DO | Dissolved Oxygen |
| DTP | Dithiophosphate |
| EDS | Energy Dispersive Spectrometer |
| EX | Ethyl Xanthate |
| FTIR | Fourier-Transform Infrared Spectroscopy |
| LA-ICP-MS | Laser Ablation microprobe-Inductively Coupled Plasma-Mass Spectroscopy |
| MLA | Mineral Liberation Analyser |
| PSD | Particle Size Distribution |
| PAX | Potassium Amyl Xanthate |
| QXRD | Quantitative X-Ray Diffraction |
| SCE | Saturated Calomel Electrode |
| SIBDTP | Sodium Diisobutyl Dithiophosphate |
| SEDTP | Sodium Ethyl Dithiophosphate |
| SEX | Sodium Ethyl Xanthate |
| SIBX | Sodium Isobutyl Xanthate |
| SHE | Standard Hydrogen Electrode |
| TBE | Tetrabromoethane |
| TAB | Trimethyl Ammonium Bromide |
| WDS | Wavelength Dispersive Spectrometer |
| XANES | X-Ray Absorption Near Edge Structure |
| XRF | X-Ray Fluorescence |

## Units

| | |
|---|---|
| A | Amps |
| Eh | Pulp Potential |
| eV | Electronvolt |
| g | Gram |
| g/ton | Gram per ton or parts per million |
| kbar | Kilo-bar |
| kg | Kilogram |

| | |
|---|---|
| kV | Kilo-volt |
| kW | Kilowatt |
| m | meters |
| mg/ton | Milligram per ton = parts per billion |
| min | Minutes |
| mL | millilitres |
| mol | moles |
| mV | millivolts |
| nA | Nanoamps |
| nm | Nanometres |
| $^{o}C$ | degrees centigrade |
| pH | Potential Hydrogen |
| µm | micrometres |
| V | volts |
| wt% | Weight percentage |
| µl | microlitres |

**Symbols**

| | |
|---|---|
| $SF_{B/A}$ | Separation Factor of B/A |

**Minerals**

| | |
|---|---|
| Arsenopyrite | $FeAsS_2$ |
| Chalcopyrite | $CuFeS_2$ |
| Dolomite | $CaMg(CO_3)_2$ |
| Muscovite | $KAl_2(AlSi_3O_{10})(FOH)_2$ |
| Pentlandite | $(Fe, Ni)_9S_8$ |
| Pyrite | $FeS_2$ |
| Pyrrhotite | $Fe_{(1-x)}S$ |
| Quartz | $SiO_4$ |
| Silica | $SiO_2$ |
| Sphalerite | (Zn,Fe)S |

# 1 INTRODUCTION

## 1.1 Background

A large portion of refractory ores are high sulphide content ores where gold is in solid solution with minerals such as pyrite, arsenian pyrite and arsenopyrite. The gold association of such ores enables pre-concentration by froth flotation of these sulphides.

In this process, semiconductor (electrical conductivity) properties of sulphide minerals make the sulphides amenable to reagents (collectors) that impart selective hydrophobicity. Fundamental studies have shown that elemental substitution in sulphide minerals alters their semi-conducting properties. An example of this is pyrite, normally an n-type semiconductor, which is observed to show alternate properties e.g. exhibiting p-type semiconductor properties when impurities such as arsenic and cobalt are present (Lalvani et al., 1990; Pridmore and Shuey, 1976; Mirronov et al., 1981). Gold bearing pyrites are characterized by varying degrees of arsenic and other elemental substitutions. Variation in semiconducting properties, as a result of different mineral composition, impacts the reagent and mineral interactions which, if not understood, translates to a loss in recovery.

The basis of this study is that gold is associated with pyrite, however pyrite from different geographical locations contains different compositional variations that causes differences in the physical and chemical properties. If collector attachment is impacted by the presence of these compositional variations, the collector reagent suite in flotation in theory can be optimised for each set of compositional variations. Recovery of pyrite can thus be maximised, resulting in a recovery of gold associated with it.

The context of the study is the gold production industry, more specifically the South African gold production industry, with a focus on gold ore from the Barberton Greenstone Belt. The Barberton Greenstone Belt hosts gold within “ore minerals” which consist of pyrite and arsenopyrite (with very minor visible gold). Gold grades from the area have been reported to be between 8 g/ton and 12.5 g/ton, with the gold being associated with pyrite and arsenopyrite (Youlton et al., 2018). The ore is refractory due to the gold being hosted by pyrite and arsenopyrite, which have to be processed via biological oxidation before cyanidation (for more about why this is necessary, see Sections 2.1.1 and 2.2). Other gold deposits in South Africa, such as the Witwatersrand Basin (largest gold resource in the world) and Sabie-Pilgrims Rest Deposit also exhibit gold association with pyrite and arsenopyrite (Meyer et al., 1994; Youlton et al., 2018), so understanding the impact of compositional variations on the flotation response of pyrite has far reaching significance.

The impact of the variation in pyrite composition has been studied at the micro-flotation scale (Bulut et al., 2004), where crystal grouping of pyrite from different areas were floated and no significant response in flotation performance was seen due to compositional variation. Even though this has been shown at the microflotation scale, the impact of compositional variations can be verified in a real ore in batch or pilot plant scale flotation.

## 1.2 Aim

The overall study aim is to relate pyrite composition, specifically the variation in pyrite composition, to its recovery in a flotation system and thus the effectiveness of reagent suites in overcoming the challenges presented by these compositional variations in valuable mineral recovery.

## 1.3 Key Questions

The Aim of the project is met if the three Key Questions can be answered. The objectives in Section 1.4 are set out to answer these questions.

1. Do compositional variations in pyrite affect the recovery of the pyrite in a flotation system?
2. Do different collectors selectively attach to pyrite particles with different compositional variations?
3. If compositional variations affect recovery, can the collector reagent suite be modified to overcome the challenge posed by these compositional variations?

## 1.4 Objectives

The objectives listed below will be referred to by their corresponding number going forward.

Objective 1: Investigate methods to quantify selective separation of pyrites with different compositional variations in case study ore.

Objective 2: Interrogate selective flotation of pyrite with different compositional variations in a batch flotation system of the case study ore.

Objective 3: Investigate recovery differences of pyrite samples with different compositional variations by floating them in a micro-flotation cell, using the same collector mixtures as used in batch flotation.

The primary objective of this study is highlighted as Objective 2 as the focus is put on on the batch flotation of the case study ore. The effect of the compositional variations of pyrite in a real ore is where the value is added by this study.

## 1.5 Approach

This section gives a brief overview of the approach used to meet the objectives. A more detailed description of each is given in Experimental Section (Section 3). Each Subsection below corresponds to an objective number in Section 1.4.

The approach of the project will be anchored around the flotation of a real ore from the Barberton Greenstone Belt. The rest of the experiments are to support and explain the observations of the flotation of the ore and to plan what experiments and variables are to be tested.

### *1.5.1 Investigate methods to quantify selective separation of pyrites with different compositional variations in case study ore*

Analytical methods were investigated into which would be suitable to meet the objectives of this study. A combination of spectroscopy and microscopy was employed to identify phases, grain structures and compositional variations within pyrite samples.

### *1.5.2 Interrogate selective flotation of pyrite with different compositional variations in a batch flotation system of the case study ore*

#### *1.5.2.1 Develop an experimental plan regarding focused on collectors and collector mixtures to use in both batch flotation and micro-flotation experiments*

Using industry relevant collectors, an experimental plan was constructed to test Objective 2 and 3.

#### *1.5.2.2 Acquire a case study ore and prepare the ore for batch flotation*

Ore was sourced from a mine and processing plant in Southern Africa and split into 1kg representative samples. Milling curves were constructed to reach a target particle size distribution that would be applicable for batch flotation experimentation.

#### *1.5.2.3 Batch Float the Case Study Ore*

The different collector mixtures selected were used in batch flotation experiments on the case study ore that was prepared. The feed, concentrates and tailings were then analysed by the methods chosen or developed in Objective 1 to interrogate whether selective flotation was taking place.

### *1.5.3 Investigate differences in pyrite flotation of samples with different compositional variations by floating them in a microflotation cell, using the same collector mixtures as used in batch flotation*

#### *1.5.3.1 Source pyrite samples that have different compositional variations, and show that these variations impact the properties of the pyrite*

Two different pyrite samples were sourced and underwent characterisation to determine the compositional variations between the two samples. The two different pyrite samples were tested using Zeta Potential tests to investigate whether a difference in surface properties existed under the same conditions with pyrite from different sources.

#### *1.5.3.2 Float the pyrite samples with different trace elements in a Micro-flotation cell*

The pyrite samples were floated in a micro-flotation cell, using the same collector mixtures applied in Objective 2 in order to investigate if the pyrite samples achieved different recoveries due to the different compositions.

# 2 LITERATURE REVIEW

The literature review section sets out the background information for the project using relevant literature sources. Each subsection starts with a general overview and then narrows the information down to the context of the project, which is flotation of sulphide gold ores.

An overview of gold ores and how they are commonly processed is displayed. Following that, gold association with pyrite, particularly arsenopyrite, is discussed. The variations in pyrite composition due to trace elements within the mineral, and the effect of these trace elements on the properties of pyrite, are then detailed.

An overview of flotation is then followed by a review of the flotation of pyrite. The aim of this section is to show that the properties of pyrite changes due to elemental impurities in the pyrite composition, and therefore should impact the flotation response, leading to a loss in of pyrite (and thus gold) recovery.

## 2.1 Gold Ores

Gold within ores most often takes the form of either invisible gold, native gold (often referred to as $Au^0$ or $gold^0$) inclusions and/or gold compounds (O Connor and Dunne, 1994; Pals et al., 2003).

"Invisible gold" is referred to as such because this type of gold is contained within the structure of pyrite, arsenopyrite and other sulphides (structurally bound, e.g. $Au^{3+}$) and/or within discrete inclusions ($Au^0$ inclusions often in sub-micron range) and are not detectable by optical or scanning electron microscopy (Arehart et al., 1993; Cook and Chryssoulis, 1990; Knipe, 1991; Pals et al., 2003). Small amounts of gold compounds within sulphides can also contribute to the total invisible gold amount. Secondary Ion Mass Spectroscopy on sulphide grains from different gold ore deposits has shown specifically invisible gold ranging from less than 0.5g/ton to over 1000g/ton (Cook and Chryssoulis, 1990).

Native gold (or $Au^0$) can be found as gold nuggets that are not attached to any other mineral but is more commonly found as inclusions or veins of gold that has formed on or within other minerals. These inclusions can be associated with other minerals, and be of a wide range of sizes (Meyer et al., 1994; Su et al., 2008).

Gold compounds form when the gold in ores chemically bound to form compounds with silver, tellurium, antimony and selenium, to name a few (Adams, 2016). This usually occurs to a much lesser extent than other forms of gold in ores. These gold compounds are often hosted within a mineral, such as a sulphide (e.g. pyrite and arsenopyrite) or silicate (O Connor and Dunne, 1994).

### *2.1.1 Classification of gold ores*

Gold ores are be classified according to the percentage of gold recovered via conventional cyanidation. The classification of the ores exists on a continuum, with free milling ores (easily recoverable gold) on one side and refractory ores (with difficult to recover gold) on the other. Ores are often described as entirely "free milling" (90% or above recovery) or "refractory" when in reality almost all ores lie between the two descriptions, where some of the gold is free milling and easily recoverable, but other gold is fully locked up in refractory ore (La Brooy et al., 1994). The ratios of each part determine how it is classed. In the ore bodies that have some sections which are mostly free milling and others that are refractory, the

free milling ores are often mined first as they are more profitable. This means that refractory ores make up more and more of the ore reserves as time proceeds, thus an increasing effort has to be made to improve the efficiency and recovery of gold from these ores.

Free milling ores are usually associated with native gold particles or nuggets that can easily come into contact with the cyanidation solutions. Refractory ores are usually associated with invisible gold where the gold is behind a "barrier" that causes cyanidation to be ineffective and thus need pretreatment before the cyanidation. Some ores are not fully refractory as acceptable gold recovery can be achieved without pretreatment, but require significantly higher cyanide or oxygen concentrations, these ores are considered complex ores (La Brooy et al., 1994).

## 2.2 Mineralogical Characteristics of Refractory Gold Ores

Generally, gold ore can be considered refractory if one or both of the following conditions are true (Natarajan, 1994):

1. The gold occurs in small particles, micrometers or sub-micrometer in diameter, and locked up within other minerals, whether in the other mineral's lattice structure or within inclusions.
2. The gold is in the vicinity of other substances (such as carbonaceous matter or certain sulphides) that interfere chemically with the cyanidation process, whether in the dissolution or recovery steps.

Within the South African context, gold is associated with pyrite and arsenopyrite, and often the refractory nature of the gold is due to the sulphide nature of the ore. Sulphide minerals compete with gold for lixiviants and therefore increase reagent consumption.

A few of the processing options are discussed in Section 0. More are available and can be studied by reading papers such as that from La Brooy et al., (1994).

## 2.3 Mineralogical Characteristics of Barberton Greenstone Belt gold ore

The mineralogical characteristics of the Barberton Greenstone Belt is discussed in this subsection as the Barberton Greenstone Belt is the case study ore for batch flotation. The Fairview and Sheba gold mines are two examples of mines that lie on the deposit.

Gold is associated with quartz veins and occurs as invisible gold and native (electrum) inclusions hosted in pyrite, with a higher content of gold found in arsenopyrite. In the main stage of gold deposition, the gold is associated with mobilization of As, Sb, Cu and Ni. Ore transporting veins were placed later in the formation process (Agangi et al., 2014), and originated from hydrothermal fluids ingress after the main rock was metamorphosed.

Mineralization of the gold ore was formed during a single tectonic stage which included the formation of porphyry dykes. Gold enrichment happened after thermal stabilisation of the crust when shear zones allowed ingress of deeply sourced hydrothermal fluids (Agangi et al., 2016; Dirks et al., 2013).

## 2.4 Gold Ore Processing

The processing route of gold ores depends on the individual ore and its properties (such as grain size, gold content, location of the gold, matrix material etc).

The first unit step is crushing and grinding the ore (normally to over 60% passing 75 µm). If the gold in the ore is associated with sulphides, flotation almost always follows this step, especially if the ore is refractory (except when the matrix is carbonaceous), in order to pre-concentrate the ore (O Connor and Dunne, 1994). Depending on the individual ore, pre-concentration and pre-treatment operations before cyanidation may vary, especially in the case of refractory gold ores. This is further discussed in Section 0.

Cyanidation is a process in which gold is leached into solution, after which the gold is recovered from this solution by contacting the solution with carbon. The gold from the processed ore is leached into a cyanide solution (cyanide being called a lixiviant in this application, normally added as NaCN), and then the gold from the cyanide solution adsorbs onto carbon. This cyanidation process may take place in tanks or over heaps of ore. Heap leaching (used more for lower grade free milling ores) results in pregnant leach solution from the base of the heap that is normally run through Carbon In Columns (CIC). The processing route with higher grade ores involves contacting the processed ore with cyanide solution and carbon within tanks, often at the same time. The entire cyanidation process is normally a mixture of pure Carbon In Pulp (CIP) and Carbon In Leach (CIL) processes. The leaching often undergoes through two stages of cyanide solution before coming into contact with carbon. In general, lower grade or faster leaching ores will have a recovery process closer to pure CIL and higher grade or slower leaching ores will have a process closer to pure CIP (Adams, 2016; La Brooy et al., 1994). Other processing options exists, such as different lixiviants (liquid medium used to extract metal from ore e.g. thiosulfate and thiourea) and other adsorbents (different resins) but these are not as widespread as the discussed methods (Adams, 2016).

After the cyanidation process, the gold loaded carbon undergoes elution stripping, where the gold is transferred from the carbon surface back into an elution or stripping solution. This pregnant eluate sometimes undergoes intermediate steps (such as clarification and deaeration) before the gold is recovered from the solution. The recovery processes that are commonly used include electrowinning (plating the gold onto electrodes using an applied electrical potential) and Merrill-Crowe (a zinc sedimentation process). The products of these processes are then sent for smelting to produce the gold ingots (Adams, 2016).

As indicated, a refractory gold ore is an ore where conventional cyanidation (20 to 30 hour leach) alone does not lead to acceptable gold recovery and therefore other methods are necessary to treat the ore to make it more amenable to leaching, typically by cyanidation (Adams, 2016; Natarajan, 1994).

### *2.4.1 Refractory ore processing options*

#### *2.4.1.1 Fine grinding*

Fine (100% passing 38 µm) or ultrafine (1 – 20 µm) grinding is sometimes required to access the gold particles that are included within other minerals (Adams, 2016; La Brooy et al., 1994). The extremely energy intensive nature of the grinding means that this is only commercially viable if the ore is first pre-concentrated before fine or ultrafine grinding, sometimes by flotation.

#### *2.4.1.2 Acid Pressure Oxidation*

Acid pressure oxidation serves to remove carbonaceous matter, typically from flotation concentrates. The process starts with removing water from the from the ore after grinding (typically thickened from a feed of 30 percent solids weight to around 50 percent solids weight). Sulphuric acid is then used to condition the slurry before it is oxidised in an autoclave using gaseous oxygen. The product of the autoclave is then cooled by flash or other means (Natarajan, 1994).

#### *2.4.1.3 Thermal Pretreatment*

Thermal pretreatment is used to break down sulphide phases to make the gold accessible (La Brooy et al., 1994). In the presence of oxygen the feed sulphides are converted to oxides in a process called roasting, but in the absence of oxygen different products are produced in pyrolysis (Adams, 2016; La Brooy et al., 1994). Roasting is usually used to treat flotation concentrates that have a high Sulphur content (Natarajan, 1994).

#### *2.4.1.4 Biological Oxidation*

Biological oxidation uses bacteria within bioreactors or tanks to oxidise a metal sulphides to sulphates in order to render cyanidation effective (Natarajan, 1994). This pretreatment is often used on flotation concentrates.

## 2.5 Pyrite and Gold Association

Gold can be found in high concentrations in pyrite and arsenopyrite (Petruk, 2000). It has been reported that up to 90% of the gold in the Emperor gold deposit in Fiji was associated with pyrite, with this high association being common as pyrite typically exists in many gold ores (Pals et al., 2003).

Gold found within pyrite has been reported to be mostly non-refractory and can be liberated by finer grinding, but gold in the arsenopyrite portion is normally refractory (Dunne, 2005). When comparing the distribution of gold adsorbed/reduced from a gold chloride solution onto pyrite and arsenopyrite, Maddox et al., (1998) observed that many small $Au^0$ particles grew on the arsenopyrite surface but few, much larger, particles grew on the pyrite surface. Arsenopyrite was seen to be more effective in concentrating gold than pyrite, and all the observations were in line with what was seen with gold in naturally occurring pyrites and arsenopyrites (Maddox et al., 1998).

### *2.5.1 The relationship between Arsenic and Gold in Pyrite*

Sites of gold growth in pyrite were related to areas of increased charge density or conductivity, such as physical or chemical defects (Knipe, 1991). Such defects could be caused by impurities within pyrite. P-type semiconductor (electronic) properties or p-n junctions in pyrite (caused by compositional variations such as arsenic) may aid the adsorption of gold from gold bearing fluids (gold in the form of $Au^{1+}(HS)_2^-$) (Simon et al., 1999, Mironov et al., 1981). It was noted that p-n junctions are believed to cause the precipitation of a broad range of base and precious metals (including gold) onto pyrite and other sulphide surfaces (Laird et al., 2015).

The highest concentration of invisible gold in iron sulphides is usually found on the boundaries of both coarse and fine grained arsenian pyrite, up to 1400 g/ton gold with 9.6 wt% arsenic in pyrite (Fairview gold deposit in South Africa) and up to 4000 g/ton gold and 13 wt% arsenic from Carlin-type gold deposits (Pals et al., 2003).

Cook and Chryssoulis (1990) put forward a mechanism of gold incorporation into arsenopyrite which includes Au forming as $Au^{3+}$ compound (such as AuAsS) through complete substitution with Fe and As within arsenopyrite. This mechanism was supported by Pals et al (2003). Knipe et al. (1992) proposed that $gold^0$ may adsorb onto the surface of arsenopyrite as the crystal grows. Sha (1993) proposed $Au(HS)^0$ chemisorption onto AS rich growth surfaces. Fleet and Mumin (1997) proposed the formation of gold from gold bearing hydrothermal fluids onto the iron deficient arsenopyrite growth surface via chemisorption.

The semiconductor properties of pyrite may play a part in the gold adsorption process. A semiconductor is a substance that has electrical conducting behaviour between that of a conductor and that of an insulator. Semiconductors are classified between having free electrons (n-type) or having “holes” that electrons can occupy (p-type). Impurities in a semiconductor lattice (such as pyrite) can cause a change in the semiconducting properties and type (Simon et al., 1999, Mironov et al., 1981).

The mineral that acts most readily as a host for invisible gold is arsenopyrite and pyrite that is otherwise rich in arsenic, with a positive correlation between gold and arsenic amounts within pyrite that suggests that the presence of arsenic facilitates the substitution of gold into the pyrite structure (Cook and Chryssoulis, 1990). The positive correlation between As and Au concentrations within pyrite was also reported by other studies (Arehart et al., 1993; Fleet and Mumin, 1997). Significant gold in the pyrite structure was only seen in pyrite that contained greater than 0.2-0.4 wt% As (Cook and Chryssoulis, 1990). In an experimental study, it was shown that pyrite with a low As content cannot contain more than 5 g/ton structurally bound Au (Tauson, 1999).

Cook and Chryssoulis, (1990) analysed samples of pyrite and arsenopyrite from nine different ore bodies and reported that in some ores gold was not detectable in pyrite grains, but almost all arsenopyrite grains had significant quantities of invisible gold. In one ore (the “Congress Ore”) it was also reported that fine grained arsenopyrite (euhedral needles smaller than 20 μm) had up to fifty times the gold content (in g/ton) than the coarse grained arsenopyrite in the same ore (Cook and Chryssoulis, 1990). The larger gold content in the finer grained arsenopyrite confirmed the findings of Simon et al., (1999) who studied the pyrite from the Twin Creeks gold deposit in Nevada.

Ores studies from the Great basin in USA showed that gold was evenly distributed in arsenian pyrite at scales of below 50 Angstrom ($10^{-10}$m), and measurements on gold containing arsenopyrite showed that gold was present in solid solution, and thus as the structure of arsenian pyrite is similar to that of arsenopyrite, it was inferred that the gold was also present in solid solution within metastable arsenian pyrite (Arehart et al., 1993).

As rich (and Fe deficient) hydrothermally synthesised arsenopyrite contained up to 3 wt% invisible gold (Fleet and Mumin, 1997). Invisible gold was reported to be spatially associated with As rich regions in pyrite (Fleet et al., 1993; Fleet and Mumin, 1997). The high Au capacity of pyrite that was As rich (whether it was arsenopyrite or arsenian pyrite), whether synthetic or natural, was shown (Fleet and Mumin, 1997).

As a general rule, gold contents of over 100 g/ton (within pyrite particles) are associated with arsenian pyrite (Cook and Chryssoulis, 1990; Fleet et al., 1993; Tauson, 1999).

The maximum solubility of gold in pyrite ores was shown to be dependent on the As content, with the direct relation as $C_{Au} = 0.02\, C_{As} + 4\, x\, 10^{-5}$, with the concentrations in Mol% which represents a maximum Au/As molar ratio of about 0.02 (Reich et al., 2005). This mathematical relationship represents the gold incorporated within the arsenian pyrite's structure and amounts over this limit would represent inclusions or nanoparticles of native gold formed within the pyrite. It is worthwhile to note that gold in arsenian pyrite below the 0.02 Au/As molar ratio was always found to be structurally bounded and not in inclusions or nanoparticles (Reich et al., 2005).

Arsenic in gold ores are attributed to arsenic minerals, such as arsenopyrite, arsenian pyrites and other pyrites with arsenic impurities or trace amounts. The silicates, on average, have been found to have a very low amount of arsenic (0-20g/ton in the silicates) compared to that of pyrite grains (Woolson et al., 1977), and arsenic in whole-rock analysis (where a sample of an entire rock is analysed) can majorly be attributed to the arsenic minerals and not the silicates.

Arsenopyrite (FeAsS) is marcasite in structure and as a result of the difference in structures between it and normal pyrite, solid solutions between the two do not exist, and thus As-bearing pyrite (Arsenian Pyrite) is associated with arsenopyrite. (Abraitis et al., 2004). This is seen as large grains of "pyrite", which is made up of smaller distinct grains of pyrite

Experimental work by Fleet and Mumin, (1997) yielded maximum amounts of arsenic incorporated into pyrite between 205 °C and 605°C at 1.3 to 1.6 kbar of 9.3 wt%, although the location of the Arsenic within the pyrite was not reported (Fleet and Mumin, 1997; Pals et al., 2003). This maximum of 9.3 wt% is in the same order of magnitude of the values reported by Vaughan and Craig, (1978) at 5 wt% and Griffin et al., (1991) at 8 wt%, but much larger than those reported by Fleet et al., (1989) at 0.5 mol% and the <0.5 wt% of Clark, (1960). The higher number reported by some could be a result of As inclusions or formations that were not part of the pyrite structure but otherwise measured (Fleet and Mumin, 1997; Griffin et al., 1991; Pals et al., 2003; Vaughan and Craig, 1978).

Arsenic in arsenian pyrites was reported to be in a crystal setting , similar to that in arsenopyrite (Simon et al., 1999).

Arsenian pyrite from the Twin Creeks deposit in Nevada was observed to have a peak in the XANES (X-ray absorption near edge structure) spectra that could correspond to Arsenic in an oxidation state more than $As^{III}$, most likely $As^{V}$ (as in arsenate $AsO_4^{3-}$) and thus arsenic was found to occur in an oxidised coating over the surfaces of arsenian pyrite grain surfaces (Simon et al., 1999). This will alter the surface properties of the arsenian pyrite grain. The arsenic within arsenian pyrite was also concluded to be $As^{1-}$ in a structural position similar to that of arsenopyrite (Simon et al., 1999).

## 2.6 Variations in Pyrite Composition and Structure

The pyrite crystal structure takes the form of a face centred cubic array where each sulphur atom is co-coordinated to three Fe atoms and bonded to another sulphur atom, and each Fe atom is coordinated to six sulphur atoms where the bond character is essentially covalent (Abraitis et al., 2004).

The stoichiometric ratio of Fe:S in pyrite is 1:2 and is not known to vary except for the cases of where impurities are found. The natural occurring pyrite Fe:S ratio is not seen to differ by more than 1% (Abraitis et al., 2004), for example, the Turkish pyrite samples of Bulut et al., (2004) was seen to vary from $FeS_{1.90}$ to $FeS_{1.97}$.

Most substitutions are stoichiometric (Such as the substitution of $Co^{2+}$ for $Fe^{2+}$), but some are non-stoichiometric (such as the substitution of As for S, forming $AsS^{3-}$ and $As_2^{3-}$ groups) and differ in valence and thus net charge and results in significant changes in the electrochemical properties of the mineral (Abraitis et al., 2004). The non-stoichiometric substitutions will also distort the crystal lattice, causing defects to more easily formed and this in conjunction with charge differences perhaps could promote more impurities to be incorporated within the pyrite structure.

In the Western Australian gold deposits, it was shown that there was a positive correlation between Au and trace elements of Pb and Bi within pyrite and arsenopyrite (Morey et al., 2008).

The maximum content of minor element impurities in pyrite were reported by Vaughan and Craig, (1978), although this was done via bulk mineral analysis and therefore included inclusions within the matrix that were not part of the pyrite structure. The maximum contents within the pyrite structure could be lower than the following reported amounts in Table 1.

Table 1: Maximum elemental content within bulk pyrite, including microscopic inclusions but excluding larger inclusions, data from Vaughan and Craig, (1978)

| Element | Maximum Content within Pyrite |
|---|---|
| **As** | 5 wt% |
| **Pb** | 5000 g/ton |
| **V** | 1000 g/ton |
| **Sb** | 700 g/ton |
| **Ti** | 600 g/ton |
| **Sn** | 400 g/ton |
| **Tl** | 340 g/ton |
| **Se** | 300 g/ton |
| **Ag** | 200 g/ton |
| **Au** | 200 g/ton |
| **Ga** | 100 g/ton |
| **Bi** | 100 g/ton |
| **Ge** | 50 g/ton |
| **Mo** | 30 g/ton |
| **Cd** | 10 g/ton |
| **In** | 10 g/ton |
| **Hg** | 0.4 g/ton |

Abraitis et al., (2004) compiled data from Arehart et al., (1993), Brill, (1989), Cabri et al., (1985), Chenery et al., (1995), Cook and Chryssoulis, (1990), Fleet et al., (1993), Griffin et al., (1991), Huston et al., (1995), Oberthür et al., (1997) and Wells and Mullens, (1973) on the maximum amount of elemental impurities found in pyrite samples from different geographical locations, and the resulting information is displayed in Figure 1 on the following page.

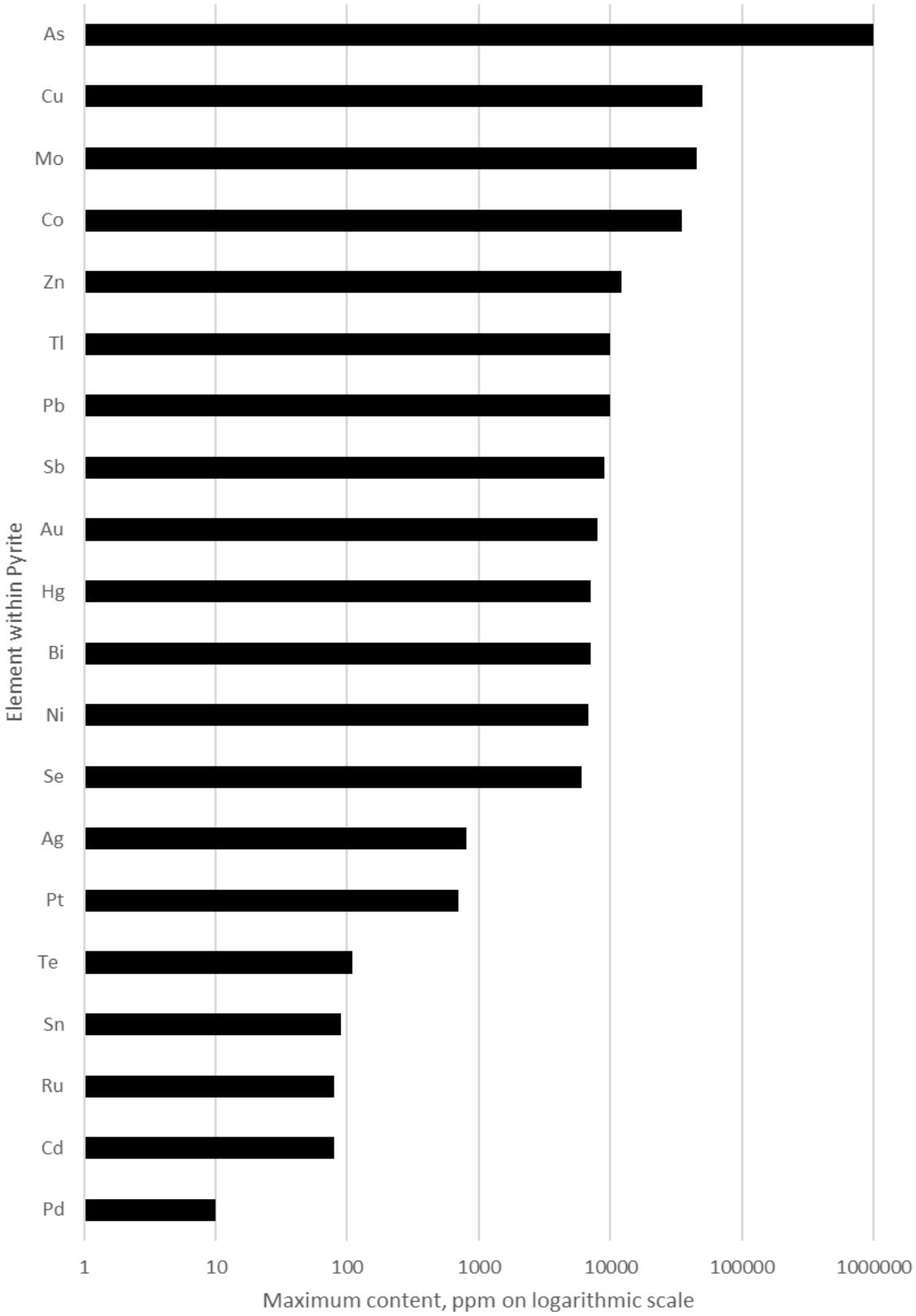


Figure 1: Compiled data from Abraitis et al., (2004) showing the maximum amount of various elements, reported in g/ton, in pyrite (Abraitis et al., 2004; Arehart et al., 1993; Brill, 1989; Cabri et al., 1985; Chenery et al., 1995; Cook and Chryssoulis, 1990; Fleet et al., 1993; Griffin et al., 1991; Huston et al., 1995; Oberthür et al., 1997; Wells and Mullens, 1973)

### *2.6.1 Substitutions for Fe and S*

Abraitis et al., (2004) and Pals et al., (2003) outlined the elemental substitutions in the pyrite system when variations in the pyrite composition were present and are summarised in Table 2 below (Abraitis et al., 2004; Bulut et al., 2004; Pals et al., 2003).

Table 2: Elemental substitutions for Fe and S in the pyrite structure

| **Substitutions for Fe** | Ag, Bi, Co, Cu, Hg, Ni, Pb and Zn |
|---|---|
| **Substitutions for S** | As, Sb, Se and Te |
| **Positions not specified** | Au, Cd, Ga, Ge, Hg, In, Mn, Mo, Ru, Sn, Tl, W, and V |

### *2.6.2 Variations in Pyrite Semiconductor Properties*

Semiconductors are classed as n-type if the substance has free electrons (electron donating) or p-type if it has “holes” (electron accepting). Semiconductor properties are related to the presence of charge carriers and in pyrite may arise from three sources, (Pridmore and Shuey, 1976):

1. Impurities or contaminants in the solid solution or inclusions
2. Deviations from Stoichiometry
3. Via thermal energy input/excitation across the energy gap

Pyrite has a band gap of 0.95eV (Pridmore and Shuey, 1976) and therefore the 3$^{rd}$ source in the previous list is insignificant at room temperature and therefore also any flotation system temperature. As mentioned in Section 2.6, pyrite has little deviation from stoichiometry (as low as 1% for Fe:S ratio) and thus the 2$^{nd}$ source in the above list is insignificant. It was however seen that sulphur deficient pyrites tend to be n-type, and it was noted that some observations of sulphur rich pyrites tended to be p-type. After reducing the sulphur content of the p-type pyrite by heating, it converted to n-type (Pridmore and Shuey, 1976), but this trend was not confirmed in later studies, such as the one by (Doyle and Mirza, 1996), who reported all pyrite samples (up to a Fe:S ratio of 1:2.015) to be n-type semiconductors.

The main source of semiconductor properties must be from the 1$^{st}$ source, i.e. impurities or contaminants, as the 2$^{nd}$ and 3$^{rd}$ sources are relatively insignificant. Different impurities, having different semiconducting properties themselves, would influence the semiconductor properties of pyrite in different ways.

Pyrite is normally a n-type semiconductor but may locally become a p-type semiconductor (Lalvani et al., 1990, Mirronov et al., 1981) (Pridmore and Shuey, 1976) which may be induced by impurities such as arsenic or lattice defects (Knipe et al., 1992). As natural pyrites contain impurities, they have been reported to be both p-type and n-type semiconductors (even within a single sample/specimen) and have had reported conductivities that vary by four orders of magnitude (Abraitis et al., 2004; Pridmore and Shuey, 1976).

P-n-bridges or p-n-type behaviour exists in pyrite between p-type locations and n-type locations within a sample, especially when impurities, such as arsenic, are present, causing the semiconductor properties

to change depending on the specific location of the impurity. This may play a role in mechanisms of gold incorporation during formation, as previously mentioned.

Due to As substitution for S in the pyrite structure, the resulting arsenian or arseno-pyrite is expected to be a p-type semiconductor (Laird et al., 2015). Arsenian pyrite, as expected, has been observed to be a p-type semiconductor (with most other pyrite samples with other impurities being n-type) with high electrical conductivity (Abraitis et al., 2004). This could be explained by the previously mentioned $AsS^{3-}$ and $As_2^{3-}$ groups which would impart the p-type semiconducting properties. P-type pyrites that are As-rich are suggested to have formed at low temperatures, while n-type pyrites generally have low As contents and suggested to have formed at higher temperatures. Substitutions for Fe, (such as Co and Cu) often results in n-type behaviour (Laird et al., 2015).

Two different pyrites (a relatively pure Peruvian pyrite versus a lower grade Australian pyrite) were floated and characterised by Owusu et al., (2013), and an oxygen demand test showed that different pyrite's from ores displayed significantly different electrochemical reactivity.

Ball and Rickard, (1976), indicated that the variability in chemical composition of pyrite, due to the deposition or formation environment, created differences in the flotation behaviour of different samples of pyrite. This was perhaps due to differences in semiconductor properties based on the different chemical compositions of the different samples of pyrite.

Schieck et al., (1990) formed synthetic pyrite crystals and compared them to naturally occurring pyrite crystals, and found significant deviations in their electronic properties, which was attributed to impurity elements.

Differences in the compositions of the Turkish pyrite of Bulut et al., (2004) (along with textural differences) were reported with significantly different isoelectric points when zeta potential (discussed in Section 2.11) was measured, although pulp potential for all pyrites were similar.

One important electronic property of pyrite is rest potential, which is the potential difference across a mineral-solution interface when the mineral surface is at electrical equilibrium. Pyrite was found to have the highest rest potential out of all sulphides at 0.66 V versus standard hydrogen electrode (SHE) (Abraitis et al., 2004). The higher the rest potential, the more difficult it is to oxidise the material, which means that pyrite is the least reactive and thus most stable out of all sulphides. Experiments by Doyle and Mirza, (1996) showed that the tested 12 pyrite samples has a minimum rest potential of 0.558 and a maximum of 0.699 vs SHE. This is put into context by chalcopyrite's rest potential of 0.56 V and galena's at 0.4 V vs. SHE, thus comparing different pyrite samples' rest potentials could be as far apart as comparing rest potentials of sulphides with completely different base metal contents.

Previous studies, such as Doyle and Mirza, (1996), failed to correlate different electrochemical properties to other properties (such as semiconductor type, rest potential or conductivity versus impurities or Fe:S ratio). The electrochemical properties are a major factor in determining the reactivity of the pyrite, including the attachment of the collector to the mineral surface.

## 2.7 Flotation of Gold Ores

Flotation is a physicochemical process that exploits the differences in hydrophobicity to achieve separation. It is often used to pre-concentrate mineral ores in the step directly after communition steps (crushing and milling) of the mined ore. The following description of flotation makes use of the word "substance" as flotation is not only used in the mining industry, but also in waste-water treatment, paper recycling and other industries. In the context of this project, the "substances" in the flotation system are minerals.

The feed is usually in a slurry form which an impeller mixes. The impeller serves to mix the slurry as well as disperses air which is bubbled up through the slurry. Reagents are added, the two most important being collectors and frothers. Collectors selectively adsorb to substances and impart hydrophobicity on them, which causes the substances to attach to the rising bubbles. The bubbles then report to and reside within the foam layer at the top which is stabilised by the frother. The froth then overflows and carries with it the hydrophobic substance, separating it from the hydrophilic (or less hydrophobic) tailings. Any undesirable or valueless mineral, rock or substance in the feed of an ore is referred to as "gangue", and the aim of flotation is to separate as much of the gangue from substances that are desired, whether this is by floating the gangue away from the valuables, or more commonly floating the valuables away from the gangue. If the substance to be floated is naturally hydrophobic, a collector may not need to be added.

For the flotation process to be successful, a number of sub-processes or steps have to occur. These sub-processes can be summarised as follows (Bradshaw, 1997):

1. Collector adsorption or attachment onto a mineral surface, rendering it hydrophobic
2. Bubbles are introduced to the pulp
3. The hydrophobic mineral particle collides with an air bubble, with a possibility of attachment of the mineral to the air bubble
4. The air bubble, loaded with hydrophobic minerals, is transported through the pulp phase. Detachment of the mineral from the air bubble may also take place
5. Mineral particles are transferred from the pulp phase to the froth phase (either via entrainment or via bubble transport) The reverse may also happen, called elutriation, where particles from the froth phase return to the pulp phase
6. The froth phase is recovered, with the loaded bubbles and mineral particles

Industrial flotation circuits most commonly involve three stages, named the roughers, cleaners and scavengers. Roughers produce the first concentrate and reject most of the gangue. This concentrate is sent to the cleaners to reject more gangue and further "clean" the concentrates. The tailings from the roughers are sent to the scavengers to recover some of the valuable minerals in the tailings from the roughers, i.e. to "scavenge" from the tailings.

### *2.7.1 The flotation system: Klimpel's Triangle*

Flotation is affected by a number of parameters which were summarized by Klimpel and Hansen, (1988), in a "summary of the interactive system of flotation". The parameters in Figure 2 are interrelated and these relationships can be viewed in a form of a triangle, as shown in below.

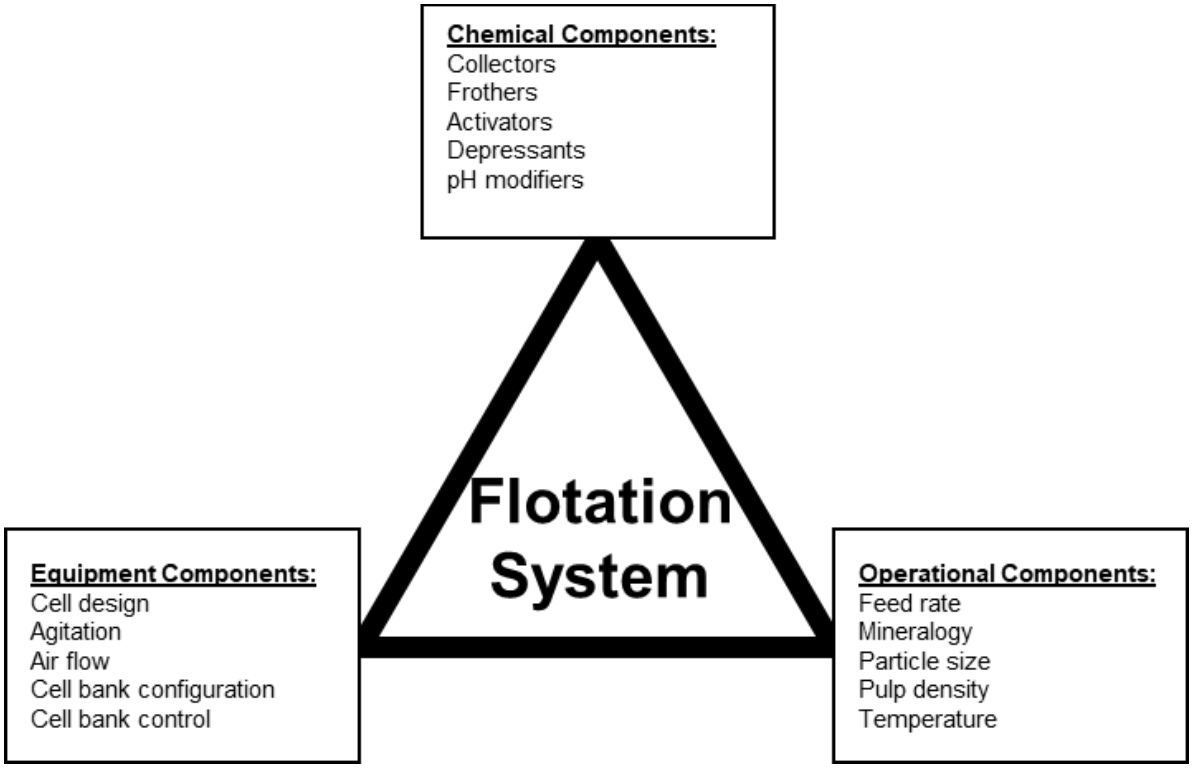


Figure 2: The Interactive flotation system redrawn (Klimpel and Hansen, 1988).

The parameters that are important in this study are the Mineralogy (found under operation components) and the Collectors (under chemical components), more specifically how the collector reagent suite should change in response to varying mineralogy in order to maximise the gold recovery when different impurities are present. A few parameters of importance are discussed further in the proceeding sections.

### *2.7.2 Pulp Potential and pH*

Pulp electrochemistry is paramount importance when considering collector attachment in flotation systems. Pulp potential, or Eh, is a measure of the oxidation or reduction potential of the pulp and has been shown to influence the floatability of sulphide minerals (Buckley and Woods, 1987; Fuernstenau et al., 1968; Fuerstenau et al., 2007; Goktepe and Williams, 1995; Hamilton and Woods, 1981; Iwasaki, I., Cooke, 1959; Lotter et al., 2016; Natarajan and Iwasaki, 1984; Woods, 2003).

The collector attachment or adsorption onto a mineral surface is an electrochemical reaction, and thus pulp potential plays an important role in controlling the attachment of the collector onto the mineral surface. The semiconducting properties of the minerals present in the pulp as well as other additives impact the Eh (V.V. Hintikka and Leppinen, 1995; Woods, 2003).

Altering the Eh in the pulp is important to the success of a flotation system as certain minerals, depending on their semiconductor properties, require either positively or negatively charged collector ions to adsorb or attach to them. Each mineral (with unique semiconducting properties) and collector combination has characteristic potential (Eh) where they start to float (Adams, 2016). Depending where in the Eh-pH domain the electrochemistry of the flotation pulp resides, a variety of collector states may exist, with the two most important states in most common collectors being the thiolate radical or dithiolate molecule.

In order to render a mineral hydrophobic, the mineral has to attach to the collector. If the mineral to be floated is a p-type semiconductor (positively charged surface), it requires a negatively charged collector (or thiolate) radical to effectively attach to it. A n-type semiconductor (negative surface) conversely requires dithiolate molecules in the pulp which will attach via a type of hydrogen bonding to render the mineral hydrophobic. Based on the mineral, the pulp electrochemistry must be changed to provide the correct conditions for collector attachment and optimum hydrophobicity (Lotter et al., 2016).

pH (on the x axis) is often plotted against Eh (on the y axis) to form a diagram known as a "Pourbaix diagram" which can be used to show different states and visualise flotation domains. A Pourbaix Diagram for butyl xanthate is shown in Figure 3 below.

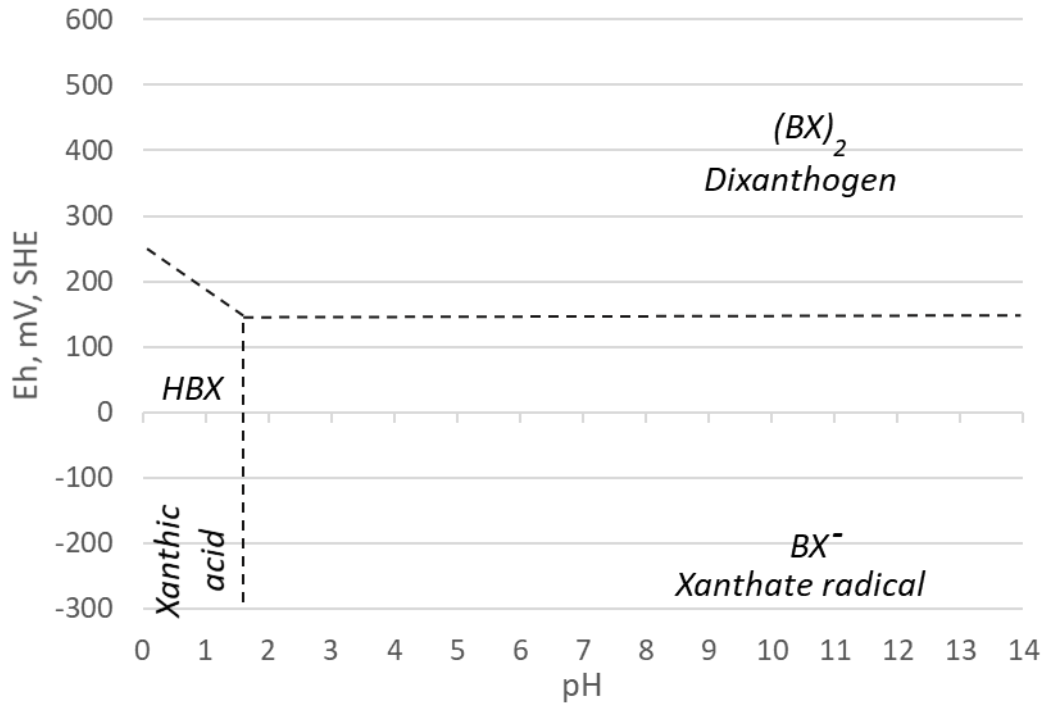


Figure 3: Pourbaix Diagram for butyl xanthate, (Iwasaki, I., Cooke, 1959; Lotter et al., 2016).

#### *2.7.2.1 pH*

Perhaps the most important parameter in flotation is pH, as in combination with Eh, it determines the flotation domain on the Pourbaix Diagrams. pH influences processes within the flotation pulp, such as hydrolysis (breakdown of chemicals) and oxidation of minerals, which are important to the success of flotation (Ozun et al., 2019). The pH of flotation pulp highly depends on the individual system (mineral to be recovered, collectors, gangue) and the system must be designed accordingly. In most flotation systems, gangue minerals may easily float at certain pH levels, so these must be avoided. Of the remaining pH band, only certain collectors would be stable and active (Guo et al., 2016; Maree et al., 2017).

#### *2.7.2.2 Eh*

Pulp potential, Eh or redox potential, is a measure of the oxidising or reducing nature of the flotation pulp. The pulp potential is almost always desired to be oxidising in nature (positive Eh) as collector attachment (in the case of xanthates and most other collectors) involves the anodic reaction of xanthate with the mineral surface to release electrons, with the reduction of oxygen as the cathodic process (This is further discussed in Section 2.8.3). Because air is the most widely used flotation gas, the combination of air and sulphide minerals lead to the average pulp potential of +200 mV to +300 mV SHE (Ralston, 1991).

Under laboratory conditions, the optimum Eh range for the flotation of native gold was seen between +10 and +60 mV (versus Saturated Calomel Electrode - SCE) the recovery of iron sulphides highest at +50mV and decreases at higher pulp potentials (Adams, 2016; V.V. Hintikka and Leppinen, 1995). Native gold however is not the focus of this study, and the appropriate flotation domain for the collector being used and pyrite should be considered when attempting to recover the pyrite, and this will be discussed later in Section 2.8.

### ***2.7.3 Particle size***

The recovery of gold in flotation is related to particle size not only for pulp properties but more so because liberation of gold from gangue is important, as the amount of native free gold in ores is diminishing and gold is more and more associated with other minerals.

A pyritic gold ore from Quebec, Canada was floated (batch flotation) with the $F_{80}$ fineness of grind being investigated versus gold recovery. An increase in gold recovery from 91.8% to 95.8% was found by decreasing particle size from an $F_{80}$ of 205 to 53 µm (Yalcin and Kelebek, 2011). This is thought to be due to better liberation of the gold which then lead to higher flotation recovery (Yalcin and Kelebek, 2011).

### *2.7.4 Collectors*

Collectors attach to the mineral surface in the flotation pulp and cause hydrophobicity to allow the minerals to attach to bubbles and rise to the froth phase and ultimately report to the concentrates. It is thus desirable for the collectors to attach to the maximum amount of mineral that is desired to be recovered to the concentrates and a minimum amount of the gangue. The collectors used to float a variety of important minerals are discussed in the next subsections. A review of pyrite flotation is given later in Section 2.8 as it is to be focussed on.

#### *2.7.4.1 Native Gold*

Native gold was reported to be floated readily without a collector and just a frother by O Connor and Dunne, (1994), due to organic contaminants. Later articles such as Dunne, (2005) reported that pure clean gold is hydrophilic and again the observed hydrophobicity of most natural occurring gold was attributed to organic contaminants but untarnished gold could still be easily floated with just a collector. Deposition of sulphur onto the gold surface was shown to render the gold hydrophobic (Dunne, 2005).

In industry, xanthates are commonly used with a mixture of other collectors (particularly amines, and dithiophosphates) for use in industry gold flotation cells (O Connor and Dunne, 1994). The recovery of gold was observed to be activated by sulphide ions and depressed by ferric ions (O Connor and Dunne, 1994).

#### *2.7.4.2 Arsenopyrite*

Because gold is more associated with arsenopyrite in a pyrite-arsenopyrite-gold system, floating the arsenopyrite from the pyrite is beneficial. Modifiers such as sodium metabisulphate and magnesia has been reported to enhance separation of arsenopyrite from pyrite in a flotation system (O Connor and Dunne, 1994).

Arsenopyrite was reported to have similar flotation properties and conditions to pyrite by (O Connor and Dunne, 1994). Under oxidising conditions, a high concentration of PAX (Potassium Amyl Xanthate) has a high recovery of pyrite and arsenopyrite (Dunne, 2005).

(Park et al., 2015) investigated the selective separation of arsenopyrite and pyrite in a Hallimond tube micro-flotation setup with a xanthate as a collector. The study found that at a pH of 4, regardless of the concentration of xanthate, arsenopyrite floated better than pyrite did. This could be because of the pulp electrochemistry in the experiments favoured the formation of either the xanthate radical or dixanthogen, one of which could have attached to the arsenopyrite better than the pyrite based on the different semiconductor properties.

### *2.7.5 Promoters*

Promoters are collectors that are added in smaller quantities than the primary collector (often called secondary collectors) and often result in better flotation recoveries than adding more primary collector alone. Dithiophosphates are the most used promoter in gold flotation circuits, but amines are also used especially in the case of gold bearing pyrites (Dunne, 2005; O Connor and Dunne, 1994). Monothiophosphates are useful for selectively recovering gold from sulphide ores (Dunne, 2005).

### *2.7.6 Frothers and Froth Stability*

Frothers are added to aid froth stability and strength. In gold flotation, a preference for polyglycol-ether based frothers has been observed (Dunne, 2005; O Connor and Dunne, 1994). Collectors and frothers sometimes have a synergistic relationship in stabilising the froth (Leja and He, 1984; Leja and Schulman, 1954; Mukai et al., 1972). With an increase in froth stability, more water is entrained into the froth phase and reports to the concentrates. With this increased froth stability, more of the mineral of interest, and/or the gangue can be also entrained to the concentrate.

Coetzer, du Preez and Bredenhann, (2003) investigated froth stability with a sulphide ore in a flotation system and found that the froth stability showed dependencies on not only the frother, but also the collector, ore and water source (Coetzer et al., 2003).

One method of determining changes in froth stability due to the collector and frother synergism or interactions in flotation is to exclude the mineral or solid phase from the flotation pulp and just the liquid and froth phase remain. The water is recovered to the “concentrate” via the froth phase and its mass can be compared to see if any change in froth stability was significant with changing inputs, as the water recovered is dependent on froth stability (Banford et al., 1998; Ekmekçi et al., 2006; Engelbrecht and Woodburn, 1975; Khoshdast and Sam, 2012).

A measuring cylinder partially filled with water, and an air source on the inside could be used to measure froth heights under different conditions, as done by Khoshdast and Sam, (2012). Conclusions can be drawn on the change in froth stability from the change in the froth height, as a more stable froth would lead to a higher froth height.

### *2.7.7 Activators*

Activators are normally soluble metal salts from which the metal ion adsorbs onto the mineral surface, thus changing the surface properties to allow other reagents, such as collectors, to better interact with it. Copper sulphate is widely used as an activator in the flotation of gold bearing pyrite but has limited use in alkaline conditions (Boulton et al., 2003; Chandra and Gerson, 2009; Teague et al., 2000).

It has been proven that up to a 5% to 20% increase in recovery of gold has been reported when adding the copper sulphate to the system (Dunne, 2005). For the arsenopyrite system, up to a 20% increase in recovery was seen when copper sulphate is introduced to the pulp before the collector, and this in turn improves gold recovery because of the arsenopyrite/pyrite and gold. The mechanism whereby copper sulphate activates gold is unknown, but one role may be the increase of the redox potential of the pulp, which in turn would allow easier oxidation of thiol collectors association (Dunne, 2005; Teague et al., 2000).

Copper sulphate can also reduce the amount of slime in the froth and, in the case of pyrite, increase the concentrate grade (Dunne, 2005). However, too high concentrations of copper sulphate affects froth stability (O Connor and Dunne, 1994). Thus an optimum exists between too little copper sulphate (too much slime/low grade concentrate) and too much copper sulphate (low froth stability, low recoveries).

### *2.7.8 Other noteworthy interactions*

The gold ore flotation systems also notably depend on the interactions between grinding media chemistry, mineralogy, process water chemistry and aeration (or dissolved oxygen) (Ball and Rickard, 1976; O Connor and Dunne, 1994; Rabieh et al., 2016).

For example, galvanic interactions between forged steel grinding media and gold or other minerals occurs and affects the system (Rabieh et al., 2016). Galvanic interaction between different minerals and indeed gold may occur in the flotation pulp as well, such as gold catalysing the increase in oxidation rate of pyrite and the reduction of Fe ions (if present), forming an extensive sulphur rich layer around the pyrite (Huai et al., 2018). The sulphur rich layer around pyrite that is formed when gold is present may explain the natural floatability of gold-pyrite systems, as the sulphur layer would be hydrophobic.

A note should be made of water contact angle, or "wettability", which is the angle of a water droplet surface to a mineral (or other) surface when a droplet is placed on the surface (interior angle inside the water droplet). In theory, the more hydrophobic a mineral is, the higher the water contact angle is, as the water droplet is repelled, and its surface tension causes the droplet to tend to a more spherical shape. Water contact angles has been used in flotation as a measure of hydrophobicity and floatability, but researchers have viewed contact angles as limited in their ability to predict flotation responses (Bradshaw and O'Connor, 1996; Leja, 1982). Flotation recovery has also been achieved where minerals of zero contact angle are floated (Crozier, 1991; Finch and Smith, 1979).

## 2.8 Flotation of Pyrite – A review

Thiol collectors are most commonly used to float pyrite (Dunne, 2005). At a pH of 4, most thiols have been shown to be effective in floating pyrite, but the instability of xanthate at this low pH has led to a preference of dithiophosphates. Xanthate with mixtures of thionocarbamates and dithiocarbamates has also shown to be successful in recovering pyrite, though collector mixtures will be covered in more detail in Section 2.8.4 (O Connor and Dunne, 1994). When using ethyl-xanthate, Fuerstenau et al., (2007) showed two maxima of recovery at a pH of 4 and 8, with a minima at 6 and depression of xanthate happening at pH's lower than 2 and over 10. A similar trend of recovery was shown by Bulut et al., (2004), where the peak recovery of pyrite with ethyl-xanthate was at a pH of 4 and had a minimum at a pH of 7.

Mixtures of collectors that have been particularly effective in floating pyrite are mostly mixtures of xanthates and dithiophosphates as well as thiocarbamates (Dunne, 2005), however collector blends and mixtures will be discussed in Section 2.8.4.

It is worth mentioning is that pyrite is often depressed when it is a gangue mineral, as non-valuable pyrite in concentrates before smelting leads to significantly higher smelting costs, the emission of sulphur oxides which then contribute to acid rain and can emit other harmful gasses (such as if arsenic is present in the pyrite) into the environment (Moslemi and Gharabaghi, 2017). Organic depressants such as starch, guar gum, dextrin, cellulose, chitosan or diethylenetriamine are used to either prevent collector attachment onto the pyrite, de-adsorb the collector from the pyrite or directly render the pyrite surface hydrophilic (Mu et al., 2016).

The semiconductor properties of pyrite plays an important role in the mechanisms of collector attachment, activation, oxidation and depression in a flotation system. The differences in trace and minor element content of the mineral can lead to the differences in the electrochemical and semiconductor properties of pyrite, which can then impact all of these interactions (Lotter et al., 2016; Moslemi and Gharabaghi, 2017).

Particle size distribution, reagent suite, dissolved oxygen, differences in surface textures and grinding conditions are known to affect the intensity of the electrochemical interactions in the flotation system (Moslemi and Gharabaghi, 2017).

A difference in the floatability of pyrite from different geographical locations was seen when Moslemi and Gharabaghi, (2017) compiled the results, and this is expected as the variations in the pyrite composition and thus properties was shown in Section 2.6. Flotation tests done by Xian et al., (2012) on "perfect" pyrite, arsenic substituted pyrite and intercrystalline Au pyrite revealed that differences existed between them, such as the floatability of pure and arsenic substituted pyrite both decreased with pulp aeration time but intercrystalline Au pyrite increased with pulp aeration time . Using electronic structure and band structure, it was noted that the stability of arsenic substituted pyrite was stronger than that of perfect pyrite, which was stronger than that of pyrite with intercrystalline Au. The stability inequalities was put forward as the reason for the differences in flotation behaviour. A relationship between the band gap value and the amount of xanthate that could be absorbed onto the pyrite surface was also reported. Since it was shown that the impurities within pyrite alters its band gap and other electrochemical properties, the amount of xanthate or other collector that can be absorbed is related to the impurities within the pyrite (Xian et al., 2012). Since the impurities differ from different geographical locations, the origin of the pyrite also influences the maximum amount of collector that can be absorbed.

Pyrite from two different genesis types were investigated by Ertekin et al., (2016) by manufacturing electrodes from them. The study showed that significant differences in electrochemical reactivity between the two, particularly with dithiophosphate type collectors, where one type of pyrite (the Carlin type- sediment hosted disseminated gold) had significantly higher rate and amount of DTP (dithiophosphate) adsorption when compared the other type (Verde Pyrite- from Arizona). One outlier of the study was that of a specific monothiophosphate that had the second highest adsorption rate for the Carlin type but the lowest on the Verde type. This was also attributed to the difference in electrochemical properties between the two pyrites. This difference in electrochemistry may be a result of different impurities in the two pyrites.

Vacancy defects due to loss of cations or anions in the pyrite lattice was also shown to affect the electrochemical properties and flotation behaviour of pyrite (Li et al., 2010). In collectorless flotation of pyrite, moderately oxidising conditions yield the best results while both highly oxidising and highly reducing environments lead to pyrite depression (Moslemi and Gharabaghi, 2017).

### *2.8.1 Oxidation of Pyrite*

If pyrite undergoes complete oxidation, ferrous ions and iron sulphates are formed, however it was experimentally observed that the oxidation does not go to completion and instead elemental sulphur is

also produced, as per Reaction 1 below (Buckley and Woods, 1987, 1984; Moslemi and Gharabaghi, 2017)

$$FeS_2 + 3.5O_2 + 0.6H_2O \rightarrow Fe^{2+} + 0.4S^0 + 1.6SO_4^{2-} + 1.2H^+ \qquad \text{Reaction 1}$$

The composition of the outer layers of a pyrite particle that has been oxidised has been studied, but a conclusion has not been drawn. Some research suggested the ferrous ions formed from Reaction 1 then ferric hydroxide, which is precipitated onto the pyrite surface as a coating that inhibits further oxidation (Chernyshova, 2003). Other research on oxidised pyrite showed an iron deficient surface layer (Buckley and Woods, 1984), iron polysulfide (Luttrell and Yoon, 1984) or multiple layers of sulphur (Hamilton and Woods, 1981) (varying form disulphide ions to elemental sulphur (Antonijević et al., 2005)).

Although the exact nature of the surface is under debate, most of the studies show that the surface of oxidised pyrite has a higher concentration of sulphur towards the outside (and thus a lower concentration of iron) (Moslemi and Gharabaghi, 2017). This sulphur rich layer is likely the cause of pyrites natural floatability in slightly oxidising conditions.

### *2.8.2 Activation of Pyrite*

Pyrite can be activated by copper, as mentioned in Section 2.7.7, but can also be activated by lead. Lead and copper containing minerals can also activate pyrite by releasing copper or lead ions that then activate the pyrite. The activation of the pyrite has been shown to increase the rate of flotation and recovery of pyrite.

### *2.8.3 Collector attachment onto pyrite*

Because of sulphide minerals and pyrites semiconductor properties, the attachment or adsorption of collectors onto the mineral surface is usually electrochemical in nature (Güler et al., 2004; Hanson and Fuerstenau, 1991; Tolley et al., 1992; Woods, 2003) and thus should be affected by variations in semiconductor properties due to varying mineral compositions (Lotter et al., 2016).

Most collectors function because of the same basic structure, as shown in Figure 4 below. The functional group attaches onto a mineral surface and the hydrophobic chain then renders the surface of the mineral hydrophobic, and amenable to recovery by froth flotation. Collectors are often named after their functional group and chain length.

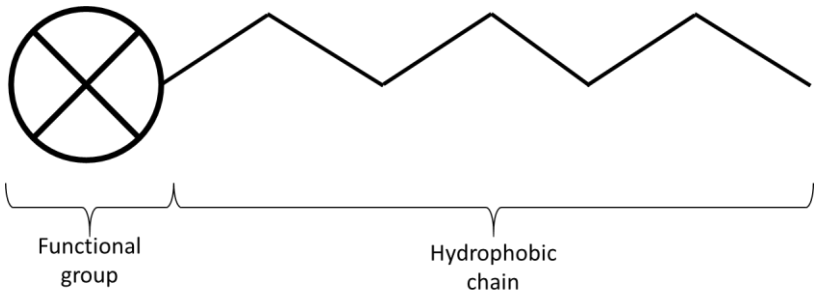


Figure 4: Basic structure of most collectors, with a reactive functional group and a hydrophobic chain

Thiol collectors, in particular xanthate, attach to mineral surfaces by the anodic oxidation of the collector with the cathodic reduction of oxygen (Dunne, 2005; Fuernstenau et al., 1968; Mendiratta, 2000; Mu et al., 2016). This may involve the half reactions given below (Dunne, 2005; Mendiratta, 2000):

1. Chemisorption of xanthate onto mineral surface:
   Xanthate → Xanthate (Absorbed) +e-
2. Reaction of Xanthate with mineral surface:
   Mineral Surface+ n*Xanthate$^-$ → Metal Xanthate$_n$ + $S^0$ +n*$e^-$
3. Dixanthogen formation near mineral surface with a xanthate ion already absorbed upon it, by:

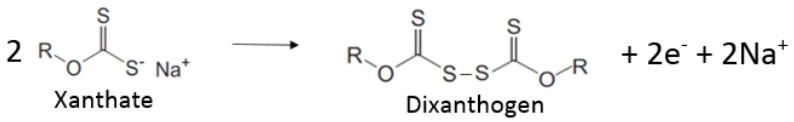


Dixanthogen is a neutral oil that plays a major part in causing hydrophobicity on mineral surfaces during flotation, and the attachment of it is the widely accepted mechanism of the flotation of free gold (Dunne, 2005; Miller et al., 1968).

FTIR (Fourier-Transform Infrared Spectroscopy) studies by Wang, (1995) identified four steps in xanthate and dixanthogen causing hydrophobicity of pyrite surfaces (Moslemi and Gharabaghi, 2017; Ralston, 1991; Wang, 1995):

1. Surface oxidation of pyrite
2. Xanthate adsorption onto pyrite surfaces and the formation of ferric xanthates
3. Dixanthogen formation by oxidation of xanthate ions
4. Dixanthogen adsorption on pyrite through ferric xanthates already present

Both the surface oxidation of a sulphide together with the oxidation of xanthates have been shown to play a vital part in the collector attachment process (Chander and Fuerstenau, 1983, 1975, 1974).

The mechanism of dixanthogen in the pulp reacting with a xanthate molecule that has already adsorbed onto the metal surface, forming an even stronger hydrophobic layer than just the adsorbed xanthate alone was shown by Yalcin and Kelebek, (2011) and was confirmed by Xiang-Huai and Forssberg, (1991) using FTIR analysis, with the best flotation results being at the pH levels where dixanthogen was co-adsorbed with xanthate ions in multiple layers. The Dixanthogen has also been shown to form a type of hydrogen bond to a mineral surface in the case of a n-type semiconductor mineral (negatively charged surface) (Lotter et al., 2016).

Longer chain xanthate molecules such as PAX oxidise more readily and thus forms dixanthogen more easily and increases hydrophobicity (Dunne, 2005; O Connor and Dunne, 1994).

Chander and Fuerstenau, (1983), (1975), (1974) has spent significant effort to understand the attachment of dithiophosphate collectors onto sulphide minerals, particularly in copper based sulphide minerals such as chalcocite, but the attachment path of the DTP onto an iron based sulphide can follow the same basic path. It is worthwhile to note that the path is very similar to the attachment path proposed by (Moslemi and Gharabaghi, 2017; Wang, 1995) of the attachment of a xanthate to a sulphide.

1. Surface oxidation of the sulphide

2. Formation of a metal-DTP salt on the surface of the mineral
3. Oxidation of the Metal-DTP salts to form a dithiophatogen $(DTP)_2$)

Even though $(DTP)_2$ is expected to form on the mineral surface, when using SEDTP (Sodium Ethyl Dithiophosphate), it was shown that $(DTP)_2$ did not form on the surface of platinum or palladium sulphides or tellurides (Tadie et al., 2015).

The corresponding reaction driving the reactions which have been discussed is the reduction of oxygen. Increasing the dissolved oxygen (DO) content in the pulp increases the pulp potential and the mechanism of collector attachment has multiple oxidation steps, the collector attachment onto pyrite benefits from a higher DO content (Chimonyo et al., 2017; M. C. Fuerstenau et al., 1990; M.C. Fuerstenau et al., 1990; Tolley et al., 1992).

The attachment of xanthate onto minerals in the semiconducting and pulp potential context was discussed in Section 2.7.2, with the mention of Pourbaix Diagrams. Figure 3 shows the Pourbaix Diagram for a xanthate collector, which has been discussed. The other collector commonly used in the gold industry context are the dithiophosphates, which are commonly mixed as an co-collector with a xanthate, as previously mentioned in Section 0. The Pourbaix Diagrams for xanthate(s) and dithiophosphates(s) can be overlaid, as in Figure 5, in order to visualise the electrochemical system at work in these systems. The new line of AE in Figure 5 when compared to Figure 3 separates the upper dithiophatogen ( $(EDTP)_2$) from the lower free dithiophosphate ($(EDTP)^-$) and dithiophosphatic acid below line AE (Lotter et al., 2016). The area EABC is a domain of importance where dixanthogen co-exists with the dithiophosphate radical, and therefore can impart hydrophobicity on minerals of both n-type and p-type semiconductor properties. This may be a reason why a dithiophosphate is commonly mixed with a xanthate in the gold recovery context, where As (and other) impurities within pyrite may render the pyrite to exhibit alternating semiconductor properties and thus a more complex collector reagent suite is needed.

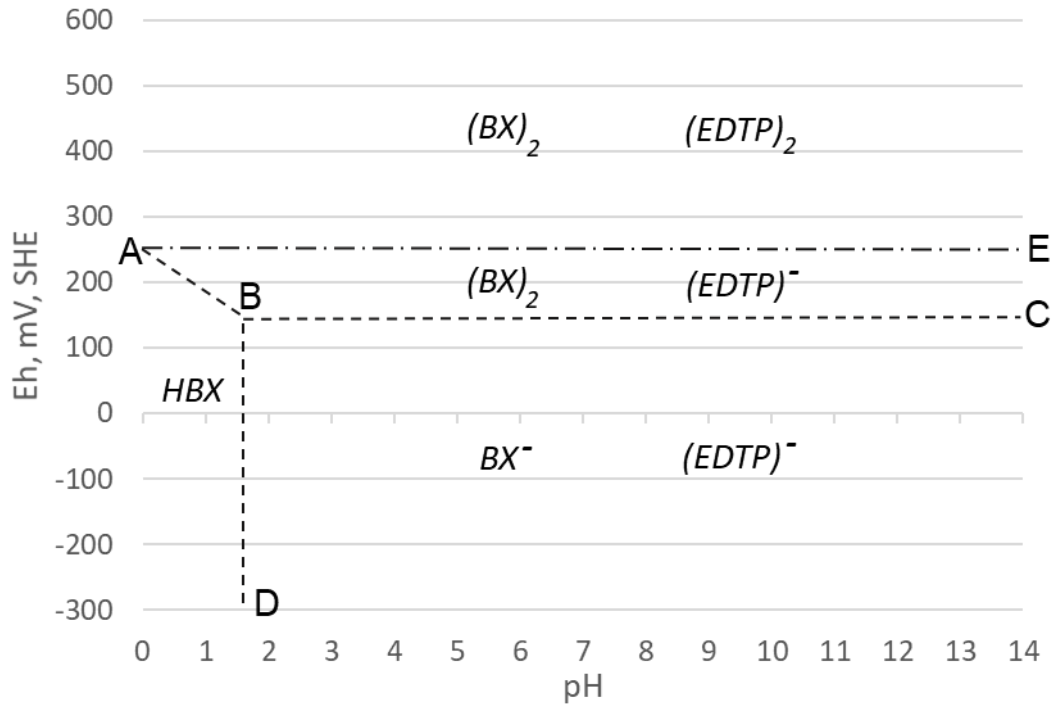


Figure 5: Overlaid Pourbaix Diagrams for butyl xanthate and ethyl dithiophosphate, from (Lotter et al., 2016)

Dithiophosphates are known to be a weak collector (low recovery) when compared to xanthates, but have higher selectivity (Lotter and Bradshaw, 2010). Dithiocarbonates are on the two extremes of this, with the highest recovery, but the lowest selectivity (Lotter and Bradshaw, 2010).

#### *2.8.3.1 Surface area coverage of Xanthate molecules*

The value of the surface area coverage of xanthate is important (for later calculations where the collector dosage is specified by percentage coverage) and has been reported from a variety of sources. Values from literature is shown in Table 3 below, with the surface area measured in Angstrom squared ($Å^2$).

Table 3: Literature values for surface area covered per molecule of Xanthate molecules

| Source | Surface area coverage per molecule Xanthate |
|---|---|
| (Grano et al., 1997) | 28.8 $Å^2$ |
| (Tipman, 1970) | 28 $Å^2$ |
| (Bilinski and Wojcik, 1996) | 30 $Å^2$ |
| (Matsuoka and Ichikoku, 1982) | 27 $Å^2$ |
| **Average** | 28.45 $Å^2$ |

### *2.8.4 Mixed or Blended Collector Systems*

Synergistic (better than the sum of its parts) behaviors of mixtures of certain collectors have been reported in sulphide ore flotation (Rao and Forssberg, 1997; Lotter and Bradshaw, 2010; Makanza et al., 2008; McFadzean et al., 2013, 2012; Pienaar et al., 2019). These can be attributed to a few mechanics, most notably faster mechanics and an increase in both recoveries and grades (Lotter and Bradshaw, 2010). The results of the studies in the mixture of collectors shows the advantage of using a mixed collector system as an increase in the recovery of these sulphides were seen. This recovery increase may be because an increase of dosage of a single collector not necessarily means increase in surface coverage of the particles, as the preferential sites for that specific collector may be already occupied. Other sites, that other collectors may occupy were left open and thus the introduction of a mixture of collectors meant that a greater surface coverage of collector was achieved which lead to higher recoveries. Another theory is that come collectors, such as DTP's, may adsorb onto the air liquid interface instead of the mineral liquid interface and help float minerals in this way (Pienaar et al., 2019).

The effect of mixtures of thiol collectors on the flotation of pyrite and galena (two mineral sulphides) was investigated by McFadzean et al., (2012). They reported clear improvements in recoveries when using a mixture of collectors, especially when using a mixture of a strong and a weak collector, with a 92,2% recovery of galena with a 10:90 mixture of sodium ethyl xanthate (SEX) with sodium ethyl dithiophosphate (SEDTP) compared to 89.0% with the best single collector. A similar thing was found with pyrite, with a 75:25 SIBX:SEDTP mixture which showed a 93.4% recovery compared to 89.8% for SIBX alone (McFadzean et al., 2012).

Another previous study by McFadzean et al. (2012), showed that mixtures of collectors resulted in improvements in flotation rate and recovery with pure galena. Pienaar et al, (2019), also showed an increase in recovery of pyrite when DTP was mixed with xanthates, even though it was shown that the DTP did not adsorb onto the pyrite surface.

Makanza et al, (2008), reported an increase in recovery of gold containing pyrite when using mixtures of thiocarbanate collectors (DTC and TTC) and xanthates, in the context of recovering gold and uranium in cyanidation tailings (Makanza et al., 2008).

Rao and Forssberg, (1997), clearly shows that mixtures of surfactant collectors in flotation improves the recoveries of targeted minerals, and furthers this review with contact angle measurements that show for example the addition of cationic dodecyl amine and neutral dodecyl alcohol show co-adsorption onto the surface but dodecyl alcohol is not adsorbed on the surface alone. This shows that interactions of collectors may play an important part in adsorbing collectors onto surfaces that they would otherwise not adsorb onto alone at all.

In sulphide flotation, xanthate in the presence of cationic alkyl trimethyl ammonium bromide (TAB) collectors showed resistance to oxidation and decomposition on the surface layer of minerals, meaning more robust flotation was achieved (Rao and Forssberg, 1997). This could also play a role in the viability of flotation of oxidised ores.

An increase of recovery of platinum of more than 5% was seen in the Raglan operation in Quebec when switching to SIBX from PAX, and it was concluded that further improvements can be made when using a mixture of the two (Lotter and Bradshaw, 2010). The South African platinum industry operated on SIBX alone until the early 1970s where the introduction of Cyanamid's 3477 as a co-collector improved recoveries (Lotter and Bradshaw, 2010). In both these cases and many more, the mechanism of the collector and surface interaction are not entirely known, just proven that they do work.

It is known that a single collector will not cover the full range in the polysulphide/complex sulphide ores (Lotter and Bradshaw, 2010), and known that mixtures may offer much better performance. What is not known is what collectors, in what ratios to be used at certain mineral compositions. This is important, particularly in the South African context where ores become less and less ideal as the "perfect" ores become depleted.

When a weaker collector is added to a stronger collector, the mixture results in a recovery gain relative to the single strong collector system (Lotter and Bradshaw, 2010). The mixture of collectors, including which collectors and at what ratios, depend on not only what main mineral is being floated, but also what other minerals and gangue are associated with it.

Other studies showing improvements in the flotation process attributed towards the synergism of collector mixtures include an improved flotation rate (Adkins and Pearse, 1992; Plaskin et al., 1954), a ratio of collectors where recovery of a sulphide was at a maximum (Bradshaw, 1997; Jiwu et al., 1984; Mingione, 1984) and improved flotation rate (Adkins and Pearse, 1992).

#### *2.8.4.1 Mechanisms of collector synergism*

The mechanism(s) that allow mixed or blended collector systems to perform better than individual collectors is not certain, with two major theories being proposed. The first theory is minerals have preferential sites for collector adsorption or attachment. These sites may be different for different collectors or collector types. Using a blend of collectors thus allows more sites (or more of the mineral surface) to be taken up by collectors and contribute towards increased hydrophobicity. The second theory is that a layer of collector that is adsorbed onto a mineral may provide a more even and uniform surface for other collectors to attach to, in another layer, thus increasing hydrophobicity (Lotter and Bradshaw, 2010; Zhong et al., 2015).

In mixed collector systems, which of the mechanisms is the reason for an increased flotation performance or if a combination of them is the reason is unclear (Lotter and Bradshaw, 2010).

The investigation into surface properties and how they vary with mineral compositional variation plays an important role in what collectors can be used and how collector mixtures must be varied according to on site changes in feed compositions.

### *2.8.5 Effect of grinding media*

Grinding media and the grinding environment before the flotation cell can have considerable effects on the properties of pyrite (Ball and Rickard, 1976; Peng and Grano, 2010a). The use of an electrochemically active grinding media, such as cast iron, can cause galvanic interactions between the pyrite and the media.

Because of the high rest potential of pyrite, the pyrite acts as a cathode and undergoes reduction (which releases hydroxide ions) while the grinding media then gets oxidised as the anode. The oxidation of the media often releases ferrous ions which then form ferric ions, and then react with the hydroxide being released from the pyrite and thus forms ferric hydroxides which can precipitate in layers onto the pyrite surface (Peng and Grano, 2010a, 2010b; Rabieh et al., 2016), which can depress the pyrite during flotation (Javadi Nooshabadi et al., 2013; Natarajan and Iwasaki, 1984; Peng and Grano, 2010b; Yelloji Rao and Natarajan, 1989).

The magnitude of the galvanic interaction is related to the difference in the electrochemical properties of the pyrite and the grinding media and the activity of the grinding media (Moslemi and Gharabaghi, 2017). When mild steel grinding media was compared to stainless steel before flotation, Chen et al., (2013) found that stainless steel (the less active grinding media) had significantly higher recoveries of pyrite from flotation than the mild steel. The amount of oxidation species formed on the pyrite surfaces after grinding was also significantly lower after grinding with stainless steel compared to grinding with mild steel (Chen et al., 2013).

## 2.9 Flotation of Other Sulphide Minerals

Many sulphides such as chalcopyrite, pentlandite and galena are pre-concentrated by froth flotation, with two relevant minerals to this study discussed in this subsection

### *2.9.1 Chalcopyrite*

Chalcopyrite can be floated without the presence of a collector, and Buckley and Woods, (1984) proposed that this was because chalcopyrite reacted in an alkaline solution, releasing iron from its surface and creating a sulphur rich layer, which is hydrophobic (Buckley and Woods, 1984). Even though chalcopyrite can be floated in the absence of a collector (Luttrell and Yoon, 1984), collectors such as xanthate are often used to increase the flotation rate and recovery.

Fuernstenau, Jameson and Yoon, (2009) constructed a Pourbaix diagram for the chalcopyrite and ethyl xanthate (EX) system, as recreated in Figure 6 below. The desired operability region is represented by the Cu(EX) space, as this is where the ethyl xanthate is adsorbed onto the chalcopyrite surface. (Fuerstenau et al., 2007).

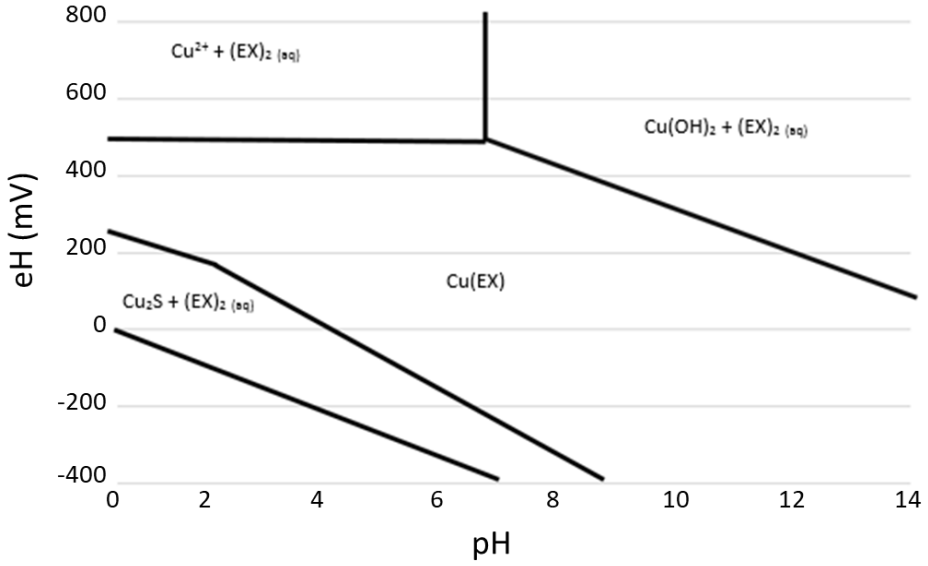


Figure 6: Pourbaix diagram for Chalcopyrite and ethyl xanthate, from Fuerstenau et al, (2007).

### *2.9.2 Pentlandite*

Pentlandite is a nickel sulphide mineral that is desired to be recovered from massive nickel ores. Flotation is often used to concentrate the pentlandite content of these ores. In pentlandite containing ores that are amenable to flotation, pyrrhotite often exists in substantial amounts and a challenge that is faced is separating the pentlandite from the pyrrhotite in a flotation circuit (Bozkurt et al., 1998; Ikotun et al., 2017; Khan and Kelebek, 2004).

Xanthate collectors are often used to float pentlandite, even from pyrrhotite (Bozkurt et al., 1998; Ikotun et al., 2017; Khan and Kelebek, 2004). Sodium Ethyl Xanthate (SEX) was seen to have the highest recovery compared to PAX and SIBX (Ikotun et al., 2017). At a pH of 9.2, with sufficient dissolved oxygen (DO), dixanthogen formation was found to be common to both pentlandite and pyrrhotite, however at lower DO, Dixanthogen was concluded to not form on pyrrhotite (Khan and Kelebek, 2004).

## 2.10 Flotation experimentation and representation

It is impractical to use large scale industrial flotation circuits to test and interrogate hypothesis formed in the flotation field, so various apparatus and methods have been developed to study phenomena in the flotation field. In the order of most alike to industry scale, the most common levels are is pilot plant scale, batch flotation and micro-flotation. A few differences of these have been discussed in Table 4 below. The properties discussed in Table 4 are a brief summary of the typical characteristics of the different levels, but may vary.

Table 4: Summary of the differences in levels of testing compared to Industry scale

| | Industry Scale | Pilot plant Scale | Batch Flotation | Micro-flotation |
|---|---|---|---|---|
| **Froth phase present** | Yes | Yes | Yes | No |
| **Pulp phase present** | Yes | Yes | Yes | "Yes"- but not to the extent of the others |
| **Ore/solids with complex mineralogy present** | Yes | Yes | Yes, but can be done with single minerals or artificial ores | No. Usually done with a single mineral or a mixture of two |
| **Continuous fed?** | Yes | Yes | No | No |
| **Approximate volume of systems** | Depends on Industry | Dozens of liters | 3 to 5 liters | Less than 500mL |

This study uses Batch Flotation and Micro-flotation to study flotation responses, with a 3-liter batch flotation cell and a 225mL micro-flotation cell. Flotation is a complex process with many interactive variables which must be varied and optimized for the system before test work can begin. Some of this pre-experimental scoping runs are discussed later in Section 3.2 later. What is needed before these scoping experiments are conducted is starting points for variables. The starting points in batch flotation were given by previous experience on the same equipment, but no experience was had on the Micro-flotation experimental setup, so literature had to be consulted for some of the starting points. Previous dissertations and thesis were consulted, primarily why the work of the research group of D.J. Bradshaw at the University Of Cape Town (UCT), as UCT has experience with the same micro-flotation equipment as was being used for this project. These and other projects that use the same experimental setup were used for preliminary air flow rate. The data found is displayed in Table 5 below.

Table 5: Parameters used by previous studies on the micro-flotation experimental setup

| Source | Air Flow rate (mL/min) | Conditioning Time (min) | Particle sizes (µm) | Ultrasonic cleaning? |
|---|---|---|---|---|
| (Vizcarra et al., 2011) | 10 | 5 | 75+ to 150- | Yes |
| (Bradshaw and O'Connor, 1996) | 8 | | Multiple, up to 150+ | 10 minutes |

Values for the parameters in a 3 litre batch flotation cell were also needed as starting points, most importantly the impeller speed and air flow rate, so literature was consulted resulting in Table 6 below.

Table 6: Batch Flotation operational Parameters form literature for 3 litre batch flotation cells

| Reference | Impeller speed (rpm) | Air flow rate (L/min) | Frother Dosage | Froth height |
|---|---|---|---|---|
| (Heyes and Trahar, 1979) | | 8 | Continuous, 5mg/min | |
| (Vera et al., 2002) | 1000 | 6 to 7 | | |
| (Melo and Laskowski, 2006) | 1300 | 5 | 30-100 g/t | 3 cm |
| (Koh and Smith, 2011) | 1050 to 1500 | 8 | Continuous, 2ml/min | 1 cm |
| (Tucker et al., 1994) | 1200 | 6 | 0-20 ppm | |
| (Koh et al., 2009) | 1200 | 8 | | 1 |
| (Barbian et al., 2003) | 1500 | 2 to 10 | 30 to 60 g/ton | |
| (Aldrich et al., 1997) | 1200 | | | 1.5 |
| (Wiese et al., 2011), other papers by same author | 1200 | | | |
| (Guy and Trahar, 1984) | | 8 | | |

### *2.10.1 Kinetics in Micro-flotation*

Micro-flotation of a single mineral is solely based on the mass recovery of the one mineral. This mass recovery can be translated to mass recovery kinetics, with constants to quantify the kinetics and allow different experiments to be compared to one another. Various kinetic models have been proposed for flotation in a micro-flotation cell (Klimpel, 2000; Kuopanportti et al., 2000), but the most commonly used is the first order rate equation (Agar et al., 1998; Çilek, 2004; Dehghani et al., 2013; Oliveira et al., 2001; Xu, 1998; Yalcin and Kelebek, 2011), as shown in Equation 1 below.

$$\mathrm{R} = \mathrm{R}^{\infty}(1 - exp(-kt)) \qquad \text{Equation 1}$$

Where $\mathrm{R}$ is the cumulative recovery at cumulative flotation time $\mathrm{t}$, $\mathrm{R}^{\infty}$ is the maximum recovery at infinite time and $k$ is the flotation rate kinetic constant in units of time$^{-1}$.

If the model applies, the value of $k$ can be calculated from the gradient of the line $\left(-ln\left(\frac{R^{\infty}-R}{R^{\infty}}\right)\right)$ versus $t$ (as the derivative of Equation 1 becomes linear, with $\left(-ln\left(\frac{R^{\infty}-R}{R^{\infty}}\right)\right)$ on one side being equal to $-kt$ on the other).

## 2.11 Zeta Potential

Zeta potential Is the measure of the electrical charge of the surface of a particle that is suspended in a liquid. It gives insight to the electrostatic repulsion or attraction of particles and is often used in colloid (particles suspended in a liquid that do not settle out) studies. The higher the absolute magnitude of the zeta potential, the more stable a colloid is. Zeta potential also gives insight into the surface properties of particles (IUPAC, 1997).

If a negatively charged particle were to exist in a liquid, positive ions in the liquid would be firmly attached to the particle surface. These positive ions are known as the counter-ions and form a layer around the particle called the Stern Layer. Yet more positive counter-ions are still attracted to the negative particle but are repelled by other positive ions in the Stern Layer and other positive ions trying to approach the particle. The greatest concentration of the counter-ions exists closest to the particle and moving further away reduces the counter-ion concentration. In an opposite sense, there is a shortage of negatively charged particles (called co-ions, as they have the same charge as the particle) close to the particle, and an increase in the concentration of negatively charged co-ions moving further away from the particle.

Both the concentration gradients of positive counter-ions and negative co-ions (in the case of a negatively charged particle) end with the bulk solution concentrations far enough away from the particle where equilibrium is restored. Before equilibrium is restored, at any point closer to the particle, there exists a difference in the concentration of the negative and positive ions, whether the particle is negatively or positively charged. Between the Stern Layer and the bulk concentration is known as the diffuse layer. The Stern Layer together with the Diffuse layer is known as the “Double Layer” and is formed in order to neutralise the charged particle. The formed Double Layer causes an electrokinetic potential between the surface of the colloid and any point of the bulk solution (Lyklema, 1995).

The magnitude of the potential can be measured (for example, in mV) and drops off first linearly through the Stern Layer and then exponentially through the diffuse layer. Electrophoresis (a charged particle's mobility in a voltage field) is related to the slip plane, which is where the Stern layer (that is rigidly attached to the particle) and the Diffuse layer (which is not attached to the particle) meet. The mobility of the particle is thus a result of the potential at this slip plane, which is called the Zeta Potential, and is considered to be the most significant potential point where electrostatic repulsion and attraction are concerned, and can be quantified by tracking particles as they migrate in a voltage field (Zeta-Meter-Inc, 2015).

Zeta potential can also be used to interrogate the change in surface properties once a collector is attached to a particle, and thus studies have measured the zeta potential of various different pyrite samples, as shown in Figure 7 below. The data points are extrapolated with lines between them for ease of reading. Figure 7 displayed below is to illustrate the general form of the Zeta Potential of pyrite as previously measured.

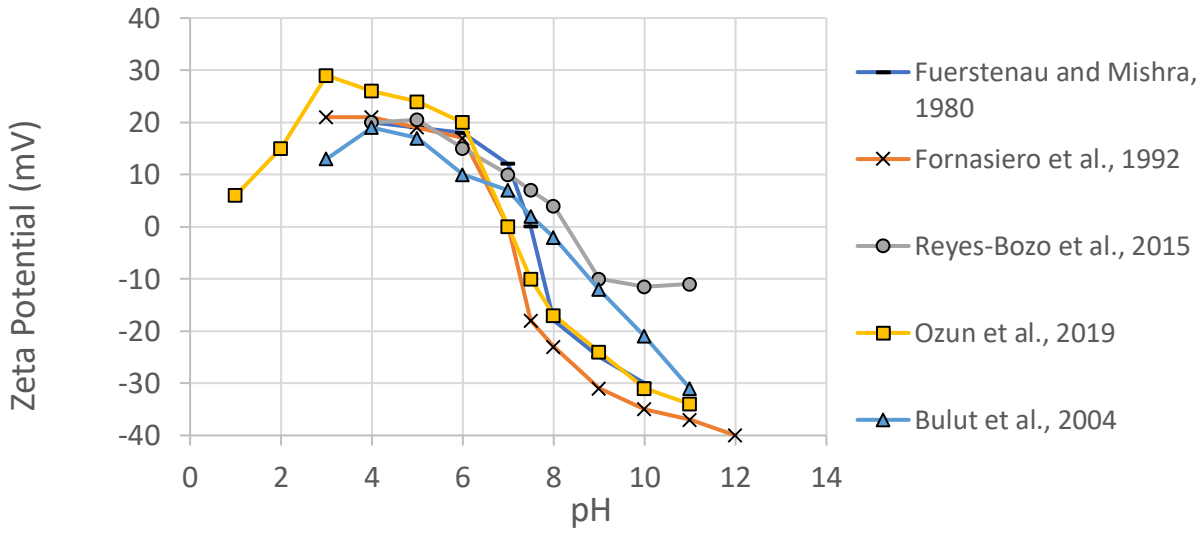


Figure 7: Zeta Potential measurements of pyrite samples, from: (Bulut et al., 2004; Fornasiero et al., 1992; Fuerstenau and Mishra, 1980; Ozun et al., 2019; Reyes-Bozo et al., 2015).

## 2.12 Separation Factor

The separation factor is a parameter often used in chemistry and separation technologies in the petrochemical setting. It is a parameter that quantifies the separation of two components by representing the change of the ratio of two substances when comparing the feed to a product (or concentrate). If $Q_{A0}$ represents the quantity of substance A in the feed and $Q_A$ represents the quantity of substance A in the product (with the analogous expressions for substance B), then the separation factor of the separation of B from A ($SF_{B/A}$) is given as Equation 2 below (Sandell, 1968).

$$SF_{B/A} = \frac{\left(\frac{Q_A}{Q_B}\right)}{\left(\frac{Q_{A0}}{Q_{B0}}\right)} \qquad \text{Equation 2}$$

## 2.13 Analysis Techniques

Table 7 below shows a summary of commonly used analysis techniques in the mineral processing field. These will be referenced later in Section 3.1 when discussing the various analysis techniques used in the analysis of the experimental results.

Table 7: Common Techniques for analysis of mineralogy. Adapted from Adams, (2016), which was adapted from Zhou et al. (2004).

| Category | Technique | Abbreviation | Application | Minimum detection limits |
|---|---|---|---|---|
| **Qualitative/ Semiquantitative** | Optical Microscopy | OM | Bulk Material qualitative and semiquantitative mineral analysis/identification | High, % |
| **Semiquantitative** | Automated Digital Image System | ADIS | Bulk Material qualitative and semiquantitative mineral analysis/identification | High, % |
| | X-Ray Diffraction | XRD | | High, % |
| | Scanning Electron Microscopy | SEM | Mineral and elemental identification, qualitative and semiquantitative analysis of individual particle | Varying, % to mg/ton |
| **Quantitative** | Mineral Liberation Analyser | MLA | Both individual and bulk sample quantitative analysis, liberation and mineral mapping data | Low, % |
| | Quantitative Evaluation of Materials using Scanning Electron Microscopy | QEMSCAN | | Low, % |
| **Quantitative** | Electron Prove microanalysis | EMPA | Quantitative analysis of individual particles | Low (g/ton) |
| | Proton Induced X-Ray emission | PIXE | | Low (g/ton) |
| | Laser Ablation microprobe-Inductively Coupled Plasma-Mass Spectroscopy | LA-ICP-MS | | Low (g/ton-mg/ton) |
| **Quantitative** | X-Ray Fluorescence | XRF | Bulk Material qualitative analysis | Low (g/ton) |

The two major groups of SEM based analysis and Optical Microscopy are discussed in the following two sections as optical microscopy and SEM is used in the methodology of this project.

### *2.13.1 SEM based analysis*

SEM based mineral analysis systems have been developed and extensively used in recent years for the determination of particle shapes and sizes (Chernet & Marmo, 2003; Lätti & Adair, 2001), determination of mineral liberation (Fandrich, Gu, Burrows, & Moeller, 2007; Mukherjee, Potapovich, Levner, & Zhang, 2009) and also gold mineralogy (Goodall & Scales, 2007), among many other uses in the mineralogy field. The two main commercial products for SEM based automated mineralogy that can recognise mineral particle composition, liberation, size and distribution are the QEMSCAN™ and Mineral Liberation Analyser (MLA) (Fandrich et al., 2007; Köse and Ikibas, 2012).

The QEMSCAN™ system used BSE (back scattered electrons) to locate particles and then EDX (an X-Ray detector) for measurement based on "particle mapping" where pixels that make up the particles are built up using thousands of measurements (Fandrich et al., 2007; Köse and Ikibas, 2012). The QEMSCAN™ analysis can be costly and time consuming due to the amount of measurements (Köse and Ikibas, 2012).

MLA system analyses each level of grayscale region in a particle (which is dependent on the atomic number of the solid) using a small number of X-ray measurements for which to report the composition of the particle (Köse and Ikibas, 2012). This is useful when differentiating phases, however when the minerals are similar in atomic mass, a large number of X-ray information should be used to differentiate the phases (Kahn et al., 2002), which again is extremely expensive and time consuming (Fandrich et al., 2007; Kahn et al., 2002).

Along with high capital costs, operating costs and time consumption, SEM based analysis also requires dust free and climate-controlled environments (Lane et al., 2008).

### *2.13.2 Optical microscopy-based analysis*

Research, such as conducted by Köse and Ikibas, (2012) have made progress in the automated analysis of samples under a reflected light microscope. The analysis, quantification, size measurement, degree of liberation and other data are obtained by image processing based on normalised colour values (Köse and Ikibas, 2012). Other studies, like that of César et al., (2018), Chopard et al, (2019), Köse & Ikibas, (2012), Lane et al., (2008) and many more, have entire projects based on forming the software based approach, methods and parameters in order to facilitate the automated mineral analysis. Phase differentiation by optical microscopy with image analysis is not easy to achieve (Kahn et al., 2002), thus developing or adapting an automated approach with software is outside the scope of this study. A manual method using a similar approach must be developed to obtain the needed outputs (César et al., 2018; Chopard et al., 2019; Köse and Ikibas, 2012; Lane et al., 2008).

Minerals that show similar colours and reflectiveness, such as chalcocite and covellite, are difficult to distinguish by automated imaging means, but a mineralogist can reply on other properties such as relative hardness, bireflectance and anisotropy to identify the mineral properly (Lane et al., 2008).

Mineral Identification Techniques under light microscopy outlined by Deer et al., (1992) allows minerals to be identified in ores or other conditions once grains are exposed and polished, such as in resin or thin section mounts. This allows for cost effective identification and characterisation of ores and rocks without needing to send samples for costly elemental analysis (Deer et al., 1992).

Before the use of SEM, one method of estimating the area of different minerals on a 2D surface has been done using “point counting” under an optical microscope (Goodall and Scales, 2007). Point counting is an indirect estimation of area, where the total the area to be surveyed is divided up into squares (or points). For each square, the underlying mineral components are identified, and the relative area estimated. For example, “pyrite occupies 10% of this square, arsenopyrite occupies 20% of this square”. This is continued for all the squares or geometric shapes in the area, and the results summed up at the end. Point counting is viable where objects or phases occupy large sections of squares, but where the objects of interest only occupy a small area relative to each square, point counting can yield unreliable results. The answer to this is to make the squares much smaller, however this would make the procedure much more time consuming and would result in many more squares of “gangue” or data that is not relevant to the study, thus point counting was not used in this study but a new method had to be developed to semi-quantitatively characterise the relationships between less common minerals on 2D surfaces.

Stereological bias (where the surface analysed is not representative of the whole underlying particles) can affect the outcome of 2D analysis (Lane et al., 2008; Lätti and Adair, 2001), such as the mineralogy done via optical microscopy. With smaller particles, such as flotation feed, concentrates and tailings (80-85% passing 75um), stereological correction is not needed as the increased particle count and number and their random nature on the surface that is analysed results in less stereologically biased results (Lane et al., 2008).

# 3 EXPERIMENTAL

This section gives a more detailed methodology according to the same subsections as Section 1.5, which corresponds to the objectives.

The approach of the project was anchored around the flotation of the Barberton case study ore. The rest of the experiments were conducted to support and explain the observations of the flotation of the case study ore.

The plan was divided into three phases, corresponding to the objectives that were set out at the start of the project. Firstly, a plan for analysing the case study ore's feed, concentrate and tailing samples for variations in the pyrite composition and quantifying selective separation was constructed.

In the second phase, batch flotation was conducted on the case study ore which was sourced from the Fairview Mine in the Barberton Greenstone Belt, Mpumalanga Province, South Africa.

The third phase consisted of conducting studies on "pure pyrite" samples from different sources to verify and support conclusions drawn from the first phase. The different pyrite samples were analysed for compositional variations and floated in a laboratory column flotation cell, commonly referred to as a micro-flotation.

## 3.1 Investigation of methods to quantify selective separation of pyrites with different compositional variations in case study ore

In this subsection, different analytical methods were investigated. The common analytical methods for identifying minerals and quantifying compositions that are used in mineral processing were discussed in Section 2.11 in Table 7.

It is important to note that all other elements found within pyrite besides Fe and S were considered compositional variations of the pyrite, including arsenic. Arsenopyrite was considered an extreme case of arsenic substitution within pyrite, as smaller amounts of arsenic within the pyrite (arsenian pyrites) were also hypothesized to change its flotation response.

### *3.1.1 Major Element and trace element analysis of samples*

Whole-rock base metal assay analysis via XRF (X-Ray Fluorescence) and trace element analysis via LA-ICP-MS was the standard analysis technique implemented. This analysis was conducted through Central Analytical Facilities (CAF) of Stellenbosch University. Both analysis types were conducted on a representative sample and delivered compositional information based on the total mass of the sample. The base metal "major" element analysis was conducted using a PANalytical Axios Wavelength Dispersive spectrometer, which is fitted with a Rh tube and the following analyzing crystals: LIF200, LIF220, PE 002, Ge 111 and PX1. The major elements were analysed on a fused glass disk using a 2.4kW Rhodium tube.

The XRF base metal assay data gave concentrations for Fe, Cu, Ni, As, Co and Pb. Optical microscopy (which is covered in Section 3.1.6) of the project's ore revealed the mineralogy present. Pyrite, arsenopyrite, pentlandite and chalcopyrite were identified which corresponded to the metals detected.

Knowledge of existing minerals in the sample, combined with the base metal compositions from XRF allowed the allocation of iron to all present minerals based on the elemental composition of each mineral (i.e. a mass balance). For example, for every copper atom, one iron atom was allocated based on chalcopyrite's stoichiometry ($CuFeS_2$). After the iron was allocated to all other minerals present, the remaining iron was assumed to be from pyrite, and thus the mass of pyrite in the feed, concentrate and tailings could be worked out. The pyrite grade and recovery could be calculated based from mass balances. Sample Calculation 1 in Appendix B gives an example of this calculation.

### *3.1.2 Selective flotation analysis using XRF Base Metal Assay results*

Base metal assay results were used to obtain compositional analysis of base metals in the whole samples of concentrate, feed and tailings in the experimental runs. All of the base metals that were reported in significant quantities (down to g/ton, none of the values were extrapolated) existed in other minerals and could not be attributed to pyrite alone, except Arsenic. In literature, arsenic was reported to only be significant in arsenic minerals, most notably arsenian pyrites and arsenopyrite, and therefore any significant amount of arsenic reported from whole-rock analysis could, and was approximated to, only be attributed to arsenic within pyrite phases. The amount of arsenic in each pyrite particle had to be quantified (and was quantified using SEM, discussed later in Section 3.1.7).

### *3.1.3 Selective flotation using Separation Factor*

The amount of arsenic reported, in g/ton, together with the pyrite content could then be used in the Separation Factor equation (Equation 1) for the feed and concentrates of each experimental run to view how well the Arsenic was separated from the pyrite, $SF_{As/pyrite}$. A value of 1 would indicate that the ratio of Arsenic: Pyrite did not change in the feed versus the concentrate, and thus pyrites with a higher arsenic content was not selectively floated or depressed over pyrites with lower (or without) Arsenic content. A value of $SF_{As/pyrite}$ higher than 1 indicated that pyrite with a higher arsenic content was floated and recovered more than those with lower Arsenic content, and a value lower than 1 of $SF_{As/pyrite}$ indicated that a higher arsenic content lead to depression and loss of pyrite with a higher arsenic content.

An example calculation of $SF_{As/pyrite}$ can be seen in Sample Calculation 2 in Appendix B

### *3.1.4 Selective flotation analysis using QXRD*

Quantitative X-Ray Diffraction (QXRD) analysis of samples allows for the identification and quantification of minerals in a sample. This analysis was used to characterise the feed in terms of the gangue, pyrite and arsenopyrite present. Small amounts of minerals, below the 1wt% mark is often not detected (Dutrow and Clark; Nuclear International Technical Working Group), but this lower limit depends on the equipment and the density and crystal structure of the sample, among other things. Trace minerals such as chalcopyrite and pentlandite thus may not show up in this analysis. QXRD for this project was done by XRD Analytical & Consulting.

Separation factor of the minerals can be applied to the results of QXRD in order to investigate selective separation.

### *3.1.5 LA-ICP-MS*

The large amount of low g/ton and mg/ton data from the LA-ICP-MS Trace Element analysis wasn't found to be useful to the batch flotation part of the project when searching for selective flotation, as it was not certain that the trace element amounts reported was hosted in the pyrite and not in any part of the silicate matrix or other parts of the ore, as the sample preparation consisted of making a fused pellet which homogenised the entire sample.

The LA-ICP-MS instrumentation consisted of a 193 nm resolution M50 SE Eximer laser ablation unit with Geostar controlling software, coupled to an Agilent 7700 ICP-MS instrument with Mass Hunter software. A photo multiplier detector was used with NIST 610 calibration standards. The data processing software was Iolite v3.34.

### *3.1.6 Optical Microscopy*

Optical microscopy is one of the tools that was used to analyse the gold ore, feed, concentrates and tailings for this project. It was therefore considered important to develop a repeatable methodology that not only investigates and achieves the aims of this project, but that could also be used in other studies and applied in industry, if required. The methodology was also designed to be inexpensive and resource efficient, as using techniques such as QEMSCAN™ can achieve similar results but are often extremely expensive for the analysis of multiple samples in small studies.

This methodology was used to determine if any specific mineral class was selectively floated. This selective flotation was then related to collector reagent suite used.

The aim of this analysis technique was to identify the different mineral phases in samples and quantify their amounts, specifically in powdered samples, in order to investigate selective flotation under different reagent suites. It is used a semi quantitative measure of determining mineral ratios on the surface when viewed under an optical microscope.

#### *3.1.6.1 Optical Microscopy Approach*

The samples to be studied (mostly powders from flotation) were first mounted in clear resin (SpeciFix-40). This process started with acquiring representative amounts of the larger sample that was to be analysed. A rotary splitter was used to split materials down to the amounts that were mounted in order to achieve the best possible representative samples, with the same procedure as discussed in Section 3.2.2 later.

Double-sided tape was placed on a sheet of glass and perspex rings, approximately 25 mm in diameter, 8mm high and 2mm thick were attached to the double-sided tape. The sample was then poured into the perspex ring, so that a layer of sample also adhered to the same double-sided tape that the bottom of the ring was attached. The resin was then mixed and poured over the sample. After the resin cured, the rings of perspex, with the resin and sample in them, were removed from the tape and glass. The layer of sample at the bottom was ground to expose the grains. After the grinding exposed the grains, the mounts were polished. The grinding and polishing were done on a RotoPol-35 machine. The result was representative grains of the samples mounted in resin and polished, ready for optical microscopy, SEM

or laser-based analysis. Additional preparation of coating the surface of the sample in a carbon layer was needed before SEM was conducted on them. Examples of these resin sample mounts are shown in Figure 8 below.

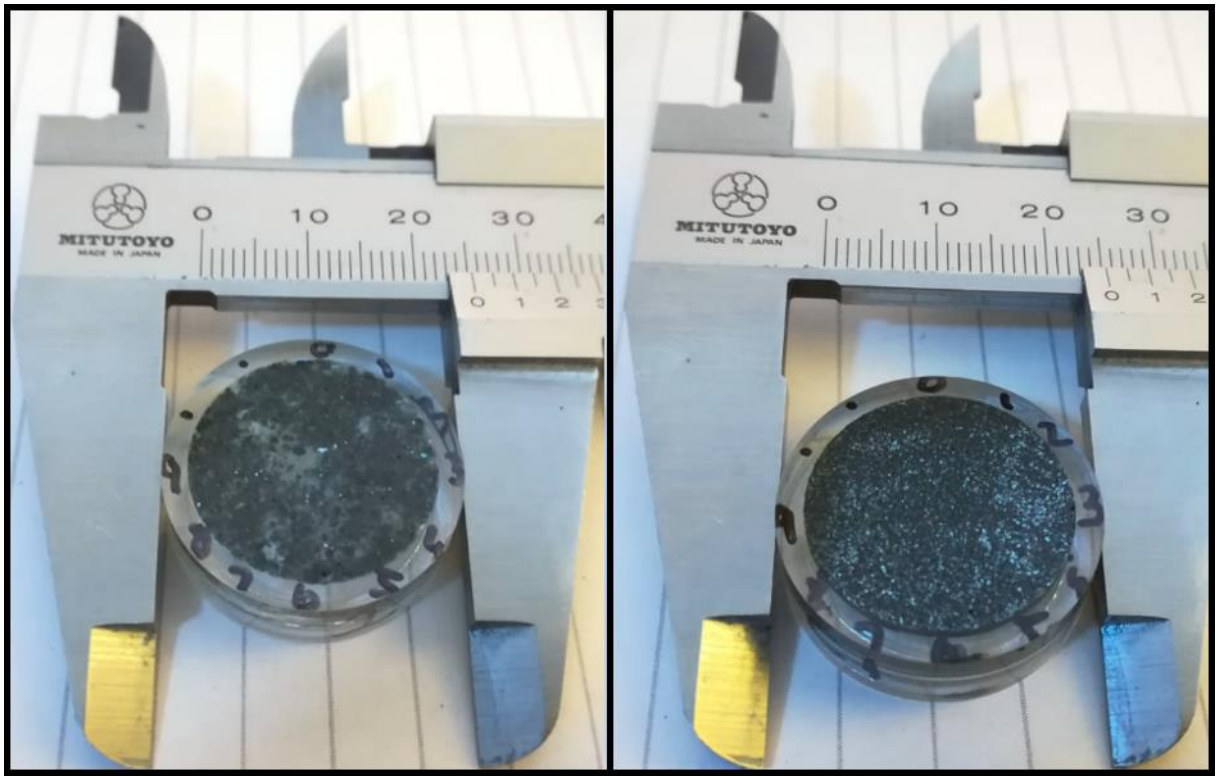


Figure 8: Examples of polished grain mounts from this study. Sample from 100% passing 1mm feed on the left, and an example of a flotation concentrate on the right.

The mounts were then taken to an optical microscope, in the reflected light setting, in order to identify the minerals and development of the methodology.

**a)** Identification and grouping of minerals or mineral phases into significant classes

Using mineral identification techniques using the properties of minerals such as colour, reflectance, hardness, bireflectance and anisotropy under light microscopy set out by Deer, Howie & Zussman (1992) and Craig and Vaughan, (1994), minerals in the samples were identified (Craig and Vaughan, 1994; Deer et al., 1992). A special note was made of each of the “important minerals” that have significance to the study or project. The minerals that were identified were then grouped into “significant mineral classes”. The “Important minerals” and “significant mineral classes” would differ for different projects.

In this project, the important minerals included Pyrite and Arsenopyrite, grains that were mixtures of the two and conglomerates that included them. Other minerals such as sphalerite and chalcopyrite existed in small amounts but were not deemed to be important to the study and thus could be ignored going forwards.

**b)** Quantitative determination of ratios of minerals

After the identification and classification of minerals in the sample, the sample slides/mounts were reasonably well characterised (in terms of mineral arrangement and surface particle sizes). A calibrated

microscope was then used to organise “size classes” for minerals on the surface of the slides. The use of the calibrated microscope was important so that the size of particles could be verified against the scale, however if a calibrated microscope is not available, the method can still be applied using the relative scale of particles in the sample.

Based on the mean area of each size class, a “area contribution” was assigned to each class. For example, the lowest size class (a 10x10µm particle) could have had an impact factor of 1, and the biggest size class (a 50x50µm particle) with a mean area of 25 times the size of the mean area of the lower size class, was assigned an impact factor of 25. In an actual project intermediate sizes would be included too but are excluded here for the sake of brevity and clarity.

In each significant class of mineral on each resin mount, the respective size classes can be counted. Carrying on the example, “60 small pyrite particles and 2 large pyrite particles, 45 small chalcopyrite particles and 1 large chalcopyrite particle” may be counted.

The count multiplied by the impact factor can yield an approximate area of coverage for each size class that can be compared to one another. In the example:

Pyrite: (60×1) + (2×25) =110

Chalcopyrite: (45×1) + (1×25) =70

Therefore, the ratio of pyrite: chalcopyrite in the sample can be approximated as 11:7

This can be continued and expanded, involving multiple mineral or mineral classes, and different ranges of particle size classes or ranges.

The size classes in the project were set. The “Small” (S) size class was set at around 30 µm across, “Medium” (M) was set at 100 µm across, “Large” (L) at 200 µm across. Examples of the grains and sizes are displayed in Figure 9, which is an image taken during the optical microscopy of the project ore. Grains larger than “L” would be uncommon later on in analysis of milled samples, so larger grains (such as the >L grain of 1000 µm across in Figure 9) were subdivided (e.g. the >L pyrite grain in Figure 9 was counted as 5 L grains).

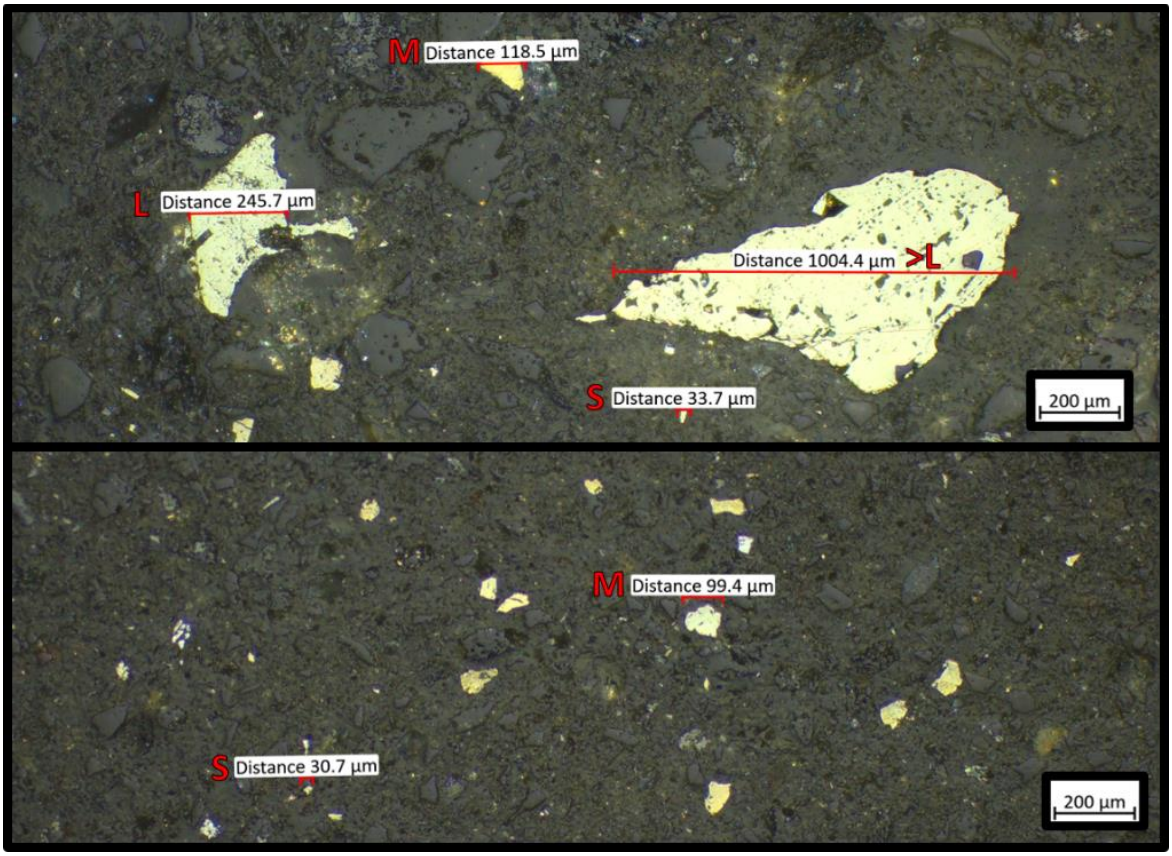


Figure 9: Size classes chosen for optical microscopy, annotated with a calibrated microscope

The area contribution were then set. This was done according to the approximate areas of coverage for each size class, as per Table 8 below.

Table 8: calculation for Area impact per particle size class

| Size | Distance Across, µm | Area, if square, µm$^2$ | Area/S Area | Area impact per particle |
|---|---|---|---|---|
| **L (large)** | 200 | 40000 | 44.4 | 50 |
| **M (medium)** | 100 | 10000 | 11.1 | 10 |
| **S (small)** | 30 | 900 | 1 | 1 |

The relative ratio of mineral classes could be then calculated once all the grains on a slide surface was counted. This result required the assumption that the surface composition was representative of the composition of the sample as a whole, which was made as the particles were small and numerous, the same condition that applied when making the assumption that stereological bias was not significant.

This methodology was applied to the feed, concentrate and tailings of the batch flotation runs in order to semi-quantitatively determine the ratio of mineral classes. The change in the ratio of these mineral classes could be quantified by the separation factor in order to interrogate selective flotation of the mineral classes.

### *3.1.7 SEM*

Since SEM microscopy is extremely cost and time sensitive, only key samples underwent this analysis technique. The second key question of "Do different collectors selectively attach to pyrite particles with different compositional variations?" was specifically targeted with this analysis by selecting the samples of the pure collectors.

SEM analysis was done at Stellenbosch University's Electron Microbeam Unit. Resin sample mounts such as the ones in Figure 8 was used in SEM microscopy. Before the samples could be attached to the SEM stage in the machine, the sample was coated with a layer of 15 nm of carbon to render the surface electronically conductive to avoid electron charge (build-up of potential) during analysis. Using carbon tape, the carbon coated resin mounts were then attached to the stage of a Zeiss MA15VP EVO Scanning Electron Microscope, fitted with both an Energy Dispersive Spectrometer (EDS- Lower detection limit of 0.1 wt%) and a Wavelength dispersive spectrometer (WDS- lower detection limit of 0.01 wt%).

Major elements were determined via EDS using an Oxford Instruments® XMax 20 $mm^2$ detector using WDS and the information in Table 9 lower concentration in the samples was quantified using Oxford Instrument ®Wave Dispersive X-ray Spectrometer. Both EDS and WDS data was processed using Oxford INCA software.

Initially, pyrite grains in resin mounts of the feed samples were first analysed for a wide range of elements that were derived from literature, from Figure 1. From the results of this, the actual elements that existed in the pyrite due to compositional variations within the case study ore could be narrowed down. To narrow down the minerals, both weight percentage compositions and probability of occurrence was taken into account, as discussed in Section 0.

It was found that all the minerals selected were over the detection limit of EDS and analysis of particles on the surface of the resin mounts from samples of the batch flotation runs could begin. The results were plotted on box and whisker diagrams to compare them to one another. The occurrence and distribution of compositional variations could then be compared to each other in the feed, concentrates and tailings of the pure collector experimental runs in order to draw conclusions with regard to selective flotation. The elements, which energy line and its corresponding peak energy is displayed Table 9 on the next page.

Table 9: SEM elements, which line was used and the corresponding peak energy

| SEM Element Line | Peak Energy keV |
|---|---|
| As L_SERIES (WD) | 1.28 |
| Se MEAN_La (WD) | 1.42 |
| Si MEAN_Ka (WD) | 1.74 |
| W MEAN_Ma (WD) | 1.77 |
| S K_SERIES (ED) | 2.30 |
| Ag MEAN_La (WD) | 2.98 |
| Sn MEAN_La (WD) | 3.44 |
| Sb MEAN_La (WD) | 3.60 |
| Ti MEAN_Ka (WD) | 4.51 |
| V MEAN_Ka (WD) | 4.95 |
| Cr MEAN_Ka (WD) | 5.41 |
| Mn MEAN_Ka (WD) | 5.90 |
| Fe K_SERIES (ED) | 6.40 |
| Co MEAN_Ka (WD) | 6.92 |
| Ni MEAN_Ka (WD) | 7.47 |
| Cu MEAN_Ka (WD) | 8.04 |
| Zn MEAN_Ka (WD) | 8.63 |
| Pt MEAN_La (WD) | 9.44 |
| Au MEAN_La (WD) | 9.71 |
| Pb M_SERIES (WD) | 10.55 |

Beam conditions during the quantitative analysis of the samples were 20 kV and approximately 1.0 A, at a working distance of 8.5 mm and a specimen beam current of -20 nA. Natural mineral and metal standards were used for standardisation and verification of the analysis.

### *3.1.8 Gold Fire Assay*

The Gold Fire Assay process is an industry standard for the determination of the gold content in ores. It is usually conducted in a furnace, where the gold is concentrated in a “button” of lead, before the lead is oxidised and removed. The gold left over can then be weighed and the mass compared to the original ore mass (Indian-Standard, 2009; Michsud, 2016). This value is reported as grams of gold per ton of ore. Gold Fire Assay analysis was done by Super Laboratory Services Springs for this project.

## 3.2 Interrogation of selective flotation of pyrite with different compositional variations in a batch flotation system of the case study ore

This subsection represents all the steps taken in order to meet Objective 2. Since the study was to be anchored around the batch flotation of the case study ore, this subsection needs to take into account all the key questions and allow them to be answered once the methodology is applied.

### *3.2.1 Developing an experimental plan regarding focused on collectors and collector mixtures to use in both batch flotation and micro-flotation experiments*

Industry relevant collectors were investigated and an experimental plan incorporating the collector mixtures was constructed to test Objective 2 and 3.

All three key questions needed to be able to be answered when this phase of planning was executed.

From literature in Table 6 and consultation with industry personnel, it was found that Sodium Isobutyl Xanthate (SIBX) was often the primary collector used in South Africa. Other areas around the world used Potassium Amyl Xanthate (PAX) as their primary collector. In most cases a Dithiophosphate was used as a secondary collector, and the one chosen for this study was SIBDTP (Sodium Diisobutyl Dithiophosphate which is referred to as simply DTP from here forwards).

The collectors were to be investigated individually and as a mixture. SIBX and PAX were both primary collectors in mixtures with DTP. The SIBX and PAX needed to be mixed with the DTP at varying ratios, so the following experimental plan as per Table 10 was devised, according to wt% fractions:

Table 10: Experimental plan with collector mixtures

| Experiment Number | | SIBX | SD25 | SD50 | SD75 | DTP | PD75 | PD50 | PD25 | PAX |
|---|---|---|---|---|---|---|---|---|---|---|
| Weight Percentage | SIBX | 100% | 75% | 50% | 25% | | | | | |
| | DTP | | 25% | 50% | 75% | 100% | 75% | 50% | 25% | |
| | PAX | | | | | | 25% | 50% | 75% | 100% |

It is also important to note that no copper sulphate or any other form of mineral activator was used in any of the flotation tests that were conducted. This was done in order to see the impact of the mineralogy of the samples on collector attachment, and also not contaminate samples with copper ions that would impact analysis.

The nomenclature used in the experimental abbreviation was as below:

SD25= Mixture of **S**IBX and **D**TP, with **25**% DTP

PD75 = Mixture of **P**AX and **D**TP, with **75**% DTP

Due to the variable nature of compositional variations and properties of a real ore, three batch flotation experiments were conducted for each experimental condition and the average was determined and reported.

It is also important to note that de-ionised water was used for batch flotation and micro-flotation as activation of the mineral surface by ions in solution from the water was to be minimized in order to remove the activation variability from the study.

### *3.2.2 Acquiring a case study ore and preparing the ore for batch flotation*

Through communication with the mine of ore origin, process conditions such as collector concentration, type of frother were determined for the experiments. These conditions will later be discussed in their relevant sections. The ore arrived from the processing plant as particles around 2000 µm and below. The ore was taken after the crushers and before the mills, and therefore referred to as "industry mill feed".

**a)** Homogenising and splitting

All of the ore from the mine (approximately 100 kg) was mixed together using a shovel and split by cone and quartering. After the preliminary mixing, all the ore was passed through a jaw crusher and crushed to 100% passing 1mm. This particle size distribution (PSD) after the jaw crushing was used for the mill feed in this project, now referred to as "project mill feed".

The mixed project mill feed, now 100% passing 1 mm was thoroughly mixed using a shovel and the cone and quartering technique was then split using a riffle splitter down to smaller amounts, halving the total each time. The riffle splitter was continued to be used, while mixing the product amounts, until 10kg portions were separated from each other. These 10 kg portions were then split down to 1 kg using rotary splitter.

Each portion, having gone through the crushing, mixing and splitting processes, was assumed to be representative of the whole industry mill feed.

**b)** Milling

A target grind, based on previous studies and industry information, was set at 85% passing 75 µm.

As previously mentioned, the project mill feed was stored as 1 kg representative samples of 100% passing 1 mm particles. The particle size distribution (PSD) plot of the project mill feed was determined using sieves to ascertain the starting point that needed to be milled to not just 85% passing 75 µm, but also a suitable distribution. This starting PSD is shown in Figure 10 below.

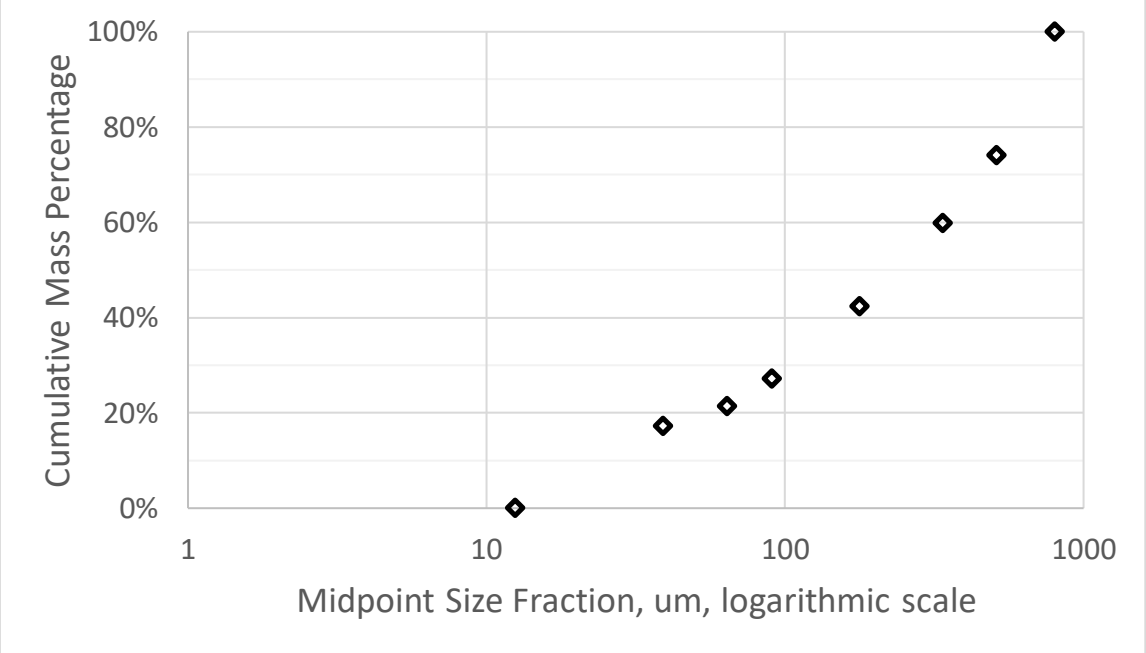


Figure 10: Project Mill Feed Particle Size Distribution

The desired grind PSD has a sigmoid curve (characteristic "S" shaped) on a logarithmic x axis, and this was targeted with scoping experiments for the milling of the ore before flotation.

In order to achieve this grind, particle size distribution plots with different grinding media compositions and milling times had to be generated. The result of not only 85% passing 75 µm but refining the entire particle size distribution to a PSD that was desirable (the characteristic sigmoid curve) was achieved after varying the grinding media type and sizes at varying milling times. The milling time settled on was 35 minutes, with the details of the mill and grinding media that were used are part of the experimental equipment in the following subsection on the equipment of batch flotation. The results of milling procedure and achieved particle size distribution are shown in Figure 27 in Section 4.2.1 as it is better placed in the Results section, under Batch Flotation Feed Characterisation.

The following milling procedure was followed for all the experimental runs:

1) Before each day of use, the mill rods were cleaned of rust by dry milling silica sand. The mill was then cleaned out.
2) Approximately 1kg of ore was added to the mill with 500mL of demineralised water.
3) The mill, with grinding media and pulp within, was placed on the rollers for 35 minutes.
4) The pulp was transferred out the mill and into a bucket by washing with deionised water.

Once the milling time and procedure was fixed, the experimental plan was completed and the ore ready to be floated in a batch flotation cell.

### *3.2.3 Floating the Case Study Ore in a Batch Flotation Cell*

The different collector mixtures selected in the previous subsection was used in batch flotation experiments of the case study ore. The feed, concentrates and tailings were then analysed by the methods chosen or developed in Objective 1 to interrogate whether selective flotation was taking place.

### *3.2.3.1 Materials*

The following materials were needed and used in the batch flotation process:

- Collectors: SIBX, PAX and DTP (Purity of >90% for xanthates, 50% for SIBDTP which was stored in stabilising solution)
- Frother: Senfroth™ 516
- De-mineralised water

### *3.2.3.2 Equipment*

The following were used in the experimental procedure:

- Rod mill:
  The case study ore was milled at 66% solids by mass by adding a representative sample of 1 kg of the ore and 500 mL (approximately 500 g) of demineralised water into a cylindrical rod mill. Demineralised water was used to eliminate the variance and effects of ions in tap water. The mill had a diameter of 215 mm with a length of 300 mm. Fourteen 20 mm diameter rods with twenty 8 mm diameter rods were used as the grinding media. Rod material was hardened steel, with a steel mill that was lined with rubber. The total weight of the grinding media was 14.1 kg.
- Batch Flotation Cell:
  A 3 litre perspex batch flotation cell was used for the flotation tests, and is shown in Figure 11 below. A diagram of this is shown in Figure 12 afterwards.

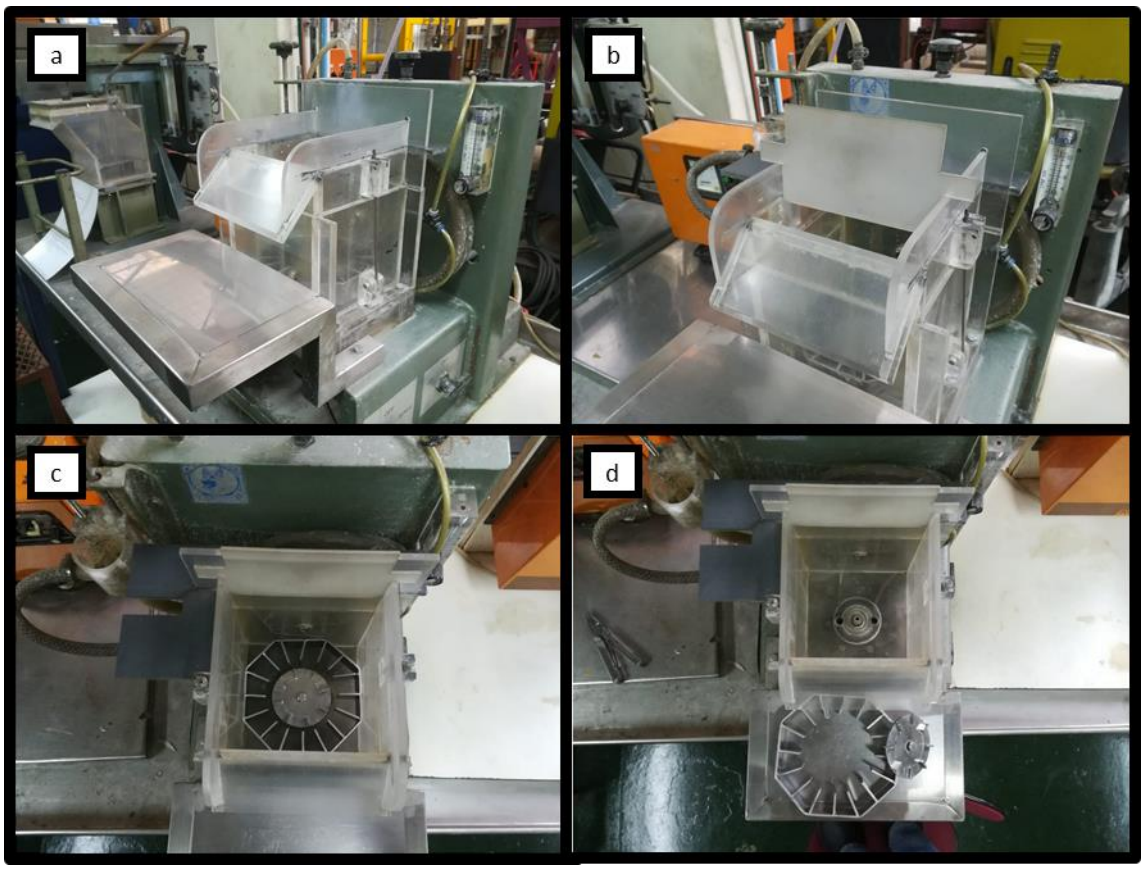


Figure 11: Pictures of the batch flotation cell, showing the: (a) entire flotation cell, (b) Batch flotation cell with the scraper used to scrape froth to concentrate trays (placed on the stainless steel “shelf” seen in (a), (c) inside showing impeller and baffling in place (d) inside without baffling and impeller, showing the two air feed lines either side of the impeller drive shaft

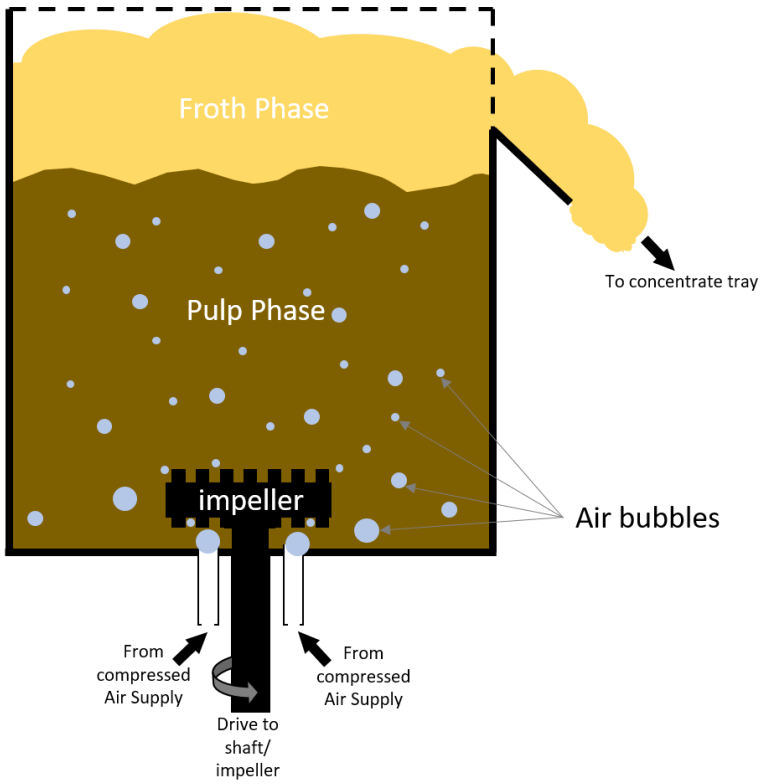


Figure 12: Diagram of the batch flotation cell, cross section. The two air inlets are rotated to the side for clarity, view the pictures of Figure 11 for the real cell. The baffle is omitted for clarity.

- Filter Press:
  A filter press was used to separate the solid particles from the liquids (water) whenever the dry solids were needed from a slurry or pulp. The filter press worked by using compressed air to push water through a filter paper, leaving the solids behind on top of the filter paper. After filter pressing, the solids were dried overnight in an oven before they were weighed or other procedures were conducted.
- Rotary Splitter:
  A rotary splitter splits a mineral sample (made up of a number of particles) into ten representative mineral samples. Each of the ten samples created are, in theory, of equal mineral composition and particle size distribution. The rotary splitter was used to split the received ore into 1kg batches and to split all samples after experiments to ensure representative samples were analysed.

**c)** Batch Flotation Procedure

The mine that the source ore was obtained from was consulted and information obtained that the pH in the industry flotation circuit was not modified and the natural pH of the ore and reagents (between 9 and 10) would be applicable in the study. A pH of approximately 9.5 was confirmed in the scoping runs.

After the collectors and pH were fixed, the next thing that needed to be set was the operational parameters of impeller RPM, air flow rate, collector and frother dosages. This was done by varying the operational parameters in scoping runs in order to see the system response and found that the

concentrations to move forward were 40 g/ton ore of frother and 25 g/ton of ore of collector respectively. The results for the scoping runs are qualitative in nature and are displayed in Appendix C.

The concentrations are based on per ton of ore in the mixture, not the total pulp mass. The percentages in Table 10 were then converted to masses for SIBX and PAX and mL to be added for DTP as in Table 11 below, which are corrected for the purity of the collectors.

Table 11: Actual masses of collectors to be added

| Experiment Number | | SIBX | SD25 | SD50 | SD75 | DTP | PD75 | PD50 | PD25 | PAX |
|---|---|---|---|---|---|---|---|---|---|---|
| Measured collector, g for SIBX and PAX, ml for DTP | SIBX | 0.0252 | 0.0189 | 0.0126 | 0.0063 | | | | | |
| | DTP | | 0.0126 | 0.0252 | 0.0378 | 0.0504 | 0.0378 | 0.0252 | 0.0126 | |
| | PAX | | | | | | 0.063 | 0.126 | 0.189 | 0.0252 |

It was decided that a bulk concentrate was to be collected, with all the concentrates for the duration of each experiment collected together. This was done because kinetics was outside the scope of the study, and a single concentrate for each float would significantly simplify analysis time and costing. The concentrate duration was set to 10 minutes (where the standard for batch flotation is 25 minutes) as the target was to investigate which particles were rendered more hydrophobic and thus faster floating by selective attachment of the collector. The single concentrate would facilitate searching for selective flotation in each case without needlessly complicating the analysis, especially because multiple forms of analysis was to be conducted for each experiment.

After each batch float was completed, the feed sample, concentrates and tailings were filter pressed and dried in an oven. Once dry, they were rotary split into the sample sizes needed for analysis.

The full list of the batch flotation procedure is given in Appendix A, which includes at which times to add which reagents and the quantities of each.

## 3.3 Investigation of differences in pyrite flotation of samples with different compositional variations by floating them in a microflotation cell, using the same collector mixtures as used in batch flotation

This subsection describes all the steps done to meet Objective 3. The same collector ratios of Objective 2 is to be used. The section focusses on the micro-flotation methodology that was used to interrogate recovery differences of pyrite with different compositional variations.

### *3.3.1 Sourcing pyrite samples that have different compositional variations, and showing that these impurities impact the properties of the pyrite*

Two different “pure” Pyrite samples were sourced from different parts of the world. These “pure” pyrites, and well as pyrite mixed with the same collector mixtures used in Objective 2 underwent Zeta Potential tests to investigate whether a difference in surface properties existed under the same conditions with pyrite from different sources and impurities. The different pyrite samples also were characterized by SEM, XRF and ICP-MS to check for differences in their composition and homogeneity of the particles in the sample.

#### *3.3.1.1 Zeta Potential*

Zeta potential tests were conducted on a Malvern™ zetasizer.

Pyrite samples were pulverized to 100% passing 25µm and sent for BET (Brunauer-Emmett-Teller) surface area analysis at the analytical facility at the Department of Process Engineering of Stellenbosch University. Based on the coverage of xanthate per molecule, the mass of xanthate for 50% monolayer coverage on 0.5g of the pyrite sample was calculated.

Demineralised water was pH adjusted to achieve targets of pH's of 3, 5, 7, 9 and 11 using NaOH to increase the pH and $H_2SO_4$ used to decrease it. Pyrite was then added to each of these pH solutions and the change of the pH measured. The solutions were then remade up, overshooting the target pH to account for the change when the pyrite was added. For example, it was seen that the pH 7 solution decreased to a pH of 6.6 when the pyrite was added. After trial and error, it was found that the original solution should be made up at a pH of 7.3 to counteract the effect of the pyrite, so that when added, the pH would settle closer to the target.

15 mL centrifuge tubes were filled up to the 10 mL mark with the pH solutions. 0.5 g of the pyrite (100% passing 25 µm) was added to this, and the pH measured, and corrected, if needed. The collector(s) were then added (in the cases when they needed to be added), the test tube capped and lightly shaken. Two minutes later, the supernatant was taken off the upper portion of the fluid and transferred to a cell for the zetasizer, and tested in the machine. Measurement of the zeta potential was done in the machine via determining the electrophoretic mobility (obtained via electrophoresis and measuring particle velocity by laser doppler volocimetry) and applying the Hendry Equation. Each sample was measured three times, with 10 to 30 runs per sample.

### ***3.3.2 Floating the pyrite samples with compositional variations in a Micro-flotation cell***

The pyrite samples were floated in a micro-flotation cell, using the same collector mixtures developed in Objective 2.

#### *3.3.2.1 Materials*

The following materials were needed and used in the micro-flotation process:

- "Pure" pyrites: Two pyrite samples from different sources
- Collectors: SIBX, PAX and DTP as in Batch flotation
- De-mineralised water
- pH modifier: NaOH
- Synthetic air from cylinder (21 % $O_2$, 79% $N_2$)
- $N_2$ from compressed $N_2$ cylinder

#### *3.3.2.2 Equipment*

The major pieces of equipment that were used in the micro-flotation experimental procedure are listed below:

- Pulveriser:

A lab scale sample pulveriser that uses hardened steel concentric rings to pulverise small amounts of samples at a time was used to reduce the particle size of the received pure pyrite samples. An example of such a pulveriser is the TM Engineering STLX Pulveriser. Sample preparation started with crushing the pyrite samples into approximately 100% passing 1cm with a hammer. The sample was then pulverised for 5 seconds before putting it into the sieve shaker. The +53µm oversized particles were put back into the pulveriser for 3 seconds and then put back into the sieve shaker to maximise the recovery into the desired size fraction.

- Sieves and Sieve shaker:
  Sieves of 38µm and 53µm were used to verify all the sample existed within the 38-53µm size fraction. A sieve shaker aided in the automation of the sieving step, so the sample could be placed above the 53µm sieve, with the 38µm sieve below it and an undersized catch pan below that.
- Rotary Splitter:
  The rotary splitter was used, as before, to split larger masses into representative smaller samples for flotation.
- Ultrasonic Cleaner:
  An ultrasonic cleaner (LaboTech Model 701 Ultrasonic bath, 50 W set at High frequency) was used to clean the pyrite sample before the collector was added.
- Column Flotation Cell/Micro-flotation cell:
  A lab scale Micro-flotation cell was used to conduct the fundamental studies. The cell was supplied with synthetic air from a cylinder via a 100 µl SGE$^{TM}$ needle. A diagram of the full setup is displayed in Figure 13. On the left is a set of burettes partially filled with water with a needle inlet point. When the needle is inserted here, bubbles from the needle displace water downwards and the volumetric flow rate of the air can be measured. The middle set of burettes allow for air pressure stabilisation and to read when the system has reached steady state.
  The micro-flotation cell is a 225 mL cell that takes 3 g of sample, making up a pulp density of 0.0133 g/cm$^3$ . Near the bottom of the cell, an outlet takes pulp to a peristaltic pump that recirculates the pulp to the bottom of the cell. In the upward part of the recirculation loop, the needle can be inserted, and the bubbles travel upwards with the recirculating pulp.
  A concentration collection area is found at the top of the chamber, where bubbles can drop the collected sample. A concentration port with a valve is used to empty this chamber.
  A port to drain the cell and collect the tailings is also found in the upwards recirculation loop. All of this can be seen in Figure 13. Figure 14 shows the path that bubbles, and pyrite, takes within the cell, and is further discussed below it.

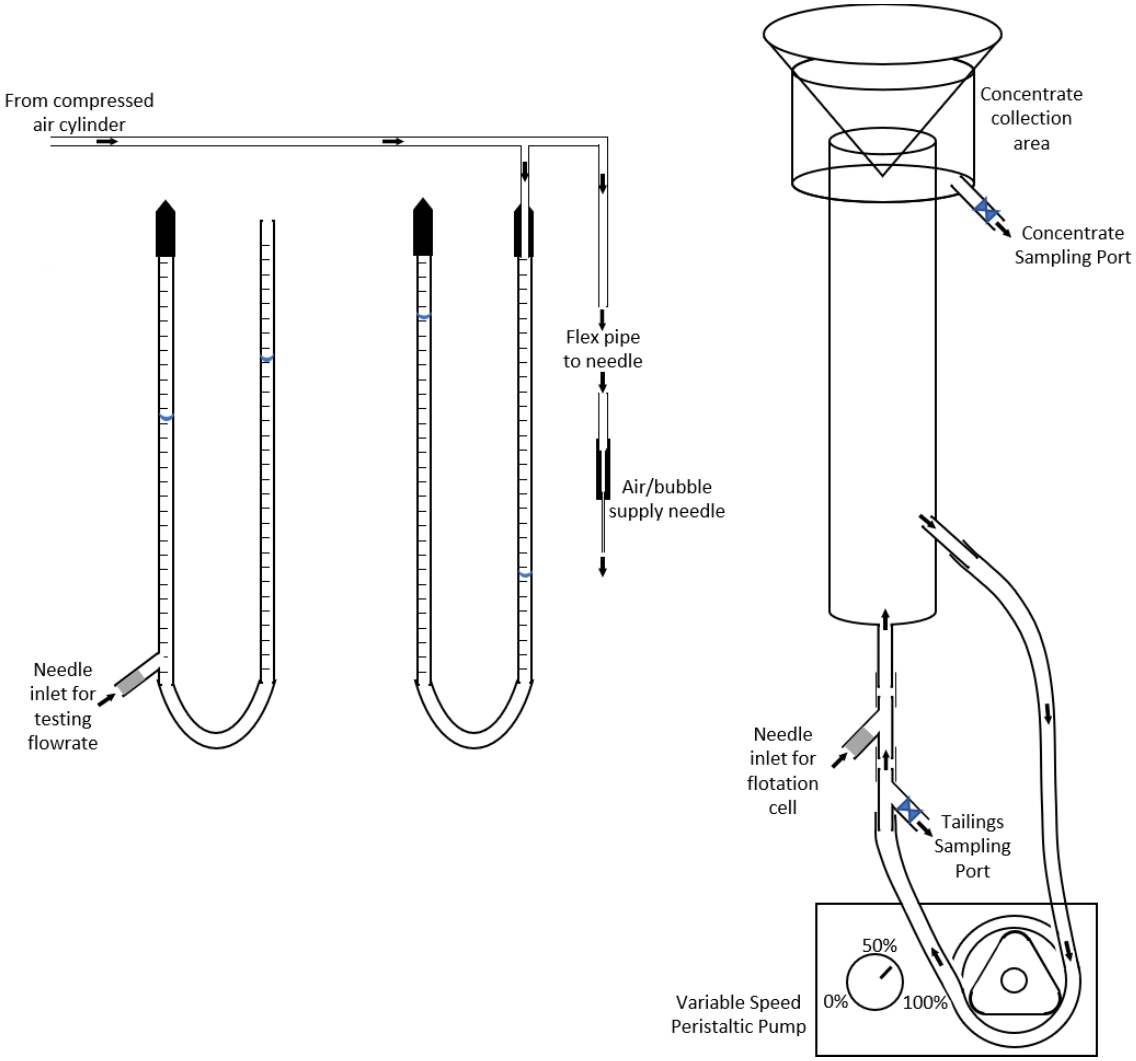


Figure 13: Diagram of Micro-flotation cell, including flow rate testing and air stabilisation burettes and peristaltic pump

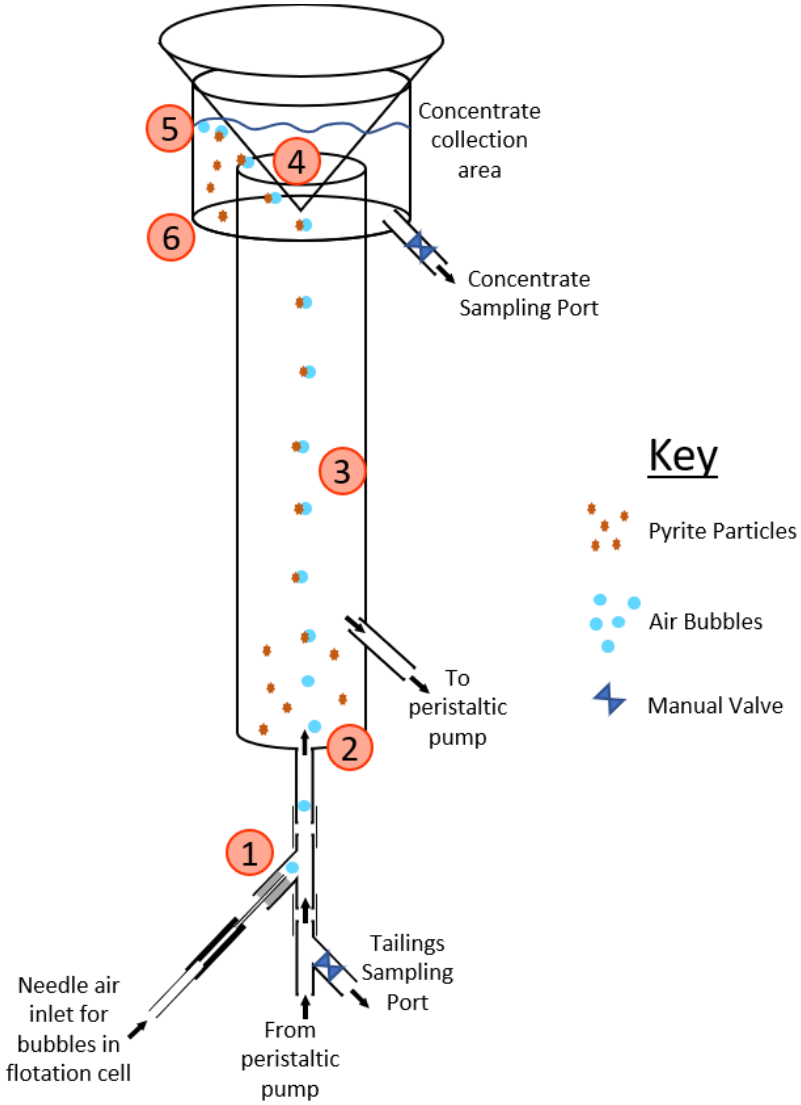


Figure 14: Operation of the micro-flotation cell with numbers showing the path of bubbles and pyrite particles

Figure 14 displays the way bubbles travel and how particles (pyrite in this case) are recovered in a micro-flotation cell. In the micro-flotation cell, air enters the upwards recirculation loop from the peristaltic pump via the needle in the needle port at ①. The bubble enters the chamber at ②, and if favorable, attaches to a pyrite particle somewhere between ① and ③. By ③, the pyrite particle(s) is attached to the bubble and rising with it. At ④, the bubble hits the glass cone that is inserted into the column, and deflects to the side as it rises, with the pyrite particle. When the bubble and pyrite particle reaches ⑤, the bubble pops or drops the pyrite particle into the concentration collection area, where it resides at ⑥ before being recovered out the concentrate sampling port.

- Vacuum filter / Buchner funnel:
  A Buchner funnel was used to filter the samples after flotation.

#### *3.3.2.3 Procedure*

**a)** Sample Preparation

After enough sample was pulverised and sieved, the 38-53 µm particles were put into the rotary splitter to be split into 3g representative samples for flotation.

The split samples were then stored in a nitrogen atmosphere at -18°C in order to prevent oxidation of the pyrite. The pyrite was not stored for more than three days before being discarded.

**b)** Micro-flotation experimental procedure

Samples of the pyrite samples were sent for BET analysis to reveal the surface area per gram of the pyrite grains within the 38-53 µm size fraction, and literature was consulted to reveal the coverage of xanthate molecules. The basis for the collector addition was to be fixed, and as in batch flotation, the amount of xanthates were used as a basis. The mass of xanthates needed for a 50% monolayer coverage was calculated based on the average molar mass of the two xanthates (172 g/mol for SIBX and 202 g/mol for PAX) and this mass is what the collector mixture masses were based on. The calculation for this is given in Appendix B.

To start the micro-flotation experiment, the synthetic air cylinder was opened, and the air flow rate was allowed to stabilize. Modification to the settings on the valves of the air lines were seldom required, though the air flow rate was verified at 8.5 mL/min and corrected if necessary.

After the micro-flotation cell was cleaned, a 3 g pyrite sample was taken out of storage and added to a 100mL beaker. A small amount of water (approximately 40 mL) was added to the pyrite and the two were mixed. The beaker was then placed into an ultrasonic bath for 5 minutes for cleaning and desliming of the pyrite grains and to break up any aggregates of particles.

The mixture from the beaker was then added to the micro-flotation cell and the cell was topped up to 75 mL. The pH was corrected before the collector was added. The peristaltic pump was then turned on at 100% flow rate (7.15 mL/s) for 5 minutes of conditioning time. The pump speed was then reduced to 50% (5 mL/s) before the cell was filled up (225 mL total), including the collection area. The conical glass bubble deflector was then placed at the top of the cell before the needle was inserted into the port of the micro-flotation cell and the timer started.

When a concentrate was due to be taken, (at aeration times of 2, 6, 12 and 20 minutes from the start) the needle was removed, the concentrate valve opened, and the concentrate collection area washed out. The concentrate collection area was refilled, and the needle reinserted for the next concentrate duration. After all the concentrates were collected, the cell was drained through the tailing collection valve. All the tailings were purged out of the cell and piping. The tailings and concentrate samples were then vacuum filtered and dried in an oven overnight before being weighed.

**c)** Data Analysis and model fitting

Data analysis started with determining the masses recovered through each concentrate step. The masses were then summed and the cumulative mass curves for the micro-flotation were obtained. The first order kinetic model, as set out by Equation 1 in Section 0, could then be fitted to the data. The model is shown again below for clarity

$$\mathrm{R} = \mathrm{R}^{\infty}(1 - exp(-kt)) \qquad \text{First order model for micro-flotation}$$

Where $\mathrm{R}$ is the cumulative recovery at cumulative flotation time t , $\mathrm{R}^{\infty}$ is the maximum recovery at infinite time and $k$ is the flotation rate kinetic constant in units of time$^{-1}$.

The application of the model to the data required two parameters, $\mathrm{R}^{\infty}$ and $k$. The value of k is calculated as the gradient of the line $\left(-ln\left(\frac{R^{\infty}-R}{R^{\infty}}\right)\right)$ versus $t$. The complexity of fitting the model is that $\mathrm{R}^{\infty}$ value for each experimental condition is needed to plot the model in order to regress $k$ from the gradient.

If the model fits well, the experimental points would fit close to the line of $\left(-ln\left(\frac{R^{\infty}-R}{R^{\infty}}\right)\right)$ versus $t$, i.e. have a $R^2$ regression parameter close to 1. This fact was used to fit the model to the data. Some previous studies "guessed" values for $\mathrm{R}^{\infty}$ and based on "good fits to the data", accepted or rejected these guesses. A more rigorous method of a similar approach was used in this study by using GRG nonlinear regression with a starting value of 15% more recovery than the cumulative recovery at the end of microflotation as an input to maximise the $R^2$ fit of $\left(-ln\left(\frac{R^{\infty}-R}{R^{\infty}}\right)\right)$ versus $t$ to experimental data. As a result of this method of searching for the best parameter for the best possible fit, the $R^{\infty}$ was chosen for the data. This is important since the kinetic constant $k$ is a measure of how quickly the system approaches the recovery at infinite time, correct values of the $R^{\infty}$ parameter is essential to an accurate kinetic constant $k$.

The excel function "LINEST" was used, which takes the inputs of x values (time points) and y values (cumulative recovery) and outputs the gradient and $R^2$ fit. The solver data analysis plugin could then be used to maximise the $R^2$ value, and the kinetic constant $k$ could then be read off the outputs of LINEST as the gradient.

## 3.4 Froth Stability Experimentation

The variation in froth stability and the synergistic or antagonistic relationships between collectors and frothers are of concern in a flotation system, especially where multiple collectors are being compared to one another, as variation in froth stability may impact flotation results. Mass, and desired minerals, can be recovered via a more stable froth phase via entrainment rather than true flotation of the collector attaching to the mineral and causing hydrophobicity.

To test the interaction between collector and frother, the mineral phase can be left out of the system and the froth was studied via two methods which are measuring the froth height in a cylinder and the water recovery in the batch flotation cell.

### *3.4.1 Froth Stability via Froth Height in a measuring cylinder*

A hole was drilled into the base of a plastic 1000 mL measuring cylinder. An air line was passed through the hole of the measuring cylinder and an aquarium air stone was placed on the air line on the inside of the measuring cylinder. The air stone was positioned at the bottom of the cylinder before the cylinder was sealed around the airline. A flow meter was placed on the feed end of the air line and connected to a compressed air supply. The intention was to measure the froth height under the same collector and frother concentrations as the batch flotation system at varying air flow rates.

The measuring cylinder was filled to 500 mL mark (with air turned off). First, the air was turned on to the three flow rates that were to be tested (1.5, 3 and 4.5 litres per minute) and the top interface of the froth was measured above the 500 mL mark. Next, just the frother was added, mixed and left to condition for 1 minute before the air was turned on and the procedure repeated. The frother case served as a control. The frother and collector mixtures were then tested, and the values plotted. An example of the experiment and the experimental set up is displayed in Figure 15 below.

Figure 15: Froth stability and froth height experiment in measuring cylinder

### *3.4.2 Froth Stability via water recovery in the Batch flotation cell*

Similar to the experiments of froth stability in the measuring cylinder, the froth stability can be interrogated in a batch flotation cell by excluding the ore phase and measuring the water recovery at the experimental concentrations of frother and collectors. When the ore is included in the experiment, mineral particles play a role in stabilising the froth, but when excluding it, the relationship between the frother and collector at the bubble and liquid interface can be studied.

The same procedure as discussed for batch flotation was followed, excluding preparing and adding the ore, up until the point that the air was turned on. The froth was still scraped every 15 seconds into the concentrates, and the experiment was ended at the 5-minute mark, where the volume of water recovered to the concentrate was measured. An increase in water recovered represented an increase in the froth stability.

## 3.5 Error analysis

Error analysis was done by means of the uncertainty parameter method. The standard deviation was taken of experimental data and this was divided by the square root of the number of experiments to yield the standard error. The standard error is widely used as a measure of experimental error in the mineral processing field, especially in froth flotation, however the standard error was then multiplied by the inverse T distribution (2 tailed) score with a confidence level of 0.95 (alpha of 0.05) and the degrees of freedom of the number of experiments minus one (usually 2, 3 repeats minus 1) to achieve the uncertainty parameter, which is seen as a more inclusive evaluation of uncertainty in analysis (Montgomery and Runger, 2014). The value of the inverse two tailed distribution at an alpha (or probability) of 5% (0.05) with the degrees of freedom being two is equal to approximately 4.3, therefore the errors of uncertainty parameter in this report are 4.3 times larger than the standard error. Examples of this error analysis are given in Appendix B.

# 4 RESULTS AND DISCUSSION

This section displays the results of the projects work and discusses them in the context of meeting the objectives and thus the aim of the study.

Following the same order and approach as presented in the approach and methodology of Section 1 and Section 3, the results of each objective are set out in their corresponding subsections. First, the methods to quantify selective separation are applied to the case study ore to acquire a baseline knowledge of the feed to the process. The batch flotation results are then displayed and discussed, and the methods finalised to quantify the selective separation are applied to the results. The micro-flotation results are also put forward and discussed, followed up by relating the batch flotation results to the micro-flotation results. The applicability of the study and the results to industry are discussed.

## 4.1 Methods to quantify selective separation of pyrites with different compositional variations in case study ore

The results of the optical microscopy, SEM, QXRD, XRF and Gold Fire Assays are displayed in the context of Batch Flotation in the Batch Flotation subsection (Section 4.2), as these methods are already developed and have been discussed in Section 3.1. The first subsection further expands on the Optical Microscopy methodology by displaying the results when using the case study ore of the project.

The minerals that were identified, including the gold (or electrum) inclusion hosted in pyrite, was consistent with literature on the area that was presented in Section 2.3.

### *4.1.1 Optical Microscopy*

This subsection focuses on the development of the optical microscopy methodology and the intermediate results obtained in order to fully develop it for the case study ore. The optical microscopy section also serves to characterise the ore in terms of the minerals present, the sizes and approximate distribution of these minerals. The format of this subsection is focussed around the aims of optical microscopy put forward in Section 3.1.6.1.

The characterisation steps discussed in this subsection was first applied and developed on representative sample mounts of the project mill feed, with 100% of particles passing 1mm.

#### *4.1.1.1 Identification of minerals that are present in the case study ore*

Minerals pictured in this section have no scale attached, as a calibrated optical microscope was only made available later in the project. The presence and identification of the minerals were the priority at this stage, and their sizes were confirmed later. Compositions of each mineral are given, along with a qualitative perspective of how much of the mineral is present, based on being familiar with the grain mounts from the samples.

**a)** Pyrite

The gold ore was known to have pyrite content, and its applicability to the study meant that this was an important minerals to identify and track. Pyrite takes the appearance of a light reflective/shiny mineral with a light-yellow tint, as visible in Figure 16 below.

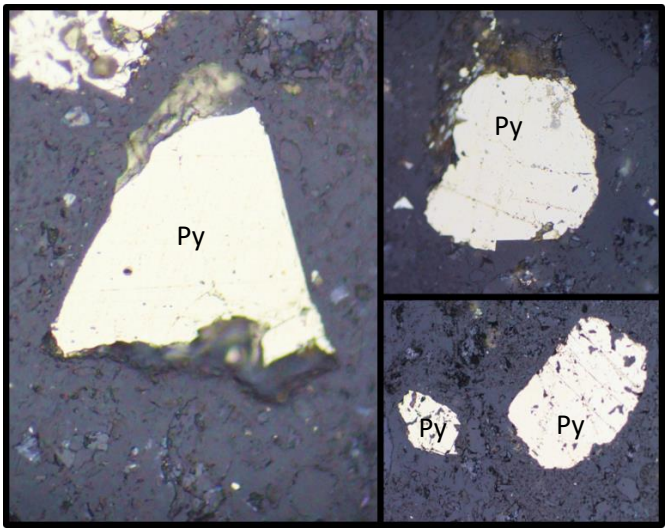


Figure 16: Pyrite in the Case study ore, under optical microscope

**b)** Arsenopyrite or Arsenian Pyrite

Arsenopyrite and arsenian pyrites were also expected to be found. Pyrites with arsenic content is differentiated from normal pyrite by its lighter, whiter colour. Arsenopyrite grains may also appear more euhedral, with straight edges and rhomboidal grain shapes. These differences in grain structures and coloration can be seen in Figure 17 below. The image on the left of Figure 17 was taken with the original light microscope that was used, while the image on the right was taken with the later calibrated microscope. The difference in the images between the original light microscope and the calibrated microscope are due to the different contrast and other image settings, as the calibrated microscope was set up to see the differences in minerals. In both images it can be observed that the grains with the more yellow tint are pyrite, and the grains that appear whiter are arsenopyrite or arsenian pyrites.

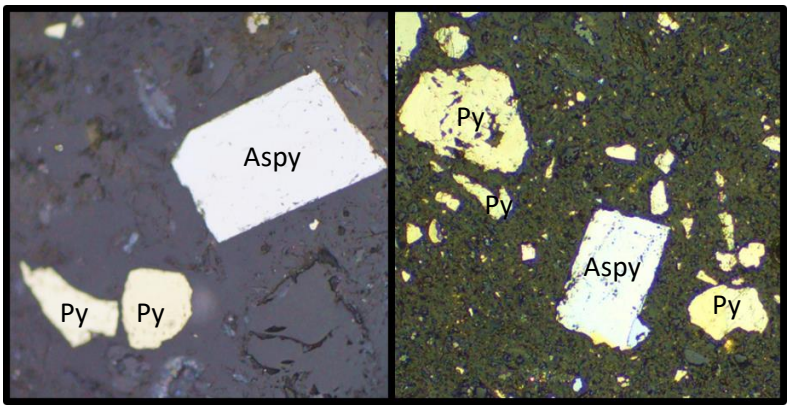


Figure 17: The difference between pyrite and arsenopyrite as shown under two different light microscopes, difference in contrast settings

Figure 18 below shows more examples of the euhedral grain structure that is often seen in arsenian pyrites and arsenopyrite, where the whole grain can be seen with straight edges or rhomboidal shapes. Figure 19 that follows that shows other cases of arsenopyrite/arsenian pyrite where the grain is made up of more complex shapes, but some breakage lines can still be seen to be straight.

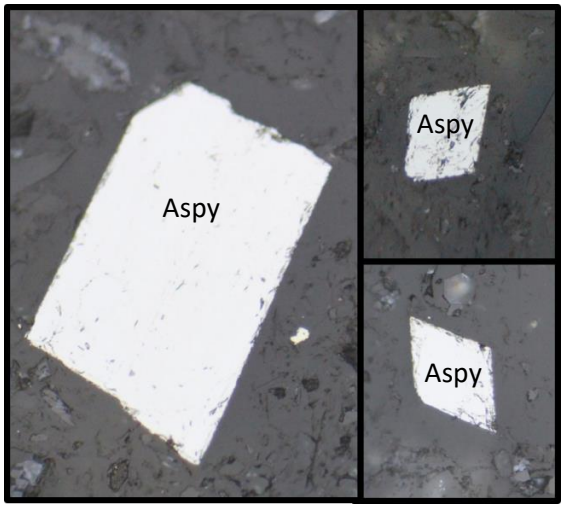


Figure 18: Euhedral shaped arsenopyrite in the case study ore

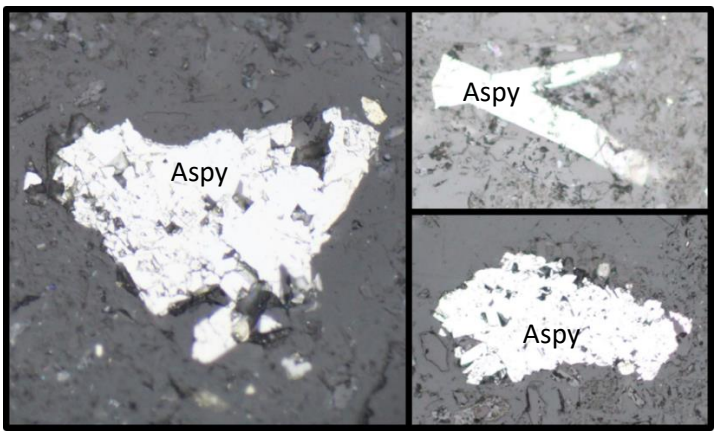


Figure 19: Arsenopyrite or arsenian pyrites in the case study ore, with complex grain structures

**c)** Mixtures of Pyrite and Arsenopyrite

Single grains visible in the ore can have both normal pyrite phases and arsenopyrite phases incorporated within the same grain. The differences in the colour within the specific grain can be used to identify such grains. Examples of these types of grains are shown in Figure 20 where pyrite content in each grain is seen as a light yellow tint and the arsenopyrite portions are seen as much whiter in certain regions of in each grain.

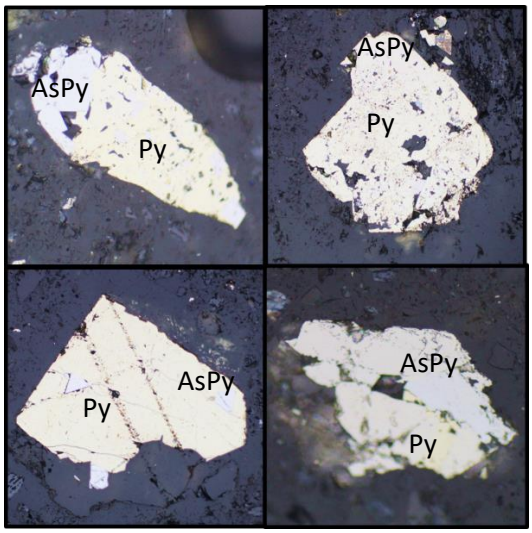


Figure 20: Examples of grains that are made up of a mixture of pyrite and arsenopyrite

**d)** Conglomerates of pyrite(s)

Conglomerates of pyrites(s) are grains that are made up of many small pieces of pyrite grains, held together by another matrix or cement. These grains can have a variety of concentrations of particles, of various sizes, as shown in Figure 21 below. The smaller particles in the conglomerates may also be made up of both pyrite and arsenopyrite, as also visible in Figure 21. Recovery of pyrite from these types of grains in froth flotation is difficult because the surface of the grain is only partly made up of pyrite and only the pyrite portion of the surface that consists of pyrite is amenable to collector attachment. Some of these grains, such as the grain in the bottom right of Figure 21, have only a small amount of its surface consisting of pyrite, is often lost to the tailings in a flotation circuit as the grain cannot be rendered hydrophobic enough by the small area that collector will attach to.

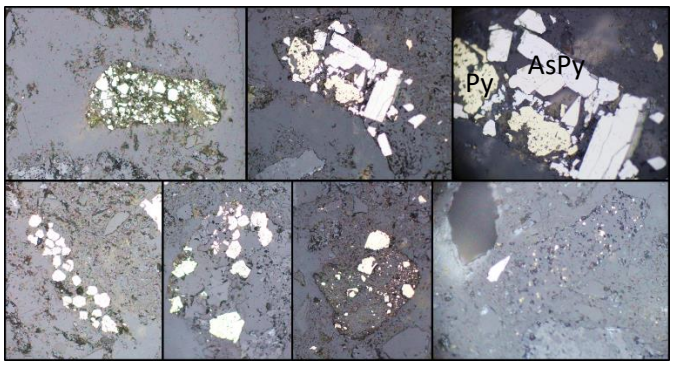


Figure 21:Grains of conglomerates of pyrite as seen in the case study ore

**e)** Chalcopyrite

Chalcopyrite was identified in the ore as very yellow grains, presenting with a much darker yellow colour than pyrite, as seen in Figure 22 below. These grains occurred rarely when compared to the abundance of pyrite and arsenopyrite. Even when found, grains of chalcopyrite were small, mostly under 10µm.

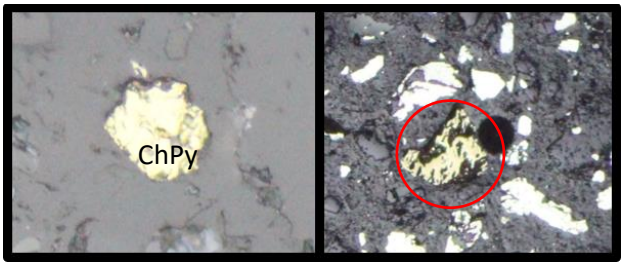


Figure 22: Images of chalcopyrite in the case study ore, highlighted in right image with red circle

**f)** Pentlandite

Pentlandite was identified in the sample, and similarly to chalcopyrite, occurred rarely.

**g)** Pyrrhotite

Pyrrhotite was identified as a light or medium yellow mineral in the samples. It was most often seen as minute inclusions within pyrite grains, with a few highlighted as examples in Figure 23 below.

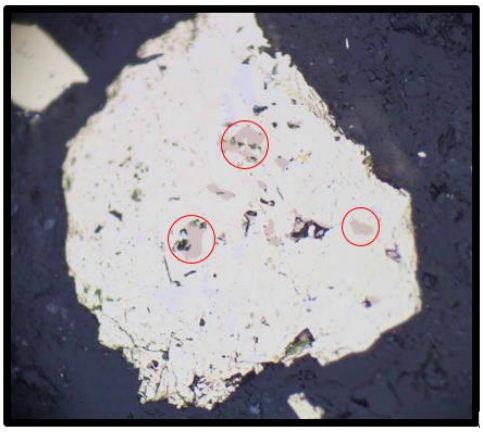

Figure 23: Image of a pyrite grain with pyrrhotite inclusions, highlighted with red circles

**h)** Sphalerite

Sphalerite, much like pyrrhotite, was identified as minor inclusions within pyrite, though less common than pyrrhotite.

**i)** Native Gold

Native gold was not specifically searched for, but in one grain, native gold was found. This native gold particle was extremely small, less than 15 µm in its longest dimension on the surface of the slide. It could have existed as a vein running perpendicular to the exposed surface, thus having more gold content than appeared, however this was the only case of native gold found and even if the vein was perpendicular, it would not contribute to a much higher gold concentration in the greater ore as seen in all of the surfaces examined. The gold assay, as discussed in Section 3.1.8 with results in 4.2.5.5, reports gold quantities far higher than just native gold that was seen on the surface of the mounts. The higher gold content is attributed to invisible gold within the pyrite and arsenopyrite. The gold ore of the area is known to have small quantities of native gold, as well as the invisible gold associated with the pyrite (Youlton et al., 2018).

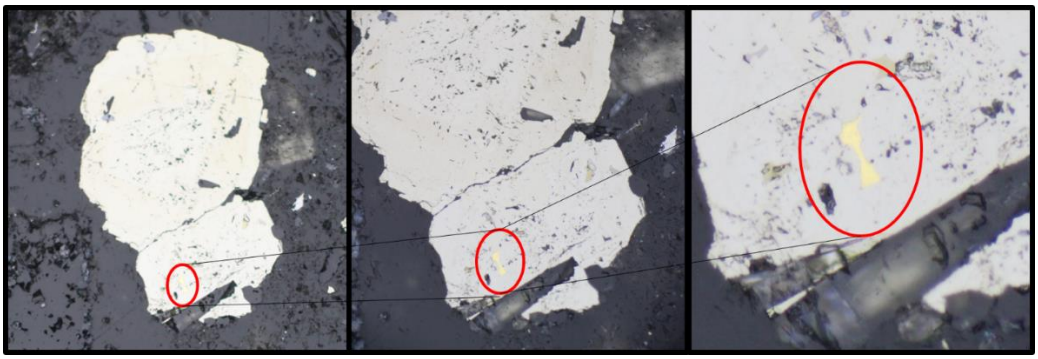

Figure 24: Native gold as seen within a pyrite grain in the case study ore

#### *4.1.1.2 Grouping minerals into functional groups*

The functional groupings for the counting of the minerals were done based on compositions and what could be seen under the optical microscope. The functional groups also had to be chosen to meet the objectives. The objectives relate to determining selective flotation in the samples to be analysed. Since trace elements cannot be seen under the optical microscope, but arsenian pyrites could be differentiated from pyrite, the focus was put on the two classes of “pyrite” and “arsenopyrite”. The class “arsenopyrite” included arsenian pyrites and arsenopyrite, both in the typical euhedral shapes of Figure 18 and those of the shapes seen in Figure 19. “Pyrite and Arsenopyrite mixes” were allocated a separate class, as the flotability of this mixed class was to be tracked. The last class allocated was to the “conglomerates”, as conglomerates occurred frequently enough to count and the recovery of these were of interest.

The result of applying the optical microscopy methodology to the case study ore is shown in Figure 25 below. This method, using the determined size classes, was applied to resin mounts of samples of the concentrates and tailings of the experimental runs in order to look for a change in the ratio of minerals. This data is visible in Section 4.2.8.

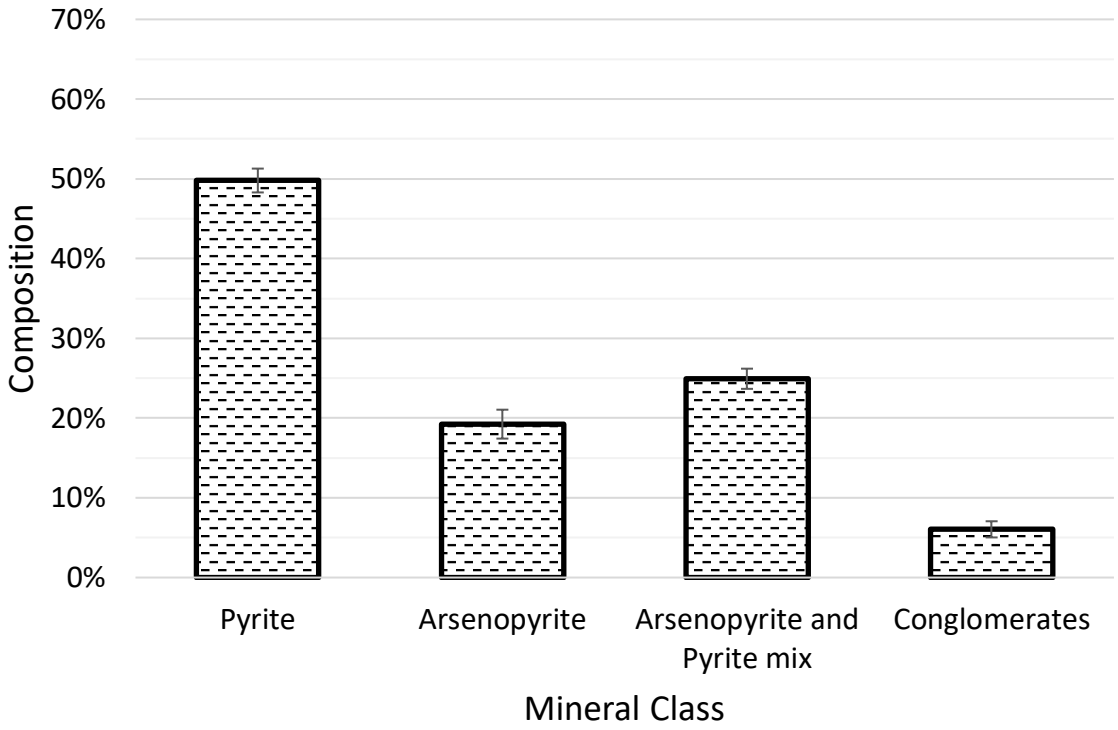


Figure 25: Relative distribution of mineral classes in the 100% passing 1 mm resin mount of the feed sample

### *4.1.2 SEM*

WDS analysis of pyrite grains with the full element list of possible impurities in pyrite revealed which of the elements of in Figure 30 existed within the pyrite phase. A box and whisker plot was chosen to represent the data, with a logarithmic scale on the left hand side, and is displayed in Figure 26 below. It is important to note that the y-axis is a logarithmic scale, especially where the box and whisker plots stretch across a wide range of weight percent, which may cause the upper ranges of the diagrams to appear compressed.

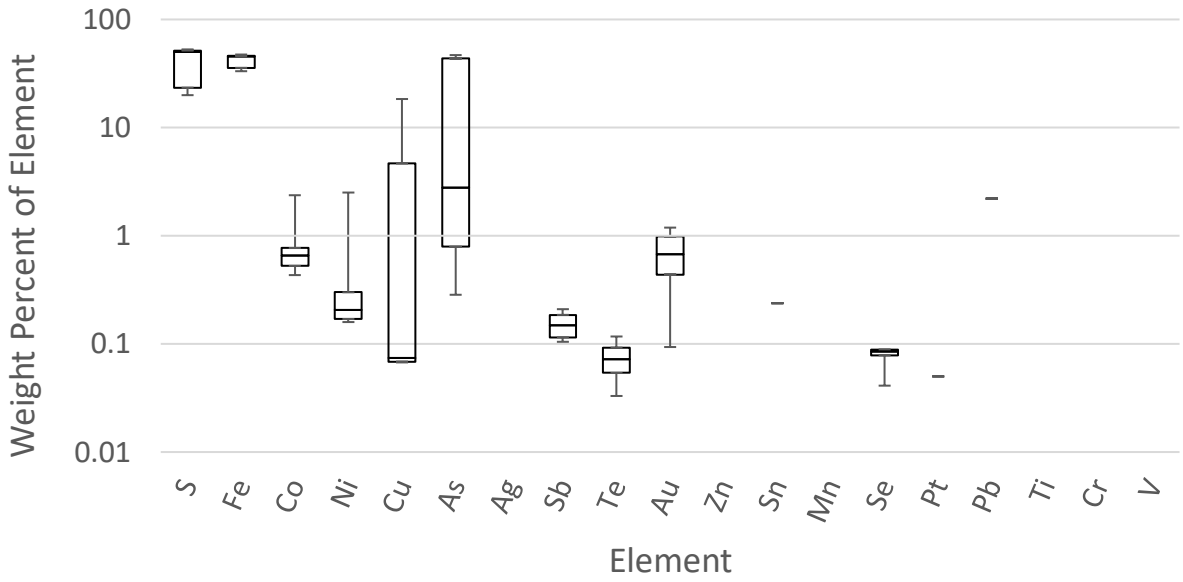


Figure 26: Box and whisker plot of WDS sensor data of pyrite grains in batch flotation feed

Table 12 shows another angle at the data obtained from the SEM WDS, where the top row represents the average weight percentage of the element when it was detected in a grain, and the bottom row represents how often it was detected in a grain. From the data in Figure 26 and Table 12, the elements to be analysed further in this project could be chosen.

Table 12: data from WDS sensor on feed pyrite grains of 100% passing 1 mm

| | S | Fe | Co | Ni | Cu | As | Sb | Te | Au | Se |
|---|---|---|---|---|---|---|---|---|---|---|
| **wt% average when present** | 41.96 | 42.394 | 0.742 | 0.369 | 4.65 | 16.49 | 0.153 | 0.074 | 0.677 | 0.084 |
| **Percent of spots with element** | 100% | 100% | 60.87 % | 30.43 % | 5.80 % | 86.96 % | 5.80 % | 5.80 % | 7.25 % | 8.70 % |

In Figure 26, it can be seen that the primary constituents of pyrite (Fe and S) have the highest composition, which is to be expected. The percentage of the spots with those elements present in Table 12 also shows that Fe and S were found in 100% of particles, which is expected since all the spots were placed on pyrite particles. In Figure 26, Fe and S compositions are seen to have extremely small differences between their medians, upper quartiles and maximum values. This is a result of the majority of pyrite having composition variations with very low weight percentage contributions (Arsenic is the only elemental variation with an upper quartile above 10 wt%), and thus upper bounds of S and Fe are saturated with values of similar weight percentages, causing the low spread in the upper quartile to max

values. The distribution below the median to the minimum in the Fe and S values is much larger as when elements are substituted into pyrite, they displace the Fe and S, thus the particles with impurities have a decreased Fe and S compositions, and this manifests as the larger distribution for the Fe and S median to minimum in Figure 26. Pyrite is the mineral of study, thus it is important to carry on analyzing for Fe and S.

Cobalt is known to substitute into pyrite, and this is found in the case study ore. When Co is present, which was 60.87% of the spots, the average composition of it is 0.742 wt% (Table 12). Co therefore occurs in significant amounts that are detectable by EDS and is present the majority of the time, thus it is reasonable to move forward with analyzing for it.

Nickel is found less commonly than cobalt, with nickel having an average composition of 0.369 wt% when present. It is still present in 30.43% of particles, often enough to still analyse for it.

Although Copper is only found in 5.8% of the particles analysed, its large weight percentage average in those particles (4.65 wt%) is significant and Cu should be analysed further. The large distribution of weight percentage% of Cu as seen in Figure 26 is a result of few particles having a higher wt%.

Arsenic is a major element of study, as Au is often associated with arsenic. The range of arsenic in the sample is large, from lower than 0.5 wt% up to 43 wt%. The upper values represent arsenopyrites with the lower values representing arsenian pyrites. The even distribution between the quartiles show that there is a large range of values, however the difference between the upper quartile and the max shows that a lot of values lie in the larger weight %, which could be a reason why the average arsenic content is high as 16.49% when arsenic is present. The large range is beneficial to the study as there may be a difference in the flotation responses of particles with a higher arsenic content over those with a lower one, as more arsenic would lead to a greater difference in pyrite properties.

Sb, or Antimony, was found in a few samples (5.8%) at levels high enough for detection with EDS and was also analysed for further in the project.

Au was found in few particles (5.8%) but was of importance to the project as the context is gold recovery in industry. The weight percentages that the gold was found at were also significant, averaging 0.677 wt%, and thus was analysed in following samples.

Te and Se also had multiple particles with them appearing, but their amounts were small, with averages of 0.074 wt% and 0.084 wt% respectively. These were lower than the EDS 0.1 wt% detection limit, and their contributions to the properties of a particle was assumed to be insignificant compared to other elements, especially because of their low occurrence (less than 10%) for each.

The other elements that were not yet mentioned (Zn, Sn, Mn, Pb, Pt, Ti, Cr and V) did not show up in significant weight percentage quantities or did not occur often enough to warrant further investigation. The element list to further analyse sample with thus consisted of S, Fe, Co, Ni, As, Sb and Au.

This element list of the significant variations in the pyrite composition relates to what was found from literature, with the same list of elements (except Co) found by Agangi et al., (2014) to be related to the gold mobilization in the area.

## 4.2 Interrogation of selective flotation of pyrite with different compositional variations in a batch flotation system of the case study ore

### *4.2.1 Batch Flotation Feed Characterisation*

#### *4.2.1.1 Particle Size distribution*

After following the milling procedure outlined in Section 3.2.2, the particle size distribution (PSD) of Figure 27 was achieved. The shape of the curve generated from the project flotation feed is in agreement with the sigmoid shape that was desired.

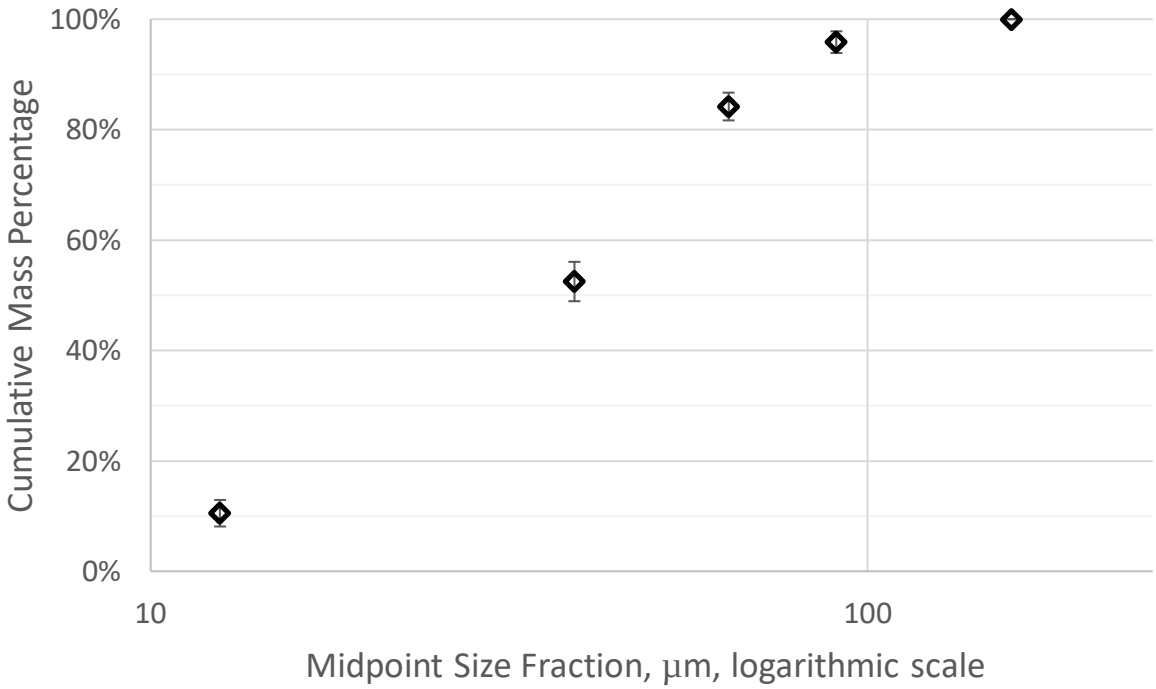


Figure 27: Cumulative particle size distribution, post mill, logarithmic x axis

The points on this PSD represent the midpoint of the size range between sieves. The third point from the left of the diagram represents the midpoint between 53 µm and 75 µm (64 µm) and 85% cumulative mass, when practically this 85% of mass all passed through the 75 µm sieve.

#### *4.2.1.2 Optical Microscopy*

The optical microscopy characterisation of the feed follows the same methodology of the previous subsection, this time using the post-mill batch flotation feed (85% passing 75 µm) instead of the pre- mill feed (100% passing 1mm). The results of the optical microscopy on the milled feed is shown in Figure 28 below. Figure 28 shows the averages obtained from three separate resin mounts from separate samples. The differences of the pre-milled optical microscopy compositions (Figure 25) should not differ significantly from the post-mill distributions. The distributions calculated for pre-mill and post-mill samples are compared in Table 13 .

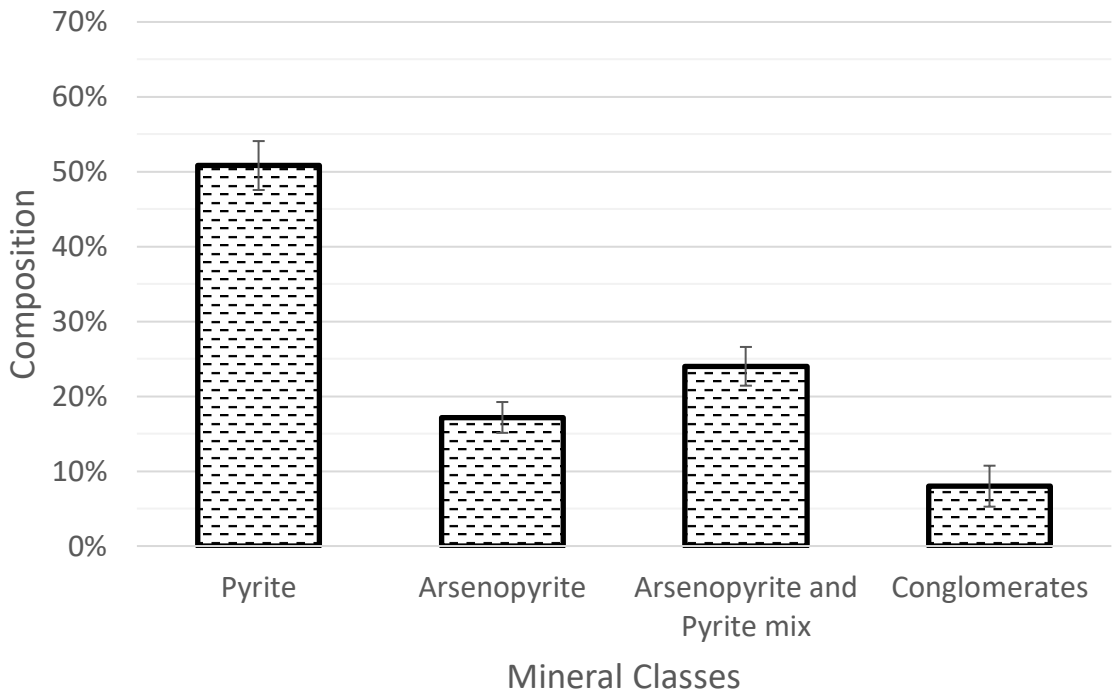


Figure 28: Percentage composition of mineral classes by optical microscopy on the project milled feed sample

As can be seen in Table 13 below, no significant differences were seen between the 100% passing 1 mm sample and the 85% passing 75 µm samples. The large difference in Conglomerate composition is a result of the values being extremely low, which results in a small change leading to a large percentage difference.

Table 13: Differences in pre-milled and post-milled optical microscopy

| | Feed, 100% passing 1 mm | Feed, 85% passing 75 um | Difference | Percentage Difference |
|---|---|---|---|---|
| **Pyrite** | 49.79% | 50.82% | 1.03% | 2.07% |
| **Arsenopyrite** | 19.24% | 17.18% | 2.06% | 10.71% |
| **Arsenopyrite and Pyrite mix** | 24.93% | 24.00% | 0.92% | 3.70% |
| **Conglomerates** | 6.04% | 8.00% | 1.95% | 32.29% |

#### *4.2.1.3 QXRD*

Quantitative X-Ray Diffraction revealed minerals that were present in the sample. In the feed samples sent, 1.73% of the feed was made up of pyrite and arsenian pyrites (with a standard deviation of 0.18% and standard error of 0.31% of the feed).

Gangue minerals included Quarts, Muscovite and Dolomite (57.4%, 20.7% and 13.6%) as per Figure 29 below. The quartz originates from metamorphosed sand (silica) and muscovite (mica) and other small

amounts of minerals resulting from metamorphosed clays. This is consistent to what is known about the area having originated from metamorphosed sediments, and these minerals are characteristic of that. The pyrite phases and other ore minerals originate from hydrothermal fluids that deposit these minerals into fractures of the rock, as described in Section 2.3.

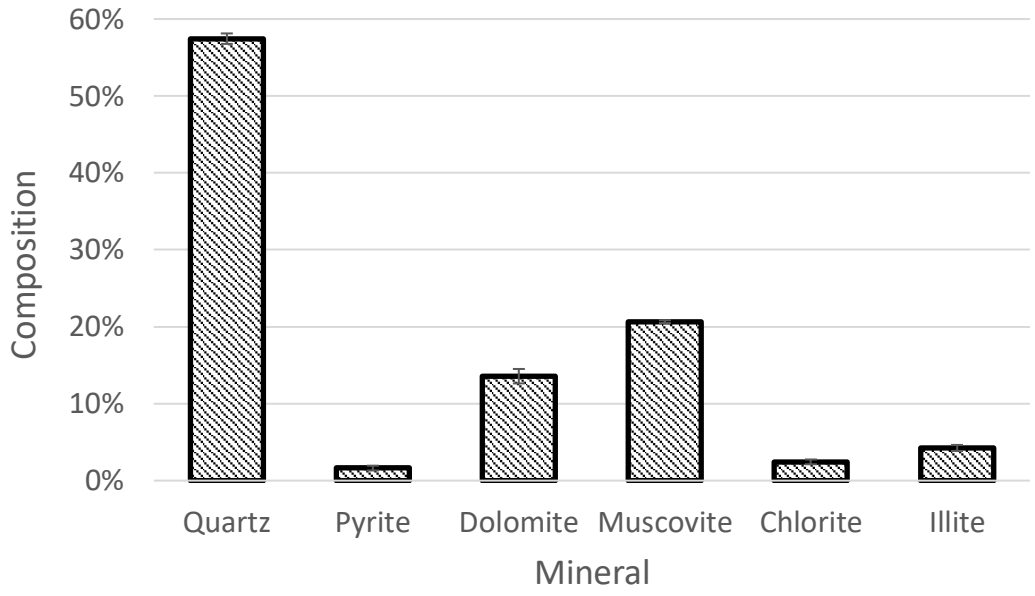


Figure 29: QXRD of case study ore

#### *4.2.1.4 LA-ICP-MS*

LA-ICP-MS revealed trace elements in the feed samples. Note that these elements are not levels within pyrite phases, but within the whole samples of the feed. The results of the trace element analysis are shown in Figure 30 below.

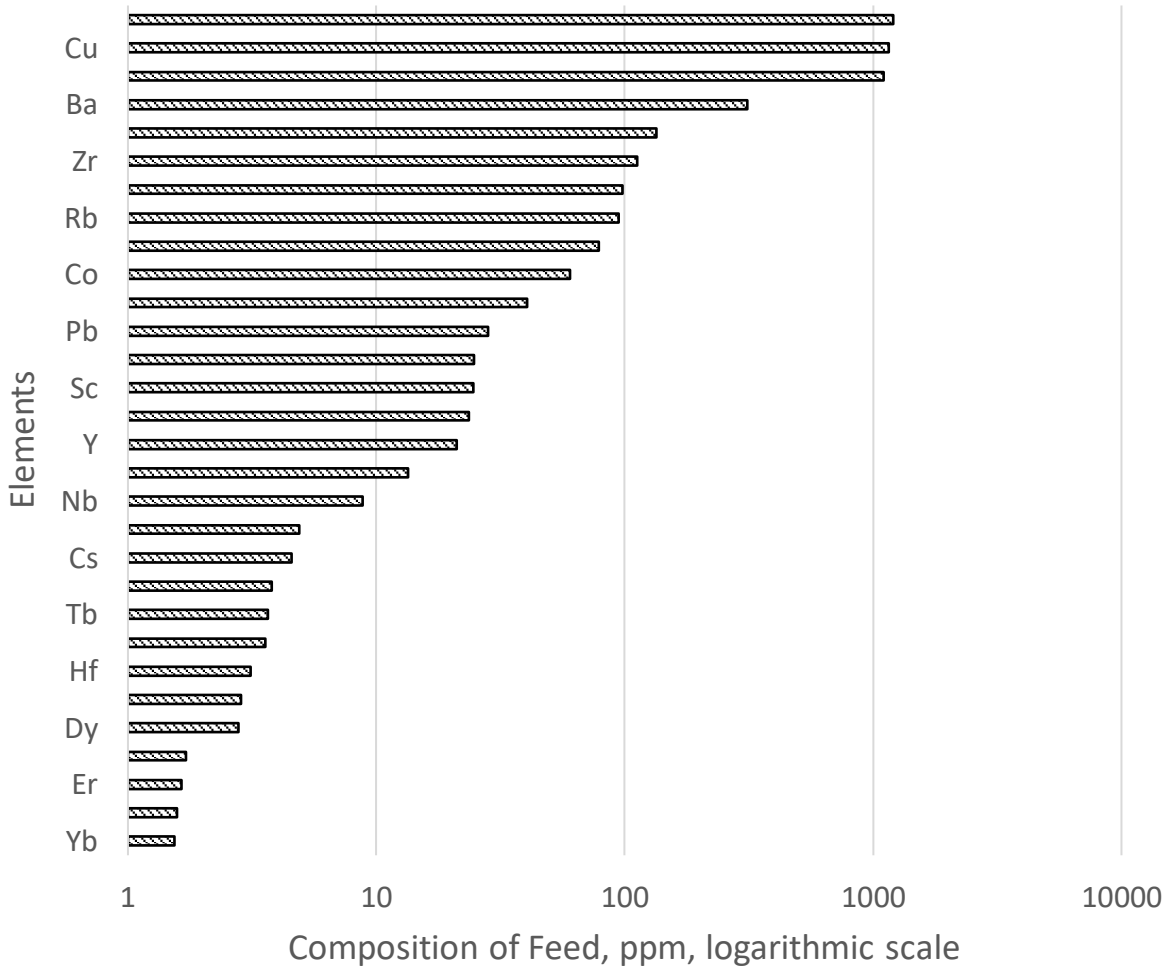


Figure 30: LA-ICP-MS of feed samples showing trace element composition

Trace elements reported to be lower than 1 g/ton have been left out of the Figure 30 for clarity.

The Ni and Cu content likely originates from small amounts of pentlandite and chalcopyrite as originally identified under optical microscopy. Cr and Ba and likely originate from gangue minerals.

#### *4.2.1.5 SEM*

The EDS sensor was used on different resin mounts of feed samples than used in Section 4.1.2. All new particles were analysed and resulted in Figure 31 and Table 14, both presented below.

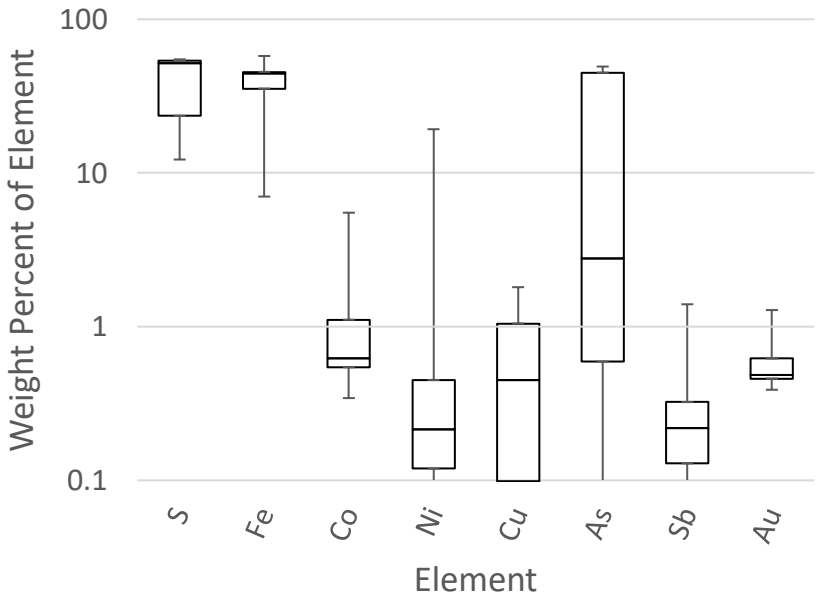


Figure 31: Box and whisker plot of EDS data from a feed sample resin mount of the case study ore

From Figure 31, it can be clearly seen that the EDS data does not differ significantly to the WDS data of Figure 26. Table 14 below is also similar to Table 12, with the major differences being that Ni was found more often in this sample and a higher Co average weight percentage was calculated. The higher Co average weight percentage of the EDS compared to the WDS is attributed to two outliers that have the maximum of around 5 wt%.

Table 14: EDS data from a feed sample resin mount of the case study ore

| | S | Fe | Co | Ni | Cu | As | Sb | Au |
|---|---|---|---|---|---|---|---|---|
| **wt% average when present** | 42.622 | 40.865 | 1.014 | 0.875 | 0.700 | 16.999 | 0.399 | 0.578 |
| **Percent of spots with element** | 100.00 % | 100.00% | 52.34% | 49.61% | 3.13% | 85.31% | 4.69% | 13.28% |

The elements listed in Table 14 were then carried forward for further analysis on the concentrates and tailings of the batch flotation experimentation.

#### *4.2.1.6 Gold Association using SEM*

All the spots found in the study that contained gold were collected and these spots were presented in the same way as all the other SEM figures, represented in Figure 32 and Table 15 below.

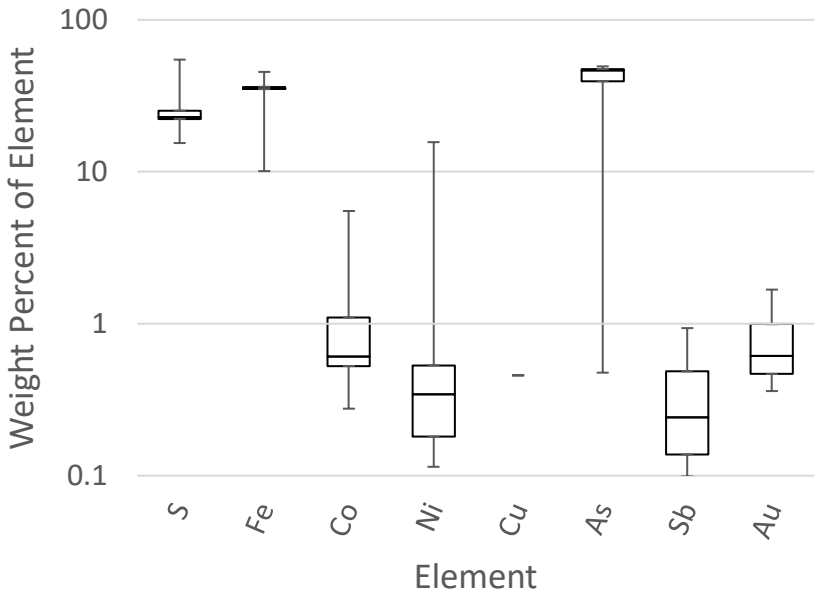


Figure 32: Composition of particles with Gold present using SEM EDS

From Figure 32, conclusions from the gold associations in the ore can be compiled. The first of these conclusions is that gold is associated with arsenopyrite and high arsenic weight percentage arsenian pyrite. The gold association with the compositional difference of pyrite having a large arsenic content is seen by the skewing of the arsenic box and whisker plot in Figure 32 to the higher weight percentages. The association of gold with high arsenic weight percentages is reinforced by accompanying Table 15 where it is shown that 100% of particles that have been represented here have Au content, but also 100% have As content (with the accompanying Fe and S).

Along with the information that all gold was associated with arsenic, Table 15 also shows that the average arsenic content of spots that contained gold was also an extremely high 36.54% arsenic (along with 35.932% iron and 28.238% sulphur). The reason why the sulphur content is much lower than previous examples is that as mentioned before, arsenic mostly substitutes for sulphur.

Table 15: Composition of Particles with gold present using SEM

| | S | Fe | Co | Ni | Cu | As | Sb | Au |
|---|---|---|---|---|---|---|---|---|
| **wt% average when present** | 28.238 | 35.932 | 1.203 | 1.509 | 0.458 | 36.536 | 0.380 | 0.741 |
| **Percent of spots with element** | 100.00 % | 100.00 % | 44.83% | 44.83% | 3.45% | 100.00 % | 13.79% | 100.00 % |

#### *4.2.1.7 Gold Fire Assay*

The gold content of the feed ore was analysed to be 8.23 g/ton. This equates to 8.23 ppm and is the feed gold grade. The known gold grade of mines around the area are 8 g/t (Barberton mines), 8.6 g/ton (Evander Mines), so the analysed result of 8.23 g/ton is well within what is known for the area (Pan African Resources, 2019). It was not known if the ore from the mine was blended.

### *4.2.2 Scoping batch flotation experiments*

As discussed in Section 3, after the feed was characterized, scoping tests of the batch flotation experiments were run. The starting point for the operational parameters was based on literature in Table 6 and experience with the experimental equipment, while the pulp chemistry starting point was provided by the mineralogist at the mine where the case study ore originated from. and refined and confirmed with the scoping tests. From the scoping runs, a combination of an air flow rate of 7 liters per minute with the impeller speed set at 1200 rpm (the impeller works to both agitate the pulp and disperse the air) was found to be the ideal combination with a frother concentration of 40 g/ton and a collector concentration of 25 g/ton. SIBX and PAX were used as single collectors in scoping runs, as these were the primary collectors and the system was to be anchored around them.

Flotation is highly reliant on froth stability, as destabilised froth causes losses of hydrophobic particles out of the froth phase and back into the pulp phase. The froth must be stable enough to hold solid particles and deliver them to the concentrate via the overflow. Froth height plays hand in hand with the froth stability, as the more stable the froth, the higher the froth height will be. The target of the scoping experiments was to find a balance between froth stability and the highest collector concentration that would allow this.

Higher agitation is beneficial as it promotes mixing and air dispersion in the system, however higher agitation than 1200 rpm caused major turbulence on the surface of the pulp phase, resulting in pulp splashing outside the bounds of the cell and into the concentrate catchment area. This was undesirable as the mass recovered by this method would not be by flotation.

A higher air flow rate than 7 liters/min caused the initial froth height to exceed the side boundaries of the cell, causing froth to overflow outside the bounds of the concentrate catchment area, causing mass (and concentrates) to be lost.

Higher dosages of collector than 25 g/ton destabilised the froth and caused the froth height to be insufficient for flotation through the entire flotation duration. This destabilisation was attributed to higher collector dosages causing more hydrophobic mineral particles to rise into the froth phase and overload the bubbles, causing them to burst and destabilise.

The entire scoping experimentation results on the impact of varying Air flow rate, agitation, frother concentration and collector concentration are visible in Appendix C.

### *4.2.3 Froth Stability*

The results of the froth stability experimentation in the measuring cylinder are displayed in Figure 33 below. The values of "no reagents" still have an increasing "froth height" with an increase in air flow rate as the bubbles displace water as they travel up the column, increasing the height above the 500 mL mark.

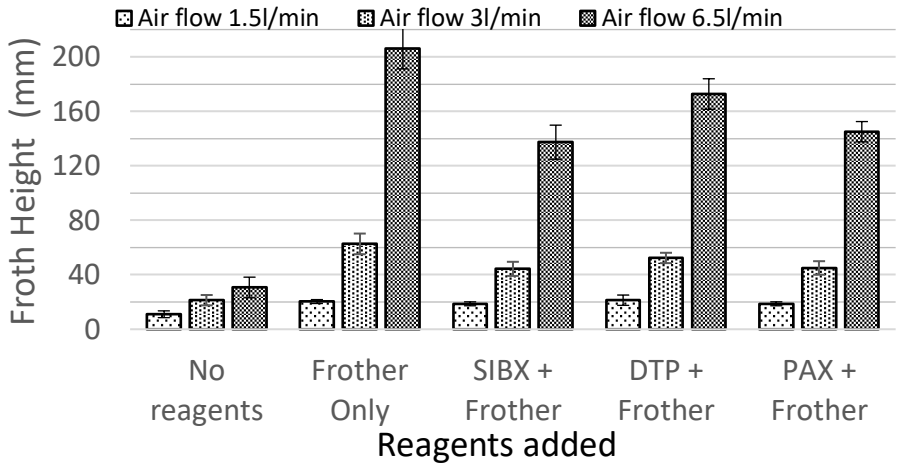


Figure 33: Froth height in measuring cylinder experimentation results

Both primary collectors (SIBX and PAX) and secondary collector (DTP), destabilised the froth as is evident in Figure 33 as the cases with collectors being present having a significantly lower froth height than when the frother was present alone, except at the lowest air flow rate, which was too low to draw any conclusions.

SIBX and PAX did not perform significantly different from each other, but both had lower froth stability than DTP in both the 3 L/min and 4.5 L/min cases.

The froth stability tests on the batch flotation cell followed these experiments, and the results can be seen in Figure 34 below, where the same trends were seen of all the collectors destabilising the froth. The froth stability and water recovery of DTP was slightly higher than that of PAX and SIBX. The collectors in this study did not act synergistically with the frother to stabilising the froth, but destabilised it, as seen in the scoping experiments when the ore was included in the system.

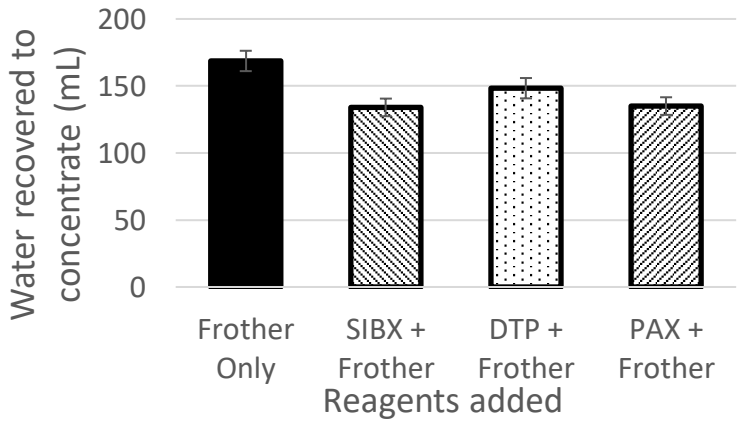


Figure 34: Water recovered to concentrates when excluding the ore phase

### *4.2.4 Mass and water recovery*

When the conditions of the experiments were fixed the batch flotation experiments were started. The first set of results focuses on the broader system of total mass and water recovery.

The nomenclature of the methodology is carried forward in this section, for example “SD50” meaning “SIBX and DTP, 50% DTP” and “PD25” mean “PAX and DTP, 25% DTP”. Graphs in this section are presented as pairs, with the first, or (a) graph, being for the SIBX and DTP system, and the second, or (b) graph, being for the PAX and DTP system. The horizontal axis label of “Collector(s) used” are ommited from every graph for clarity. The approach of discussing the figures and results in this section is to first discuss the results of the single collectors alone and compare them with each other, and then to discuss the trends visible as the DTP content is increased in the SIBX and PAX systems.

The first set of figures to be displayed is the mass pull (total dry mass recovered to the concentrates), and is displayed in Figure 35 below.

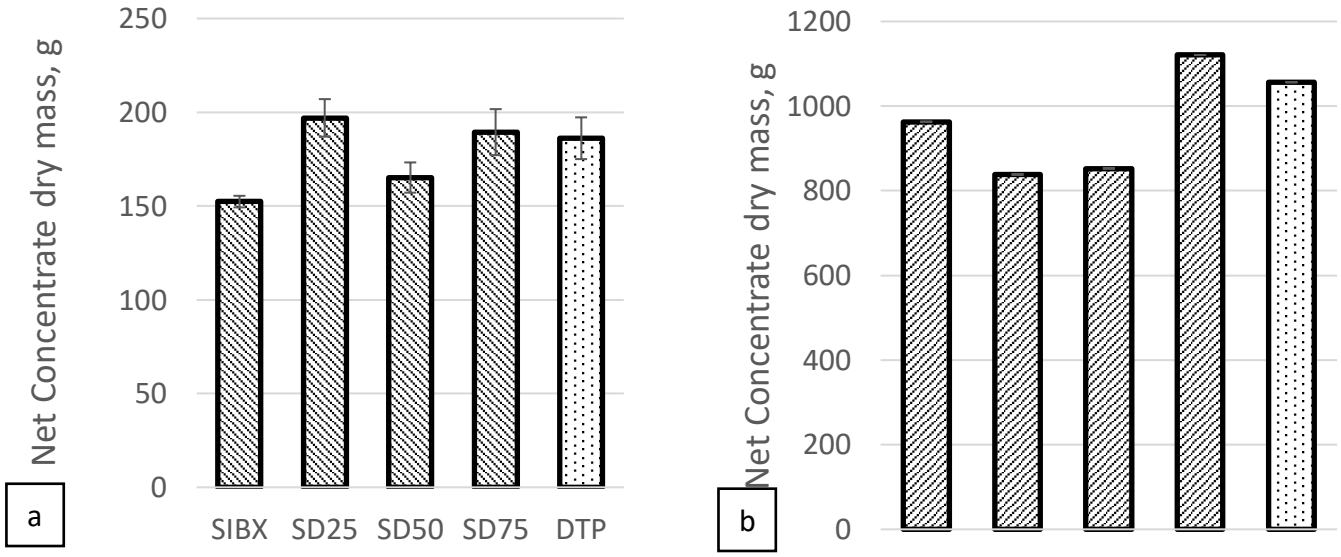


Figure 35:Dry mass recovered to concentrate, or "mass pull", in (a) SIBX and DTP batch flotation and (b) PAX and DTP Batch flotation

From Figure 35, it can be seen that DTP recovered more mass than PAX, and SIBX recovered the least mass out of the pure collectors. Looking at other trends, addition of DTP to SIBX seemed to recover more mass across all experiments. 25% of DTP and 75% PAX recovered the least mass, but the mass recovery improved as more DTP was included. Knowing that DTP has a more stable froth than SIBX and PAX, it is important to check for entrainment, as the extra froth stability from DTP may recover more mass via entrainment than the effect of the collector.

#### *4.2.4.1 Entrainment*

To check for entrainment in the batch flotation system, the first point to be considered is water recovery in the different cases. If an increase in water recovery and a corresponding increase in mass pull is seen, entrainment may be a concern for the mass recovery in the system. Figure 36 below shows the water recovered to concentrates for the various experiments.

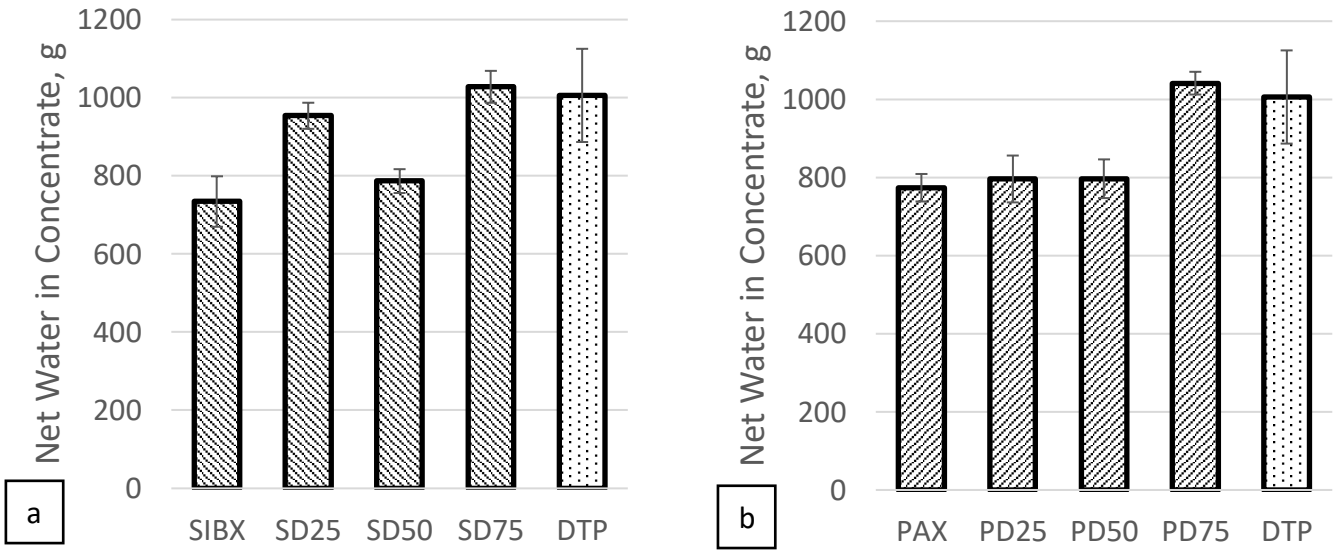


Figure 36: Water recovery to concentrates in batch flotation

Here it can be seen that collector compositions of only DTP and xanthates mixed with 75% DTP have significantly higher water recoveries than the rest, which corresponds to the peaks in mass recovery seen in Figure 35. The high water recovery of SD25 in Figure 36 is also seen to have a high mass recovery in Figure 35, however the variations in mass and water recovery through the other experiments show no correlations. This correlation can be checked by drawing a graph of mass recovery versus water recovery, which is plotted in Figure 37 below. Although no correlation is seen and a low $R^2$ value is obtained, it is worthwhile to note that the three values on the right-hand side are from SD75, PD75 and DTP experiments.

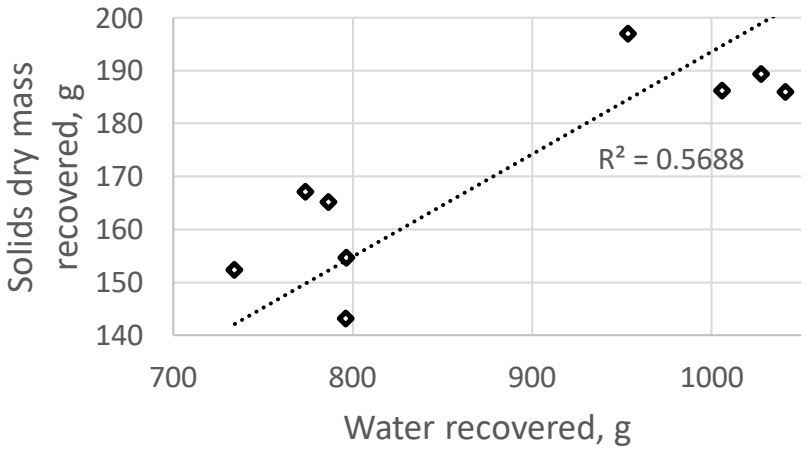


Figure 37: Mass recovery versus water recovery in Batch Flotation, with trendline to check for correlation

### *4.2.5 Recovery and Grade*

The recovery of pyrite, chalcopyrite and pentlandite are discussed in this section. The primary focus of this study is pyrite, and pyrite with elemental substitutions as impurities. While chalcopyrite and pentlandite are two completely different minerals from pyrite, they can be considered as extreme cases of pyrite with Cu and Ni substitution. The low amount of actual Cu and Ni found in some of the pyrite grains cannot account for the amount of Cu and Ni reported in the Base Metal Assay, and because chalcopyrite and pentlandite was identified during optical microscopy, it can be assumed that the Ni and Cu originates from the chalcopyrite and pentlandite, and the error associated with small amounts of Cu and Ni in some pyrite grains considered to be negligible.

#### *4.2.5.1 Pyrite*

Pyrite masses in the experimental cases are calculated from the mass of Fe content of the samples from XRF base metal analysis. Recovery of pyrite was calculated by comparing the mass of pyrite in the feed compared to the mass of pyrite in the concentrate, while grade data was obtained from comparing the total mass of pyrite in the concentrate to the total mass of concentrate. Sample calculations for this are given in Appendix B.

The results of the grade and recovery data are shown in Figure 38 and Figure 39 respectively. The large jump in SIBX grade and recovery when adding DTP were unexpected, but a mass balance done with the pyrite amount in the feed minus the amounts in the tailings and concentrates yielded less than 4% errors across all experiments, with most errors reporting less than a 2% error.

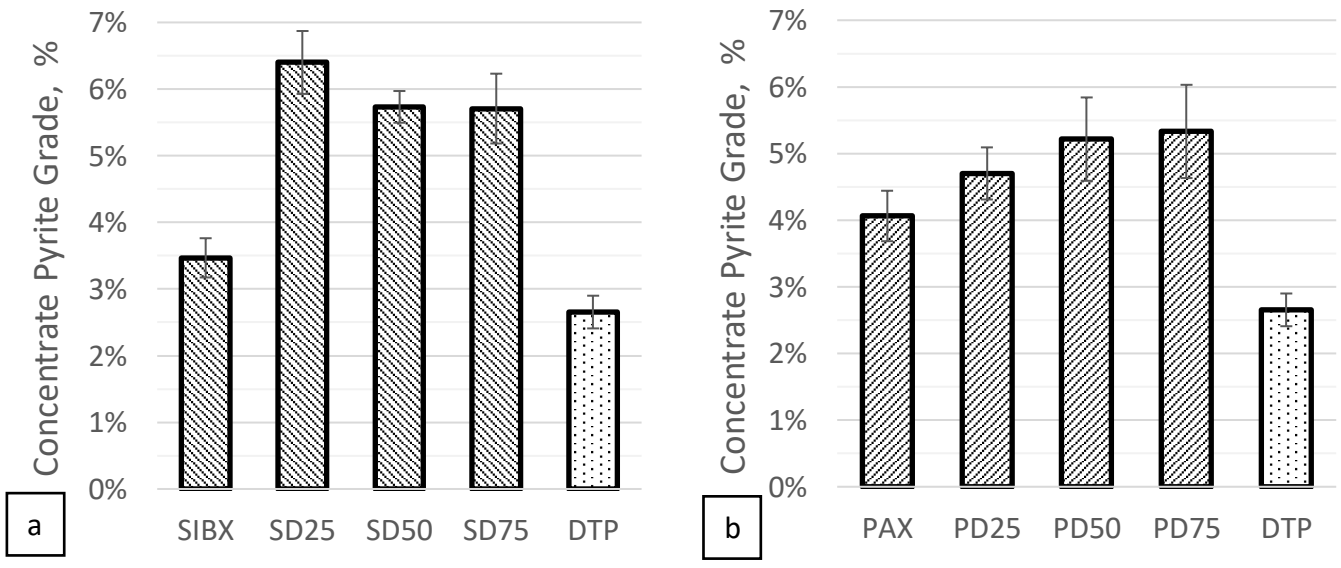


Figure 38: Pyrite grade in batch flotation experiments

When viewing Figure 38, it is worthwhile noting that the pyrite grade in the feed is 1.73%. It can be seen that SIBX as a single collector performs less favourably than PAX as a single collector, but the difference is barely significant. DTP alone performs poorly compared to SIBX and PAX with grade. SIBX almost doubles in its grade with 25% DTP is added, but as more DTP is introduced the grade lowers slightly, but still stays approximately double that of SIBX alone. The trend for PAX is much smoother, with the grade

of PAX steadily increasing with an increase in DTP content. The grades obtained relate to the recoveries pictured in Figure 39 via the total mass of concentrate.

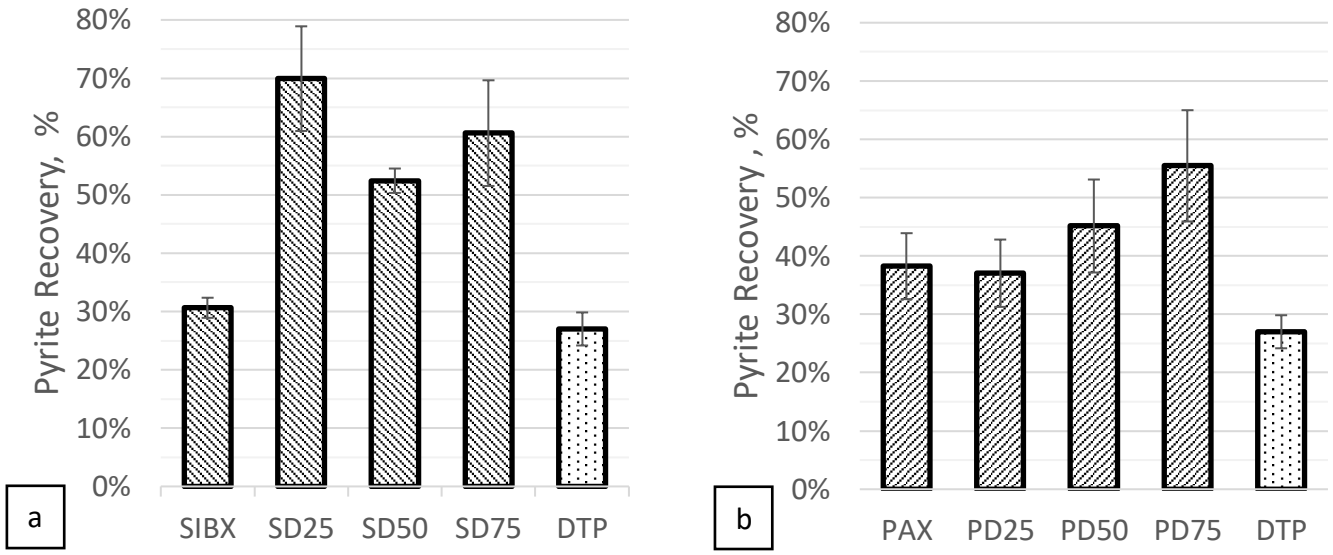


Figure 39: Pyrite Recovery in batch flotation experiments

Because the total masses in the concentrate remain relatively constant throughout the experiments (as visible in Figure 35), the trends in recovery are almost exactly the same as the trends in the grade.

Outliers from the relatively constant mass pull include DTP, which benefits in recovery even though its grade was still low because of its greater concentrate mass pull, although the DTP recovery is still lower than PAX and SIBX. Because of the lower mass pull of PD25, an increase in recovery is not apparent even though the grade increases, but as the DTP content increases, an increase in grade is seen.

Both PAX and SIBX benefit from having DTP in the system, as expected according to previous studies. What was not expected was the increase in grade and recovery even when the system comprised of 75% DTP, as DTP is a weak collector (as seen by its poor performance alone). In the scoping experiments, it was put as a priority that a high collector concentration or dose must be used, as information from a metallurgist where the case study ore originated from listed the collector dosage at 300g/ton, which is over 10x what was settled on in the scoping experiments This could have been an error in correspondence. A lower total collector concentration or dosage may have benefited from seeing smoother trends, as even at 25% of the primary collector the grades and recoveries were high.

Small amounts of DTP in SIBX (as in SD25) proved successful, as both the grade and recovery doubled. SD25 compared to SIBX alone is especially effective as usually grade and recovery have an inverse relationship, where changes that improve the grade adversely affect the recovery, and vice versa. If the concentrates were split into different concentrates in different time intervals, the kinetics could also be studied, but because of the short flotation time of 10 minutes, the results presented are of faster floating minerals in order to interrogate the objectives of selective collector attachment. A longer flotation time may lead to the grades and recoveries evening out as the slower particles that less collector attached to would also float out.

#### *4.2.5.2 Arsenopyrite*

Arsenopyrite recovery was calculated from XRF base metal analysis data of samples from the batch flotation experimentation and displayed in Figure 40 below.

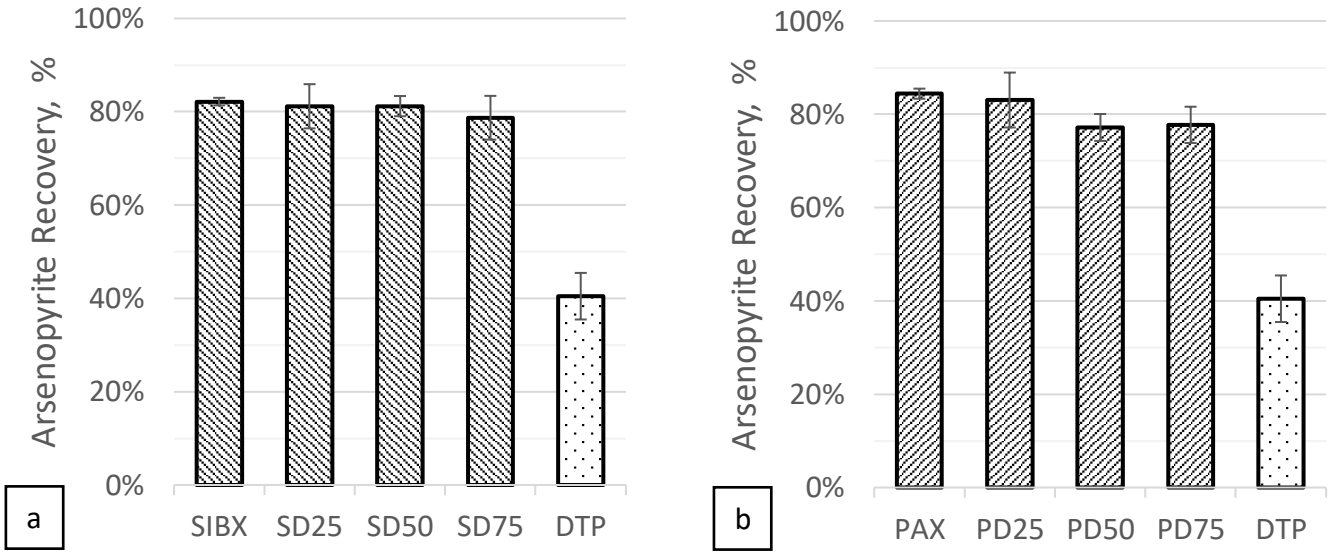


Figure 40: Arsenopyrite Recovery in batch flotation experiments

Unlike the other minerals of interest in the study, arsenopyrite recovery did not significantly increase when using collector mixtures over the recovery seen with xanthates alone. This is attributed to DTP not recovering arsenopyrite as well as xanthates, which is a trend that continues throughout the results and discussion section. This loss of arsenopyrite and arsenic containing pyrites when using DTP as a collector is seen in Figure 40 as DTP having a arsenopyrite recovery of 40.47%, which is less than half of the xanthates (82.19% for SIBX and 84.42% for PAX).

#### *4.2.5.3 Chalcopyrite*

Chalcopyrite is a naturally floating mineral and can be floated without the presence of a collector. This is perhaps why the recoveries of chalcopyrite are significantly higher than pyrite across the experiments. Because of the values reported in the base metal assay, the results of the chalcopyrite recovery had to be constrained to one significant figure. Similar trends can be seen in the recovery of chalcopyrite in Figure 41 to the pyrite recovery discussed earlier. When SIBX was used as a collector it benefited from the increasing DTP content, with a significant increase in recovery when the two collectors were mixed over the base collectors alone. A maximum in the SIBX-DTP system was seen with a mix of 50% SIBX and 50% DTP. The larger error bar in the SD75 is a result of the concentrations of copper and chalcopyrite being low, and one outlier (could be a larger piece of chalcopyrite in this sample) causing the large error. Mixtures of PAX and DTP recovered more chalcopyrite than PAX alone, with PD25 performing the best. Interestingly compared to all other minerals, PAX alone produced the lowest recovery, being beaten by both SIBX and DTP. This can be related to both the natural floating ability of chalcopyrite, combined with literature that showed that dithiophosphates readily recovered chalcopyrite, such as the work from Zhong et al., (2015).

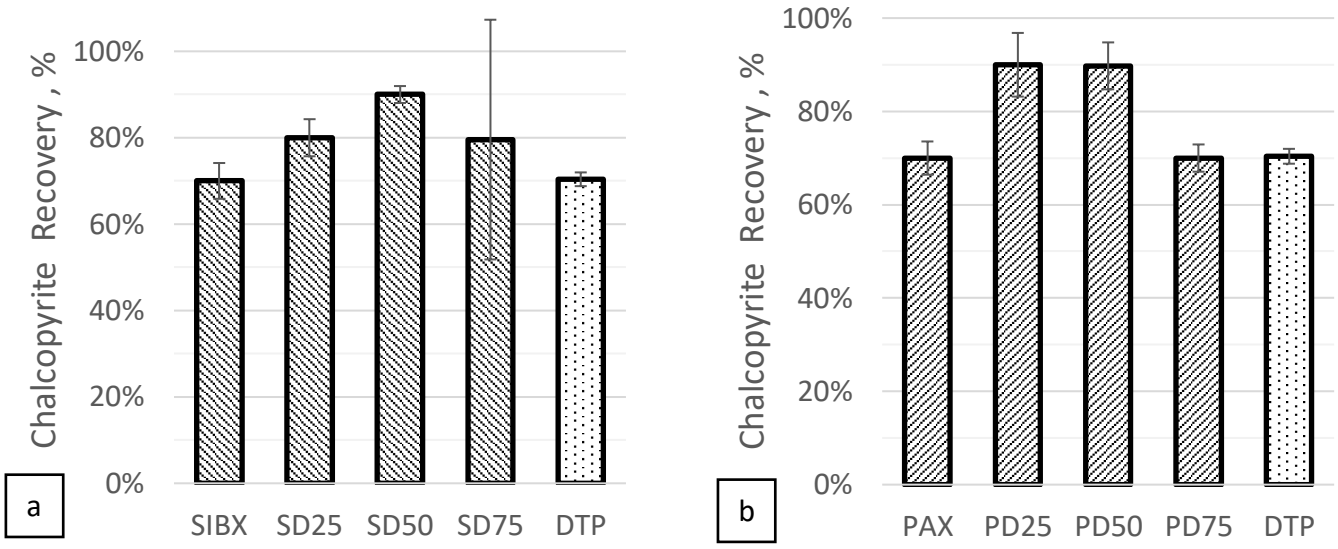


Figure 41: Chalcopyrite recovery in batch flotation experiments

#### *4.2.5.4 Pentlandite*

As with chalcopyrite, because the base metal assay only reported nickel as one significant figure, the recovery results had to be constrained to one significant figure as well. The recoveries of pentlandite when using mixtures of either SIBX and DTP or the PAX and DTP performed better than the single collectors alone but did not significantly differ from one another. For example, SD25 did not significantly differ from SD50, SD75. PD25, PD50 or PD75. However, the mixtures of xanthates and DTP performed better than the individual collectors alone. This information can be seen in Figure 42 below.

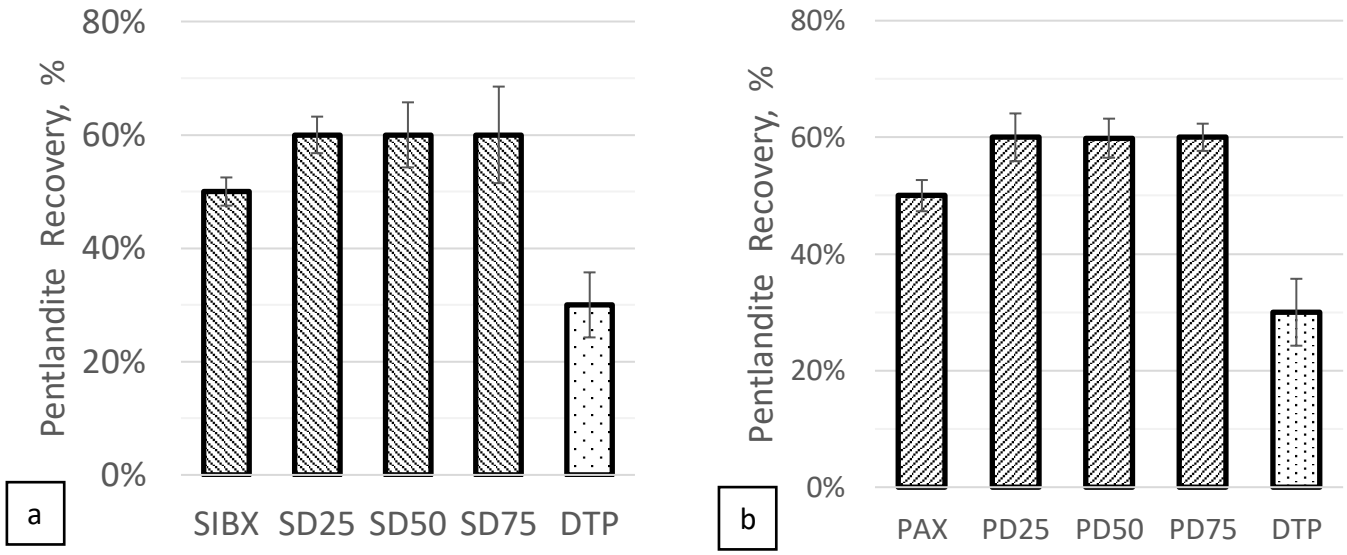


Figure 42: Pentlandite Recovery in batch flotation

#### *4.2.5.5 Gold*

As the study is in the gold ore context, it is important to discuss the gold recovery. The figures for this subsection was generated from the gold fire assay data. Initially, only the three single collectors were sent for gold fire assay but after the pyrite grade results were obtained, further samples of the well performing batch flotation runs were also sent to sample the data. The two highest performing pyrite grade and recovery experiments were the SD25 and the PD75 runs, and the correlation between pyrite performance and gold performance was to be investigated by including these experimental points.

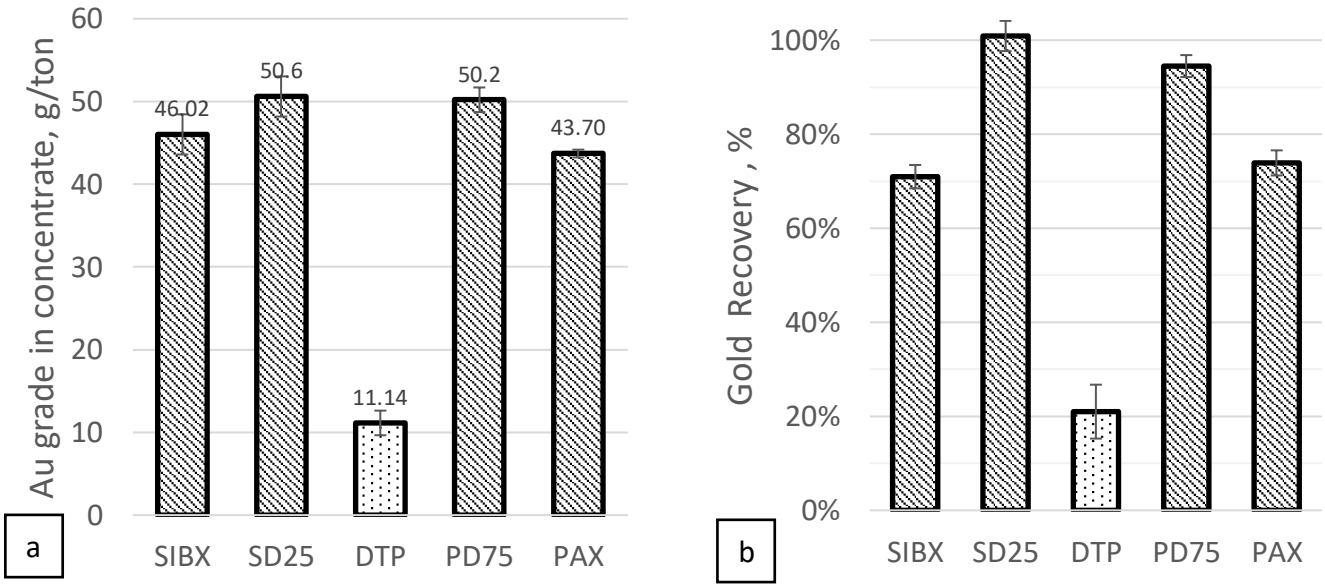


Figure 43: Gold grade and recovery in concentrate of selected batch flotation experiments

The high SD25 grade combined with a high mass pull resulted in an extremely high calculated gold recovery of close to 100%, as seen in Figure 43. The higher recovery of SD25 is in line with what was expected since SD25 had the highest pyrite recovery, as seen in Figure 39 earlier, however recovering all of the gold was not expected. The corresponding second highest recovery of pyrite in PD75 lead to the second highest gold recovery. DTP did not recover or concentrate the gold nearly as well as the primary collectors of the Xanthates. The DTP recovered around a third of the gold compared to the Xanthates, even though the pyrite recovery of the DTP was only marginally lower. This difference in gold trend when compared to the pyrite trend is one of the first indications that a “pyrite recovery” metric is not a perfect parameter as a proxy for gold recovery. If gold is associated mostly with a pyrite of a certain compositional variation (e.g. arsenic content as shown in this ore), and selective flotation takes place where pyrite without arsenic content is recovered, the pyrite recovery will not relate to the gold recovery. It is clear from comparing the gold grade and recovery data in this section and the pyrite grade and recovery data from Section 4.2.5.1 that the gold trends are not directly related to just the pyrite trends, but are also affected by total mass pull and possible selective flotation of different types of pyrite. It is also worth noting that native gold was seen under optical microscopy (Figure 24) and liberated grains of native gold may be more prone to recovery due to mass pull or DTP content. This supports the high peak of gold recovery of SD25, as it not only had the highest pyrite recovery, but also the highest mass pull.

The pyrite recovery compared to gold recovery is plotted in Figure 44 below. Here, the extreme outlier of DTP can be seen as the lower left value. When this data point is excluded, the linear trendline has a $R^2$ fit parameter of 0.9485, however when it is included the $R^2$ drops to 0.6694, which is no longer a good fit.

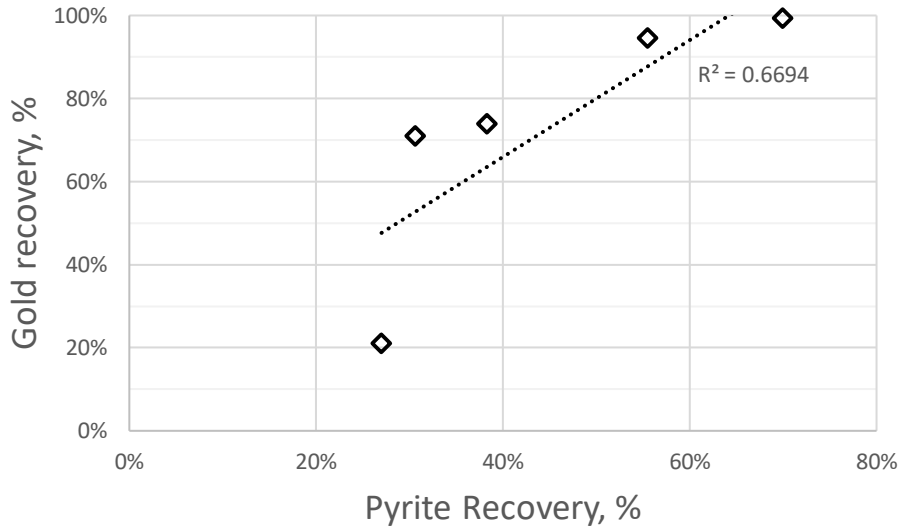


Figure 44: Pyrite Recovery versus Gold Recovery in select batch flotation systems

The gold recovery is related to the pyrite recovery, but again, it is seen that the relationship is far more complex than a simple linear fit across the entire range. The fact that almost 100% of gold can be recovered when not all of the pyrite is recovered also shows that the gold distribution is not even through all pyrite particles, and not all pyrite has to be recovered to recover all the gold. The mixture of 75% SIBX and 25% DTP may be extremely similar to what is used in industry, as it is known that SIBX and DTP is used but the ratios and mixtures are understandably a trade secret. If the performance in industry relates to what has been seen in the laboratory scale of this experiment, a loss in pyrite may not be directly proportional to the losses in gold, and the mixture of SD25 or similar is economically the best option, which is why industry has a high possibility of using this mixture.

### *4.2.6 Separation factor based on Base Metal Assay analysis*

The quantification of the separation factors of arsenic (or arsenopyrite) and pyrite will allow the interrogation of selective flotation when it comes to pyrite with arsenic impurity.

The values seen in Figure 45 below are calculated from the base metal assay values of arsenic and the pyrite calculated for the pyrite grade and recovery.

The definition of Separation Factor (of arsenic over pyrite) is the change in the ratio of arsenic to pyrite in the concentrate compared to the feed. A value higher than one means that arsenic occupied a higher ratio when compared to pyrite in the concentrate than the feed, and thus arsenic was selected for during the flotation process. It is also worthwhile to note that the values presented in Figure 45 is not the separation of arsenopyrite from pyrite, but arsenic from pyrite, as arsenic content is contributed from both arsenian pyrite and arsenopyrite, but conclusions can still be drawn from the results.

All the values in Figure 45 are above 1, which shows that arsenic was selected for and the concentrates had higher arsenic: pyrite ratio than the feed. The trends in arsenic seen can be summarised as higher arsenic content in the xanthate concentrate cases compared to DTP. The uncertainty parameters make it unclear what the trends are within the SIBX and DTP mixtures, however a steady decrease is seen in the PAX and DTP mixtures as more DTP proportion is included in the mixture. The lower arsenic content in the DTP concentrates is the first preview of selective separation based on collector, and the lower arsenic content than expected of the DTP concentrates may relate to the lower gold recovery than expected from the previous subsection, and is revisited after more data is presented.

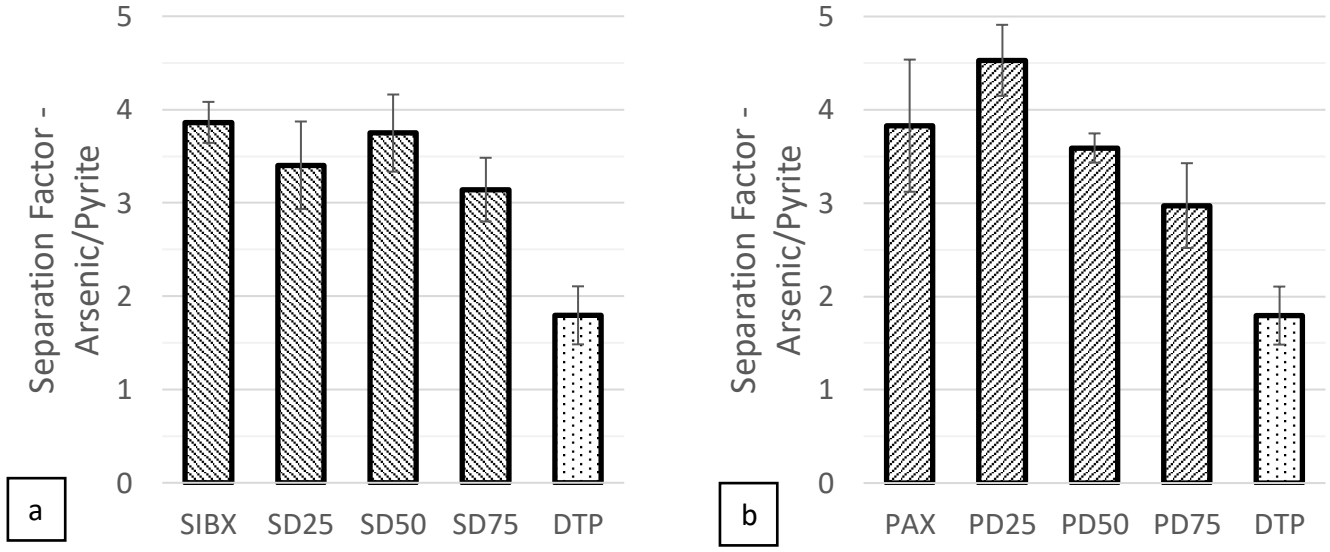


Figure 45: Separation factor of Arsenic from Pyrite in Batch flotation. Base metal assay data

SD25 is seen to have the lower Separation Factor than SIBX and PAX alone. This is because SD25 recovered the most pyrite in total with the greatest mass pull, meaning the Separation Factor decreases as more of the total pyrite was rendered hydrophobic and recovered, as not only the pyrite with high arsenic content was recovered, but also pyrite with lower arsenic content. The second highest pyrite recovery of PD75 supports this observation, as SD75 also had a lower Separation Factor than the SIBX and PAX cases. In the other cases, a much smaller portion of the pyrite was recovered, as only a portion of the more hydrophobic pyrite was floated, and selective attachment of collector could be better quantified. This is not however the same reason that the DTP separation factor being lower, as these three experiments had low pyrite recoveries, so the recovered pyrite was selected for hydrophobicity over the unrecovered pyrite.

### *4.2.7 QXRD*

QRD samples of the three single collector runs were sent for analysis in order to semi-quantitatively determine the ratio of pyrite to arsenopyrite in the samples. The pyrite grades from the QXRD reports slightly higher values than calculated in Section 4.2.5.1, however the values from QXRD show large uncertainty parameters, possibly because of the semi quantitative nature of the analysis and because the values are close to the 1wt% detection limit. The value for DTP's arsenopyrite is reported, although below the detection limit, and was possibly extrapolated, even though the uncertainty is very low.

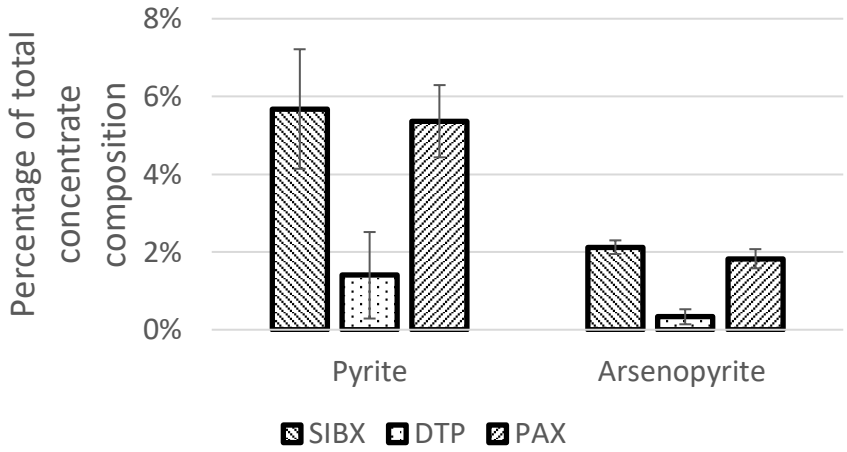


Figure 46: QXRD data for SIBX, DTP and PAX of pyrite and arsenopyrite composition of concentrates

The QXRD data can be used to construct $SF_{arsenopyrite/pyrite}$ values to compare the selective flotation of Pyrite and arsenopyrite, but because of the high uncertainty in the pyrite and arsenopyrite the uncertainty in the Separation Factor values mean that they are not significant when compared to each other, as seen in Figure 47 and at most the trend of SIBX and PAX having a higher $SF_{arsenopyrite/pyrite}$ than DTP. The values of this $SF_{arsenopyrite/pyrite}$ show the same trends when comparing the separation factors of $SF_{arsenic/pyrite}$ from Section 4.2.6, although the separation factors presented here for the xanthate cases are much lower (though still above 1).

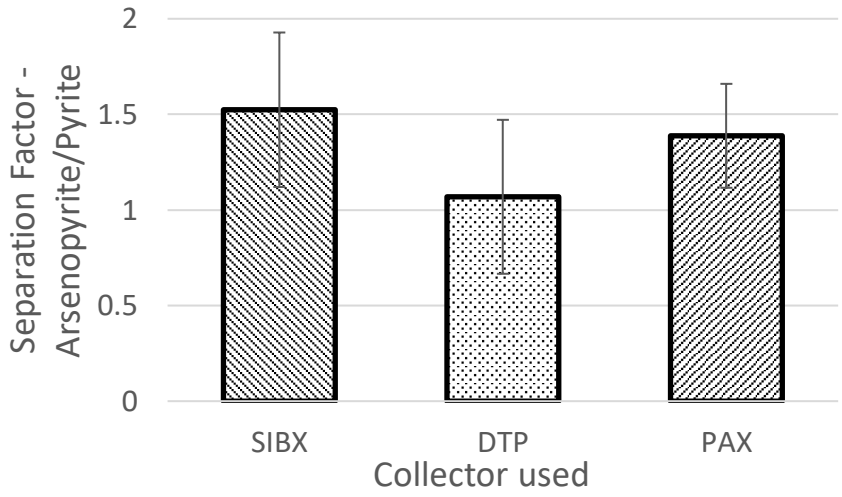


Figure 47: Separation Factor of arsenopyrite versus pyrite in SIBX, PAX and DTP in the batch flotation experiments, QXRD data

The difference between the two cases is that Figure 47 lists separation factors based on arsenopyrite, while Figure 45 is based on Arsenic. The arsenic content of the feed and concentrates consist not only of arsenopyrite, but also arsenian pyrites that have arsenic content but still would report as pyrite (and not arsenopyrite) in QXRD analysis. Selective recovery of this pyrite with significant weight percentage of arsenic would further skew the of SF $_{arsenic/pyrite}$ towards higher values as it carries arsenic away from the feed to the concentrates, while simultaneously decreasing the values of SF $_{arsenopyrite/pyrite}$ as more “pyrite” would register under QXRD for the concentrates. Further investigation into the complete distribution of arsenic in pyrite grains is conducted in the SEM analysis (Section 4.2.9).

### *4.2.8 Optical Microscopy*

The target of the optical microscopy section is to produce semi quantitative results on the relative distribution of minerals in the study for the different collectors. Because the relative distributions of arsenopyrite and pyrite are quantified in optical microscopy for the feed and concentrate ( including tailings), the separation factor of SF $_{arsenopyrite/pyrite}$ can be calculated for each of the pure collector cases.

In all the cases, conglomerates are not well recovered to the concentrates. This is because even though the conglomerate particle contains pyrite, the surface of the particle is a mixture between gangue and pyrite, and only certain portion of the surface could be rendered hydrophobic by collectors.

The trends seen in the SF $_{arsenopyrite/pyrite}$ from the QXRD section is seen to continue in this section in Figure 48, Figure 49, and Figure 50. The xanthates performed extremely similarly, having SF $_{arsenopyrite/pyrite}$ of 1.37 for SIBX and 1.36 for PAX, values over 1 which show the selective flotation of arsenopyrite over pyrite. DTP exhibited a SF $_{arsenopyrite/pyrite}$ of 0.86, which shows that the selective flotation of pyrite took place, and arsenopyrite was not recovered well.

For the cases of SIBX and PAX, it was also seen that the concentrates recovered more of the particles with mixed arsenopyrite and pyrite regions as well. If arsenopyrite was being selectively floated, these particles would be rendered more hydrophobic based on their arsenopyrite content as well.

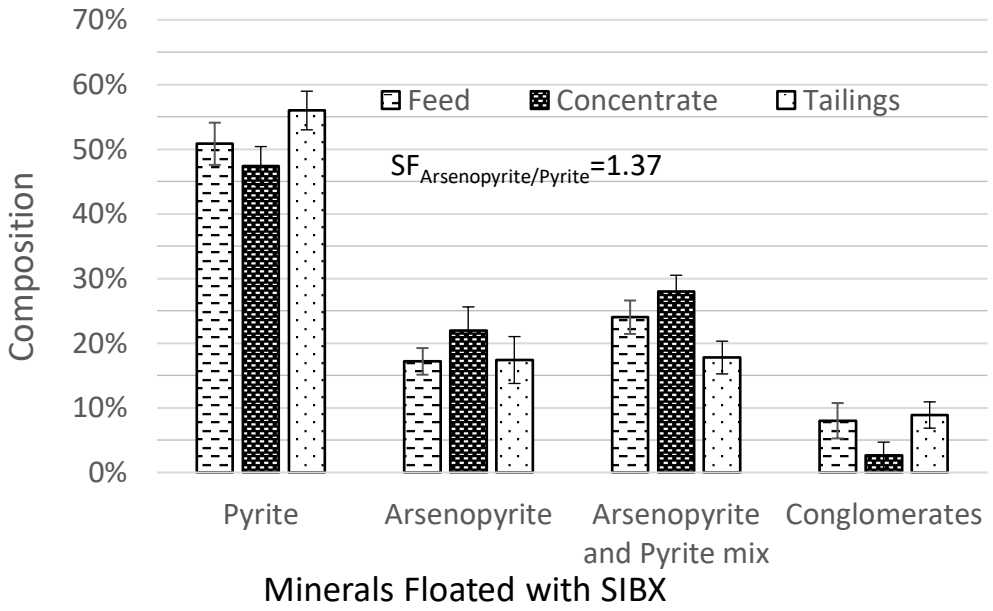


Figure 48: Optical Microscopy of mineral class composition of concentrates in SIBX experiment

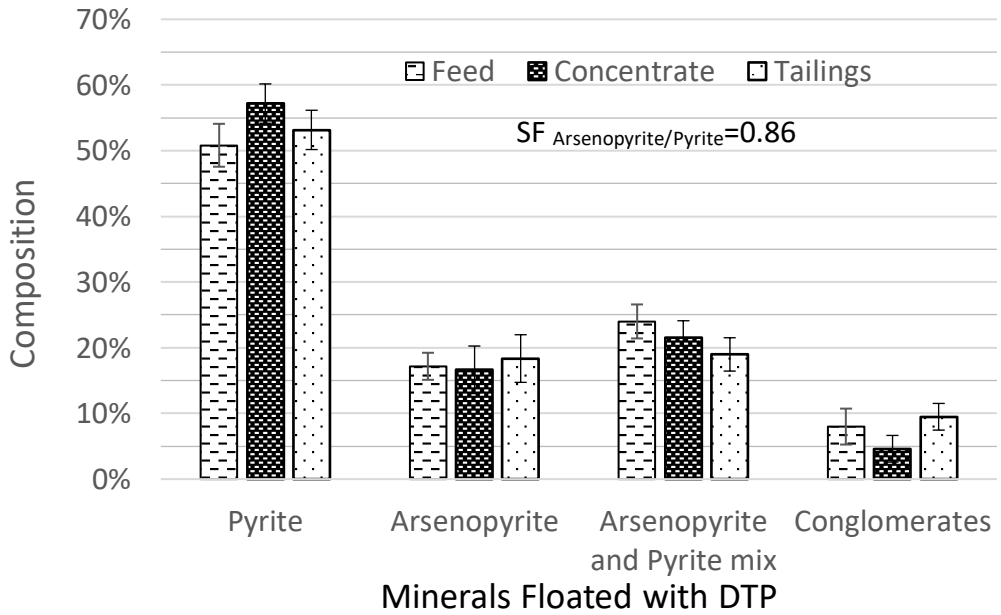


Figure 49: Optical Microscopy of mineral class composition of concentrates in DTP experiment

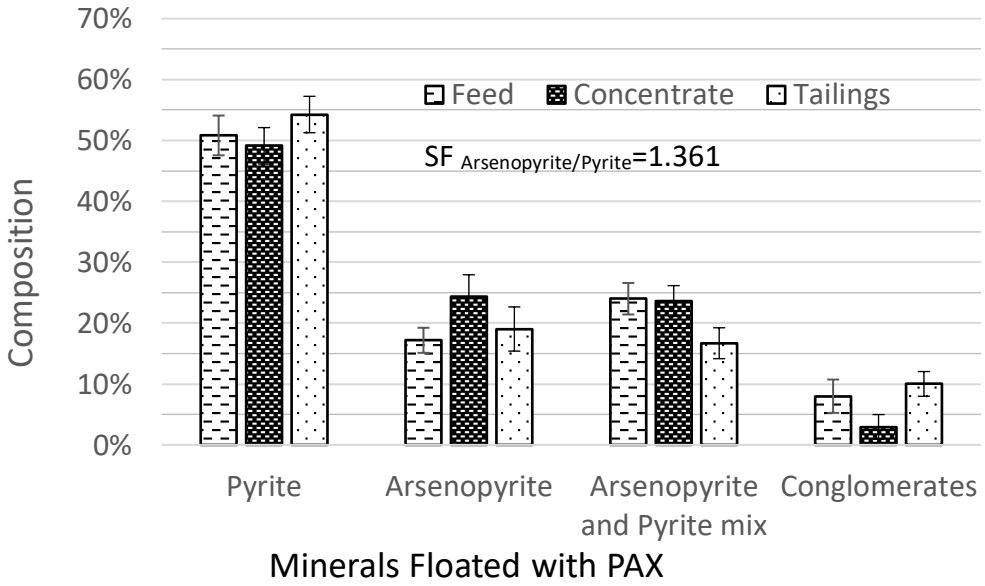


Figure 50: Optical Microscopy of mineral class composition of concentrates in PAX experiment

### *4.2.9 SEM*

The figures in this section are again presented in pairs, but this time the figure on the left is the compositional distribution of the concentrate sample, while the figure on the right is the compositional distribution of the tailings. Below the figures, the tables for both the concentrate and tailing of the experimental runs are presented to view the data of the average weight percentage and occurrence of the elements.

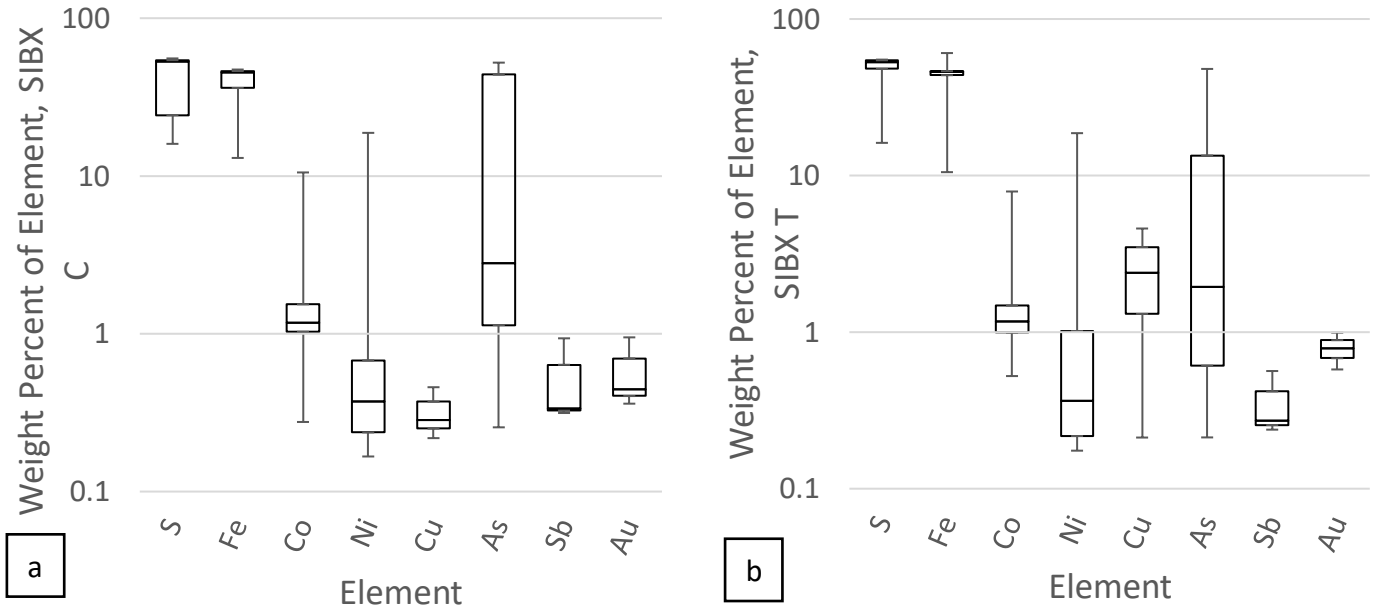


Figure 51: SEM EDS data of pyrite particles, SIBX concentrate versus SIBX Tailings

The discussion on the compositional variations of pyrite grains begins with arsenic content. When Figure 51 is consulted, the observation can be made that the arsenic content in the concentrates is skewed to the upper weight percentages of the arsenic range when compared to the arsenic box and whisker of the tailings. When the arsenic data of Table 16 and Table 17 is compared, it is seen that arsenic content shows up in the concentrates more often (88.68% compared to 78%) and at a much higher weight percentage average (16.598 wt% compared to 12.376 wt%). This further strengthens the argument of pyrite with higher arsenic content being selectively floated over pyrite with lower arsenic content that were presented by previous sections. The value of this section is that it shows not only arsenopyrite is selectively recovered, but also arsenian pyrites.

Table 16: SEM EDS data of pyrite particles, SIBX Concentrates

| SIBX C | S | Fe | Co | Ni | Cu | As | Sb | Au |
|---|---|---|---|---|---|---|---|---|
| **Average wt% when element is present** | 43.871 | 41.066 | 1.999 | 1.996 | 0.320 | 16.598 | 0.529 | 0.585 |
| **Percent of spots with element** | 100.00 % | 100.00 % | 37.74% | 43.40% | 5.66% | 88.68% | 5.66% | 5.66% |

Table 17: SEM EDS data of pyrite particles, SIBX Tailings

| SIBX T | S | Fe | Co | Ni | Cu | As | Sb | Au |
|---|---|---|---|---|---|---|---|---|
| **Average wt% when element is present** | 46.979 | 42.951 | 2.101 | 3.499 | 2.402 | 12.376 | 0.358 | 0.785 |
| **Percent of spots with element** | 100.00 % | 100.00% | 36.00% | 32.00% | 4.00% | 78.00% | 6.00% | 4.00% |

When looking at other compositional variations, it is important to note that the dominant variation in the pyrite composition was that of arsenic. Particles with other impurities rarely existed without arsenic also being present, as on average 90% of particles in the case study ore had some arsenic content present.

The other significant difference to be seen when SIBX was used as a collector is with copper. Copper is known to be beneficial in flotation circuits and is often used as an activator by adding copper salts such as copper sulphate to the system. Minerals with copper impurities has also been shown to be recovered by flotation better than those without, and this was attributed to the release of these copper ions from the mineral into solution to aid in activation. In this study, it was seen that in the case when SIBX was used as a collector, particles with high copper content reported to the tailings. If the case was made where copper ions in solution would activate the pyrite, the copper ions from the copper rich particles would be in solution and activate any mineral it comes into contact with, not just the original source of the copper. The variation in the electronic properties due to the presence of the copper would play a more significant role in whether the particle was recovered, and in the case where SIBX was used as a collector, the particles that had a copper content were more likely to not get recovered, as seen by the box and whisker diagrams in Figure 51 of copper in the concentrate being skewed towards the lower weight percentages compared to copper in the tailings. The information in

Table 16 and Table 17 confirm this, with the average copper content, when present, of 0.32 wt% in the concentrates compared to 2.4 wt% in the tailings.

The higher sulphur content of the tailings of the SIBX collector experiment (46.979 wt% compared to 43.871 wt%) is due to the decreased arsenic content of the tailings. Arsenic substitutes for sulphur in the pyrite structure, resulting in less sulphur present in the concentrates as the concentrate has a higher arsenic content.

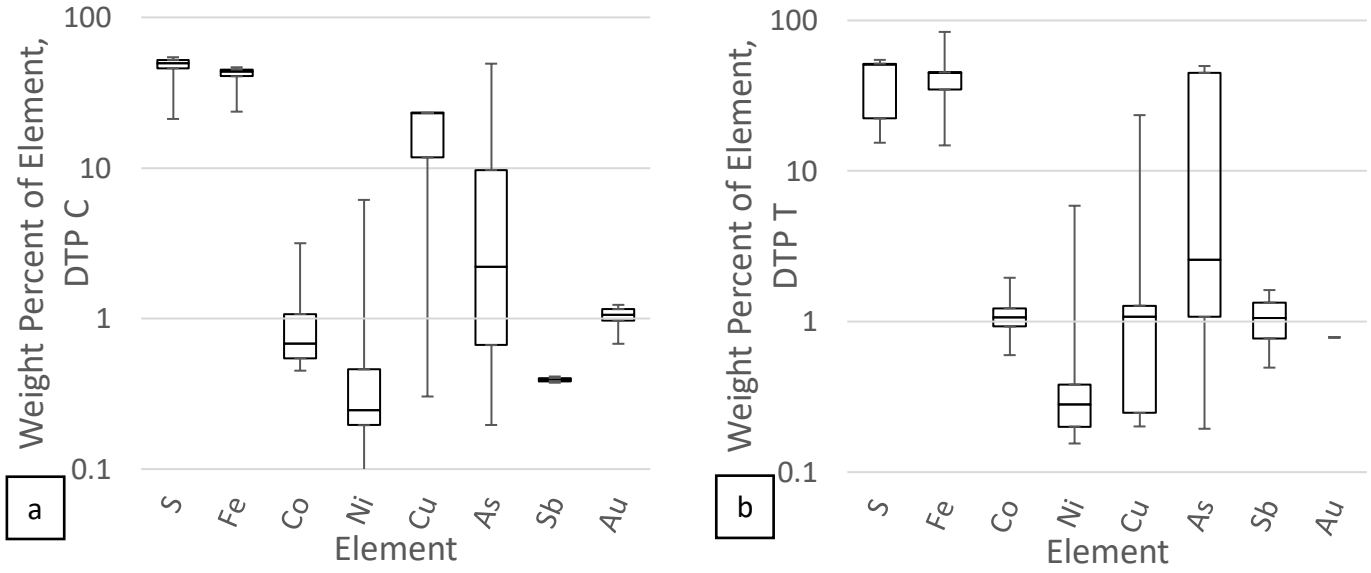


Figure 52: SEM EDS data of pyrite particles, DTP concentrate versus DTP Tailings

Again, the data for the DTP collector experimental run is opposite that to SIBX (and PAX, shown next). In

Figure 52, the arsenic content in the concentrate is significantly lower than the arsenic content in the tailings. This supports data of previous sections, showing that pyrite with a higher arsenic content was not recovered as well as arsenic with a lower or no arsenic content.

The data in Table 18 and Table 19 show this further, with an average arsenic content of just 10.985 wt% in the concentrate, the lowest of any sample tested. In the concentrates where DTP was used as the collector, 92.68% of particles still had some arsenic content, but the average content was much lower and this is reflected in the box and whisker plot of Figure 52 and the lower arsenic average.

Table 18: SEM EDS data of pyrite particles, DTP Concentrates

| DTP C | S | Fe | Co | Ni | Cu | As | Sb | Au |
|---|---|---|---|---|---|---|---|---|
| **wt% average when present** | 44.706 | 41.533 | 0.930 | 0.992 | 15.559 | 10.985 | 0.393 | 1.018 |
| **Percent of spots with element** | 100.00 % | 100.00% | 46.34% | 41.46% | 7.32% | 92.68% | 4.88% | 12.20% |

Table 19: SEM EDS data of pyrite particles, DTP Tailings

| DTP T | S | Fe | Co | Ni | Cu | As | Sb | Au |
|---|---|---|---|---|---|---|---|---|
| **wt% average when present** | 41.060 | 41.342 | 1.108 | 0.551 | 5.260 | 17.602 | 1.057 | 0.785 |
| **Percent of spots with element** | 98.98% | 100.00% | 33.67% | 34.69% | 5.10% | 90.82% | 2.04% | 1.02% |

Also opposite to the results of the experimental run where SIBX was used as the collector, particles with a high copper weight percent was recovered. This is observed the box and whisker diagram of copper for the concentrates of the DTP collector experiment is massively skewed to the particles with a higher copper weight percentage. The recovery of high copper weight percentages pyrite when DTP was used as a collector is verified by the data in Table 18 and

Table 19, where only 7.32% of particles have copper content, however these particles have a much higher copper content than the copper containing particles in the tailings (15.559wt% in the concentrates versus 5.26 wt% in the tailings).

DTP was shown to not attach to or recover pyrite nearly as well as xanthates, but did recover chalcopyrite extremely well in micro-flotation experiments (Zhong et al., 2015). Chalcopyrite is a completely different mineral than pyrite but can be viewed as a pyrite with an extreme case of copper substitution. It can therefore be understood why DTP also recovers pyrite with a high copper content so readily in the case study ore.

Figure 53 shows the box and whisker plots of the data from the flotation experiments that used PAX as a collector. Once again, the data for the experiments that used PAX are similar to the ones that used SIBX. Higher arsenic content pyrite is shown to be recovered over the pyrite with a lower arsenic content, which is backed up by the data in Table 20 and Table 21, with the average arsenic content when it is present of 14.515 wt% in the concentrates compared to 12.536 wt% in the tailings. Although the average values for arsenic weight percentage is a when comparing PAX concentrate to tailings shows significant difference, the concentrate average for PAX (14.515 wt%) is lower than that of SIBX (16.598 wt%) and the tailing arsenic weight percentage is higher when PAX was used as a collector (12.536 wt%) when compared to SIBX (12.376 wt%). Although similar to PAX, this shows that SIBX is more selective towards the higher arsenic content pyrite than PAX.

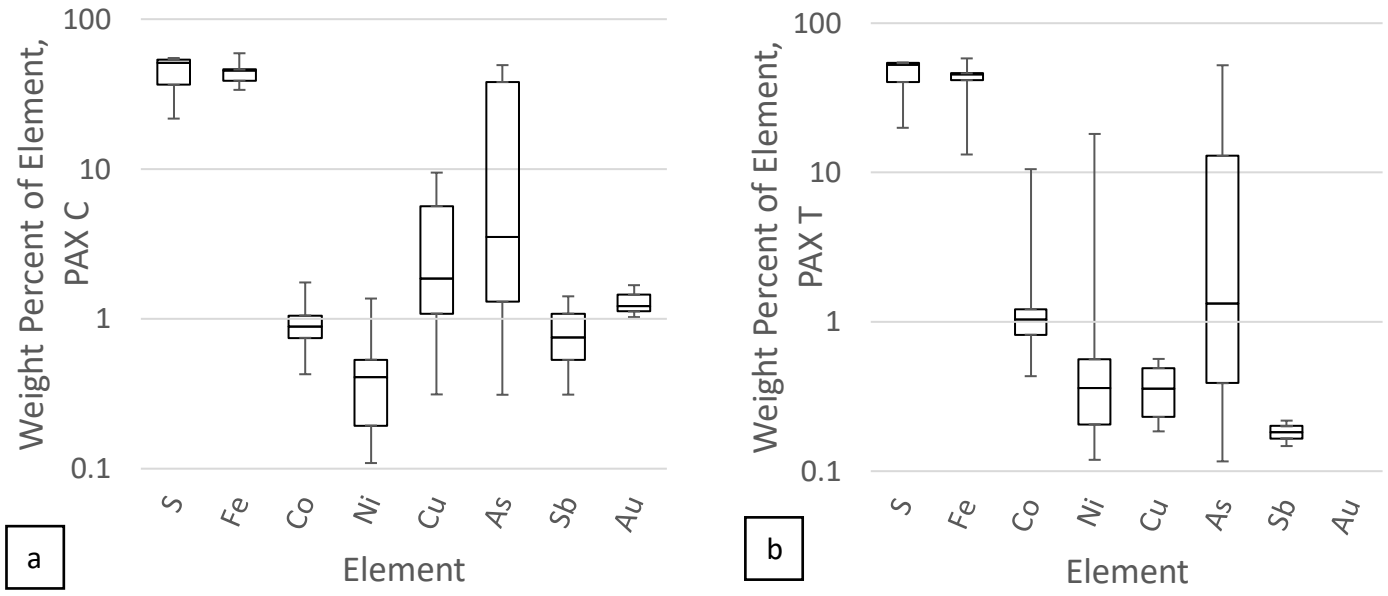


Figure 53: SEM EDS data of pyrite particles, PAX concentrate versus PAX Tailings

Table 20: SEM EDS data of pyrite particles, PAX concentrates

| PAX C | S | Fe | Co | Ni | Cu | As | Sb | Au |
|---|---|---|---|---|---|---|---|---|
| **wt% average when present** | 45.013 | 43.191 | 1.684 | 0.434 | 3.876 | 14.515 | 0.826 | 1.306 |
| **Percent of spots with element** | 100.00 % | 100.00% | 37.25% | 43.14% | 5.88% | 90.20% | 5.88% | 5.88% |

Table 21: SEM EDS data of pyrite particles, PAX Tailings

| PAX T | S | Fe | Co | Ni | Cu | As | Sb | Au |
|---|---|---|---|---|---|---|---|---|
| **wt% average when present** | 45.235 | 42.252 | 0.908 | 1.851 | 0.365 | 12.536 | 0.183 | N/A |
| **Percent of spots with element** | 100.00 % | 100.00% | 36.07% | 29.51% | 6.56% | 91.80% | 3.28% | 0.00% |

From Figure 53, Table 20 and Table 21, the other two differences that are evident are higher nickel weight percent average in the tailings, however looking at the box and whisker diagrams in Figure 53, the midrange of data was not skewed for nickel, but a one or a few outliers of high nickel weight percentage caused high maximum of Ni in Figure 53 (b), which impacted the average of Ni in Table 21 . The outlier of high nickel content was likely pentlandite or a grain close to pentlandite.

### *4.2.10 Pourbaix Diagram*

The Pourbaix diagrams for the ethyl xanthate and ethyl dithiophosphate system (Figure 3) were overlaid with the conditions measured during the experimental runs to form Figure 54. Although the chain lengths of the collectors that were used to generate the figures are not all the same as in the study, the functional groups still remain the same and conclusions can still be drawn about the state and flotation domains that the experiments existed in.

Figure 54 below shows the Eh and pH region of the conducted experiments in batch flotation. All experiments were in the range of a pH of 9.3 to 9.6 with no trend between them, so the left and right organisation of the values are placed in the same range but are not significant. The SIBX-DTP system is displayed on the left and PAX-DTP on the right of one another for clarity in Figure 54.

In the context of this discussion the work of Lotter et al., (2016), as reviewed from literature in Section 0, related the attachment of dixanthogen (and by extension dithiophatogen) to n-type (negative) semiconductors via hydrogen bonding. The collector radicals, being negatively charged, would adsorb more readily onto positive surfaces or p-type semiconductors. The inclusion of other elements into the pyrite structure, such as arsenic, was shown in literature to change the pyrites semiconductor properties from its normally n-type to a p-type semiconductor.

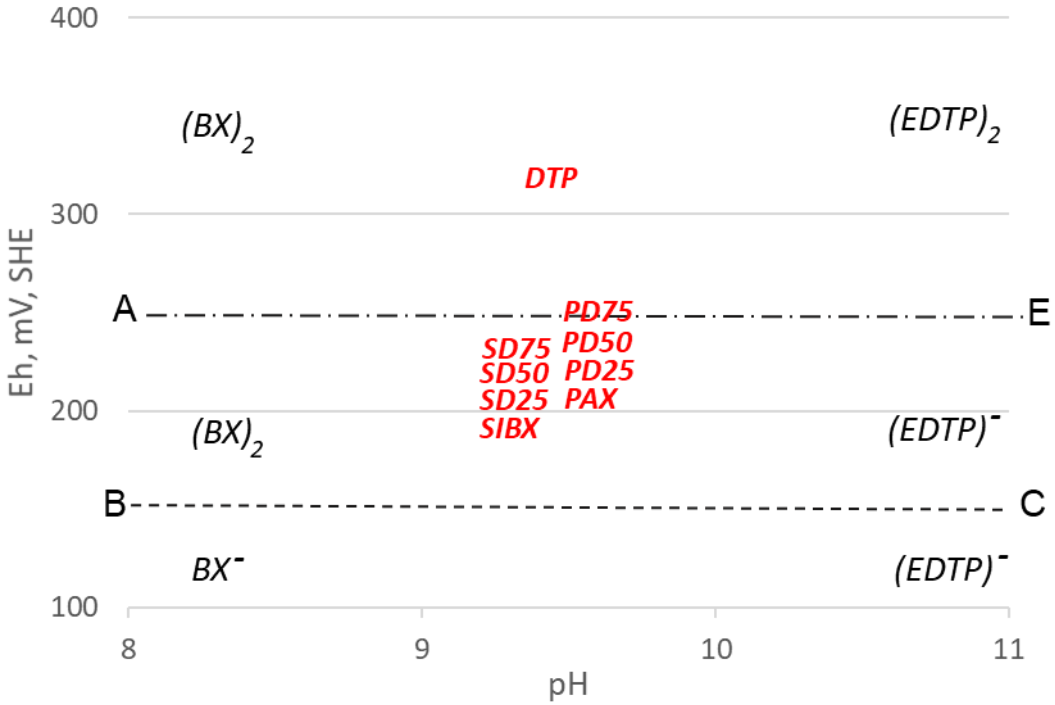


Figure 54: Pourbaix diagram of pyrite, xanthate and DTP with experimental conditions overlaid

For the mixed collector systems of both SIBX-DTP and PAX-DTP, the experimental conditions were measured to be in the “desired operability” region of ABCE. In this region, both a dixanthogen and thiolate radical would exist in the pulp, and in theory, both n-type semiconductors and p-type semiconductors would be amenable to collector attachment and thus both would be recovered, leading to an overall increase in recovery over the single collectors alone. This was reflected in the experimental results.

The DTP collector system is the outlier when compared to the large grouping of other experimental conditions. The flotation collector system with DTP as a collector was measured to have an average Eh of 321 mV, which put it in the flotation domain of dithiophatogen. The batch flotation experiments that used DTP as a collector were found to selectively recover pyrite over arsenian pyrites and arsenopyrite. The reason that is attributed to the selective flotation of pyrite over arsenopyrite is that the pulp conditions favoured the dithiophatogen formation and attachment to pyrite (as a n-type semiconductor) over that of attachment to arsenopyrite and arsenian pyrites (which would have exhibited p-type semiconductor properties). The pyrite was thus rendered more hydrophobic and recovered over the pyrite with arsenic content.

The xanthates used in the study showed measured pulp potentials of 136 mV for SIBX and 214 mV for PAX. These pulp potentials both fell in the region of dixanthogen formation. From literature, dixanthogen formation leads to better hydrophobicity and flotation recovery, even though it was established that direct dixanthogen attachment onto the mineral surface would favour minerals that were n-type semiconductors, but it was seen in this project that both the xanthates selectively floated arsenopyrite and arsenian pyrites. This is not what was expected, and no simple explanation could be provided. The cause of this could be related to the attachment process of dixanthogen, where in the cases of the highest hydrophobicity, Yalcin and Kelebek, (2011) and Xiang-Huai and Forssberg, (1991) showed that dixanthogen in the pulp co-adsorbed into another layer with xanthates that already attached to the mineral surface. The initial adsorption of xanthate to the mineral surface could have been favoured onto minerals with p-type semiconducting properties, then allowing dixanthogen to form or co-adsorb onto these minerals and recovering them.

The mechanisms of collector adsorption and the phase of the collector on the different surfaces could be better studied in the case of the real ore used in batch flotation.

## 4.3 Investigation of differences in pyrite flotation of samples with different compositional variations by floating them in a microflotation cell, using the same collector mixtures as used in batch flotation

### *4.3.1 Characterisation of Pyrite Samples*

The two different pyrite samples used in this study were characterized using SEM and XRF to find the compositional variation of the pyrite to be floated in the micro-flotation cell.

#### *4.3.1.1 XRF Oxides*

XRF of the two pyrite samples, labeled “Pyrite 1” and “Pyrite 2” are given in Table 22 below.

The major differences between the two pyrite samples is that $SiO_2$ content was seen in Pyrite 2 compared to pyrite 1. Silica ($SiO_2$) formed 6.53 weight percent of pyrite 2. When pyrite 2 was pulverized down to the correct size fraction to be used in the experiments, the silica was seen in SEM imaging to not be compositional variations of the pyrite, but discreet grains of silica that do not impact the pyrite grains that are to be floated. As a result of the silica content, the maximum recovery of pyrite 2 will be capped to 93.47% because silica should not float out of the micro-flotation cell. The other element oxides listed

for pyrite 2 may be hosted in the silica gangue phase and not the pyrite phase so cannot be definitively allocated to compositional variations within pyrite 2. SEM analysis that followed the XRF would more confidently allocate variations in the pyrite structure, but the XRF was still valuable to see that pyrite 1 contained no silica content while pyrite 2 did.

Table 22: XRF data of micro-flotation pyrites

| | $Al_2O_3$ (%) | CaO (%) | $Cr_2O_3$ (%) | $Fe_2O_3$ (%) | $K_2O$ (%) | MgO (%) | MnO (%) | $Na_2O$ (%) | $P_2O_5$ (%) | $SiO_2$ (%) | $TiO_2$ (%) |
|---|---|---|---|---|---|---|---|---|---|---|---|
| Pyrite 1 | 0.03 | 0.30 | 0.08 | 65.57 | 0.01 | 0.03 | bdl | 0.01 | 0.03 | 0.01 | 0.01 |
| Pyrite 2 | 0.53 | 0.03 | 0.05 | 61.64 | 0.12 | bdl | bdl | 0.03 | 0.02 | 6.53 | 0.03 |

#### *4.3.1.2 BET Surface Area*

The BET surface area was reported to be 1.28 $m^2/g$ for pyrite 1 and 1.32 $m^2/g$ for pyrite 2. Since both samples were of the same size class (38-53µm) and exhibited surface area results that were within 3% of each other, the influence of shape factors (such as particle roundness) could be assumed to be negligible when comparing the flotation results of the two samples.

The average surface area of 1.3 $m^2/g$ was used to calculate the mass of xanthate that needed to be added to achieve the 50% monolayer surface coverage of collector. This calculation can be seen in Appendix B.

#### *4.3.1.3 SEM*

SEM EDS of the pyrite samples reveals the compositional variations of the pyrite, just as in the batch flotation section. 20 different elements were searched for, but it was found that the only significant elements (above 0.1 wt%) were the primary pyrite constituents (iron and sulphur), along with copper, lead and cobalt.

Pyrite 1's compositional variations are displayed in Figure 55 and Table 23 below.

The iron and sulphur content of the pyrite grains are tightly constrained, as the entire sample is from one crystal grouping. Compositional variations include a small amount of copper (33.33% particles at an average of 0.15wt%) and more widely spread amounts of lead (66.67% of particles, at an average of 0.51 wt%).

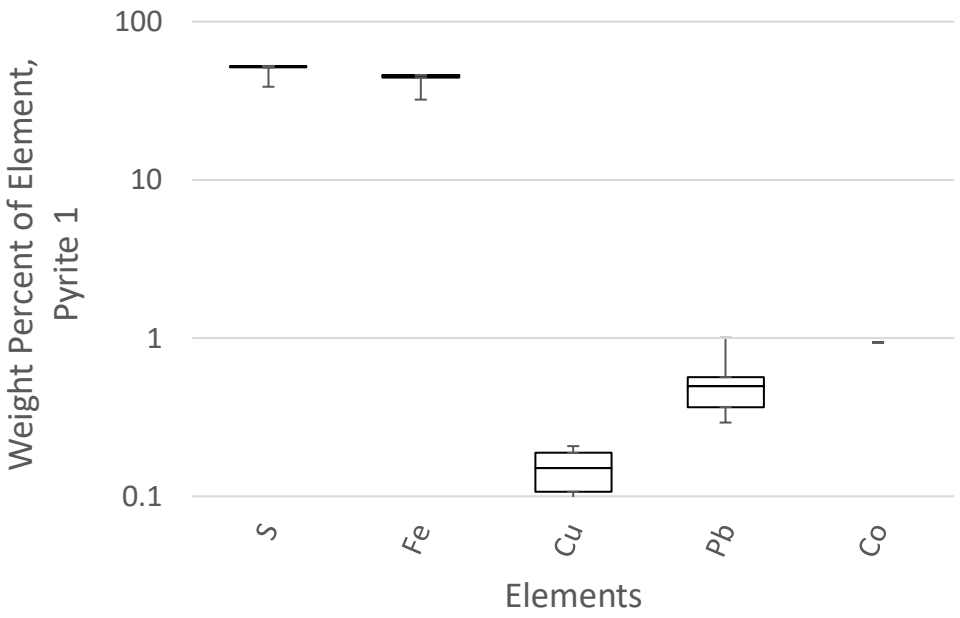


Figure 55: SEM analysis of Pyrite 1 sample

Table 23: SEM EDS data of Pure Pyrite 1 sample

| Pyrite 1 | S | Fe | Cu | Pb | Co |
|---|---|---|---|---|---|
| **wt% average when present** | 50.287 | 44.037 | 0.150 | 0.510 | 0.940 |
| **Percent of spots with element** | 100.00% | 100.00% | 33.33% | 66.67% | 5.56% |

Pyrite 2's grains were targeted for compositional information and only cobalt was seen as a significant compositional variation in pyrite 2. In 18.92% of samples, cobalt was seen at an average weight percentage of 1.156 wt%.

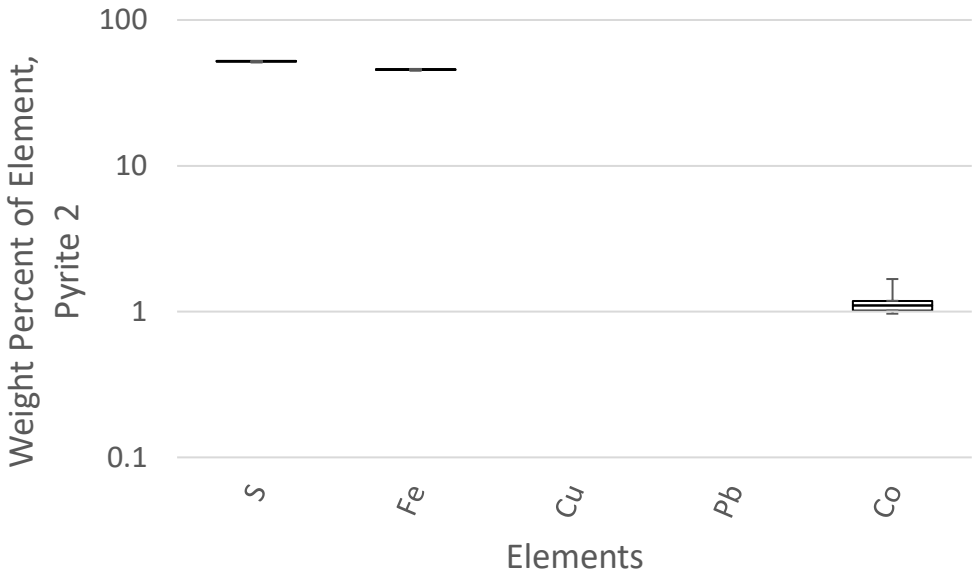


Figure 56: SEM analysis of Pyrite 2 sample

Table 24: SEM EDS data of Pure Pyrite 2 sample

| Pyrite 2 | S | Fe | Cu | Pb | Co |
|---|---|---|---|---|---|
| **wt% average when present** | 51.791 | 45.548 | N/A | N/A | 1.156 |
| **Percent of spots with element** | 100.00% | 100.00% | 0.00% | 0.00% | 18.92% |

What was thought to be the gangue particles of silica was also targeted for compositional information, and it was confirmed what gangue particles existed of $SiO_2$. The gangue and pyrite were fully liberated from each other, and only 20% of the gangue grains contained some traces of pyrite, but lower than 1 wt%. a small amount of potassium was also found in the gangue.

| Pyrite 2 Gangue | Si | O | Fe | S | K |
|---|---|---|---|---|---|
| **wt% average when present** | 44.513 | 54.971 | 0.197 | 0.371 | 0.104 |
| **Percent of spots with element** | 100.00% | 100.00% | 20.00% | 20.00% | 26.67% |

#### *4.3.1.4 Trace elements using XRF*

Trace elements were reported via XRF analysis and is shown in Table 25 below. The entry of "bdl" designates "below detection limit".

Table 25: Trace element analysis via XRF of Pyrite samples used in micro-flotation

| | Cu | Pb | Co | Ni | Ti | La | Cl | Sr | V |
|---|---|---|---|---|---|---|---|---|---|
| **Pyrite 1** | 407 | 1218 | 572 | bdl | 59 | 53 | 7 | 12 | 3 |
| **Pyrite 2** | 28 | 14 | 920 | bdl | 170 | 50 | 3 | 9 | bdl |

The XRF analysis agrees with the data from SEM EDS analysis with regards to the elements present and the distribution of them.

The compositional variations in the pyrite samples obtained for microflotation were expected to be less than that of the batch flotation ore, as these pyrite samples were of high purity and originated from single crystals. This higher purity and lower compositional variations were seen in both pyrite 1 and pyrite 2 with an average weight percentage between 0.1 wt% and 1.5 wt% of elemental substitutions when they were present. The effect of this compositional variations was tested by comparing the flotation response of each sample to each other to see if significant differences could be seen. The differences in their flotation response between pyrite 1 and pyrite 2 was compared to the results obtained from batch flotation where more pronounced differences in compositional variation of the pyrite grains existed.

#### *4.3.1.5 Zeta Potential*

Zeta potential measurements of the experimental pyrite are compared to literature values of pyrite from Section 2.11 in Figure 57 below. The average of literature values from Figure 7 are displayed as circles in Figure 57 and the lines are omitted for clarity on the trends of the experimental pyrite. The characteristic sigmoid shape was seen more in pyrite 1 than pyrite 2, although the lack of the characteristic shape could be due to a larger gap between the pH values tested. Even though the characteristic shapes were not seen, values for the pH for both pyrites were within literature values, except Pyrite 2 was slightly lower than literature in the pH 2 to 3 range. Pyrite 1 displayed a consistently higher zeta potential than pyrite 2 across the whole pH range.

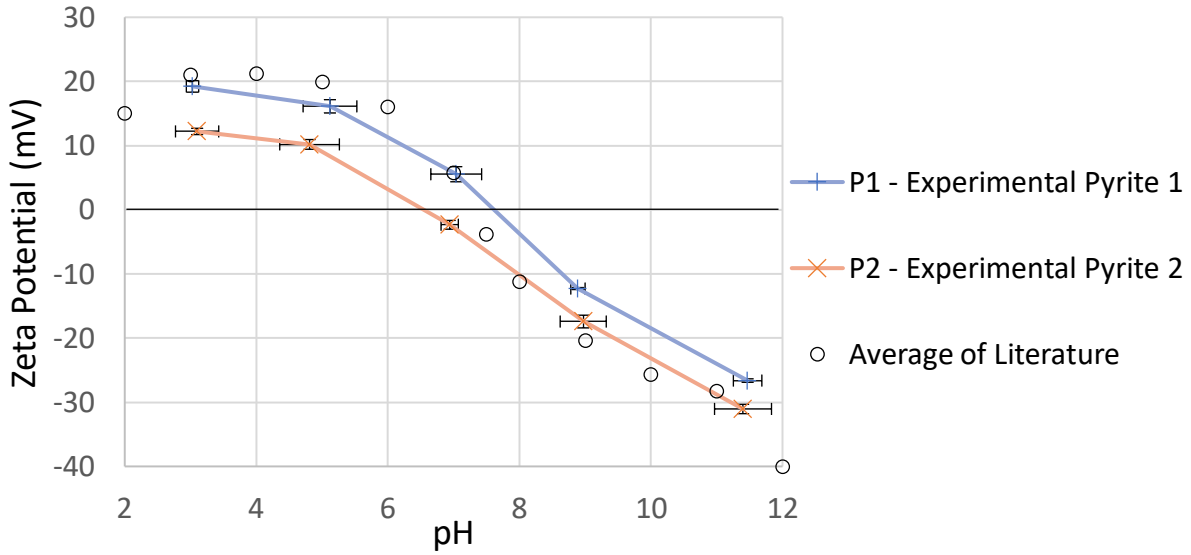


Figure 57: Zeta potential of Experimental pyrite 1 and 2 compared to literature values

Zeta potential tests were also carried out on both of the pyrite samples using the collectors and collector mixtures. The results are displayed in Figure 58, Figure 59, Figure 60 and Figure 61 on the next page. Error bars were excluded for clarity as the error in Zeta potential in Figure 57 were not significant in their magnitude. The calculated error for each data point can be viewed in Appendix D, under the Zeta Potential Heading.

Micro-flotation took place at a pH of 9, so discussion around the zeta potential will be concentrated on this value. It is important to note that DTP did not change the zeta potential significantly in either of the samples. In Pyrite 1, SD25 caused the biggest difference at a pH of 9, followed by pure SIBX, both being lower than the pure pyrite 1.

In pyrite 2, PD25, PD50 and PD75 all had very similar zeta potentials, lower than the pure pyrite as well.

Looking at the range of the changes in zeta potential, pyrite 1 had a larger change in zeta potential for the SIBX-DTP system than the PAX-DTP system, while pyrite 2 had a larger change for the PAX-DTP system than the SIBX-DTP system. This can be seen by looking at the width of the line bundles in the figures on the following page.

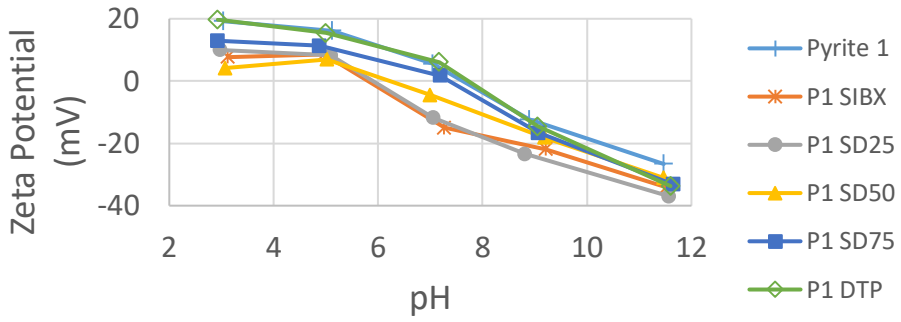


Figure 58: Zeta Potential of Pyrite 1, SIBX and DTP mixtures

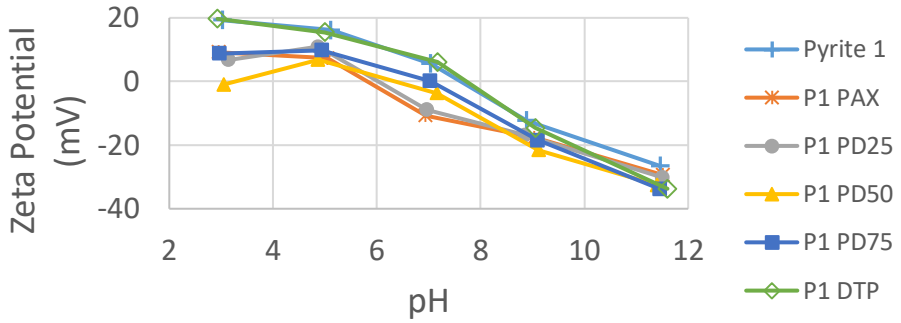


Figure 59: Zeta Potential of Pyrite 1, PAX and DTP mixtures

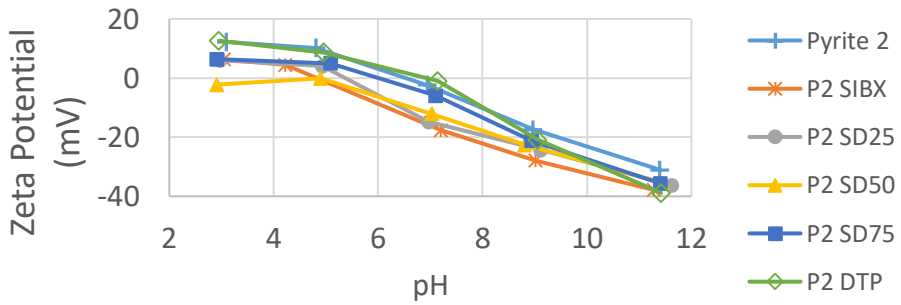


Figure 60: Zeta Potential of Pyrite 2, SIBX and DTP mixtures

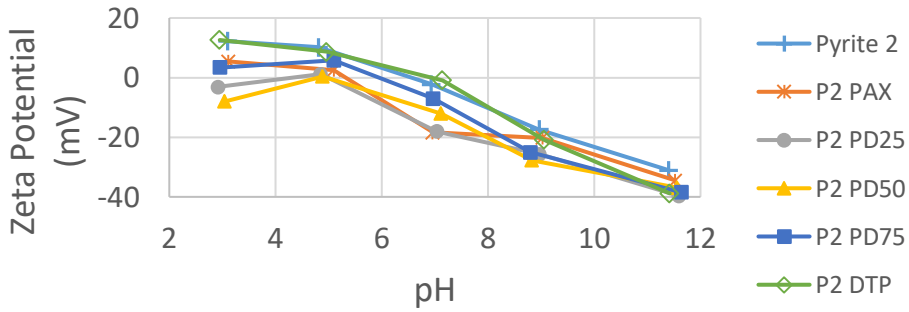


Figure 61: Zeta Potential of Pyrite 1, PAX and DTP mixtures

### *4.3.2 Mass Recovery*

#### *4.3.2.1 Discussion on cumulative recovery and model application*

This subsection is structured to visualise the characteristic trends of a micro-flotation experiment together with how the first order model for flotation is applied to the data generated from all the experiments.

For clarity, this subsection uses just the data from pyrite 1 and the pure collector runs, and omits error bars as the trends are the focus.

Figure 62 below shows the cumulative mass recovery at the cumulative flotation time of pyrite 1 where no collector was used, as well as the micro-flotation with the three collectors were applied alone. The instantaneous gradient at any point of a model or trend fitted to these graphs would yield the instantaneous rate of flotation.

The trends for each experiment follow the standard shape for the first order model, which is first exhibiting a large gradient as the faster floating material is recovered, and the gradient tapering off as the faster floating material in the pulp is depleted. Since the same representative pyrite samples were used for each of the experiments shown in Figure 62, differences in both the recovery and rate of flotation are due to collector influences on increasing the hydrophobicity (and thus recovery) from the base case of no collector.

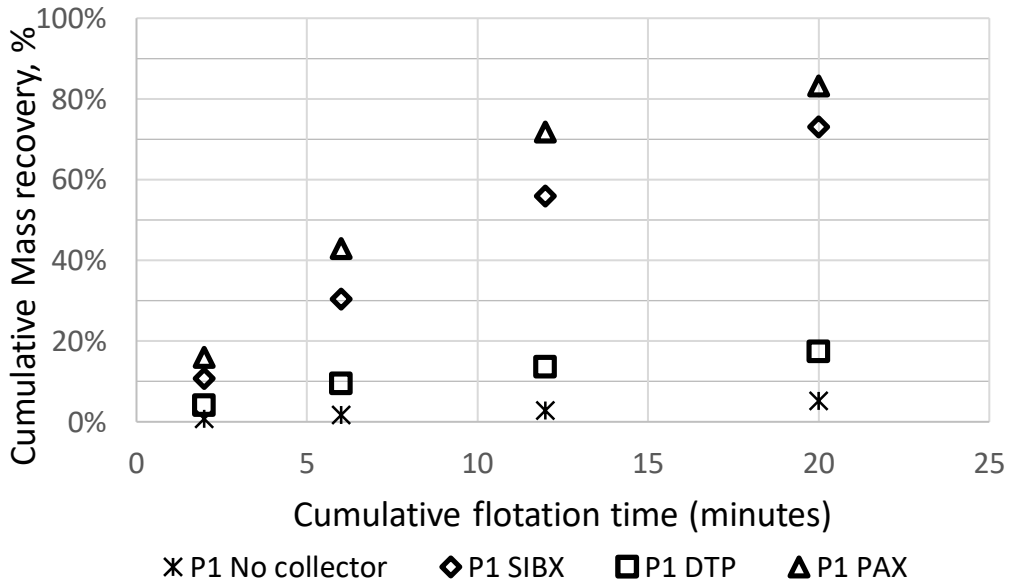


Figure 62: Cumulative mass recovery of select experiments

In order to apply the first order model of $\mathrm{R} = \mathrm{R}^{\infty}(1 - exp(-kt))$ to the system, the method as put forward in Section 3.3.2.3 was followed. Points of the lines of the linearised factor of $(-ln\left(\frac{R^{\infty}-R}{R^{\infty}}\right))$ versus $t$ were plotted. The value of $\mathrm{R}^{\infty}$was then regressed to yield the best fitting linear relationship. The result of the process of plotting the linearised factor versus t, regressing $\mathrm{R}^{\infty}$ for the best value of $\mathrm{R}^2$ and the linear fits are displayed in Figure 63 below.

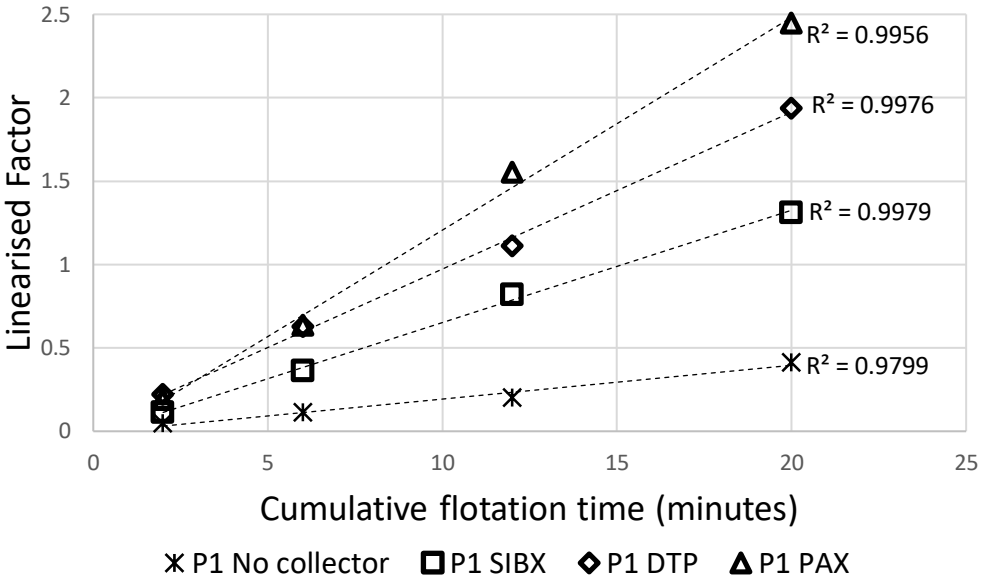


Figure 63: Linearised factor to calculate kinetic constant for microflotation

The kinetic constants $k$ were then determined from the gradients of the lines in Figure 63. The models thus had all the parameters. The parameters of $R^{\infty}$ and $k$ were then substituted back into the first order model and points were plotted for every 0.1 minute to verify the model fit, with the results displayed in Figure 64 below, where it can be seen that the method and model fitting approach lead to acceptable models being fitted to the data.

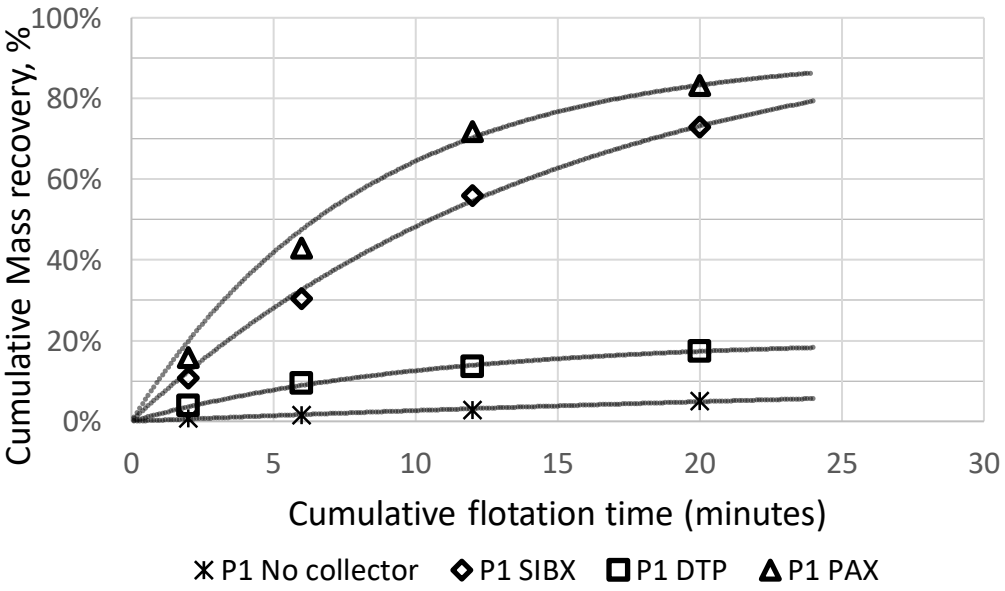


Figure 64: Model fitted applied to select experimental runs

All of the models fitted to the data obtained from experimental runs had a regression $R^2$ fit parameter of over 0.993, showing the model fit to the data. This was a result of using the GRG nonlinear solver to converge on the best fit. The $R^2$ fit parameters combined with values of the recovery at time infinity that

were sensible (none over 100%, all of them marginally larger than the achieved recovery after 20 minutes of flotation) as well as the visually fit of Figures such as in Figure 64 leads to the conclusion that the fitted models are accurate for the data obtained.

#### *4.3.2.2 Total Recovery at 20 minutes of flotation*

The recovery of the pyrite 1 and pyrite 2 under the PAX-DTP system than the SIBX-DTP system are shown in Figure 65 and Figure 66. Each figure has both the actual recovery after 20 minutes of micro-flotation, and also the model fit parameter of $R^{\infty}$ (Recovery at infinite time).

Figure 65 and Figure 66 include error bars for the cumulative recovery, but are insignificant enough in most cases to not be visible outside the border of the recovery bar. The largest error that was calculated was for pyrite 2 in the PD25 case which had a positive and negative value of 1.3%, which barely can be seen outside the outline of the bar. This shows good repeatability of the micro-flotation experiments.

Figure 65 displays the data for the SIBX-DTP collector system. The natural floatability of pyrite 2 was higher than pyrite 1 (5.08% for pyrite 1 compared to 6.51% for pyrite 2 in the 20 minutes of micro-flotation). DTP alone also recovered much less pyrite than other cases, though this value was still higher than the natural floatability of the pyrite which shows that DTP still caused hydrophobicity and collected pyrite. The copper content of pyrite 1 could have made pyrite 1 more amenable to flotation with DTP, resulting in a higher recovery with DTP alone (17.36% for pyrite 1 compared to the 14.56% for pyrite 2 recovery with DTP). The higher recovery of pyrite 1 with DTP is the reverse trend when compared to the natural floatability of the pyrite samples, showing that DTP did attach better to pyrite 1 and impart hydrophobicity better than DTP did with pyrite 2. This again could be related to the high recovery of chalcopyrite with DTP that Zhong et al., (2015) found in micro-flotation experiments with a corresponding low recovery of pyrite. The copper content in pyrite 1 could have also activated the pyrite, leading to better collector attachment.

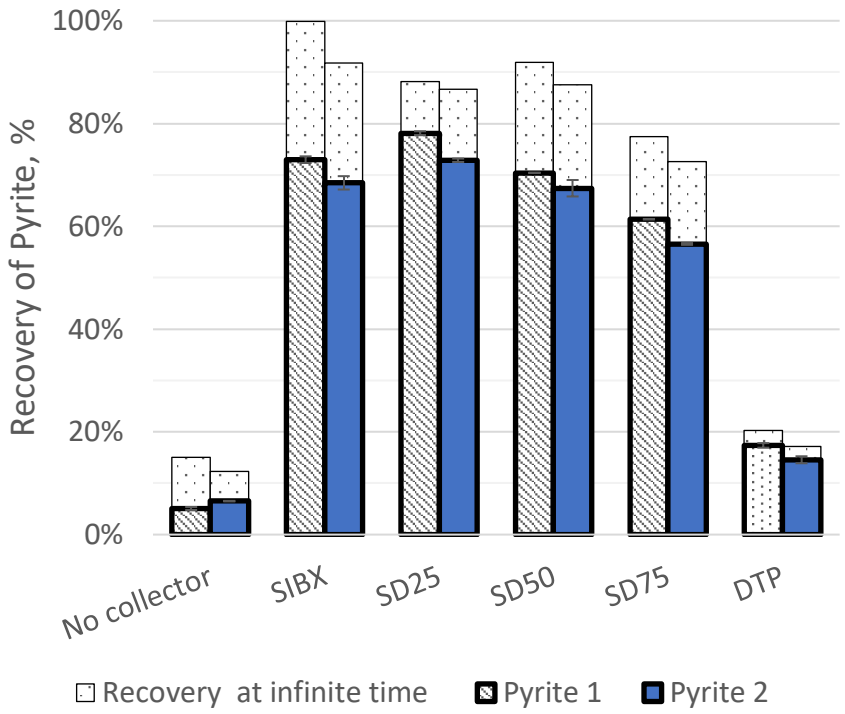


Figure 65: Recovery of Pyrite in Micro-flotation, using SIBX and DTP with the model fit parameter of Recovery at infinite time

SIBX as a collector alone showed a recovery of 72.97% for pyrite 1 and 68.46% for pyrite 2. An increase in recovery of both pyrite 1 and pyrite 2 was seen with a mixture of 75% SIBX and 25% DTP compared to the single SIBX collector with an increase in recovery of 5.88% for pyrite 1 and 4.39% for pyrite 2. when more DTP content was included above 25%, the recovery steadily decreased for both pyrite samples. The model fit parameter of recovery at infinity shows that SIBX alone theoretically has the potential to recover 99.9% of pyrite 1, which was the most theoretical recovery at infinite time, even when compared to the SD25 case that recovered more pyrite in the 20 minutes of flotation.

In Figure 65, the overall recoveries were lower for the pyrite 2 system than the pyrite 1 system using the same collectors, however this was expected since silica particles contributed to the total mass but was not expected to be recovered in the system. The same trend was seen in pyrite 2 as was seen in pyrite 1 for the SIBX-DTP system.

Figure 66 shows the recovery of the two pyrite samples with the PAX-DTP collector system. The difference in trends when compared to the SIBX-DTP system can be seen that a collector mixture of DTP and PAX did not improve the recovery of pyrite 1 over the single collector of PAX alone. For pyrite 1, PAX alone recovered the most pyrite 1 for the 20 minutes of micro-flotation at 83.2% and the recovery of pyrite 1 steadily decreased with increasing DTP content. The theoretical recoveries at infinite time for the PAX-DTP system when floating both pyrite samples also predicted lower achievable recoveries than the SIBX-DTP system, across all corresponding experiments, except PD75 compared to SD75.

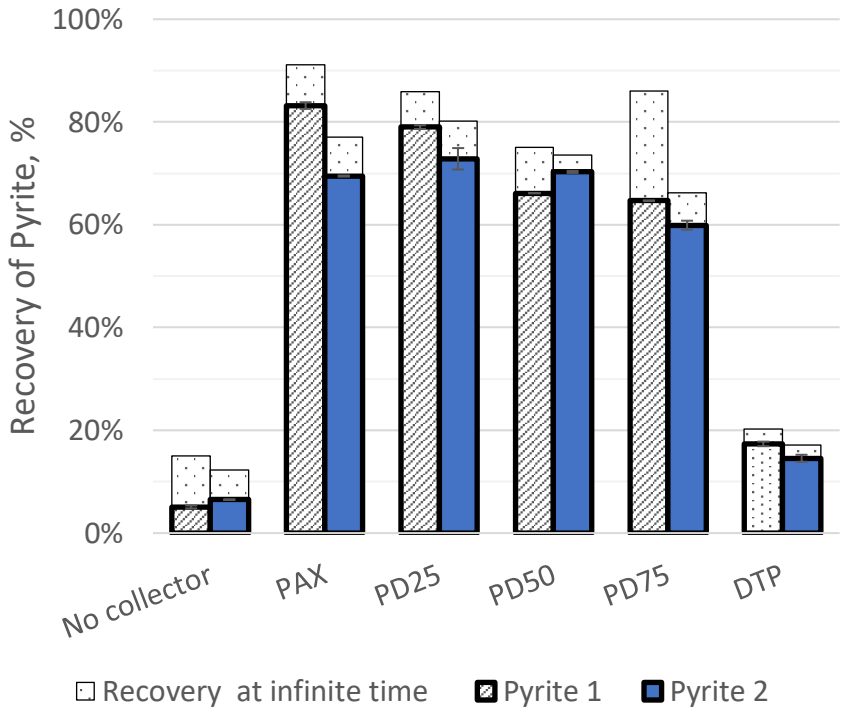


Figure 66: Recovery of Pyrite in Micro-flotation, using PAX and DTP with the model fit parameter of Recovery at infinite time

Unlike in pyrite 1, pyrite 2 still showed an increase in recovery when adding a small amount of DTP to PAX, as PD25 was tied with SD25 for the highest recovery of pyrite 2 during the 20 minutes of micro-flotation at 72.85%. It should be noted that the model predicts a higher recovery at infinite time for the SD25 case for pyrite 2 (91.77% recovery at infinite time for SD25 compared to 80.18% for PD25 in pyrite 2's case).

The trends shown in three out of the four cases of pyrite and collector system combination, 25% DTP and 75% xanthates improved recovery over the xanthates alone shows that even in pyrite with significantly lower compositional variations than that was found in the pyrite of the batch flotation pyrite, a collector mixture is beneficial and improves recovery.

Because of the silica content in pyrite 2, concrete conclusions could not be drawn about the effect of compositional variations between the two pyrite samples after 20 minutes of flotation, as the limiting factor for pyrite 2 would have been the silica content and thus recovery alone cannot lead to conclusions

on comparing the performance of the two pyrites. In every case, the recovery at infinity model parameter was less for pyrite 2 than pyrite 1, showing the effect of the silica content of pyrite 2 that could not be recovered. In every case besides PD50, the overall recovery of pyrite 2 after 20 minutes was also lower than pyrite 1.

### *4.3.3 Mass recovery at 2 minutes- fast floating mass*

Because of the silica content of pyrite 2, conclusions about trends comparing pyrite 1 and 2 to each other could not be made at the end of 20 minutes of flotation. The faster floating material that was recovered in the first two minutes to the first concentrate however does not have the limiting factor of silica making up a large portion of the remaining pulp and limiting recovery as was in Pyrite 2's case closer to the end of the 20 minutes of flotation.

The efficiency of recovery of pyrite in flotation is related to the sub-processes of flotation, as discussed in Section 2.7. The overall collection efficiency made up of the product of the efficiencies of each of the sub-processes. In order to compare the recovery values of pyrite 1 and pyrite 2 to each other, the efficiency of the other factors that are not related to the pyrite composition have to be as close to one another as possible.

One of sub process efficiencies to be considered is the efficiency, or probability, that a mineral particle would collide with a bubble. Because of the silica content in pyrite 2, the probability of the bubble colliding with a particle is made up of the sum of the probabilities of colliding with a particle of pyrite and colliding with a particle of silica. The probability of the bubble colliding with a particle of silica does not contribute to collection, thus lowering the collection efficiency of pyrite. After the majority of the pyrite is recovered, the proportion of pyrite to silica in pyrite 2 would decrease and thus the probability of a bubble colliding with a particle of pyrite 2 would be lower than pyrite 1. The difference in these efficiencies can be minimised by looking at the data from where the pyrite: gangue ratios are the most similar where the least amount of pyrite was removed from both systems, during the first concentrates.

Figure 67 shows the recovery of pyrite to the first concentrate for the SIBX-DTP system.

In the case of pyrite 1, the SIBX showed improvements in recovery when a mixture of 25% DTP and 75% SIBX was used. Pyrite 2 did not show any improvements with a collector mixture. DTP exhibited the same trend as seen in the total recovery at 20 minutes with Pyrite 1 being recovered more than pyrite 2, as it is likely that due to the low recovery of DTP that the silica in pyrite 2 was not as much a recovery limiting factor as in the case of the higher recovering xanthates.

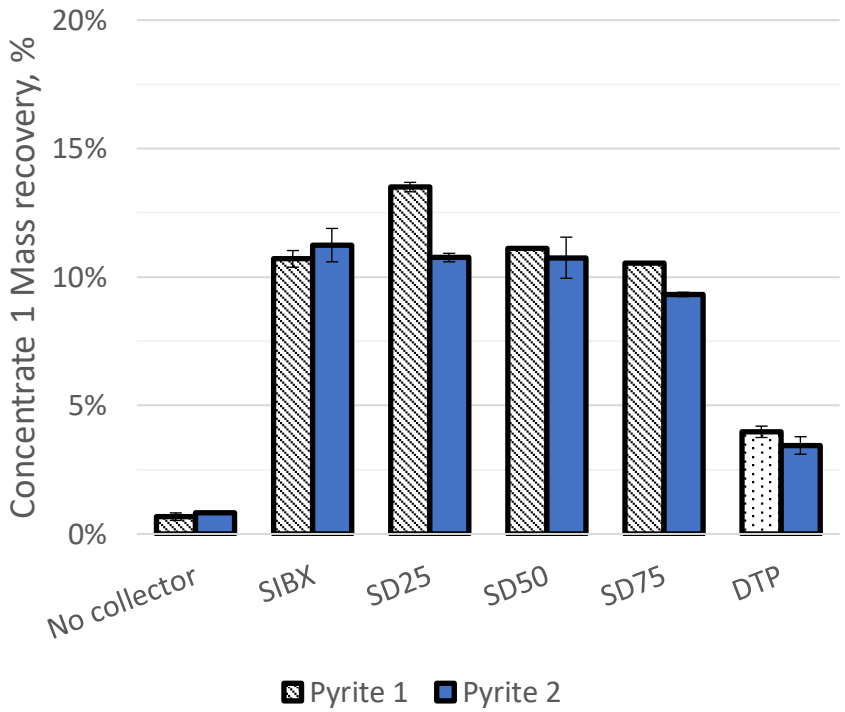


Figure 67: Recovery at 2 minutes of pyrite for the SIBX-DTP system in Micro-flotation

When comparing pyrite 1 to pyrite 2 in each case, no trend was seen in the SIBX-DTP system. In some cases the error bars overlapped and the recovery differences were not significant. No trends were able to be made with the first concentrate recovery differences of pyrite 1 compared to pyrite 2 across the SIBX-DTP system.

Figure 68 displays the recovery of pyrite 1 and pyrite 2 to the first concentrate for the PAX-DTP system.

For both pyrite 1 and pyrite 2, an increase was seen in the recovery to the first concentrate for the mixture of 25% DTP and 75% PAX. In the case of PAX and PD25, pyrite 1 was recovered more than pyrite 2. However, In the cases of PD50 and PD75, pyrite 2 was recovered over pyrite 1, and this changed for DTP where pyrite 1 was again recovered over pyrite 2. As a result of these changing differences in recovery to the first concentrate, no trends could be drawn when comparing pyrite 1 and pyrite 2 to each other.

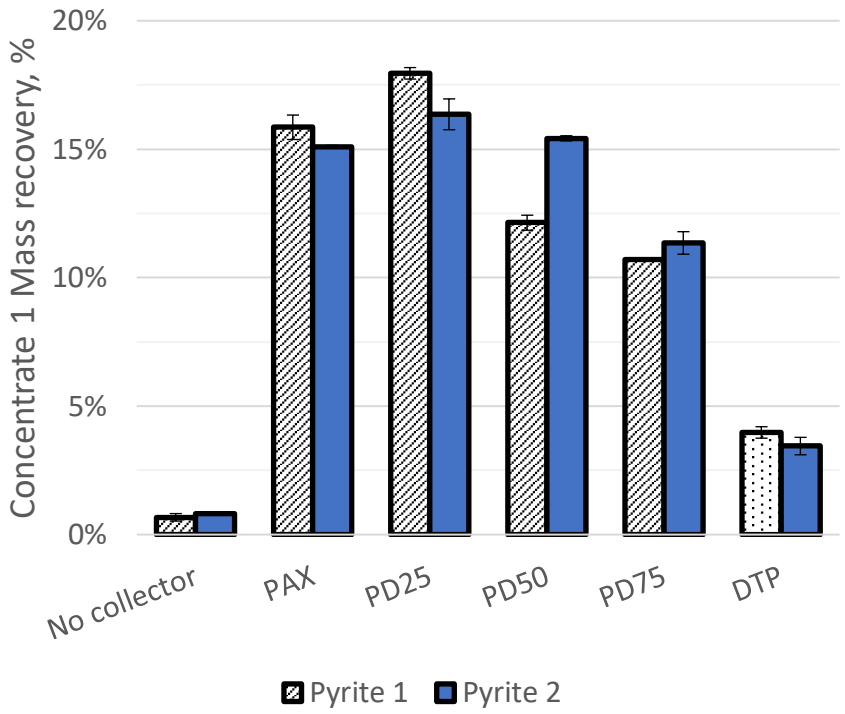


Figure 68: Recovery at 2 minutes of pyrite for the PAX-DTP system in Micro-flotation

Overall, in both the cumulative recovery at 20 minutes and in the first concentrate (at 2 minutes), no significant trends could be seen when comparing the recovery of pyrite 1 to the recovery of pyrite 2 in the context of the collector systems tested recovering one pyrite over another. Pyrite 1 thus did not perform any differently to pyrite 2 concerning single collectors attaching to one pyrite and floating it more over the other pyrite, as if this was the case, the recovery of the pyrite in the system that contained the collector that would attach selectively to it would be higher across the collector range where a significant portion of that collector existed.

### *4.3.4 Kinetic constant*

Figure 69 and Figure 70 shows the kinetic constant that was calculated using the first order model for flotation. Note that the unit for the kinetic constant is $min^{-1}$ and does not include a mass unit, thus is not a measure of mass recovery over time. When the first order model is studied, two parameters are fit to predict the recovery at any time t. The first parameter has already been discussed, which is the recovery at infinite time. The second parameter is the kinetic constant, which is a measure of how quickly the recovery of the system approaches the predicted recovery at infinite time.

The reason why the DTP rate constants are among the highest constants calculated for both pyrite 1 and pyrite 2 even though DTP exhibited a low recovery and predicted recovery at infinite time therefore has its explanation that the mass recoveries of DTP approached the theoretical maximum fairly quickly compared to how most other experiments approached their theoretical maximum recoveries.

The calculated kinetic constants for both pyrite 1 and pyrite 2 with the SIBX-DTP system is shown in Figure 69 while the kinetic constants for the PAX-DTP system is displayed in Figure 70 on the following page.

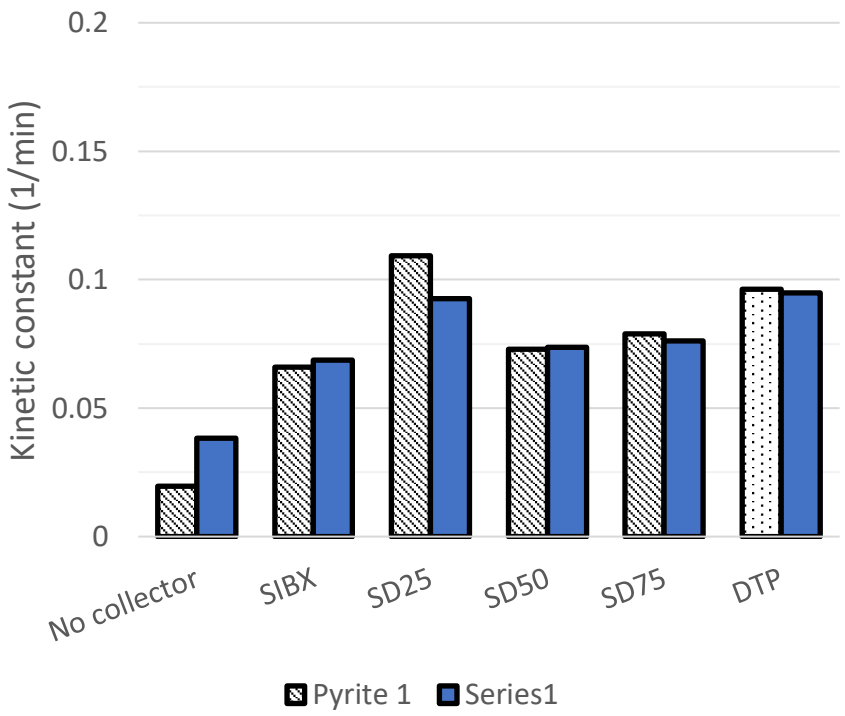


Figure 69: Kinetic model constant of micro-flotation runs using SIBX and DTP

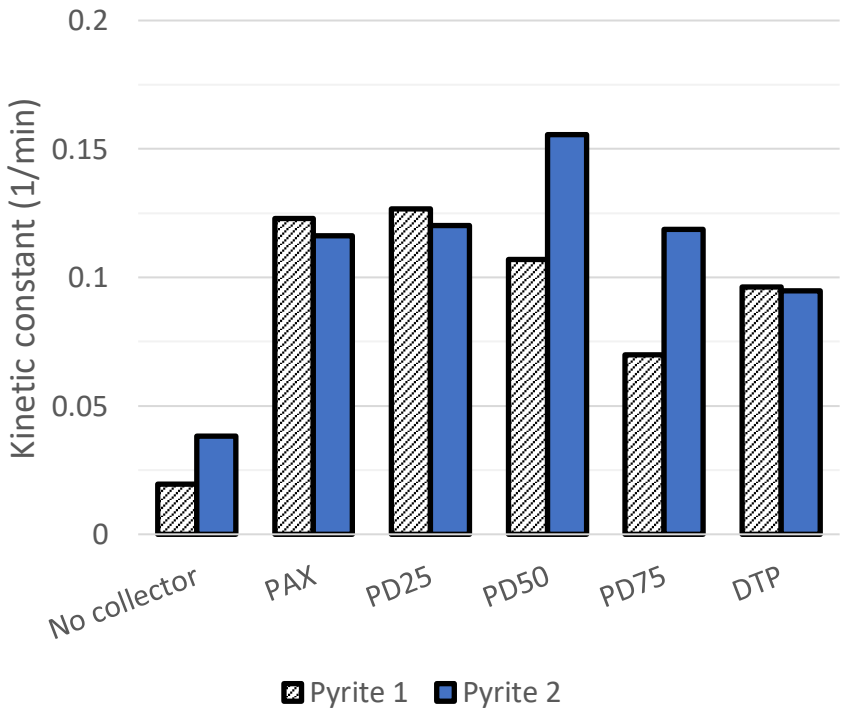


Figure 70: Kinetic model constant of micro-flotation runs using PAX and DTP

The SIBX-DTP system performed similarly in both pyrite cases when it came to kinetic constants. Only in the best recovering case of pyrite 1, SD25, the kinetic constants of the two different pyrites were significantly different with pyrite 1 being higher at 0.1093$min^{-1}$ compared to pyrite 2's constant of 0.0925 $min^{-1}$.

The PAX-DTP system had significantly higher kinetic constants compared to the corresponding cases of the SIBX-DTP system, except the case of pyrite 1's PD75 test compared to SD75, where SD75 had a calculated kinetic constant of 0.079 $min^{-1}$ compared to PD75's 0.07 $min^{-1}$, which are similar. The mixture of collectors did not improve the kinetic constants of flotation, except for the SD25 case in both pyrites and PD50 case when pyrite 2 was floated. The PD50 test was seen as an outlier in the recovery at 20 minutes and in the first concentrate where pyrite 2 was recovered more than pyrite 1 in both, contrary to what was expected.

If the DTP only experimental runs are excluded from the discussion due to their low recovery, when comparing pyrite 1 and pyrite 2 to one another in each case for the kinetic constant, very few significant differences are seen. Besides the discussed difference of SD25 where pyrite 1 had a higher kinetic constant than pyrite 2, two additional observations of a significantly differing kinetic constant were in the case of PD50 and PD75, where pyrite 2 had a flotation kinetic constant of 0.1556 $min^{-1}$ for PD50 and 0.119 $min^{-1}$ for PD75 compared to 0.1069 $min^{-1}$ and 0.07 $min^{-1}$ respectively for pyrite 1.

## 4.4 Discussion on Zeta Potential and Pulp Potential for Batch Flotation and Microflotation

When Figure 57 though to Figure 61 are studied in relation to the flotation responses, a few correlations can be drawn. The values of Figure 57 though to Figure 61 at a pH of 9 are referenced, as this pH is the closest to the flotation system and is representative of the conditions in the micro-flotation cell. One of the large discrepancies in the trends of the flotation responses is in Figure 68 (First concentrate mass recovery) and Figure 70 (kinetic contestant) that Pyrite 2 had significantly more faster floating mass than Pyrite 1 when 50% of PAX and 50% of DTP was used as a collector, which is opposite to the majority of other collector mixtures. When the corresponding the Zeta Potential is searched for PD50, it is noted that Pyrite 2 has the largest negative Zeta potential at -27.7mV (followed by Pyrite 2 PD75 at -25.05 mV as the second lowest) when compared to all other zeta potential measurements at a pH of 9, where other values were in the range of 20 to 22mV. PD75 Also exhibited similar behaviour to PD50 in Figure 68 and Figure 70, though the difference between Pyrite 2 and Pyrite 1 was less pronounced than the PD50 system.

Two possible reasons are put forward for this increase in faster floating masses at the higher magnitude of negative zeta potentials. The first reason is related to the particles of pyrite in the system being ore dispersed. The bigger the magnitude of the zeta potential, the more particles are repelled from each other and thus the more stable a colloid or suspension of particles are. This would have increased the distance from the bottom that is occupied by the “pulp” phase in the Pd50 and PD75 case, meaning that the bubble travelling upwards would have been in contact with particles with a longer period of time, allowing more particles to attach. The slower loading of the bubble due the particles being more dispersed could have allowed the bubble not to get overloaded early on, and more particles stick to the bubble and report to the concentrate rather than fall of it. Once all the particles that were rendered hydrophobic were recovered, this process would have slowed down, leading to the same trends in overall recovery, which was seen. The second reason that could have contributed to this phenomena is the more negatively charged pyrite particles could have led to the attraction of positively charged $FeOH^+$ ions to their surface, and iron hydroxide xanthates ($FeOH\ (X)^2$ or $Fe(OH)_2X$) formation could lead to greater hydrophobicity earlier on, leading to faster floating material. Again here, once the hydrophobic particles were recovered, the process slows and leads to similar overall recovery. The second theory is supported by Fornasiero and Ralston, (1992), who found a relation between the flotation maximum recovery at pH of 9 was related to the formation of $FeOH^+$ ions in solution. Both reasons stated here would be less pronounced in batch flotation where the pulp phase has a higher solids density and many other minerals besides pyrite, though the formation of $FeOH^+$ may still take place on pyrite surface.

When Figure 54 (Pulp potential for different test cases) is consulted, it is seen that most experimental conditions exist in the range of approximately 200 to 250mV. This is in line with literature, where its stated that most plants use air as a flotation gas and air set potentials are from +100 to +300mV (V. V. Hintikka and Leppinen, 1995). When Figure 54 is consulted, the outlier of DTP exists at +312mV. V. V. Hintikka and Leppinen, (1995) also states that reduced selectivity due to excessive oxidation of easily oxidised minerals may take place at high pulp potentials, which may explain the loss of arsenopyrite in the DTP test case. The arsenopyrite may have become excessively oxidised and inhibited collector attachment, which resulted in the arsenopyrite not being recovered with DTP as a collector. Pyrite would also have been oxidised under these conditions (more so than in the other cases) which could have lead

to the lower pyrite recoveries seen with DTP. Reducing agents can be used to bring the pulp potential back into the range of other experiments, though other interactions may occur due to their presence.

The other test cases, besides DTP, correspond to the desirable flotation domain, as discussed in Section 974.2.10. For xanthates, this flotation domain correspond to the formation of ferric xanthates, which may link to the second reason for the PD50 case in micro-flotation to have more faster floating minerals.

## 4.5 Relating Micro-flotation to Batch flotation

No direct relationship can be constructed between the compositional variations of the micro-flotation experiments to the flotation performance, unlike in the batch flotation experimentation where a difference in flotability of particles with compositional variations were observed. The difference between the mineralogy of the pyrite samples in microflotation and the pyrite samples in batch flotation was that a different order of magnitude of elemental variation was present. The batch flotation ore had a complex set of compositional variations with arsenic being the dominant compositional variation that drove selective flotation. Elemental variations of 10 wt% of other elements besides iron and sulphur were common, while the variations in the micro-flotation samples were less common and rarely exceeded 1 wt%.

Differences in the zeta potential and thus surface properties when comparing pyrite 1 and pyrite 2 were found. These differences also lead to differences in surface properties when collectors were introduced into the system, though these differences in zeta potential did not lead to trends in the flotation performance. This agrees with the work done by Bulut et al., (2007) on the microflotation of pyrite samples from different parts of Turkey. Bulut et al., (2007) did not study the effects in a real ore.

In all cases of micro-flotation, a mixture of 75% xanthate and 25% DTP lead to improvements in recovery over the single collectors alone (whether overall or at the first concentrate). In the batch flotation, 75% SIBX and 25% DTP achieved the highest recovery of pyrite and gold, thus both flotation systems showed an increase in recovery (and faster kinetics the case of micro-flotation) when collector mixtures were used over single collectors alone.

In this study, the pyrite samples used in micro-flotation did not have the properties of the pyrite in the real ore or exhibit trends that the real ore exhibited, and that itself is a result that can be learnt from. The applicability of micro-flotation to batch flotation and industry should be investigated further at the starting phase of projects. In this project, the pyrite samples used for micro-flotation were not similar to the pyrite types seen in the case study ore. The micro-flotation pyrite samples had different elemental variations at different orders of magnitude than the case study ore. When microflotation experimentation is to be conducted, it is important to compare the samples used in the experimentation to the industry that the research is being used in. Fundamental studies at the micro-flotation level may not agree with what is seen in batch flotation of an ore, as in this project. When advances are made at the micro-flotation level, the next step is to test these advances in the batch flotation setup, and then in the pilot plant scale (before potential application in industry), but if the theories tested at the micro-flotation level are not conducted with the actual industry mineralogy in mind, this advancement process may be hindered.

## 4.6 Answering Key Questions

### *4.6.1 Do compositional variations in pyrite affect the recovery of the pyrite in a flotation system?*

Compositional variations were seen to affect the flotation results of pyrite in the real ore from the Barberton Greenstone Belt. In the ore, multiple elements caused variations in the pyrite composition, including arsenic, copper and nickel. Arsenic was the most prominent compositional variation, detected in approximately 90% of grains and covered a range from 0.1 wt% to 43 wt%. In the cases where SIBX and PAX was used as a collector, the system recovered pyrite that had a higher weight percentage of arsenic and did not recover pyrite with a low weight percentage arsenic. When using DTP, the opposite trend was observed where the recovered pyrite was seen to have a lower weight percentage of arsenic and the pyrite with a larger arsenic content was not recovered to the same extent. Separation factors from base metal analysis, QXRD and optical microscopy supported the SEM analysis of the selective recoveries of the pyrite with compositional variations. An emphasis has to be placed on that not only was the mineral identity of arsenopyrite selectively recovered from pyrite, but also pyrite with arsenic content (arsenian pyrites) was selectively recovered from the pyrite without or with low amounts of arsenic.

Selective recovery of one set of minerals is coupled with the selective loss of the minerals that were not recovered. The compositional variations thus impacted the flotation response in the batch flotation of the case study ore, as certain particles were recovered over other particles because of compositional differences.

The compositional variations in batch flotation were significant but to the contrary, the compositional variation in micro-flotation were not. The compositional variations of the two pyrite samples in micro-flotation was not seen to impact the flotation response, and this was attributed to the low magnitude and occurrence of the compositional variations found in the pyrite samples used for micro-flotation.

The difference in the magnitude of the variation is what determines if the compositional variation affects the flotation recovery.

### *4.6.2 Do different collectors selectively attach to pyrite particles with different compositional variations?*

As discussed for the previous key question, in the batch flotation system, it was seen that the different pure collectors recovered pyrite with different compositional variations. By extension, the recovered particles were recovered because of the collectors selectively attaching onto them and causing hydrophobicity of those particles, making the particles amenable to recovery through froth flotation.

In the microflotation case, this selective flotation of one pyrite with certain variations was not seen. The lack of a difference between the two pyrite samples tested in micro-flotation again is related to the lower amount of compositional variation in the micro-flotation case. The more compositional variation a particle has, the more surface of the particle would vary, for example the change from a n-type semiconductor to a p-type semiconductor where arsenic was present that was shown in literature. If compositional variations that cause the change in properties are not significant enough or not common

enough, the surface properties of the particle would reflect this in being similar to the original mineral identity properties. This is shown by the batch flotation data where the particles with a high arsenic content were either recovered or not recovered, but the particles with a small amount of arsenic (less than 1 wt%) showed the opposite trend. Even though arsenic was present, the particles with the lower weight percentage of elements other than iron or sulphur did not exhibit the same trends as that with the higher weight percentage of element other than the components of the mineral identity of pyrite.

#### *4.6.3 If compositional variations affect recovery, can the collector reagent suite be modified to overcome the challenge posed by these compositional variations?*

The compositional variations were shown to affect the recovery of pyrite in the case study ore, and collector mixtures improved the recovery of the pyrite. The mixture of 75% DTP and 25% SIBX was shown to have the highest pyrite recovery and grade, not only in the batch flotation case study ore but also in some of the microflotation tests.

In the batch flotation tests where the compositional variations made a difference in recovery, the overall recovery was increased when using a mixture of collectors. The mixture of 75% SIBX and 25% DTP resulted in the separation ratio of arsenic/pyrite to decrease, showing that the mixture succeeded in recovering both arsenopyrite and arsenian pyrites (that the SIBX as a collector alone recovered), as well as the pyrite with no or smaller amount of arsenic contents (that the DTP recovered alone when used as a collector). The synergistic relationship between the SIBX and DTP, whether each collector floated and recovered separate minerals or acted together in all minerals, improved the recovery and overcame the mineralogical barrier posed by the compositional variation in the real ore from the Barberton Greenstone Belt.

### 4.7 Applicability to Industry

In some industrial applications, secondary collectors are used with primary collectors to improve recovery in the flotation network. This works in the same way that was shown in the batch flotation section of this project, increasing the recovery with only a small amount of the secondary collector added to the pulp.

The value of this study is showing that compositional variations impact the attachment of the collector to minerals, whether this is the primary collector or the secondary collector, in a real ore.

This has various potential impacts:

1. Minerals with the same “identity” tend to be treated the same way- i.e. “Use PAX to float pyrite”. Even if the method of floating the mineral is using a mixture of collectors, it may be well known worldwide that a certain mineral should be treated with the same mixture of collectors.
   This translates to the same collectors being used on the same “mineral identity”, even though the compositional variations present could differ in different geographical locations, resulting in a loss of the desired mineral due to differences in their properties. This study shows that different collectors and mixtures should be studied and optimised for every scenario.
2. As different areas of ore are mined around an existing plant, compositional variations in the ores could change due to a changing location, layer, formation time, condition or other factors of the

ore. If a drop in recovery is seen, one of the checks in the troubleshooting procedure that should be put in place is to check for a change in the trace element mineralogy of the desired mineral.

3. Due to the range of compositional variations in the feed of the desired mineral, some of the mineral may not be recovered in the original rougher flotation cells, due to the collector(s) not attaching to certain particles of the desired mineral well enough due to their impurities or trace elements. These particles then report to the scavenger flotation cell with the rest of the rougher tailings, where they are supposed to be scavenged and recovered. If the same collector(s) are used in the scavenger phase, the collector(s) will again not attach well to the same minerals that got rejected in the feed, resulting in ineffective scavenging of the desired mineral. The mineralogy not only in the original ore, but also in subsequent stages therefore must be checked and collector reagent suites have to be optimised in each stage.

   This may be more difficult than expected, as collector reagent suites remain in the system throughout the flotation stages in the process, and the collector(s) added in the rougher stages will still be in the system at the scavenger and cleaner stages.

# 5 CONCLUSIONS

The case study ore was characterised with pyrite existing in the ore with compositional variations, the most important compositional variation being a variable amount of arsenic within the pyrite. The gold found in the system was associated with pyrite with high weight percentage arsenic. SIBX and PAX, both being xanthates, performed similarly where a pyrite recovery of 30.63% and 38.25% respectively was achieved. DTP showed the lowest pyrite recovery of 27%.

Although the DTP recovery was in the same region as the xanthates, a major disparity was seen in the gold recovery of DTP where DTP was seen to only recover 20.97% of gold, compared to 70.97% when SIBX was used and 73.89% when PAX was used. The reason for DTP lower gold recovery, even though it recovered nearly the same amount of pyrite, was attributed to the fact that DTP was seen to selectively recover pyrite with no arsenic or a low weight percentage arsenic, compared to SIBX and PAX which selectively recovered pyrite with a higher weight percentage arsenic. Even though DTP recovered pyrite, the pyrite it recovered had a composition of a low weight percentage of arsenic and the gold was not associated with it.

When DTP and the xanthates were mixed together, a higher recovery of pyrite was seen. The best case of 75% SIBX and 25% DTP recovered the most pyrite (69.92%) at the best pyrite grade (6.4%) and the most gold (100%) at the highest gold grade of 50.6 g/ton. All of these metrics represent the best of all of the experiments and conditions, which is not a situation that is common since grade and recovery often have an inverse relationship.

Two pyrite samples were sourced for micro-flotation and were characterised. Pyrite 1 was found to on average have less than 1 wt% of other elements besides iron and sulphur, with the most common two being copper and lead. Pyrite 2 was found to have silica grains that were separate from pyrite grains, along with an average of 1.1 wt% Cobalt that appeared in 18.92% of spots. The wt% compositional variations seen in the pyrite samples used in microflotation were of an order magnitude less than seen in the batch flotation ore.

As a result of the silica content in pyrite 2, the mass recovery of pyrite 2 could not be compared to the mass recovery of pyrite 1 after 20 minutes of flotation. The faster floating masses of the first concentrate were thus compared, because the impact of the silica would be minimised. No trends or differences were seen when the first concentrate of pyrite 1 and pyrite 2 were compared to one another or when comparing the two pyrite samples using the calculated kinetic rate constant either, so the conclusion was drawn that the smaller order of magnitude of compositional variation in the microflotation samples did not lead to an impact on recovery, collector attachment or kinetics.

An improvement in recovery after 20 minutes of flotation was seen in the case of both pyrite 1 and pyrite 2 with a ratio of 75% SIBX and 25% DTP over SIBX alone, with an increase in recovery of 5.88% for pyrite 1 and 4.39% for pyrite 2 when using the collector mixture over SIBX only. An increase in recovery for pyrite 2 after 20 minutes was seen when 75% PAX and 25% DTP was used over PAX (increase of 3.37%), but the corresponding increase for pyrite 1 was not seen after 20 minutes of flotation.

In microflotation, it was shown that collector mixtures can still be beneficial to recovery even when the compositional variations in the pyrite sample were minimal. The result of increased recovery in the microflotation tests when 75% of a xanthate was combined with 25% of DTP coupled with the batch flotation experiment with the highest pyrite grade and recovery with the highest gold grade and recovery being when 75% SIBX and 25% DTP was used as the collector suite, the conclusion is made that collector mixtures are beneficial to the recovery of pyrite when applied in the correct ratio.

In the batch flotation system, as a result of compositional variations, the recovery of pyrite was impacted. Selective flotation of pyrite with a higher arsenic content in the case where xanthates were used as a collector resulted in the pyrite without or with a lower arsenic content to be lost. When DTP was used as a collector, the recovery of pyrite with a low arsenic content was seen, which was coupled to a loss of pyrite with a higher arsenic content. The compositional variations in pyrite thus impacted the recovery of the pyrite, and this was related to the selective attachments of different collectors to pyrite with different compositional variations. When mixing collectors, specifically 75% SIBX and 25% DTP, the separation of pyrite and arsenic decreased with a corresponding increase in the pyrite recovery, and thus the collector reagent suite was used to overcome the mineralogical barrier posed by the variations in composition of the pyrite.

# 6 RECOMMENDATIONS

A better option than the LA-ICP-MS of the whole-rock analysis for selective flotation of trace element within pyrite would have been to separate the pyrite grains from the silicates, dissolve the pyrite and its trace elements into solution and then send this solution through a mass spectroscopy device. Pyrite grains from the feed, concentrate and tailings could have undergone this analysis, allowing comparisons between the distributions of the trace elements in each to be made to draw conclusions. This method was in development, but due to time constraints, could not be completed. The method development got to the stage of separating the pyrite grains from the silicates. The separation of the pyrite grains was first achieved by washing with water and allowing the heavier and larger particles to settle down before discarding the supernatant. Due to the large density of pyrite (5.01 g/cm$^3$, compared to silicates of around 2.65g/cm$^3$), the pyrite particles would settle out and not get discarded. Discarding the smaller grains of silicates then allowed the sample to undergo heavy liquid gravitational separation, where the samples were immersed in Tetrabromoethane (TBE, density of 2.97 g/cm$^3$). Most of the silicates floated on the TBE, while the pyrite and some of the heavier gangue minerals sank to the bottom. After washing and drying, the pyrite grains were then individually picked out of the heavier materials that sank in the TBE to yield the pyrite grains separated from everything else in the original sample.

SEM analysis of various samples were already conducted and LA-ICP-MS of the separated pyrite grains would not yield valuable results, as both SEM and LA-ICP-MS are both spot analysis which require ablation of the surface of a spot to read results. The advantage of dissolving the entire sample's worth of pyrite grains would be that the whole pyrite grain (and complete pyrite representative samples of each condition) would be dissolved and analysed, not just the surface of an exposed grain. The results of this methodology would have served as a confirmation of the results of other methods used in this study.

To further study the selective attachment of collectors to minerals with compositional variations form the same ore, FTIR or laser microscopy on particles such as the ones displayed in Figure 20 (where arsenopyrite and arsenian pyrites exist in the same particle with normal pyrite) after exposing the grain to different collectors could show which collectors are attached to which mineral surface, and the extent of the attachment on the surface. These images could be related to elemental mapping of the surface of the particle to draw conclusions of the compositional variation to collector attachment

# 7 REFERENCES

Abraitis, P.K., Pattrick, R.A.D., Vaughan, D.J., 2004. Variations in the compositional, textural and electrical properties of natural pyrite: A review. Int. J. Miner. Process. 74, 41–59. https://doi.org/10.1016/j.minpro.2003.09.002

Adams, M.D., 2016. Gold Ore Processing, Gold Ore Processing. https://doi.org/10.1016/c2015-0-00699-2

Adkins, S.J., Pearse, M.J., 1992. The influences of collector chemistry on kinetics and selectivity in base-metal sulphide flotation. Miner. Eng. 5, 295–310. https://doi.org/10.1016/0892-6875(92)90212-R

Agangi, A., Hofmann, A., Eickmann, B., Marin-Carbonne, J., Reddy, S.M., 2016. An atmospheric source of S in Mesoarchaean structurally-controlled gold mineralisation of the Barberton Greenstone Belt. Precambrian Res. 285, 10–20. https://doi.org/10.1016/j.precamres.2016.09.004

Agangi, A., Hofmann, A., Przybyłowicz, W., 2014. Trace element zoning of sulfides and quartz at sheba and fairview gold mines: Clues to mesoarchean mineralisation in the barberton greenstone belt, south africa. Ore Geol. Rev. 56, 94–114. https://doi.org/10.1016/j.oregeorev.2013.08.016

Agar, G.E., Chia, J., Requis, C.L., 1998. Flotation rate measurements to optimize an operating circuit. Miner. Eng. 11, 347–360.

Aldrich, C., Moolman, D.W., Bunkell, S.J., Harris, M.C., Theron, D.A., 1997. Relationship between surface froth features and process conditions in the batch flotation of a sulphide ore. Miner. Eng. 10, 1207–1218. https://doi.org/10.1016/s0892-6875(97)00107-6

Antonijević, M.M., Dimitrijević, M.D., Šerbula, S.M., Dimitrijević, V.L.J., Bogdanović, G.D., Milić, S.M., 2005. Influence of inorganic anions on electrochemical behaviour of pyrite. Electrochim. Acta 50, 4160–4167. https://doi.org/10.1016/j.electacta.2005.01.036

Arehart, G.B., Chryssoulis, S.L., Kesler, S.E., 1993. Gold and Arsenic in Iron Sulfides from Sediment hosted Disseminated Gold Deposits: Implication for Depositional Processes. Econ. Geol. 88, 171–185. https://doi.org/10.1177/0047287594033002123

Ball, B., Rickard, R.S., 1976. The chemistry of Pyrite Flotation. A.M. Gaudin Meml. Vol. AIME. 458–484.

Banford, A.W., Aktas, Z., Woodburn, E.T., 1998. Interpretation of the ef- fect of froth structure on the performance of froth flotation using image analysis. Powder Technol 98, 61–73.

Barbian, N., Ventura-Medina, E., Cilliers, J.J., 2003. Dynamic froth stability in froth flotation. Miner. Eng. 16, 1111–1116. https://doi.org/10.1016/j.mineng.2003.06.010

Bilinski, B., Wojcik, W., 1996. Correlation between surface free energy and floatability of galena with potassium ethyl xanthate. J. Adhes. Sci. Technol. 10.

Boulton, A., Fornasiero, D., Ralston, J., 2003. Characterisation of sphalerite and pyrite flotation samples by XPS and ToF-SIMS. Int. J. Miner. Process. 70, 205–219. https://doi.org/10.1016/S0301-7516(03)00003-6

Bozkurt, V., Xu, Z., Finch, J.A., 1998. Pentlandite/pyrrhotite interaction and xanthate adsorption. Int. J. Miner. Process. 52, 203–214.

Bradshaw, D.J., 1997. Synergistic effects between thiol collectors used in the flotation of pyrite. University of Cape Town.

Bradshaw, D.J., O'Connor, C.T., 1996. Measurement of the sub-process of bubble loading in flotation. Miner. Eng. 9, 443–448. https://doi.org/10.1016/0892-6875(96)00029-5

Brill, B.A., 1989. Trace element contents and partitioning of ele- ments in ore minerals from the CSA Cu–Pb–Zn deposit, Australia. Can. Miner. 27, 263–274.

Buckley, A.N., Woods, R., 1987. The surface oxidation of pyrite. Appl. Surf. Sci. 27, 437–452.

https://doi.org/10.1016/0169-4332(87)90153-X

Buckley, A.N., Woods, R., 1984. X-RAY PHOTOELECTRON SPECTROSCOPIC INVESTIGATION OF THE SURFACE OXIDATION OF SULFIDE MINERALS. Proc. Int. Symp. Electrochem. Miner. Met. Process. 84–10, 286–302.

Bulut, F., Arslan, F., Atak, S., 2004. Flotation behaviors of pyrites with different chemical compositions 21, 86–92.

Cabri, L.J., Campbell, J.L., Gilles Laflamme, J.H., Leigh, R.G., Maxwell, J.A., Scott, J.D., 1985. Proton microprobe analysis of trace elements in sulfides from some massive sulfide deposits. Can. Mineral. 23, 133–148.

César, J., Iglesias, Á., Soares, K., Martins, F., Leite, A., Domingues, A., Beatriz, M., Casagrande, C., Paciornik, S., 2018. Automatic characterization of iron ore by digital microscopy and image analysis &. Integr. Med. Res. 7, 376–380. https://doi.org/10.1016/j.jmrt.2018.06.014

Chander, S., Fuerstenau, D.W., 1983. Electrochemical flotation separation of chalcocite from molybdenite. Int. J. Miner. Process. 10, 89–94. https://doi.org/10.1016/0301-7516(83)90035-2

Chander, S., Fuerstenau, D.W., 1975. Electrochemical reaction control of contact angles on copper and synthetic chalcocite in aqueous potassium diethyldithiophosphate solutions. Int. J. Miner. Process. 2, 333–352. https://doi.org/10.1016/0301-7516(75)90027-7

Chander, S., Fuerstenau, D.W., 1974. The effect of potassium diethyldithiophosphate on the electrochemical properties of platinum, copper and copper sulfide in aqueous solutions. J. Electroanal. Chem. 56, 217–247. https://doi.org/10.1016/S0022-0728(74)80330-X

Chandra, A.P., Gerson, A.R., 2009. A review of the fundamental studies of the copper activation mechanisms for selective flotation of the sulfide minerals, sphalerite and pyrite. Adv. Colloid Interface Sci. 145, 97–110. https://doi.org/10.1016/j.cis.2008.09.001

Chen, X., Peng, Y., Bradshaw, D., 2013. Effect of regrinding conditions on pyrite flotation in the presence of copper ions. Int. J. Miner. Process. 125, 129–136. https://doi.org/10.1016/j.minpro.2013.08.007

Chenery, S., Cook, J.M., Stylus, M., Cameron, E.M., 1995. Determination of the 3-dimensional distributions of precious metals in sulfide minerals by laser-ablation microprobe inductively coupled plasma-mass spectrometry (LAMP-ICP-MS). Chem. Geol. 124, 55–65.

Chernyshova, I. V., 2003. An in situ FTIR study of galena and pyrite oxidation in aqueous solution. J. Electroanal. Chem. 558, 83–98. https://doi.org/10.1016/S0022-0728(03)00382-6

Chimonyo, W., Wiese, J., Corin, K., O'Connor, C., 2017. The use of oxidising agents for control of electrochemical potential in flotation. Miner. Eng. 109, 135–143. https://doi.org/10.1016/j.mineng.2017.03.011

Chopard, A., Marion, P., Royer, J., Taza, R., Bouzahzah, H., 2019. Automated sul fi des quanti fi cation by multispectral optical microscopy 131, 38–50. https://doi.org/10.1016/j.mineng.2018.11.005

Çilek, E.C., 2004. Estimation of flotation kinetic parameters by considering interactions of the operating variables. Miner. Eng. 16, 109–123.

Coetzer, G., Du Preez, H.S., Bredenhann, R., 2003. Influence of water resources and metal ions on galena flotation of Rosh Pinah ore. J. South African Inst. Min. Metall. 103, 193–201.

Cook, N.J., Chryssoulis, S.L., 1990. Concentrations of "Invisible gold" in the common sulfides.

Craig, J.R., Vaughan, D.J., 1994. Ore microscopy and ore petrography, 2nd ed.

Crozier, R.D., 1991. Sulphide collector bonding and the mechanism of flotation. Miner. Eng. 4, 839.

Deer, W.A., Howie, R.A., Zussman, J., 1992. An introduction to the rock-forming minerals.

Dehghani, F., Rahimi, M., Rezai, B., 2013. Influence of particle shape on the flotation of magnetite, alone and in the presence of quartz particles. J. South. African Inst. Min. Metall.

Dirks, P.H.G.M., Charlesworth, E.G., Munyai, M.R., Wormald, R., 2013. Stress analysis, post-orogenic extension and 3.01Ga gold mineralisation in the Barberton Greenstone Belt, South Africa. Precambrian Res. 226, 157–184. https://doi.org/10.1016/j.precamres.2012.12.007

Doyle, F.M., Mirza, A.H., 1996. Electrochemical oxidation of pyrite samples with known composition and electrical properties. Electrochem. Proc. 96, 203–214.

Dunne, R., 2005. Flotation of gold and gold-bearing ores, Developments in Mineral Processing. Elsevier B.V. https://doi.org/10.1016/S0167-4528(05)15014-5

Dutrow, B.L., Clark, C.M., n.d. X-ray Powder Diffraction (XRD) [WWW Document]. Geochemical Instrum. Anal.

Ekmekçi, Z., Bradshaw, D.., Harris, P.., Buswell, M.A., 2006. Interactive effects of the type of milling media and CuSO4 additionon the flotation performance of sulphide minerals from Merensky ore part II: froth stability. Int. J. Miner. Process 78, 164–174.

Engelbrecht, J.A., Woodburn, E.T., 1975. The effects of froth height, aeration rate, and gas precipitation on flotation. S. Afr. Inst. Min. Met. 76, 125–132.

Ertekin, Z., Pekmez, K., Ekmekçi, Z., 2016. Evaluation of collector adsorption by electrochemical impedance spectroscopy. Int. J. Miner. Process. 154, 16–23. https://doi.org/10.1016/j.minpro.2016.06.012

Fandrich, R., Gu, Y., Burrows, D., Moeller, K., 2007. Modern SEM-based mineral liberation analysis. Int. J. Miner. Process. 84, 310–320. https://doi.org/10.1016/j.minpro.2006.07.018

Finch, J.A., Smith, G.W., 1979. Contact angle and wetting. Miner. Sci. Eng. 11, 36.

Fleet, M.E., Chryssoulis, S.L., Maclean, P.J., Davidson, R., Weisener, C.G., 1993. Arsenian pyrite from gold deposits: Au and As distribution investigated by SIMS and EMP, and color staining and surface oxidation by XPS and LIMS. Can. Mineral. 31, 1–17.

Fleet, M.E., Mumin, A.H., 1997. Gold-bearing arsenian pyrite and marcasite and arsenopyrite from Carlin Trend gold deposits and laboratory synthesis. Am. Mineral. 82, 182–193. https://doi.org/10.2138/am-1997-1-220

Fornasiero, D., Eijt, V., Ralston, J., 1992. An electrokinetic study of pyrite oxidation. Colloids and Surfaces 62, 63–73. https://doi.org/10.1016/0166-6622(92)80037-3

Fornasiero, D., Ralston, J., 1992. Iron hydroxide complexes and their influence on the interaction between ethyl xanthate and pyrite. J. Colloid Interface Sci. 151, 225–235. https://doi.org/10.1016/0021-9797(92)90253-I

Fuernstenau, M., Kuhn, M., Elgillani, D., 1968. Flotation. Soc. Mining, Metall. Explor. 145–155, 227–250.

Fuerstenau, D.W., Mishra, R.K., 1980. Complex Sulphide Ores. Inst. Min. Met.

Fuerstenau, M., Jameson, G., Yoon, R., 2007. Froth Flotation: A century of innovation. Soc. Mining, Metall. Explor.

Fuerstenau, M.C., Misra, M., Palmer, B.R., 1990. Xanthate adsorption on selected sulfides in the virtual absence and presence of oxygen, Part 2. Int. J. Miner. Process. 29, 111–119.

Fuerstenau, M. C., Natalie, C.A., Rowe, R.M., 1990. Xanthate adsorption on selected sulfides in the virtual absence and presence of oxygen, Part 1. Int. J. Miner. Process. 29, 89–98. https://doi.org/10.1016/0301-7516(90)90007-L

Goktepe, F., Williams, K.P., 1995. Electrochemical effects in flotation 8, 1035–1048.

Goodall, W.R., Scales, P.J., 2007. An overview of the advantages and disadvantages of the determination

of gold mineralogy by automated mineralogy. Miner. Eng. 20, 506–517. https://doi.org/10.1016/j.mineng.2007.01.010

Grano, S.R., Prestidge, C.A., Ralston, J., 1997. Solution interaction of ethyl xanthate and sulphite and its effect on galena flotation and xanthate adsorption. Int. J. Miner. Process. 52, 161–186.

Griffin, W.L., Ashley, P.M., Ryan, C.G., Soey, H.S., Suter, G.F., 1991. Pyrite geochemistry in the North Arm epithermal Ag–Au deposit, Queensland, Australia: a proton-microprobe study. Can. Mineral. 29, 185–198.

Güler, T., Hiçyilmaz, C., Gökağaç, G., Ekmekçi, Z., 2004. Voltammetric and drift spectroscopy investigation in dithiophosphinate- chalcopyrite system. J. Colloid Interface Sci. 279, 46–54. https://doi.org/10.1016/j.jcis.2004.06.036

Guo, B., Peng, Y., Parker, G., 2016. Electrochemical and spectroscopic studies of pyrite-cyanide interactions in relation to the depression of pyrite flotation. Miner. Eng. 92, 78–85. https://doi.org/10.1016/j.mineng.2016.03.003

Guy, P.J., Trahar, W.J., 1984. The influence of grinding and flotation environments on the laboratory batch flotation of galena. Int. J. Miner. Process. 12, 15–38. https://doi.org/10.1016/0301-7516(84)90020-6

Hamilton, I.C., Woods, R., 1981. An investigation of surface oxidation of pyrite and pyrrhotite by linear potential sweep voltammetry. J. Electroanal. Chem. 118, 327–343. https://doi.org/10.1016/S0022-0728(81)80551-7

Hanson, J.S., Fuerstenau, D.W., 1991. The electrochemical and flotation behavior of chalcocite and mixed oxide/sulfide ores. Int. J. Miner. Process. 33, 33–47. https://doi.org/10.1016/0301-7516(91)90041-G

Heyes, G.W., Trahar, W.J., 1979. Oxidation-Reduction effects in the flotation of chalcocite and cuprite. Int. J. Miner. Process. 6, 229–252. https://doi.org/10.1016/0301-7516(79)90039-5

Hintikka, V. V., Leppinen, J.O., 1995. Potential control in the flotation of sulphide minerals and precious metals. Miner. Eng. 8, 1151–1158. https://doi.org/10.1016/0892-6875(95)00080-A

Hintikka, V.V., Leppinen, J.O., 1995. Potential control in the flotation of sulfide minerals and precious metals. Miner. Eng 8 (10).

Huai, Y., Plackowski, C., Peng, Y., 2018. The galvanic interaction between gold and pyrite in the presence of ferric ions. Miner. Eng. 119, 236–243. https://doi.org/10.1016/j.mineng.2018.01.040

Huston, D.L., Sie, S.H., Suter, G.F., Cooke, D.R., Both, R.A., 1995. Trace elements in sulfide minerals from Eastern Australian volcanic-hosted massive sulfide deposits: Part 1. Proton microprobe analyses of pyrite, chalcopyrite and sphalerite, and Part II. Selenium levels in pyrite: comparison with values and implications. Econ. Geol. 90, 1167–1196.

Ikotun, B.D., Adams, F. V., Ikotun, A.G., 2017. Application of three xanthates collectors on the recovery of nickel and pentlandite in a low-grade nickel sulfide ore using optimum flotation parameters. Part. Sci. Technol. 35.

Indian-Standard, 2009. How To assay gold ore 3.

IUPAC, 1997. Compendium of Chemical Terminology. https://doi.org/10.1351

Iwasaki, I., Cooke, R.W.B., 1959. Dissociation constant of xanthic acid as determined by spectrophotometric method. Phys. Chem. 6, 1321–1322.

Javadi Nooshabadi, A., Larsson, A.C., Kota, H.R., 2013. Formation of hydrogen peroxide by pyrite and its influence on flotation. Miner. Eng. 49, 128–134. https://doi.org/10.1016/j.mineng.2013.05.016

Jiwu, M., Longling, Y., Kouxiong, S., 1984. l frother collectors for flotation of sulfide minerals. Reagents

Miner. Ind. London Inst. Min. Metall. 287–290.

Kahn, H., Mano, E.S.M., Tassinari, M.M.M.L., 2002. Image Analaysis Coupled With A SEM-EDS Applied To The Characaterization Of A Zn-Pb Partially Weathered Ore. J. Miner. Mater. Charact. Eng. 01, 1–9. https://doi.org/10.4236/jmmce.2002.11001

Khan, A., Kelebek, S., 2004. Electrochemical Aspects of Pyrrhotite and Pentlandite in Relation to their Flotation with Xanthate. Part-I: Cyclic Voltammetry and Rest Potential Measurements. J. Appl. Electrochem. 34, 849–856.

Khoshdast, H., Sam, A., 2012. An efficiency evaluation of iron concentrates flotation using rhamnolipid biosurfactant as a frothing reagent. Environ. Eng. Res. 17, 9–15. https://doi.org/10.4491/eer.2012.17.1.009

Klimpel, R., Hansen, R., 1988. The interaction of flotation chemistry and size reduction in the recovery of a porphyry copper ore. Int. J. Miner. Process. 22, 169–181.

Klimpel, R.R., 2000. Optimizing the industrial flotation performance of sulfide minerals having some natural floatability. Int. J. Miner. Process. 58, 77–84.

Knipe, S., 1991. Hydrothermal precipitation of precious metals on sulphide substrates .

Knipe, S., Foster, R., Stanley, J., 1992. Role of sulphide surfaces in sorption of precious metals from hydrothermal fluids.pdf.

Koh, P.T.L., Hao, F.P., Smith, L.K., Chau, T.T., Bruckard, W.J., 2009. The effect of particle shape and hydrophobicity in flotation. Int. J. Miner. Process. 93, 128–134. https://doi.org/10.1016/j.minpro.2009.07.007

Koh, P.T.L., Smith, L.K., 2011. The effect of stirring speed and induction time on flotation. Miner. Eng. 24, 442–448. https://doi.org/10.1016/j.mineng.2010.12.007

Köse, C., Ikibas, C., 2012. Statistical methods for segmentation and quantification of minerals in ore microscopy 30, 19–32. https://doi.org/10.1016/j.mineng.2012.01.008

Kuopanportti, H., Suorsa, T., Dahlo, O., Niinimaki, J., 2000. A model of conditioning in the flotation of a mixture of pyrite and chalcopyrite ores. Int. J. Miner. Process. 59, 327–338.

La Brooy, S.R., Linge, H.G., Walker, G.S., 1994. Review of gold extraction from ores. Miner. Eng. 7, 1213–1241. https://doi.org/10.1016/0892-6875(94)90114-7

Laird, J.S., Macrae, C.M., Halfpenny, A., Large, R., Ryan, C.G., 2015. Microelectronic junctions in arsenian pyrite due to impurity and mixed sulfide heterogeneity. Am. Mineral. 100, 26–34. https://doi.org/10.2138/am-2015-4648

Lalvani, S.B., Weston, A., Masden, J.T., 1990. Characterization of semiconducting properties of naturally occurring polycrystalline FeS 2 ( Pyrite ). J. Mater. Sci. 25, 107–112.

Lane, G.R., Martin, C., Pirard, E., 2008. Techniques and applications for predictive metallurgy and ore characterization using optical image analysis. Miner. Eng. 21, 568–577. https://doi.org/10.1016/j.mineng.2007.11.009

Lätti, D., Adair, B.J.I., 2001. An assessment of stereological adjustment procedures. Miner. Eng. 14, 1579–1587. https://doi.org/10.1016/S0892-6875(01)00176-5

Leja, J., 1982. Surface Chemistry of Froth Flotation. Plenum Press, New York.

Leja, J., He, B.Q., 1984. The role of flotation frothers in the particle-bubble attachment process. Principles of Mineral Flotation. Princ. Miner. Flot. ust. Inst. Min. Met. 73–89.

Leja, J., Schulman, J.H., 1954. Flotation theory: molecular interactions between frothers and collectors at solid–liquid–air interfaces. Trans. AIME 199, 221–228.

Li, Y.-Q., Chen, J.-H., Chen, Y., 2010. Electronic structures and flotation behavior of pyrite containing

vacancy defects. Wuli Huaxue Xuebao/ Acta Phys. - Chim. Sin. 26, 1435–1441.

Lotter, N.O., Bradshaw, D.J., 2010. The formulation and use of mixed collectors in sulphide flotation. Miner. Eng. 23, 945–951. https://doi.org/10.1016/j.mineng.2010.03.011

Lotter, N.O., Bradshaw, D.J., Barnes, A.R., 2016. Classification of the Major Copper Sulphides into semiconductor types, and associated flotation characteristics. Miner. Eng. 96–97, 177–184. https://doi.org/10.1016/j.mineng.2016.05.016

Luttrell, G.H., Yoon, R.H., 1984. Surface studies of the collectorless flotation of chalcopyrite. Colloids and Surfaces 12, 239–254. https://doi.org/10.1016/0166-6622(84)80103-1

Lyklema, J., 1995. Fundamentals of Interface and Colloid Science.

Maddox, L.M., Bancroft, G.M., Scaini, M.J., Lorimer, J.W., 1998. Invisible gold: Comparison of Au deposition on pyrite and arsenopyrite. Am. Mineral. 83, 1240–1245. https://doi.org/10.2138/am-1998-11-1212

Makanza, A.T., Vermaak, M.K.G., Davidtz, J.C., 2008. The flotation of auriferous pyrite with a mixture of collectors. Int. J. Miner. Process. 86, 85–93. https://doi.org/10.1016/j.minpro.2007.11.004

Maree, W., Kloppers, L., Hangone, G., Oyekola, O., 2017. The effects of mixtures of potassium amyl xanthate (PAX) and isopropyl ethyl thionocarbamate (IPETC) collectors on grade and recovery in the froth flotation of a nickel sulfide ore. South African J. Chem. Eng. 24, 116–121. https://doi.org/10.1016/j.sajce.2017.07.001

Matsuoka, I., Ichikoku, T., 1982. Study on Collection of Galena by Dithiophosphates. J. Min. Metall. Inst. Japan 98.

Mcfadzean, B., Castelyn, D.G., O'connor, C.T., 2012. The effect of mixed thiol collectors on the flotation of galena. Miner. Eng. 36–38, 211–218. https://doi.org/10.1016/j.mineng.2012.03.027

Mcfadzean, B., Mhlanga, S.S., O'Connor, C.T., 2013. The effect of thiol collector mixtures on the flotation of pyrite and galena. Miner. Eng. 50–51, 121–129. https://doi.org/10.1016/j.mineng.2013.06.018

Melo, F., Laskowski, J.S., 2006. Fundamental properties of flotation frothers and their effect on flotation. Miner. Eng. 19, 766–773. https://doi.org/10.1016/j.mineng.2005.09.031

Mendiratta, N., 2000. Kinetic studies of sulfide mineral oxidation and xanthate Adsorption. Univ. Libr. Virginia Polytech. Inst. State Univ.

Meyer, F.M., Moller, P., de Bruin, D., Przybylowicz, W.J., Prozesky, V.M., 1994. The Gold-Pyrite Association in Witwatersrand Reefs: Evidence of Electrocehmical Precipitation of Gold.

Michsud, D., 2016. Gold Fire Assay Process [WWW Document]. 911 Metal. URL https://www.911metallurgist.com/blog/gold-fire-assay-process

Miller, J.D., Misra, M., Gopalakrishnan, S., 1968. Gold flotation from Colorado river sand with air sparged hydrocyclone. Miner. Met. Process.

Mingione, P.A., 1984. Use of dialkyl and diaryl dithiophosphate promoters as mineral flotation agents. Inst. Min. Met. London.

Montgomery, D.C., Runger, G.C., 2014. Statistical intervals for a single sample, in: Montgomery, D.C., Runger, G.C. (Eds.), Applied Statistics and Probability for Engineers. John Wiley & Sons, Singapore, p. 277.

Morey, A.A., Tomkins, A.G., Bierlein, F.P., Weinberg, R.F., Davidson, G.J., 2008. Bimodal distribution of gold in pyrite and arsenopyrite: Examples from the archean boorara and bardoc shear systems, Yilgarn Craton, Western Australia. Econ. Geol. 103, 599–614. https://doi.org/10.2113/gsecongeo.103.3.599

Moslemi, H., Gharabaghi, M., 2017. A review on electrochemical behavior of pyrite in the froth flotation

process. J. Ind. Eng. Chem. 47, 1–18. https://doi.org/10.1016/j.jiec.2016.12.012

Mu, Y., Peng, Y., Lauten, R.A., 2016. The depression of pyrite in selective flotation by different reagent systems – A Literature review. Miner. Eng. 96–97, 143–156. https://doi.org/10.1016/j.mineng.2016.06.018

Mukai, S., Wakamatsu, T., Takahashi, K., 1972. Mutual interaction between collectors and frothers in flotation. Mem. Fac. Eng. Kyoto Univ. 34, 279–228.

Natarajan, K.A., 1994. Biological processing of refractory gold ores. J. Mines, Met. Fuels 42, 325–332. https://doi.org/10.1016/0892-6875(91)90081-6

Natarajan, K.A., Iwasaki, I., 1984. ELECTROCHEMICAL ASPECTS OF GRINDING MEDIA--MINERAL INTERACTIONS IN MAGNETITE ORE GRINDING. Int. J. Miner. Process. 13, 53–71.

Nuclear-International-Technical-Working-Group, n.d. ITWG GUIDELINE ON POWDER X-RAY DIFFRACTION (XRD).

O Connor, C.T., Dunne, R.C., 1994. The flotation of gold bearing ores - A review. Miner. Eng. 7, 839–849. https://doi.org/10.1016/0892-6875(94)90128-7

Oberthür, T., Cabri, L.J., Weiser, T.W., Mcmahon, G., Müller, P., 1997. Pt, Pd and other trace elements in sulfides of the Main Sulfide Zone, Great Dyke, Zimbabwe: A reconnaissance study. Can. Mineral. 35, 597–609.

Oliveira, J.F., Saraiva, S.M., Pimenta, J.S., Oliveira, A.P.A., 2001. Kinetic of pyrochlore flotation from Araxa mineral deposits. Miner. Eng. 14, 99–105.

Owusu, C., Addai-Mensah, J., Fornasiero, D., Zanin, M., 2013. Estimating the electrochemical reactivity of pyrite ores-their impact on pulp chemistry and chalcopyrite flotation behaviour. Adv. Powder Technol. 24, 801–809. https://doi.org/10.1016/j.apt.2013.05.006

Ozun, S., Vaziri Hassas, B., Miller, J.D., 2019. Collectorless flotation of oxidized pyrite. Colloids Surfaces A Physicochem. Eng. Asp. 561, 349–356. https://doi.org/10.1016/j.colsurfa.2018.10.064

Pals, D.W., Spry, P.G., Chryssoulis, S., 2003. Invisible Gold and Tellurium in Arsenic-Rich Pyrite from the Emperor Gold Deposit, Fiji: Implications for Gold Distribution and Deposition. Econ. Geol. 98, 479–493.

Pan_African_Resources, 2019. Operations at a glance- Pan African Resources [WWW Document]. URL http://www.panafricanresources.com/gold/btrp/operations-at-a-glance-2/

Park, K., Choi, J., Gomez-Flores, A., Kim, H., 2015. Flotation Behavior of Arsenopyrite and Pyrite, and Their Selective Separation. Mater. Trans. 56, 435–440. https://doi.org/10.2320/matertrans.m2014369

Peng, Y., Grano, S., 2010a. Effect of grinding media on the activation of pyrite flotation. Miner. Eng. 23, 600–605. https://doi.org/10.1016/j.mineng.2010.02.003

Peng, Y., Grano, S., 2010b. Inferring the distribution of iron oxidation species on mineral surfaces during grinding of base metal sulphides. Electrochim. Acta 55, 5470–5477. https://doi.org/10.1016/j.electacta.2010.04.097

Petruk, W., 2000. Applied mineralogy in the mining industry.

Pienaar, D., Jordaan, T., McFadzean, B., O'Connor, C.T., 2019. The synergistic interaction between dithiophosphate collectors and frothers at the air-water and sulphide mineral interface. Miner. Eng. 138, 125–132. https://doi.org/10.1016/j.mineng.2019.04.038

Plaskin, I.N., Glembotskii, V.A., Okolovich, A.M., 1954. Investigations of the possible intensification of the flotation process using combinations of collectors. Tech. Rep. Transl. Feb 1989, Mintek.

Pridmore, D.F., Shuey, R.T., 1976. The electrical resistivity of galena, pyrite, and chalcopyrite. Am. Mineral. 61, 248–259.

Rabieh, A., Albijanic, B., Eksteen, J.J., 2016. A review of the effects of grinding media and chemical conditions on the flotation of pyrite in refractory gold operations. Miner. Eng. 94, 21–28. https://doi.org/10.1016/j.mineng.2016.04.012

Ralston, J., 1991. Eh and its consequences in sulphide mineral flotation. Miner. Eng. 4, 859–878. https://doi.org/10.1016/0892-6875(91)90070-C

Rao, K.H., Forssberg, K.S.E., 1997. Mixed collector systems in flotation. Int. J. Miner. Process. 51, 67–79. https://doi.org/10.1016/s0301-7516(97)00039-2

Reich, M., Kesler, S.E., Utsunomiya, S., Palenik, C.S., Chryssoulis, S.L., Ewing, R.C., 2005. Solubility of gold in arsenian pyrite. Geochim. Cosmochim. Acta 69, 2781–2796. https://doi.org/10.1016/j.gca.2005.01.011

Reyes-Bozo, L., Escudey, M., Vyhmeister, E., Higueras, P., Godoy-Faúndez, A., Salazar, J.L., Valdés-González, H., Wolf-Sepúlveda, G., Herrera-Urbina, R., 2015. Adsorption of biosolids and their main components on chalcopyrite, molybdenite and pyrite: Zeta potential and FTIR spectroscopy studies. Miner. Eng. 78, 128–135. https://doi.org/10.1016/j.mineng.2015.04.021

Sandell, E.B., 1968. Meaning of the term “separation factor.” Anal. Chem. 40, 834–835.

Schieck, R., Hartmann, A., Fiechter, S., Könenkamp, R., Wetzel, H., 1990. Electrical properties of natural and synthetic pyrite (FeS 2) crystals. J. Mater. Res. 5, 1567–1572. https://doi.org/10.1557/JMR.1990.1567

Simon, G., Huang, H., Penner-Hahn, J.E., Kesler, S.E., Kao, L.S., 1999. Oxidation state of gold and arsenic in gold-bearing arsenian pyrite. Am. Mineral. 84, 1071–1079. https://doi.org/10.2138/am-1999-7-809

Su, W., Xia, B., Zhang, H., Zhang, X., Hu, R., 2008. Visible gold in arsenian pyrite at the Shuiyindong Carlin-type gold deposit, Guizhou, China: Implications for the environment and processes of ore formation. Ore Geol. Rev. 33, 667–679. https://doi.org/10.1016/j.oregeorev.2007.10.002

Tadie, M., Corin, K.C., Wiese, J.G., Nicol, M., O’Connor, C.T., 2015. An investigation into the electrochemical interactions between platinum group minerals and sodium ethyl xanthate and sodium diethyl dithiophosphate collectors: Mixed potential study. Miner. Eng. 83, 44–52. https://doi.org/10.1016/j.mineng.2015.08.003

Tauson, V.L., 1999. Gold solubility in the common gold-bearing minerals: Experimental evaluation and application to pyrite. Eur. J. Mineral. 11, 937–947.

Teague, A.J., Van Deventer, J.S.J., Swaminathan, C., 2000. The effect of copper activation on the behaviour of free and refractory gold during froth flotation. Int. J. Miner. Process. 59, 113–130. https://doi.org/10.1016/S0301-7516(99)00060-5

Tipman, N.R., 1970. THE REACTIONS OF POTASSIUM ETHYL XANTHATE IN AQUEOUS SOLUTION.

Tolley, W., Kotlyar, D., Van Wagoner, R., 1992. FUNDAMENTAL ELECTROCHEMICAL STUDIESOF SULFIDE MINERAL FLOTATION 5, 867–881.

Tucker, J.P., Deglon, D.A., Franzidis, J.P., Harris, M.C., O’Connor, C.T., 1994. An evaluation of a direct method of bubble size distribution measurement in a laboratory batch flotation cell. Miner. Eng. 7, 667–680. https://doi.org/10.1016/0892-6875(94)90098-1

Vaughan, D.J., Craig, J.R., 1978. Mineral Chemistry of Metal Sulfides. Cambridge Univ. Press. Cambridge.

Vera, M.A., Mathe, Z.T., Franzidis, J.P., Harris, M.C., Manlapig, E. V., O’Connor, C.T., 2002. The modelling of froth zone recovery in batch and continuously operated laboratory flotation cells. Int. J. Miner. Process. 64, 135–151. https://doi.org/10.1016/S0301-7516(01)00068-0

Vizcarra, T.G., Harmer, S.L., Wightman, E.M., Johnson, N.W., Manlapig, E. V., 2011. The influence of particle shape properties and associated surface chemistry on the flotation kinetics of chalcopyrite.

Miner. Eng. 24, 807–816. https://doi.org/10.1016/j.mineng.2011.02.019

Wang, X.-H., 1995. Interfacial pyrite oxidation electrochemistry and flotation. J. Colloid Interface Sci.

Wells, J.D., Mullens, T.E., 1973. Gold-bearing arsenian pyrite determined by microprobe analysis, Cortez and Carlin gold mines, Nevada. Econ. Geol. 68, 187–201.

Wiese, J., Harris, P., Bradshaw, D., 2011. The effect of the reagent suite on froth stability in laboratory scale batch flotation tests. Miner. Eng. 24, 995–1003. https://doi.org/10.1016/j.mineng.2011.04.011

Woods, R., 2003. Electrochemical potential controlling flotation. Int. J. Miner. Process. 72, 151–162. https://doi.org/10.1016/S0301-7516(03)00095-4

Woolson, E.A., Moore, L., Fleischer, M., Pollutants., N.R.C. (US) C. on M. and B.E. of E., 1977. Arsenic: Medical and Biologic Effects of Environmental Pollutants.

Xian, Y., Wen, S., Chen, X., Deng, J., Liu, J., 2012. Effect of lattice defects on the electronic structures and floatability of pyrites. Int. J. Miner. Metall. Mater. 19, 1069–1076.

Xiang-Huai, W., Forssberg, E.K., 1991. Mechanisms of pyrite flotation with xanthates. Int. J. Miner. Process. 33, 275–290.

Xu, M., 1998. Modified flotation rate constant and selectivity index. 1Minerals Eng. 11, 271–278.

Yalcin, E., Kelebek, S., 2011. Flotation kinetics of a pyritic gold ore. Int. J. Miner. Process. 98, 48–54. https://doi.org/10.1016/j.minpro.2010.10.005

Yelloji Rao, M.K., Natarajan, K.A., 1989. Electrochemical effects of mineral-mineral interactions on the flotation of chalcopyrite and sphalerite. Int. J. Miner. Process. 27, 279–293. https://doi.org/10.1016/0301-7516(89)90069-0

Youlton, K.L., Kinnaird, J.A., Youlton, B.J., 2018. Mineralization processes - the primary control on gold recovery 6–8.

Zeta-Meter-Inc, 2015. Zeta Potential: A complete course in 5 minutes.

Zhong, H., Huang, Z., Zhao, G., Wang, S., Liu, G., Cao, Z., 2015. The collecting performance and interaction mechanism of sodium diisobutyl dithiophosphinate in sulfide minerals flotation. J. Mater. Res. Technol. 4, 151–161. https://doi.org/10.1016/j.jmrt.2014.12.003

## APPENDIX A – BATCH FLOTATION METHODOLOGY

Apparatus besides flotation cell and mill:

- Bucket to collect pulp after milling and tails after float
- Wash bottle
- 2 liter measuring cylinder
- 1 litre measuring cylinder
- Syringe to take 50mL samples
- Filter paper

1. Weigh Ore bag to be used and note mass. Prepare 0.025g of collector mixture (SIBX, DTP and PAX)) and 0.04mL of frother (Senfroh 516) that is refrigerated.
2. Prepare a wash bottle and weigh it, note its mass.
3. Prepare Concentrate tray, weigh and note its mass.
4. Fill the 1 litre top up measuring cylinder to the 1 litre mark with demineralised water.
5. Mill ore to required grind in a laboratory scale rod/ball mill using demineralised water (66% solids- approximately 1kg ore with 500g water).

   Requirement: 85% passing 75 micron: Milling Calibration curve determines time- 35 minutes.
6. Fill 2 liter measuring cylinder (to 2 liter mark) with demineralised water.
7. Transfer milled ore (pulp) to bucket using demineralised water from the measuring cylinder. Try to keep water usage to a minimum, target is around 1 litre.
8. Ensure Drain of flotation cell is closed
9. Transfer milled pulp to Perspex flotation cell using the remainder of the demineralised water in the 2 liter measuring cylinder.

   Note the water used to transfer pulp from mill and to cell. DO NOT EXCEED 2 liters of water for these steps. Total water in cell should be 2500mL now.
10. Set impeller speed to 1200 rpm
11. Take 50mL of feed sample using syringe.

12. Conduct Batch flotation:

At time:
0 minutes: Add 25g/ton (0.025g) collector(s)

4 minutes: Add frother: Senfroh 516 40g/ton solids- 0.04mL

5 minutes: Turn air on (Air flow rate 7L/min) and allow froth to develop

Concentrates are collected by scraping froth into collecting pan every 15 seconds

At 6:45 minute Mark: Top water up to 4cm mark

At 7:45 minute Mark: Top water up to 3cm mark

At 9:45 minute Mark: Top water up to 2.5cm mark

At 15 Minute: Turn air off

13. Ensure bucket is placed below drain pipe, open drain valve. Wash out all solids using water. Clear air feed lines of any solids by disconnecting them and blowing through them, capturing any solids.
14. Weigh wash bottle after each run and record mass.
15. Weigh the concentrate tray including the solids and water and record masses.
16. Filter press all samples, concentrates and tailings. Dry overnight in an oven at 60-80$^{o}$C. Weigh and record masses of dry solids.

NOTES: Scraper and weir are “washed off” periodically as required to ensure all solids belonging to the concentrate end up in the concentrate tray.

## APPENDIX B – SAMPLE CALCULATIONS

Throughout the sample calculations, wet masses and dry masses are used.

The dry mass of a sample was calculated as the weighed dry mass of the sample and filter paper minus the filter paper mass that was weighed before the sample was put onto it.

The wet mass was calculated as the weighed mass of the sample minus the mass of the container that held it.

### 1. Pyrite Recovery and Grade

The pyrite recovery and grade calculations were based on calculating the mass of pyrite in each mass (Concentrate, tailings and feed). This was based on the XRF data and dry mass data.

$$Mass\ of\ pyrite\ in\ the\ sample = (Mass\ of\ Fe\ in\ sample - Fe\ contributions\ to\ other\ minerals)\ x\ (\frac{Molar\ mass\ of\ Pyrite}{Molar\ mass\ of\ Fe})$$

Where the mass of Fe in the sample is calculated as:

$$Mass\ of\ Fe\ in\ the\ sample = (Percentage\ of\ Fe\ in\ the\ sample)\ x\ (dry\ mass\ of\ the\ sample)$$

Where the percentage of Fe in the sample is calculated from XRF data. For example, 3% Fe in the concentrate of 175 grams of dry mass.

$$Mass\ of\ Fe\ in\ the\ sample = (3\%)\ x\ (175g) = 5.25g$$

The Fe contributions to other minerals, chalcopyrite and pentlandite, are calculated as follows, with the masses of copper and nickel being calculated in the same was as Fe in the previous calculation

$$Fe\ contributions\ to\ chalcopyrite = \frac{(Copper\ mass)\ x\ (Fe\ Molar\ mass)}{chalcopyrite\ molar\ mass}\ x\ Molar\ ratio\ Fe{:}Cu\ in\ Chalcopyrite$$

$$= \frac{(0.05\%\ x\ 175g)\ x\ \left(55.845\frac{g}{mol}\right)}{63.546\frac{g}{mol}}\ x\frac{1}{1}$$

$$= 0.077g$$

$$Fe\ contributions\ to\ Pentlandite = \frac{(Nickel\ mass)\ x\ (Fe\ Molar\ mass)}{Ni\ Molar\ mass}\ x\ Molar\ ratio\ Fe{:}Ni\ in\ Pentlandite$$

$$= \frac{(0.18\%\ x\ 175g)\ x\ (55.845\frac{g}{mol})}{58.6934\frac{g}{mol}}\ x\frac{4.5}{4.5}$$

$$= 0.3g$$

Therefore

$$Mass\ of\ pyrite\ in\ the\ sample = (5.25g - (0.077g + 0.3g)\ x\ (\frac{119.965}{55.845})$$

$$= 10.468\text{g of pyrite}$$

The Grade of Pyrite can be calculated as:

$$Pyrite\ grade = \frac{mass\ of\ pyrite}{Total\ mass} x100\%$$

$$= \frac{10.468g}{175g} x100\%$$

$$= 5.98\%$$

The recovery of pyrite is simply the mass of pyrite in the concentrate divided by the mass of pyrite in the feed, both calculated as described above for calculating the pyrite mass.

$$Pyrite\ Recovery = \frac{mass\ of\ pyrite\ in\ concentrate}{mass\ of\ pyrite\ in\ feed} x100\%$$

$$= \frac{10.468g}{34.4g} x100\%$$

$$= 30.043\%$$

## 2. Separation Factor

$$Separation\ Factor\ of\ A\ from\ B = SF_{A/B}$$

$$SF_{\frac{Arsenopyrite}{Pyrite}} = \frac{\left(\frac{mass\ A\ in\ concentrate}{mass\ B\ in\ concentrate}\right)}{\left(\frac{mass\ A\ in\ feed}{mass\ B\ in\ feed}\right)}$$

Example:

$Separation\ Factor\ of\ Arsenopyrite\ from\ Pyrite = SF_{Arsenopyrite/Pyrite}$

*Data for this example is from QXRD data, for SIBX runs, in percentages. Because it is the change in the ratio of A and B, as long as the units are in absolute mass or percentage, the units no not matter as the SF is dimensionless*

$$SF_{\frac{Arsenopyrite}{Pyrite}} = \frac{\left(\frac{mass\ aresenopyrite\ in\ concentrae}{mass\ pyrite\ in\ concentrate}\right)}{\left(\frac{mass\ aresenopyrite\ in\ feed}{mass\ pyrite\ in\ feed}\right)}$$

$$= \frac{\left(\frac{2.12\%}{5.03\%}\right)}{\left(\frac{0.587\%}{1.73\%}\right)}$$

$$= 1.03$$

## 3. Error Analysis

***Error in Directly measured parameters: Uncertainty Parameter***

$$Uncertainty = (Standard\ Error)\ x\ (T, Inverse, 2\ tailed\ Score)$$

$$= \left(Standard\ Deviation\ of\ data\ x\ \sqrt{Number\ of\ data\ points}\right)\ x\ (T, Inverse, 2\ tailed)$$

Where parameters of the "T, Inverse, two tailed" term are:

$$Alpha = \alpha = 1 - confidence\ level = 1 - 0.95 = \ 0.05$$

$$Degrees\ of\ freedom = Number\ of\ data\ points - 1$$

Example:

Again, data from this is taken from the *QXRD data, from the feed samples. All values are again in percentage*

| Feed samples | Quartz |
|---|---|
| sample 1 | 57.9 |
| sample 2 | 57.22 |
| sample 3 | 57.22 |
| Average | 57.44667 |
| StDev | 0.392598 |
| Standard Error | 0.68 |
| Uncertainty Parameter | 2.93 |

$$Uncertainty\ of\ quarts = (Standard\ Error)\ x\ (T, Inverse, 2\ tailed\ Score)$$

$$Uncertainty\ of\ quarts = (0.68)\ x\ (4.30265273)$$
$$= 2.93$$

## 4. Amount of Xanthate for 50% monolayer coverage in micro-flotation

The surface coverage for a single xanthate particle from literature is converted to meters squared:

$$Area\ of\ xanthate\ per\ particle\ in\ meters\ squared = area\ in\ Angstrom\ squared\ x\ \frac{10^{-20} m^2}{1\ Å^2}$$

$$= 28.485\ x\ 10^{-20} m^2$$

The BET particle surface area and the mass of pyrite in the Micro-flotation cell is then used to calculate the total pyrite surface area in the cell:

$$Total\ pyrite\ surface\ area = (pyrite\ surface\ area\ per\ gram)\ x\ (grams\ of\ pyrite)$$

$$= 1.3\frac{m^2}{g}\ x\ 3g$$

$$= 3.9m^2$$

The number of molecules of xanthate needed is then calculated:

$$Number\ of\ xanthate\ molecules\ needed$$

$$= (total\ area\ of\ pyrite\ in\ sample)\ x\frac{(desired\ coverage)}{(area\ of\ xanthate\ per\ molecule)}$$

$$= (3.9m^2)\ x\frac{50\%}{28.485\ x\ 10^{-20}m^2/molecule}$$

$$= 6.84x10^{18}\ molecules\ of\ xanthate$$

The mass of xanthate to be added can then be calculated, for example PAX:

$$Mass\ of\ xanthate = (Mol\ of\ xanthate)x\ (molar\ mass\ of\ xanthate)$$

$$= \frac{Molecules\ of\ xanthate}{Avogadro's number}x\ (molar\ mass\ of\ xanthate)$$

$$= \frac{6.84x10^{18}\ molecules\ of\ xanthate}{6.022 \times 10^{23}\frac{molecules}{mol}}x\ (202.37\ \mathrm{g/mol})$$

$$= 2.3\ x\ 10^{-3}g\ of\ xanthate$$

$$= 0.0023\ g\ of\ xanthat$$

## 5. Collector Dosage Calculation for Batch Flotation

The example of SD25 will be used, where the total collector dosage is 25.2g/ton, with 75% SIBX and 25% SIBDTP.

$$Total\ Mass\ of\ Collector = Collector\ dosage\ x\ mass\ core$$

$$= 25.2\frac{g}{ton}\ x\ 1\ kg\ x\frac{1\ ton}{1000\ kg}$$

$$= 0.0252g$$

The total mass of collector then has to be split up into the two collector components and corrected for purity, for example, SIBTPD:

$$Mass\ of\ DTP = Total\ Mass\ of\ Collector\ x\ Percentage\ DTP\ x\ \frac{1}{Percentage\ Purity}$$

$$= 252\ \mu g\ \ x\ 25\%\ x\frac{1}{50\%}$$

$$= 126\ \mu g$$

## APPENDIX C: BATCH FLOTATION SCOPING EXPERIMENTS

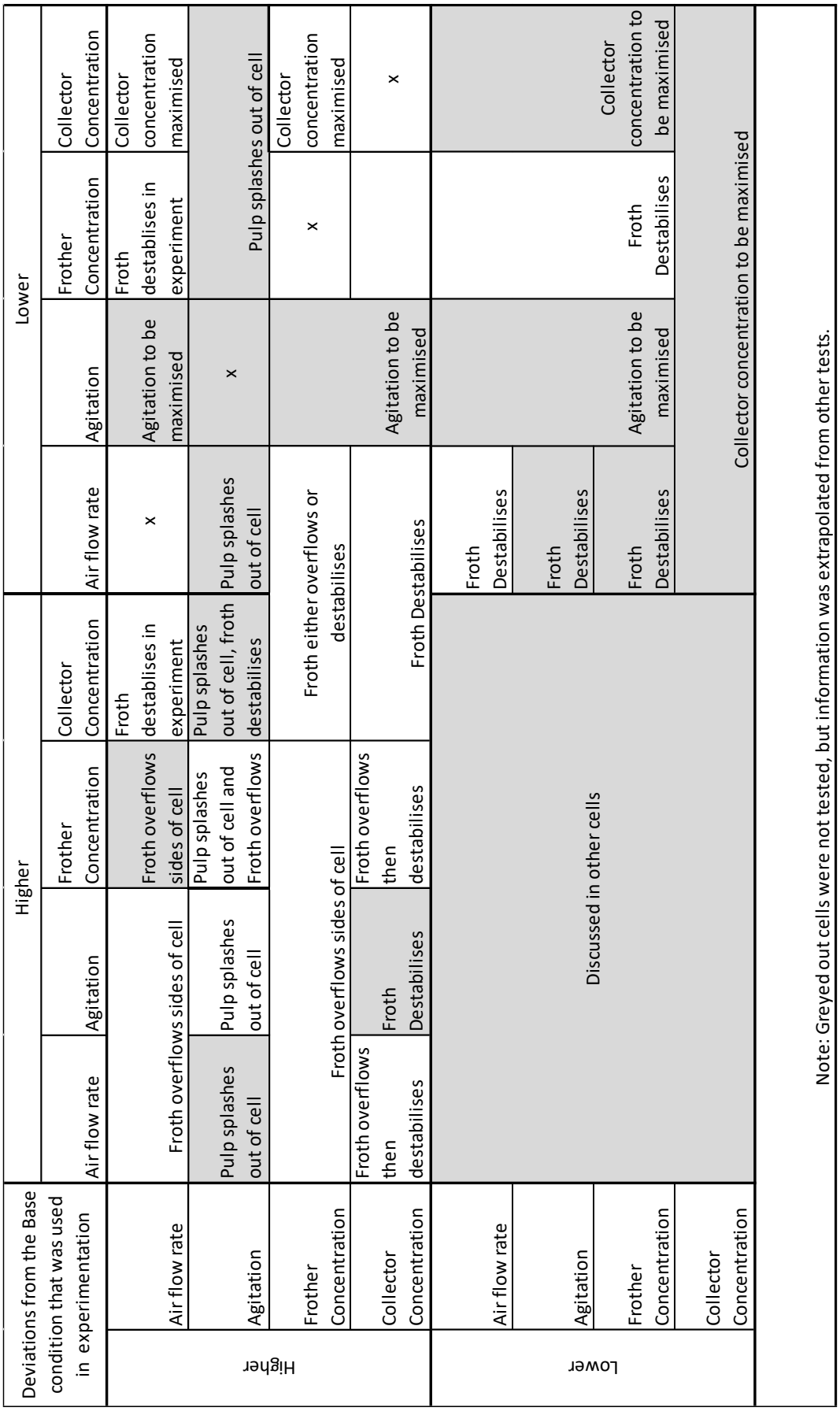

## APPENDIX D: EXPERIMENTAL RAW DATA

### *Batch Flotation Mass recovery Data*

| Experiment | SIBX 1 |
|---|---|
| | |
| Raw ore mass, incl Bag, g | 1000.8 |
| Wash water mass before, g | 598.7 |
| Wash water mass after, g | 397 |
| Concentrate wet mass, incl pan, g | 1171 |
| Concentrate dry mass, incl bag, g | 161.5 |
| Tailing dry mass, incl bag, g | 867.7 |

| Experiment | SIBX 2 |
|---|---|
| | |
| Raw ore mass, incl Bag, g | 1027.1 |
| Wash water mass before, g | 634.4 |
| Wash water mass after, g | 412.4 |
| Concentrate wet mass, incl pan, g | 1241.2 |
| Concentrate dry mass, incl bag, g | 159.3 |
| Tailing dry mass, incl bag, g | 858.3 |

| Experiment | SIBX 3 |
|---|---|
| | |
| Raw ore mass, incl Bag, g | 1023.3 |
| Wash water mass before, g | 412.4 |
| Wash water mass after, g | 205.6 |
| Concentrate wet mass, incl pan, g | 1213.7 |
| Concentrate dry mass, incl bag, g | 159.4 |
| Tailing dry mass, incl bag, g | 854.9 |

| Experiment | PAX 1 |
|---|---|
| | |
| Raw ore mass, incl Bag, g | 1041.4 |
| Wash water mass before, g | 617.3 |
| Wash water mass after, g | 444.9 |
| Concentrate wet mass, incl pan, g | 1225.5 |
| Concentrate dry mass, incl bag, g | 174.4 |
| Tailing dry mass, incl bag, g | 863.5 |

| Experiment | PAX 2 |
|---|---|

| | |
|---|---|
| Raw ore mass, incl Bag, g | 1033.1 |
| Wash water mass before, g | 444.9 |
| Wash water mass after, g | 222.8 |
| Concentrate wet mass, incl pan, g | 1257.6 |
| Concentrate dry mass, incl bag, g | 178.8 |
| Tailing dry mass, incl bag, g | 844.8 |

| Experiment | PAX 3 |
|---|---|
| | |
| Raw ore mass, incl Bag, g | 1027.8 |
| Wash water mass before, g | 612.2 |
| Wash water mass after, g | 438.5 |
| Concentrate wet mass, incl pan, g | 1198.8 |
| Concentrate dry mass, incl bag, g | 171.1 |
| Tailing dry mass, incl bag, g | 846.8 |

| Experiment | DTP 1 |
|---|---|
| | |
| Raw ore mass, incl Bag, g | 1085.6 |
| Wash water mass before, g | 449.6 |
| Wash water mass after, g | 393.4 |
| Concentrate wet mass, incl pan, g | 1372.8 |
| Concentrate dry mass, incl bag, g | 197.3 |
| Tailing dry mass, incl bag, g | 844.8 |

| Experiment | DTP 2 |
|---|---|
| | |
| Raw ore mass, incl Bag, g | 1046.2 |
| Wash water mass before, g | 393.4 |
| Wash water mass after, g | 337.6 |
| Concentrate wet mass, incl pan, g | 1276.5 |
| Concentrate dry mass, incl bag, g | 188.8 |
| Tailing dry mass, incl bag, g | 869.1 |

| Experiment | DTP 3 |
|---|---|
| | |
| Raw ore mass, incl Bag, g | 1065.2 |
| Wash water mass before, g | 337.6 |
| Wash water mass after, g | 298.5 |
| Concentrate wet mass, incl pan, g | 1312.2 |
| Concentrate dry mass, incl bag, g | 195.5 |
| Tailing dry mass, incl bag, g | 866.5 |

| Experiment | SD25 1 |
|---|---|

| | |
|---|---|
| Raw ore mass, incl Bag, g | 1034.7 |
| Wash water mass before, g | 298.5 |
| Wash water mass after, g | 251.8 |
| Concentrate wet mass, incl pan, g | 1277.4 |
| Concentrate dry mass, incl bag, g | 203 |
| Tailing dry mass, incl bag, g | 800 |

| Experiment | SD25 2 |
|---|---|
| | |
| Raw ore mass, incl Bag, g | 1054.8 |
| Wash water mass before, g | 251.8 |
| Wash water mass after, g | 214.8 |
| Concentrate wet mass, incl pan, g | 1256.2 |
| Concentrate dry mass, incl bag, g | 209.3 |
| Tailing dry mass, incl bag, g | 812.6 |

| Experiment | SD25 3 |
|---|---|
| | |
| Raw ore mass, incl Bag, g | 1061.7 |
| Wash water mass before, g | 214.8 |
| Wash water mass after, g | 190.5 |
| Concentrate wet mass, incl pan, g | 1228.2 |
| Concentrate dry mass, incl bag, g | 201.8 |
| Tailing dry mass, incl bag, g | 831.5 |

| Experiment | SD50 1 |
|---|---|
| | |
| Raw ore mass, incl Bag, g | 1036.2 |
| Wash water mass before, g | 612.2 |
| Wash water mass after, g | 566.8 |
| Concentrate wet mass, incl pan, g | 1082.2 |
| Concentrate dry mass, incl bag, g | 170.2 |
| Tailing dry mass, incl bag, g | 833 |

| Experiment | SD50 2 |
|---|---|
| | |
| Raw ore mass, incl Bag, g | 1065.4 |
| Wash water mass before, g | 566.8 |
| Wash water mass after, g | 520.4 |
| Concentrate wet mass, incl pan, g | 1102 |
| Concentrate dry mass, incl bag, g | 176.5 |
| Tailing dry mass, incl bag, g | 845.9 |

| Experiment | SD50 3 |
|---|---|

| | |
|---|---|
| Raw ore mass, incl Bag, g | 1054.3 |
| Wash water mass before, g | 520.4 |
| Wash water mass after, g | 493.5 |
| Concentrate wet mass, incl pan, g | 1086.8 |
| Concentrate dry mass, incl bag, g | 172 |
| Tailing dry mass, incl bag, g | 828.7 |

| Experiment | SD75 1 |
|---|---|
| | |
| Raw ore mass, incl Bag, g | 1062.8 |
| Wash water mass before, g | 636 |
| Wash water mass after, g | 578.1 |
| Concentrate wet mass, incl pan, g | 1355.2 |
| Concentrate dry mass, incl bag, g | 202.5 |
| Tailing dry mass, incl bag, g | 858.4 |

| Experiment | SD75 2 |
|---|---|
| | |
| Raw ore mass, incl Bag, g | 1043.5 |
| Wash water mass before, g | 578.1 |
| Wash water mass after, g | 536.8 |
| Concentrate wet mass, incl pan, g | 1315 |
| Concentrate dry mass, incl bag, g | 192.8 |
| Tailing dry mass, incl bag, g | 843.8 |

| Experiment | SD75 3 |
|---|---|
| | |
| Raw ore mass, incl Bag, g | 1013.2 |
| Wash water mass before, g | 536.8 |
| Wash water mass after, g | 597.5 |
| Concentrate wet mass, incl pan, g | 1244.6 |
| Concentrate dry mass, incl bag, g | 196 |
| Tailing dry mass, incl bag, g | 793 |

| Experiment | PD25 1 |
|---|---|
| | |
| Raw ore mass, incl Bag, g | 1026.2 |
| Wash water mass before, g | 578.1 |
| Wash water mass after, g | 564.8 |
| Concentrate wet mass, incl pan, g | 1046.5 |
| Concentrate dry mass, incl bag, g | 143.8 |
| Tailing dry mass, incl bag, g | 883 |

| Experiment | PD25 2 |
|---|---|

| | |
|---|---|
| Raw ore mass, incl Bag, g | 1069.3 |
| Wash water mass before, g | 564.8 |
| Wash water mass after, g | 512.2 |
| Concentrate wet mass, incl pan, g | 1121 |
| Concentrate dry mass, incl bag, g | 157.1 |
| Tailing dry mass, incl bag, g | 912.5 |

| Experiment | PD25 3 |
|---|---|
| | |
| Raw ore mass, incl Bag, g | 1080 |
| Wash water mass before, g | 512.2 |
| Wash water mass after, g | 451.5 |
| Concentrate wet mass, incl pan, g | 1140.1 |
| Concentrate dry mass, incl bag, g | 151.7 |
| Tailing dry mass, incl bag, g | 922.9 |

| Experiment | PD50 1 |
|---|---|
| | |
| Raw ore mass, incl Bag, g | 1054.3 |
| Wash water mass before, g | 467.7 |
| Wash water mass after, g | 373.7 |
| Concentrate wet mass, incl pan, g | 1158 |
| Concentrate dry mass, incl bag, g | 161.4 |
| Tailing dry mass, incl bag, g | 865.7 |

| Experiment | PD50 2 |
|---|---|
| | |
| Raw ore mass, incl Bag, g | 1025.9 |
| Wash water mass before, g | 653 |
| Wash water mass after, g | 600.3 |
| Concentrate wet mass, incl pan, g | 1092.3 |
| Concentrate dry mass, incl bag, g | 159 |
| Tailing dry mass, incl bag, g | 847.5 |

| Experiment | PD50 3 |
|---|---|
| | |
| Raw ore mass, incl Bag, g | 1044.4 |
| Wash water mass before, g | 600.3 |
| Wash water mass after, g | 579 |
| Concentrate wet mass, incl pan, g | 1100.4 |
| Concentrate dry mass, incl bag, g | 166.7 |
| Tailing dry mass, incl bag, g | 819.1 |

| Experiment | PD75 1 |
|---|---|

| | |
|---|---|
| Raw ore mass, incl Bag, g | 1042.6 |
| Wash water mass before, g | 373.7 |
| Wash water mass after, g | 275.9 |
| Concentrate wet mass, incl pan, g | 1406.7 |
| Concentrate dry mass, incl bag, g | 191 |
| Tailing dry mass, incl bag, g | 865 |

| Experiment | PD75 2 |
|---|---|
| | |
| Raw ore mass, incl Bag, g | 1059.3 |
| Wash water mass before, g | 619.8 |
| Wash water mass after, g | 523 |
| Concentrate wet mass, incl pan, g | 1412 |
| Concentrate dry mass, incl bag, g | 200.1 |
| Tailing dry mass, incl bag, g | 822.2 |

| Experiment | PD75 3 |
|---|---|
| | |
| Raw ore mass, incl Bag, g | 1023 |
| Wash water mass before, g | 523 |
| Wash water mass after, g | 479.3 |
| Concentrate wet mass, incl pan, g | 1336.2 |
| Concentrate dry mass, incl bag, g | 189.9 |
| Tailing dry mass, incl bag, g | 839.8 |

***Particle size distribution Data***

| Pre Mill | |
|---|---|
| Sive Size, um | Mass Sieve Before, g |
| 0 | 0 |
| 25 | 452.51 |
| 53 | 469.74 |
| 75 | 278.57 |
| 106 | 461.8 |
| 250 | 462.24 |
| 425 | 508.15 |
| 600 | 510.69 |
| 1000 | 0 |

| Post mill | |
|---|---|
| Sive Size, um | Mass incl Bag g |
| 0 | 103.25 |
| 25 | 354.32 |
| 53 | 276.25 |
| 75 | 95.36 |
| 106 | 43.56 |
| 212 | 0 |
| | |
| Sive Size, um | Mass incl Bag g |
| 0 | 18.26 |
| 25 | 52.62 |
| 53 | 43.86 |
| 75 | 21.59 |
| 106 | 11.59 |
| 212 | 0 |
| | |
| Sive Size, um | Mass incl Bag g |
| 0 | 39.58 |
| 25 | 135.81 |
| 53 | 96.26 |
| 75 | 43.35 |
| 106 | 22.58 |
| 212 | 0 |

***XRF Data***

| Experimental Data | SIBX 1 | SIBX 2 | SIBX 3 | SD25 1 | SD25 2 | SD25 3 | SD50 1 | SD50 2 | SD50 3 |
|---|---|---|---|---|---|---|---|---|---|
| | | | | | | | | | |
| Feed Dry Mass | 1000.8 | 1027. 1 | 1023. 3 | **1027** | **1047. 1** | 1054 | 1028. 5 | 1057. 7 | 1046. 6 |
| Net Concentrate dry mass, g | 153.8 | 151.6 | 151.7 | 195.3 | 201.6 | 194.1 | 162.5 | 168.8 | 164.3 |
| Net Tailing dry mass, g | 860 | 850.6 | 847.2 | 792.3 | 804.9 | 823.8 | 825.3 | 838.2 | 821 |
| Eh | 187 | 204 | 199 | **210** | **204** | 213 | 235 | 231 | 223 |
| | | | | | | | | | |
| XRF Feed | SIBX 1 | SIBX 2 | SIBX 3 | SD25 1 | SD25 2 | SD25 3 | SD50 1 | SD50 2 | SD50 3 |
| Cu - % | 0.01 | 0.01 | 0.01 | 0.01 | 0.01 | 0.01 | 0.01 | 0.01 | 0.01 |
| Ni - % | 0.06 | 0.05 | 0.05 | 0.05 | 0.05 | 0.05 | 0.05 | 0.05 | 0.05 |
| As - g/ton | 249.26 | 257.6 3 | 258.1 8 | 146 | 136 | 151 | 155 | 165 | 154 |
| Co - % | bdl | bdl | bdl | bdl | bdl | bdl | bdl | bdl | bdl |
| Fe - % | 5.12 | 5.16 | 5.15 | 6.81 | 6.80 | 6.79 | 6.73 | 6.69 | 6.74 |
| Pb - g/ton | 22.22 | 18.97 | 22.59 | 20 | 24 | 16 | 18 | 23 | 21 |
| S - % | 0.39 | 0.49 | 0.49 | 1.47 | 1.44 | 1.42 | 1.42 | 1.37 | 1.39 |
| | | | | | | | | | |
| XRF Conc | SIBX 1 | SIBX 2 | SIBX 3 | SD25 1 | SD25 2 | SD25 3 | SD50 1 | SD50 2 | SD50 3 |
| Cu - % | 0.05 | 0.05 | 0.05 | 0.04 | 0.04 | 0.04 | 0.06 | 0.06 | 0.06 |
| Ni - % | 0.18 | 0.15 | 0.15 | 0.15 | 0.15 | 0.15 | 0.19 | 0.20 | 0.19 |
| As - g/ton | 1777.41 | 1751. 97 | 1762. 93 | 891 | 870 | 875 | 1184 | 1163 | 1182 |
| Co - % | 0.02 | 0.02 | 0.02 | 0.01 | 0.01 | 0.01 | 0.02 | 0.02 | 0.02 |
| Fe - % | 9.21 | 9.23 | 9.2 | 12.29 | 12.10 | 12.21 | 13.32 | 13.27 | 13.55 |
| Pb - g/ton | 117.8 | 136.5 5 | 117.6 7 | 100 | 81 | 96 | 122 | 120 | 121 |
| S - % | 2.57 | 2.1 | 2.05 | 5.56 | 5.16 | 5.44 | 7.22 | 7.17 | 7.48 |

| | | | | | | | | | |
|---|---|---|---|---|---|---|---|---|---|
| XRF Tail | SIBX 1 | SIBX 2 | SIBX 3 | SD25 1 | SD25 2 | SD25 3 | SD50 1 | SD50 2 | SD50 3 |
| Cu - % | bdl | bdl | bdl | bdl | bdl | bdl | bdl | bdl | bdl |
| Ni - % | 0.03 | 0.03 | 0.03 | 0.03 | 0.03 | 0.03 | 0.03 | 0.03 | 0.03 |
| As - g/ton | 67.37 | 69.18 | 68.39 | 56 | 44 | 50 | 57 | 51 | 55 |
| Co - % | bdl | bdl | bdl | bdl | bdl | bdl | bdl | bdl | bdl |
| Fe - % | 4.37 | 4.33 | 4.32 | 5.63 | 5.60 | 5.62 | 5.77 | 5.77 | 5.76 |
| Pb - g/ton | 15.26 | 11.92 | 14.12 | 11 | 9 | 10 | 11 | 10 | 11 |
| S - % | 0.08 | 0.1 | 0.09 | 0.22 | 0.20 | 0.23 | 0.18 | 0.19 | 0.18 |

| | SD75 1 | SD75 2 | SD75 3 | DTP 1 | DTP 2 | DTP 3 | PD75 1 | PD75 2 | PD75 3 |
|---|---|---|---|---|---|---|---|---|---|
| | | | | | | | | | |
| Feed Dry Mass | 1055.1 | 1035.8 | 1005.5 | 1077.9 | 1038.5 | 1057.5 | 1034.9 | 1051.6 | 1015.3 |
| Net Concentrate dry mass, g | 194.8 | 185.1 | 188.3 | 189.6 | 181.1 | 187.8 | 183.3 | 192.4 | 182.2 |
| Net Tailing dry mass, g | 850.7 | 836.1 | 785.3 | 837.1 | 861.4 | 858.8 | 857.3 | 814.5 | 832.1 |
| Eh | 236 | 240 | 232 | 312 | 325 | 327 | 261 | 269 | 257 |
| | | | | | | | | | |
| XRF Feed | SD75 1 | SD75 2 | SD75 3 | DTP 1 | DTP 2 | DTP 3 | PD75 1 | PD75 2 | PD75 3 |
| Cu - % | 0.01 | 0.01 | 0.01 | 0.01 | 0.01 | 0.01 | 0.01 | 0.01 | 0.01 |
| Ni - % | 0.05 | 0.05 | 0.05 | 0.05 | 0.05 | 0.05 | 0.05 | 0.05 | 0.05 |
| As - g/ton | 172 | 184 | 181 | 160 | 146 | 162 | 207 | 206 | 195 |
| Co - % | 0.00 | bdl | bdl | bdl | bdl | bdl | bdl | 0.01 | bdl |
| Fe - % | 6.78 | 6.75 | 6.80 | 6.64 | 6.63 | 6.63 | 6.80 | 6.77 | 6.78 |
| Pb - g/ton | 24 | 36 | 25 | 24 | 20 | 23 | 29 | 29 | 26 |
| S - % | 1.40 | 1.40 | 1.44 | 1.33 | 1.41 | 1.46 | 1.41 | 1.45 | 1.43 |
| | | | | | | | | | |

| XRF Conc | SD75 1 | SD75 2 | SD75 3 | DTP 1 | DTP 2 | DTP 3 | PD75 1 | PD75 2 | PD75 3 |
|---|---|---|---|---|---|---|---|---|---|
| Cu - % | 0.05 | 0.04 | 0.04 | 0.04 | 0.04 | 0.04 | 0.04 | 0.04 | 0.04 |
| Ni - % | 0.16 | 0.15 | 0.16 | 0.09 | 0.09 | 0.10 | 0.16 | 0.16 | 0.16 |
| As - g/ton | 966 | 947 | 957 | 373 | 361 | 348 | 969 | 974 | 1019 |
| Co - % | 0.01 | 0.02 | 0.01 | 0.01 | 0.01 | bdl | 0.02 | 0.02 | 0.02 |
| Fe - % | 11.58 | 11.57 | 11.50 | 8.57 | 8.57 | 8.57 | 11.12 | 11.13 | 11.14 |
| Pb - g/ton | 115 | 103 | 109 | 55 | 50 | 48 | 112 | 102 | 122 |
| S - % | 5.74 | 5.70 | 5.44 | 1.42 | 1.46 | 1.44 | 5.21 | 5.40 | 5.30 |
| | | | | | | | | | |
| XRF Tail | SD75 1 | SD75 2 | SD75 3 | DTP 1 | DTP 2 | DTP 3 | PD75 1 | PD75 2 | PD75 3 |
| Cu - % | bdl | bdl | bdl | bdl | bdl | bdl | bdl | bdl | bdl |
| Ni - % | 0.03 | 0.03 | 0.03 | 0.04 | 0.04 | 0.04 | 0.03 | 0.03 | 0.03 |
| As - g/ton | 53 | 58 | 69 | 133 | 115 | 102 | 64 | 67 | 58 |
| Co - % | bdl | bdl | bdl | bdl | bdl | bdl | bdl | bdl | bdl |
| Fe - % | 5.79 | 5.75 | 5.76 | 6.31 | 6.34 | 6.36 | 5.82 | 5.80 | 5.78 |
| Pb - g/ton | 15 | 11 | 13 | 18 | 16 | 14 | 12 | 13 | 11 |
| S - % | 0.17 | 0.19 | 0.17 | 1.28 | 1.39 | 1.41 | 0.18 | 0.20 | 0.21 |

| | PD50 1 | PD50 2 | PD50 3 | PD25 1 | PD25 2 | PD25 3 | PAX 1 | PAX 2 | PAX 3 |
|---|---|---|---|---|---|---|---|---|---|
| | | | | | | | | | |
| Feed Dry Mass | 1046.6 | 1018.2 | 1036.7 | 1018.5 | 1061.6 | 1072.3 | 1033.7 | 1025.4 | 1020.1 |
| Net Concentrate dry mass, g | 153.7 | 151.3 | 159 | 136.1 | 149.4 | 144 | 166.7 | 171.1 | 163.4 |
| Net Tailing dry mass, g | 858 | 839.8 | 811.4 | 875.3 | 904.8 | 915.2 | 855.8 | 837.1 | 839.1 |
| Eh | 244 | 255 | 237 | 228 | 224 | 219 | 214 | 202 | 227 |
| | | | | | | | | | |

| XRF Feed | PD50 1 | PD50 2 | PD50 3 | PD25 1 | PD25 2 | PD25 3 | PAX 1 | PAX 2 | PAX 3 |
|---|---|---|---|---|---|---|---|---|---|
| Cu - % | 0.01 | 0.01 | 0.01 | 0.01 | 0.01 | 0.01 | 0.01 | 0.01 | 0.01 |
| Ni - % | 0.05 | 0.05 | 0.05 | 0.05 | 0.05 | 0.05 | 0.05 | 0.05 | 0.05 |
| As - g/ton | 170 | 178 | 182 | 173 | 176 | 178 | 229.17 | 255.77 | 255.74 |
| Co - % | bdl | bdl | bdl | bdl | bdl | bdl | bdl | bdl | bdl |
| Fe - % | 6.79 | 6.77 | 6.76 | 6.80 | 6.75 | 6.75 | 5.15 | 5.17 | 5.17 |
| Pb - g/ton | 24 | 25 | 28 | 24 | 23 | 26 | 22.76 | 24.88 | 19.87 |
| S - % | 1.42 | 1.39 | 1.38 | 1.37 | 1.37 | 1.45 | 0.39 | 0.49 | 0.49 |
| | | | | | | | | | |
| XRF Conc | PD50 1 | PD50 2 | PD50 3 | PD25 1 | PD25 2 | PD25 3 | PAX 1 | PAX 2 | PAX 3 |
| Cu - % | 0.06 | 0.06 | 0.06 | 0.07 | 0.07 | 0.07 | 0.04 | 0.04 | 0.04 |
| Ni - % | 0.20 | 0.20 | 0.20 | 0.21 | 0.21 | 0.21 | 0.15 | 0.15 | 0.15 |
| As - g/ton | 1206 | 1231 | 1249 | 1622 | 1565 | 1659 | 1783.93 | 1736.97 | 1712.13 |
| Co - % | 0.02 | 0.02 | 0.02 | 0.02 | 0.02 | 0.02 | 0.02 | 0.02 | 0.02 |
| Fe - % | 13.13 | 13.15 | 13.08 | 13.73 | 13.76 | 13.72 | 9.64 | 9.63 | 9.39 |
| Pb - g/ton | 127 | 140 | 133 | 195 | 173 | 187 | 78.48 | 69.58 | 67.9 |
| S - % | 7.04 | 7.40 | 7.15 | 8.08 | 7.79 | 7.76 | 2.03 | 1.99 | 1.9 |
| | | | | | | | | | |
| XRF Tail | PD50 1 | PD50 2 | PD50 3 | PD25 1 | PD25 2 | PD25 3 | PAX 1 | PAX 2 | PAX 3 |
| Cu - % | bdl | bdl | bdl | bdl | bdl | bdl | bdl | bdl | bdl |
| Ni - % | 0.03 | 0.03 | 0.03 | 0.03 | 0.03 | 0.03 | 0.03 | 0.03 | 0.03 |
| As - g/ton | 68.74 | 63.77 | 68.93 | 59 | 55 | 44 | 61.97 | 65.65 | 63.54 |
| Co - % | bdl | bdl | bdl | bdl | bdl | bdl | bdl | bdl | bdl |
| Fe - % | 575.0% | 575.0% | 574.0% | 5.81 | 5.83 | 5.79 | 4.24 | 4.27 | 4.28 |
| Pb - g/ton | 1314.0 % | 1239.0 % | 1318.0 % | 11 | 11 | 9 | 12.76 | 13.17 | 12.19 |

***Froth Stability tests***

| Batch Froth stability | | | |
|---|---|---|---|
| | Test 1 (mL) | Test 2 (mL) | Test 3 (mL) |
| Frother Only | 172 | 168 | 166 |
| SIBX + Frother | 131 | 135 | 136 |
| DTP + Frother | 151 | 149 | 145 |
| PAX + Frother | 136 | 132 | 137 |

| Froth height in measuring cylinder | | | |
|---|---|---|---|
| Froth height 1.5 | Test 1 (mm) | Test 2 (mm) | Test 3 (mm) |
| No reagents | 12 | 10 | 11 |
| Frother Only | 20 | 21 | 20 |
| SIBX + Frother | 18 | 19 | 19 |
| DTP + Frother | 20 | 23 | 21 |
| PAX + Frother | 18 | 19 | 19 |
| | | | |
| Froth height 3 | | | |
| | Test 1 (mm) | Test 2 (mm) | Test 3 (mm) |
| No reagents | 20 | 21 | 23 |
| Frother Only | 60 | 62 | 66 |
| SIBX + Frother | 42 | 45 | 46 |
| DTP + Frother | 52 | 51 | 54 |
| PAX + Frother | 45 | 43 | 47 |
| | | | |
| Froth height 4.5 | | | |
| | Test 1 (mm) | Test 2 (mm) | Test 3 (mm) |
| No reagents | 34 | 28 | 30 |

| | | | |
|---|---|---|---|
| Frother Only | 212 | 200 | 206 |
| SIBX + Frother | 142 | 138 | 132 |
| DTP + Frother | 173 | 168 | 177 |
| PAX + Frother | 148 | 142 | 145 |

| Experiment | C1 Filter paper mass, g | C1 total mass, g | C2 Filter paper mass, g | C2 total mass, g | C3 Filter paper mass, g | C3 total mass, g | C4 Filter paper mass, g | C4 total mass, g | T Filter pa | T total mass, g | eH, mV |
|---|---|---|---|---|---|---|---|---|---|---|---|
| P1 No collector | 1.527 | 1.541 | 1.532 | 1.556 | 1.525 | 1.558 | 1.53 | 1.601 | 1.526 | 4.351 | 482 |
| P1 No collector | 1.518 | 1.544 | 1.529 | 1.559 | 1.535 | 1.571 | 1.528 | 1.596 | 1.517 | 4.338 | 447 |
| P1 SIBX | 1.52 | 1.843 | 1.522 | 2.108 | 1.522 | 2.293 | 1.521 | 2.04 | 1.525 | 2.313 | 214 |
| P1 SIBX | 1.533 | 1.851 | 1.528 | 2.12 | 1.518 | 2.275 | 1.53 | 2.032 | 1.532 | 2.362 | 226 |
| P1 SD25 | 1.518 | 1.931 | 1.541 | 2.311 | 1.516 | 2.342 | 1.526 | 1.9 | 1.534 | 2.187 | 266 |
| P1 SD25 | 1.527 | 1.927 | 1.536 | 2.289 | 1.534 | 2.337 | 1.524 | 1.889 | 1.528 | 2.192 | 271 |
| P1 SD50 | 1.532 | 1.855 | 1.533 | 2.098 | 1.522 | 2.227 | 1.523 | 1.999 | 1.533 | 2.401 | 236 |
| P1 SD50 | 1.521 | 1.853 | 1.537 | 2.117 | 1.52 | 2.241 | 1.523 | 1.971 | 1.541 | 2.417 | 228 |
| P1 SD75 | 1.522 | 1.807 | 1.542 | 1.956 | 1.519 | 2.125 | 1.528 | 1.875 | 1.526 | 2.566 | 254 |
| P1 SD75 | 1.537 | 1.824 | 1.537 | 1.973 | 1.52 | 2.141 | 1.532 | 1.864 | 1.526 | 2.581 | 263 |
| P1 DTP | 1.519 | 1.634 | 1.535 | 1.698 | 1.518 | 1.648 | 1.532 | 1.644 | 1.525 | 3.927 | 329 |
| P1 DTP | 1.525 | 1.64 | 1.528 | 1.682 | 1.53 | 1.64 | 1.526 | 1.631 | 1.537 | 3.916 | 344 |
| P1 PD75 | 1.525 | 1.821 | 1.525 | 1.994 | 1.518 | 2.1 | 1.534 | 1.954 | 1.526 | 2.516 | 237 |
| P1 PD75 | 1.518 | 1.828 | 1.525 | 2.009 | 1.53 | 2.21 | 1.531 | 1.949 | 1.524 | 2.531 | 234 |
| P1 PD50 | 1.537 | 1.887 | 1.533 | 2.187 | 1.533 | 2.179 | 1.529 | 1.867 | 1.531 | 2.551 | 215 |
| P1 PD50 | 1.526 | 1.908 | 1.531 | 2.161 | 1.518 | 2.183 | 1.53 | 1.854 | 1.522 | 2.543 | 209 |
| P1 PD25 | 1.537 | 2 | 1.538 | 2.31 | 1.535 | 2.307 | 1.526 | 1.8 | 1.522 | 2.095 | 211 |
| P1 PD25 | 1.537 | 2.061 | 1.527 | 1.988 | 1.533 | 2.315 | 1.522 | 1.817 | 1.52 | 2.101 | 205 |
| P1 PAX | 1.524 | 2.007 | 1.53 | 2.301 | 1.533 | 2.334 | 1.522 | 1.826 | 1.535 | 2.031 | 251 |
| P1 PAX | 1.527 | 1.956 | 1.539 | 2.322 | 1.525 | 2.389 | 1.525 | 1.876 | 1.532 | 2.002 | 248 |
| | | | | | | | | | | | |
| P2 No collector | 1.524 | 1.551 | 1.528 | 1.562 | 1.525 | 1.601 | 1.533 | 1.587 | 1.524 | 4.292 | 432 |
| P2 No collector | 1.536 | 1.558 | 1.524 | 1.568 | 1.533 | 1.612 | 1.528 | 1.578 | 1.522 | 4.301 | 419 |
| P2 SIBX | 1.502 | 1.81 | 1.524 | 2 | 1.534 | 2.222 | 1.532 | 1.98 | 1.533 | 2.363 | 202 |
| P2 SIBX | 1.486 | 1.827 | 1.523 | 2.07 | 1.533 | 2.213 | 1.528 | 1.992 | 1.531 | 2.522 | 214 |
| P2 SD25 | 1.522 | 1.856 | 1.524 | 2.163 | 1.531 | 2.38 | 1.52 | 1.897 | 1.524 | 2.357 | 214 |
| P2 SD25 | 1.52 | 1.83 | 1.533 | 2.187 | 1.533 | 2.346 | 1.528 | 1.913 | 1.52 | 2.312 | 221 |
| P2 SD50 | 1.527 | 1.838 | 1.526 | 2.064 | 1.522 | 2.167 | 1.522 | 1.949 | 1.528 | 2.39 | 236 |
| P2 SD50 | 1.528 | 1.822 | 1.539 | 2.061 | 1.534 | 2.172 | 1.521 | 1.939 | 1.528 | 2.5 | 222 |
| P2 SD75 | 1.535 | 1.779 | 1.537 | 1.919 | 1.515 | 2.075 | 1.523 | 1.845 | 1.522 | 2.672 | 244 |
| P2 SD75 | 1.537 | 1.791 | 1.54 | 1.93 | 1.525 | 2.087 | 1.527 | 1.834 | 1.521 | 2.691 | 252 |
| P2 DTP | 1.535 | 1.635 | 1.531 | 1.672 | 1.528 | 1.632 | 1.527 | 1.631 | 1.537 | 4.037 | 371 |
| P2 DTP | 1.529 | 1.628 | 1.54 | 1.657 | 1.533 | 1.627 | 1.539 | 1.621 | 1.525 | 3.96 | 352 |
| P2 PD75 | 1.524 | 1.825 | 1.529 | 1.95 | 1.534 | 2.252 | 1.522 | 1.757 | 1.534 | 2.615 | 236 |
| P2 PD75 | 1.519 | 1.829 | 1.535 | 1.962 | 1.524 | 2.153 | 1.529 | 1.713 | 1.524 | 2.6 | 235 |
| P2 PD50 | 1.522 | 1.956 | 1.538 | 2.232 | 1.535 | 2.225 | 1.535 | 1.731 | 1.518 | 2.361 | 241 |
| P2 PD50 | 1.53 | 1.973 | 1.533 | 2.203 | 1.522 | 2.2 | 1.529 | 1.721 | 1.527 | 2.373 | 231 |
| P2 PD25 | 1.534 | 1.96 | 1.538 | 2.242 | 1.525 | 2.242 | 1.532 | 1.816 | 1.539 | 2.254 | 286 |
| P2 PD25 | 1.527 | 2.01 | 1.525 | 1.944 | 1.517 | 2.247 | 1.538 | 1.823 | 1.526 | 2.32 | 281 |
| P2 PAX | 1.517 | 1.919 | 1.534 | 2.107 | 1.526 | 2.184 | 1.532 | 1.818 | 1.517 | 2.384 | 217 |
| P2 PAX | 1.528 | 1.964 | 1.542 | 2.1 | 1.521 | 2.171 | 1.534 | 1.827 | 1.525 | 2.352 | 222 |

## APPENDIX E: PROCESSED DATA

***Batch Flotation data***

| Experimental Data | SIBX 1 | SIBX 2 | SIBX 3 | SD25 1 | SD25 2 | SD25 3 |
|---|---|---|---|---|---|---|
| | | | | | | |
| Net Concentrate wet mass, g | 906.8 | 977 | 949.5 | 1013.2 | 992 | 964 |
| Net Concentrate dry mass, g | 153.8 | 151.6 | 151.7 | 195.3 | 201.6 | 194.1 |
| Net Tailing dry mass, g | 860 | 850.6 | 847.2 | 792.3 | 804.9 | 823.8 |
| Net Water in Concentrate, g | 705.1 | 755 | 742.7 | 966.5 | 955 | 939.7 |
| Mass recovery, % | 16.1% | 0.155097 | 0.155771 | 0.196192 | 0.198426 | 0.190073 |
| Concentrate Solids % | 21.8% | 0.200795 | 0.204255 | 0.202069 | 0.211099 | 0.206555 |
| Eh | 187 | 204 | 199 | 210 | 204 | 213 |
| | | | | | | |
| Grade in Concentrate | SIBX 1 | SIBX 2 | SIBX 3 | SD25 1 | SD25 2 | SD25 3 |
| Concentrate Pyrite - % | 3.331052 | 3.533827 | 3.53881 | 6.507802 | 6.510343 | 6.180012 |
| Separation Factor Arsenic:Pyrite | 3.964109 | 3.801705 | 3.822364 | 3.390583 | 3.598301 | 3.221658 |
| | | | | | | |
| Recovery - % | SIBX 1 | SIBX 2 | SIBX 3 | SD25 1 | SD25 2 | SD25 3 |
| Pyrite | 31.43041 | 30.14989 | 30.32451 | 71.53524 | 72.45362 | 65.78519 |
| Chalcopyrite | 76.83853 | 73.80002 | 74.12294 | 76.06621 | 77.0127 | 73.66224 |
| Pentlandite | 46.10312 | 44.28001 | 44.47376 | 57.04966 | 57.75953 | 55.24668 |
| | | | | | | |
| | | | | | | |
| Averages | SIBX | | | SD25 | | |
| | | | | | | |

| | | | | | | |
|---|---|---|---|---|---|---|
| Net Concentrate wet mass, g | 944.4 | | | 989.7 | | |
| Net Concentrate dry mass, g | 152.4 | | | 197.0 | | |
| Net Tailing dry mass, g | 852.6 | | | 807.0 | | |
| Net Water in Concentrate, g | 734.3 | | | 953.7 | | |
| Mass recovery, % | 15.7% | | | 19.5% | | |
| Concentrate Solids % | 20.8% | | | 20.7% | | |
| Eh | 196.67 | | | 209.00 | | |
| Concentrate Grades | | | | | | |
| Concentrate Pyrite - % | 3.47% | | | 6.40% | | |
| Separation Factor Arsenic:Pyrite | 3.862725673 | | | 3.403513918 | | |
| | | | | | | |
| Pyrite Recovery- % | 30.63% | | | 69.92% | | |
| Chalcopyrite Recovery- % | 70% | | | 80% | | |
| Pentlandite Recovery- % | 50% | | | 60% | | |
| Gold Recovery | 70.97% | | | 100.89% | | |
| | | | | | | |
| Eh | 196.6667 | | | 209 | | |
| | | | | | | |
| **Uncertainty Parameter Error** | **SIBX** | | | **SD25** | | |
| | | | | | | |
| Net Concentrate wet mass, g | 87.87190204 | | | 61.30403611 | | |
| Net Concentrate dry mass, g | 3.086068318 | | | 10.00771497 | | |
| Net Tailing dry mass, g | 16.47041377 | | | 39.38513972 | | |
| Net Water in Concentrate, g | 64.58009581 | | | 33.39879811 | | |
| Mass recovery, % | 0.008556239 | | | 0.010743497 | | |
| Concentrate Solids % | 0.022783317 | | | 0.011216151 | | |
| Concentrate Grades | | | | | | |
| Concentrate Pyrite - % | 0.002944625 | | | 0.004719554 | | |
| Separation Factor Arsenic:Pyrite | 0.219612131 | | | 0.4686429 | | |

| | | | | | | |
|---|---|---|---|---|---|---|
| Pyrite Recovery- % | 0.017250226 | | | 0.089781681 | | |
| Chalcopyrite Recovery- % | 0.041457652 | | | 0.042907477 | | |
| Pentlandite Recovery- % | 0.024874591 | | | 0.032180608 | | |

| Experimental Data | SD50 1 | SD50 2 | SD50 3 | SD75 1 | SD75 2 | SD75 3 |
|---|---|---|---|---|---|---|
| | | | | | | |
| Net Concentrate wet mass, g | 818 | 837.8 | 822.6 | 1091 | 1050.8 | 980.4 |
| Net Concentrate dry mass, g | 162.5 | 168.8 | 164.3 | 194.8 | 185.1 | 188.3 |
| Net Tailing dry mass, g | 825.3 | 838.2 | 821 | 850.7 | 836.1 | 785.3 |
| Net Water in Concentrate, g | 772.6 | 791.4 | 795.7 | 1033.1 | 1009.5 | 1041.1 |
| Mass recovery, % | 0.164254 | 0.165665 | 0.163141 | 0.190534 | 0.184763 | 0.193447 |
| Concentrate Solids % | 0.210329 | 0.213293 | 0.206485 | 0.188559 | 0.183358 | 0.180866 |
| Eh | 235 | 231 | 223 | 236 | 240 | 232 |
| | | | | | | |
| Grade in Concentrate | SD50 1 | SD50 2 | SD50 3 | SD75 1 | SD75 2 | SD75 3 |
| 5.633983758 | 5.633984 | 5.740709 | 5.825102 | 5.696275 | 5.502391 | 5.923554 |
| 3.866123639 | 3.866124 | 3.55756 | 3.820051 | 3.284997 | 3.010941 | 3.129532 |
| | | | | | | |
| Recovery - % | SD50 1 | SD50 2 | SD50 3 | SD75 1 | SD75 2 | SD75 3 |
| 51.45393064 | 51.45393 | 52.95773 | 52.85843 | 60.79112 | 56.83761 | 64.12163 |
| 94.79824988 | 94.79825 | 95.75494 | 94.19071 | 92.31352 | 71.48098 | 74.90801 |
| 60.03889159 | 60.03889 | 63.83663 | 59.65412 | 59.08066 | 53.61074 | 59.9264 |
| | | | | | | |
| | | | | | | |

| Averages | SD50 | | | SD75 | | |
|---|---|---|---|---|---|---|
| | | | | | | |
| Net Concentrate wet mass, g | 826.1 | | | 1040.7 | | |
| Net Concentrate dry mass, g | 165.2 | | | 189.4 | | |
| Net Tailing dry mass, g | 828.2 | | | 824.0 | | |
| Net Water in Concentrate, g | 786.6 | | | 1027.9 | | |
| Mass recovery, % | 16.4% | | | 19.0% | | |
| Concentrate Solids % | 21.0% | | | 18.4% | | |
| Eh | 229.67 | | | 236.00 | | |
| Concentrate Grades | | | | | | |
| 5.633983758 | 5.73% | | | 5.71% | | |
| 3.866123639 | 3.747911498 | | | 3.141823205 | | |
| | | | | | | |
| Pyrite Recovery- % | 52.42% | | | 60.58% | | |
| Chalcopyrite Recovery- % | 90% | | | 80% | | |
| Pentlandite Recovery- % | 60% | | | 60% | | |
| Gold Recovery | #REF! | | | #REF! | | |
| | | | | | | |
| Eh | 229.6667 | | | 236 | | |
| | | | | | | |
| **Uncertainty Parameter Error** | **SD50** | | | **SD75** | | |
| | | | | | | |
| Net Concentrate wet mass, g | 25.74090938 | | | 139.0694159 | | |
| Net Concentrate dry mass, g | 8.061017306 | | | 12.27827628 | | |
| Net Tailing dry mass, g | 22.23592355 | | | 85.2784372 | | |
| Net Water in Concentrate, g | 30.51784495 | | | 40.81250018 | | |
| Mass recovery, % | 0.003142371 | | | 0.010978942 | | |
| Concentrate Solids % | 0.00847956 | | | 0.009749866 | | |
| Concentrate Grades | | | | | | |

| | | | | | | |
|---|---|---|---|---|---|---|
| 5.6 | 0.002379219 | | | 0.005236624 | | |
| 3.9 | 0.413488086 | | | 0.341421539 | | |
| | | | | | | |
| Pyrite Recovery- % | 0.020892118 | | | 0.09058271 | | |
| Chalcopyrite Recovery- % | 0.019589448 | | | 0.277492651 | | |
| Pentlandite Recovery- % | 0.05742624 | | | 0.085165836 | | |

| Experimental Data | DTP 1 | DTP 2 | DTP 3 | PD75 1 | PD75 2 | PD75 3 |
|---|---|---|---|---|---|---|
| | | | | | | |
| Net Concentrate wet mass, g | 1108.6 | 1012.3 | 1048 | 1142.5 | 1147.8 | 1072 |
| Net Concentrate dry mass, g | 189.6 | 181.1 | 187.8 | 183.3 | 192.4 | 182.2 |
| Net Tailing dry mass, g | 837.1 | 861.4 | 858.8 | 857.3 | 814.5 | 832.1 |
| Net Water in Concentrate, g | 1052.4 | 956.5 | 1008.9 | 1044.7 | 1051 | 1028.3 |
| Mass recovery, % | 0.181743 | 0.180463 | 0.183534 | 0.183196 | 0.188898 | 0.18563 |
| Concentrate Solids % | 0.18016 | 0.189336 | 0.186143 | 0.175457 | 0.183064 | 0.177186 |
| Eh | 312 | 325 | 327 | 261 | 269 | 257 |
| | | | | | | |
| Grade in Concentrate | DTP 1 | DTP 2 | DTP 3 | PD75 1 | PD75 2 | PD75 3 |
| 2.752046425 | 2.752046 | 2.554514 | 2.657041 | 5.107451 | 5.647795 | 5.239959 |
| 1.806920135 | 1.80692 | 1.913452 | 1.663917 | 2.860022 | 2.876482 | 3.184804 |
| | | | | | | |
| Recovery - % | DTP 1 | DTP 2 | DTP 3 | PD75 1 | PD75 2 | PD75 3 |
| 27.98140476 | 27.9814 | 25.74982 | 27.27516 | 52.29043 | 59.72929 | 54.35453 |
| 70.35903145 | 70.35903 | 69.75445 | 71.03546 | 70.84742 | 73.18372 | 71.78174 |

| | | | | | | |
|---|---|---|---|---|---|---|
| 31.66156415 | 31.66156 | 31.3895 | 35.51773 | 56.67794 | 58.54698 | 57.42539 |
| | | | | | | |
| | | | | | | |
| Averages | DTP | | | PD75 | | |
| | | | | | | |
| Net Concentrate wet mass, g | 1056.3 | | | 1120.8 | | |
| Net Concentrate dry mass, g | 186.2 | | | 186.0 | | |
| Net Tailing dry mass, g | 852.4 | | | 834.6 | | |
| Net Water in Concentrate, g | 1005.9 | | | 1041.3 | | |
| Mass recovery, % | 18.2% | | | 18.6% | | |
| Concentrate Solids % | 18.5% | | | 17.9% | | |
| Eh | 321.33 | | | 262.33 | | |
| Concentrate Grades | | | | | | |
| 2.752046425 | 2.65% | | | 5.33% | | |
| 1.806920135 | 1.794762897 | | | 2.973769241 | | |
| | | | | | | |
| Pyrite Recovery- % | 27.00% | | | 55.46% | | |
| Chalcopyrite Recovery- % | 70% | | | 70% | | |
| Pentlandite Recovery- % | 30% | | | 60% | | |
| Gold Recovery | 20.99% | | | 94.49% | | |
| | | | | | | |
| Eh | 321.3333 | | | 262.3333 | | |
| | | | | | | |
| **Uncertainty Parameter Error** | **DTP** | | | **PD75** | | |
| | | | | | | |
| Net Concentrate wet mass, g | 120.9366925 | | | 105.1193431 | | |
| Net Concentrate dry mass, g | 11.12697756 | | | 13.90747406 | | |
| Net Tailing dry mass, g | 33.14470303 | | | 53.43918555 | | |
| Net Water in Concentrate, g | 119.2852649 | | | 29.11037743 | | |

| | | | | | | |
|---|---|---|---|---|---|---|
| Mass recovery, % | 0.003831906 | | | 0.00710802 | | |
| Concentrate Solids % | 0.011572207 | | | 0.009905536 | | |
| Concentrate Grades | | | | | | |
| 2.8 | 0.002454077 | | | 0.006995841 | | |
| 1.8 | 0.3110412 | | | 0.454465547 | | |
| | | | | | | |
| Pyrite Recovery- % | 0.028333372 | | | 0.095397118 | | |
| Chalcopyrite Recovery- % | 0.015919335 | | | 0.029211545 | | |
| Pentlandite Recovery- % | 0.057356411 | | | 0.023369236 | | |

| Experimental Data | PD50 1 | PD50 2 | PD50 3 | PD25 1 | PD25 2 | PD25 3 |
|---|---|---|---|---|---|---|
| | | | | | | |
| Net Concentrate wet mass, g | 893.8 | 828.1 | 836.2 | 782.3 | 856.8 | 875.9 |
| Net Concentrate dry mass, g | 153.7 | 151.3 | 159 | 136.1 | 149.4 | 144 |
| Net Tailing dry mass, g | 858 | 839.8 | 811.4 | 875.3 | 904.8 | 915.2 |
| Net Water in Concentrate, g | 799.8 | 775.4 | 814.9 | 769 | 804.2 | 815.2 |
| Mass recovery, % | 0.153087 | 0.154986 | 0.159613 | 0.140129 | 0.146919 | 0.140463 |
| Concentrate Solids % | 0.192173 | 0.195125 | 0.195116 | 0.176983 | 0.185775 | 0.176644 |
| Eh | 244 | 255 | 237 | 228 | 224 | 219 |
| | | | | | | |
| Grade in Concentrate | PD50 1 | PD50 2 | PD50 3 | PD25 1 | PD25 2 | PD25 3 |
| 5.052672086 | 5.052672 | 5.089307 | 5.506044 | 4.586079 | 4.880747 | 4.637356 |
| 3.66245333 | 3.662453 | 3.565891 | 3.543615 | 4.648977 | 4.357685 | 4.585287 |
| | | | | | | |
| Recovery - % | PD50 1 | PD50 2 | PD50 3 | PD25 1 | PD25 2 | PD25 3 |
| 42.89119514 | 42.8912 | 43.71378 | 48.81324 | 35.42359 | 39.7036 | 35.99735 |

| | | | | | | |
|---|---|---|---|---|---|---|
| 88.1138926 | 88.11389 | 89.15734 | 92.02276 | 93.53952 | 98.51168 | 94.00354 |
| 58.74259507 | 58.7426 | 59.43822 | 61.34851 | 56.12371 | 59.10701 | 56.40213 |
| | | | | | | |
| | | | | | | |
| Averages | PD50 | | | PD25 | | |
| | | | | | | |
| Net Concentrate wet mass, g | 852.7 | | | 838.3 | | |
| Net Concentrate dry mass, g | 154.7 | | | 143.2 | | |
| Net Tailing dry mass, g | 836.4 | | | 898.4 | | |
| Net Water in Concentrate, g | 796.7 | | | 796.1 | | |
| Mass recovery, % | 15.6% | | | 14.3% | | |
| Concentrate Solids % | 19.4% | | | 18.0% | | |
| Eh | 245.33 | | | 223.67 | | |
| Concentrate Grades | | | | | | |
| 5.052672086 | 5.22% | | | 4.70% | | |
| 3.66245333 | 3.590653107 | | | 4.530649679 | | |
| | | | | | | |
| Pyrite Recovery- % | 45.14% | | | 37.04% | | |
| Chalcopyrite Recovery- % | 90% | | | 90% | | |
| Pentlandite Recovery- % | 60% | | | 60% | | |
| Gold Recovery | 0.00% | | | #REF! | | |
| | | | | | | |
| Eh | 245.3333 | | | 229.6667 | | |
| | | | | | | |
| **Uncertainty Parameter Error** | **PD50** | | | **PD25** | | |
| | | | | | | |
| Net Concentrate wet mass, g | 88.9900513 | | | 122.8582119 | | |
| Net Concentrate dry mass, g | 9.787418518 | | | 16.61651086 | | |

| | | |
|---|---|---|
| Net Tailing dry mass, g | 58.34075557 | 51.41645008 |
| Net Water in Concentrate, g | 49.51292156 | 59.9502947 |
| Mass recovery, % | 0.008338383 | 0.009507535 |
| Concentrate Solids % | 0.004227354 | 0.012859293 |
| Concentrate Grades | | |
| 5.1 | 0.006256198 | 0.003910673 |
| 3.7 | 0.156923967 | 0.380419461 |
| | | |
| Pyrite Recovery- % | 0.079693768 | 0.057711851 |
| Chalcopyrite Recovery- % | 0.050278208 | 0.068227922 |
| Pentlandite Recovery- % | 0.033518805 | 0.040936753 |

| Experimental Data | PAX 1 | PAX 2 | PAX 3 |
|---|---|---|---|
| | | | |
| Net Concentrate wet mass, g | 961.3 | 993.4 | 934.6 |
| Net Concentrate dry mass, g | 166.7 | 171.1 | 163.4 |
| Net Tailing dry mass, g | 855.8 | 837.1 | 839.1 |
| Net Water in Concentrate, g | 788.9 | 771.3 | 760.9 |
| Mass recovery, % | 0.167467 | 0.173071 | 0.166472 |
| Concentrate Solids % | 0.211307 | 0.221833 | 0.214746 |
| Eh | 214 | 202 | 227 |
| | | | |
| Grade in Concentrate | PAX 1 | PAX 2 | PAX 3 |
| 4.22832862 | 4.033761 | 4.228329 | 3.92802 |
| 3.645919953 | 4.158631 | 3.64592 | 3.686067 |
| | | | |
| Recovery - % | PAX 1 | PAX 2 | PAX 3 |
| 40.78301471 | 37.60149 | 40.78301 | 36.36946 |
| 66.744685 | 64.50614 | 66.74469 | 64.07215 |

| | | | |
|---|---|---|---|
| 50.05851375 | 48.37961 | 50.05851 | 48.05411 |
| | | | |
| | | | |
| Averages | PAX | | |
| | | | |
| Net Concentrate wet mass, g | 963.1 | | |
| Net Concentrate dry mass, g | 167.1 | | |
| Net Tailing dry mass, g | 844.0 | | |
| Net Water in Concentrate, g | 773.7 | | |
| Mass recovery, % | 16.9% | | |
| Concentrate Solids % | 21.6% | | |
| Eh | 214.33 | | |
| Concentrate Grades | | | |
| 4.22832862 | 4.06% | | |
| 3.645919953 | 3.830205943 | | |
| | | | |
| Pyrite Recovery- % | 38.25% | | |
| Chalcopyrite Recovery- % | 70% | | |
| Pentlandite Recovery- % | 50% | | |
| Gold Recovery | 73.89% | | |
| | | | |
| Eh | 214.3333 | | |
| | | | |
| **Uncertainty Parameter Error** | **PAX** | | |
| | | | |
| Net Concentrate wet mass, g | 73.13623747 | | |
| Net Concentrate dry mass, g | 9.596405429 | | |
| Net Tailing dry mass, g | 25.50690538 | | |
| Net Water in Concentrate, g | 35.159106 | | |
| Mass recovery, % | 0.008838198 | | |

| | | | |
|---|---|---|---|
| Concentrate Solids % | 0.013333747 | | |
| Concentrate Grades | | | |
| 4.2 | 0.003784039 | | |
| 3.6 | 0.708307139 | | |
| | | | |
| Pyrite Recovery- % | 0.056573846 | | |
| Chalcopyrite Recovery- % | 0.035627917 | | |
| Pentlandite Recovery- % | 0.026720938 | | |

***Micro-Flotation Data***

| Experiment | C1 Floated Mass, g | C2 Floated Mass, g | C3 Floated Mass, g | C4 Floated Mass, g | Tailing mass |
|---|---|---|---|---|---|
| P1 No collector | 0.014 | 0.024 | 0.033 | 0.071 | 2.825 |
| P1 No collector | 0.026 | 0.03 | 0.036 | 0.068 | 2.821 |
| P1 SIBX | 0.323 | 0.586 | 0.771 | 0.519 | 0.788 |
| P1 SIBX | 0.318 | 0.592 | 0.757 | 0.502 | 0.83 |
| P1 SD25 | 0.413 | 0.77 | 0.826 | 0.374 | 0.653 |
| P1 SD25 | 0.4 | 0.753 | 0.803 | 0.365 | 0.664 |
| P1 SD50 | 0.323 | 0.565 | 0.705 | 0.476 | 0.868 |
| P1 SD50 | 0.332 | 0.58 | 0.721 | 0.448 | 0.876 |
| P1 SD75 | 0.285 | 0.414 | 0.606 | 0.347 | 1.04 |
| P1 SD75 | 0.287 | 0.436 | 0.621 | 0.332 | 1.055 |
| P1 DTP | 0.115 | 0.163 | 0.13 | 0.112 | 2.402 |
| P1 DTP | 0.115 | 0.154 | 0.11 | 0.105 | 2.379 |
| P1 PD75 | 0.296 | 0.469 | 0.582 | 0.42 | 0.99 |
| P1 PD75 | 0.31 | 0.484 | 0.68 | 0.418 | 1.007 |
| P1 PD50 | 0.35 | 0.654 | 0.646 | 0.338 | 1.02 |
| P1 PD50 | 0.382 | 0.63 | 0.665 | 0.324 | 1.021 |
| P1 PD25 | 0.463 | 0.772 | 0.772 | 0.274 | 0.573 |
| P1 PD25 | 0.524 | 0.461 | 0.782 | 0.295 | 0.581 |
| P1 PAX | 0.483 | 0.771 | 0.801 | 0.304 | 0.496 |
| P1 PAX | 0.429 | 0.783 | 0.864 | 0.351 | 0.47 |
| | | | | | |
| | | | | | |
| P2 No collector | 0.027 | 0.034 | 0.076 | 0.054 | 2.768 |
| P2 No collector | 0.022 | 0.044 | 0.079 | 0.05 | 2.779 |
| P2 SIBX | 0.308 | 0.476 | 0.688 | 0.448 | 0.83 |
| P2 SIBX | 0.341 | 0.547 | 0.68 | 0.464 | 0.991 |
| P2 SD25 | 0.334 | 0.639 | 0.849 | 0.377 | 0.833 |
| P2 SD25 | 0.31 | 0.654 | 0.813 | 0.385 | 0.792 |
| P2 SD50 | 0.311 | 0.538 | 0.645 | 0.427 | 0.862 |
| P2 SD50 | 0.294 | 0.522 | 0.638 | 0.418 | 0.972 |
| P2 SD75 | 0.244 | 0.382 | 0.56 | 0.322 | 1.15 |
| P2 SD75 | 0.254 | 0.39 | 0.562 | 0.307 | 1.17 |
| P2 DTP | 0.1 | 0.141 | 0.104 | 0.104 | 2.5 |
| P2 DTP | 0.099 | 0.117 | 0.094 | 0.082 | 2.435 |
| P2 PD75 | 0.301 | 0.421 | 0.718 | 0.235 | 1.081 |
| P2 PD75 | 0.31 | 0.427 | 0.629 | 0.184 | 1.076 |
| P2 PD50 | 0.434 | 0.694 | 0.69 | 0.196 | 0.843 |
| P2 PD50 | 0.443 | 0.67 | 0.678 | 0.192 | 0.846 |
| P2 PD25 | 0.426 | 0.704 | 0.717 | 0.284 | 0.715 |
| P2 PD25 | 0.483 | 0.419 | 0.73 | 0.285 | 0.794 |
| P2 PAX | 0.447 | 0.573 | 0.658 | 0.286 | 0.867 |
| P2 PAX | 0.391 | 0.558 | 0.65 | 0.293 | 0.827 |

| Experiment | C1 Floated Mass, g | C2 Floated Mass, g | C3 Floated Mass, g | C4 Floated Mass, g | T |
|---|---|---|---|---|---|
| Averages mass recovery | | | | | |
| P1 No collector | 0.02 | 0.027 | 0.0345 | 0.0695 | 2.823 |
| P1 SIBX | 0.3205 | 0.589 | 0.764 | 0.5105 | 0.809 |
| P1 SD25 | 0.4065 | 0.7615 | 0.8145 | 0.3695 | 0.6585 |
| P1 SD50 | 0.3275 | 0.5725 | 0.713 | 0.462 | 0.872 |
| P1 SD75 | 0.286 | 0.425 | 0.6135 | 0.3395 | 1.0475 |
| P1 DTP | 0.115 | 0.1585 | 0.12 | 0.1085 | 2.3905 |
| P1 PD75 | 0.303 | 0.4765 | 0.631 | 0.419 | 0.9985 |
| P1 PD50 | 0.366 | 0.642 | 0.6555 | 0.331 | 1.0205 |
| P1 PD25 | 0.4935 | 0.6165 | 0.777 | 0.2845 | 0.577 |
| P1 PAX | 0.456 | 0.777 | 0.8325 | 0.3275 | 0.483 |
| P2 No collector | 0.0245 | 0.039 | 0.0775 | 0.052 | 2.7735 |
| P2 SIBX | 0.3245 | 0.5115 | 0.684 | 0.456 | 0.9105 |
| P2 SD25 | 0.322 | 0.6465 | 0.831 | 0.381 | 0.8125 |
| P2 SD50 | 0.3025 | 0.53 | 0.6415 | 0.4225 | 0.917 |
| P2 SD75 | 0.249 | 0.386 | 0.561 | 0.3145 | 1.16 |
| P2 DTP | 0.0995 | 0.129 | 0.099 | 0.093 | 2.4675 |
| P2 PD75 | 0.3055 | 0.424 | 0.6735 | 0.2095 | 1.0785 |
| P2 PD50 | 0.4385 | 0.682 | 0.684 | 0.194 | 0.8445 |
| P2 PD25 | 0.4545 | 0.5615 | 0.7235 | 0.2845 | 0.7545 |
| P2 PAX | 0.419 | 0.5655 | 0.654 | 0.2895 | 0.847 |

| | | | | | | | Percentage Cumulative mass recovery | | | |
|---|---|---|---|---|---|---|---|---|---|---|
| Cumulative mass recovery | | | | | | | C1 | C2 | C3 | C4 |
| P1 No collector | 0.02 | 0.047 | 0.0815 | 0.151 | 2.974 | | 0.67% | 1.58% | 2.74% | 5.08% |
| P1 SIBX | 0.3205 | 0.9095 | 1.6735 | 2.184 | 2.993 | | 10.71% | 30.39% | 55.91% | 72.97% |
| P1 SD25 | 0.4065 | 1.168 | 1.9825 | 2.352 | 3.0105 | | 13.50% | 38.80% | 65.85% | 78.13% |
| P1 SD50 | 0.3275 | 0.9 | 1.613 | 2.075 | 2.947 | | 11.11% | 30.54% | 54.73% | 70.41% |
| P1 SD75 | 0.286 | 0.711 | 1.3245 | 1.664 | 2.7115 | | 10.55% | 26.22% | 48.85% | 61.37% |
| P1 DTP | 0.115 | 0.2735 | 0.3935 | 0.502 | 2.8925 | | 3.98% | 9.46% | 13.60% | 17.36% |
| P1 PD75 | 0.303 | 0.7795 | 1.4105 | 1.8295 | 2.828 | | 10.71% | 27.56% | 49.88% | 64.69% |
| P1 PD50 | 0.366 | 1.008 | 1.6635 | 1.9945 | 3.015 | | 12.14% | 33.43% | 55.17% | 66.15% |
| P1 PD25 | 0.4935 | 1.11 | 1.887 | 2.1715 | 2.7485 | | 17.96% | 40.39% | 68.66% | 79.01% |
| P1 PAX | 0.456 | 1.233 | 2.0655 | 2.393 | 2.876 | | 15.86% | 42.87% | 71.82% | 83.21% |
| P2 No collector | 0.0245 | 0.0635 | 0.141 | 0.193 | 2.9665 | | 0.83% | 2.14% | 4.75% | 6.51% |
| P2 SIBX | 0.3245 | 0.836 | 1.52 | 1.976 | 2.8865 | | 11.24% | 28.96% | 52.66% | 68.46% |
| P2 SD25 | 0.322 | 0.9685 | 1.7995 | 2.1805 | 2.993 | | 10.76% | 32.36% | 60.12% | 72.85% |
| P2 SD50 | 0.3025 | 0.8325 | 1.474 | 1.8965 | 2.8135 | | 10.75% | 29.59% | 52.39% | 67.41% |
| P2 SD75 | 0.249 | 0.635 | 1.196 | 1.5105 | 2.6705 | | 9.32% | 23.78% | 44.79% | 56.56% |
| P2 DTP | 0.0995 | 0.2285 | 0.3275 | 0.4205 | 2.888 | | 3.45% | 7.91% | 11.34% | 14.56% |
| P2 PD75 | 0.3055 | 0.7295 | 1.403 | 1.6125 | 2.691 | | 11.35% | 27.11% | 52.14% | 59.92% |
| P2 PD50 | 0.4385 | 1.1205 | 1.8045 | 1.9985 | 2.843 | | 15.42% | 39.41% | 63.47% | 70.30% |
| P2 PD25 | 0.4545 | 1.016 | 1.7395 | 2.024 | 2.7785 | | 16.36% | 36.57% | 62.61% | 72.85% |
| P2 PAX | 0.419 | 0.9845 | 1.6385 | 1.928 | 2.775 | | 15.10% | 35.48% | 59.05% | 69.48% |

SL= -ln((R*-R)/R*)

| | | C1 | C2 | C3 | C4 | R* | k | R2 |
|---|---|---|---|---|---|---|---|---|
| P1 No collector | 0.15% | 0.045869 | 0.111331 | 0.201742 | 0.413229 | 0.15 | 0.019598 | 0.992681 |
| P1 SIBX | 0.32% | 0.113381 | 0.362662 | 0.820288 | 1.310927 | 0.999004 | 0.065864 | 0.999081 |
| P1 SD25 | 0.18% | 0.166295 | 0.580176 | 1.375047 | 2.175345 | 0.881361 | 0.109283 | 0.998198 |
| P1 SD50 | 0.02% | 0.128817 | 0.403689 | 0.904568 | 1.451521 | 0.919455 | 0.072885 | 0.999242 |
| P1 SD75 | 0.00% | 0.146365 | 0.413229 | 0.995769 | 1.571122 | 0.774668 | 0.079013 | 0.998305 |
| P1 DTP | 0.22% | 0.218148 | 0.62759 | 1.110597 | 1.934843 | 0.202854 | 0.096277 | 0.999034 |
| P1 PD75 | 0.22% | 0.132938 | 0.386014 | 0.86624 | 1.39274 | 0.860722 | 0.069917 | 0.99932 |
| P1 PD50 | 0.29% | 0.176364 | 0.589332 | 1.327578 | 2.129528 | 0.75079 | 0.106867 | 0.999073 |
| P1 PD25 | 0.03% | 0.234489 | 0.635157 | 1.605702 | 2.522648 | 0.858999 | 0.126715 | 0.997511 |
| P1 PAX | 0.48% | 0.191192 | 0.635931 | 1.552441 | 2.444787 | 0.911091 | 0.122813 | 0.997794 |
| P2 No collector | 0.03% | 0.069773 | 0.191979 | 0.490797 | 0.756946 | 0.122546 | 0.038219 | 0.997045 |
| P2 SIBX | 0.65% | 0.130677 | 0.379198 | 0.852845 | 1.370181 | 0.917724 | 0.068792 | 0.999294 |
| P2 SD25 | 0.17% | 0.132589 | 0.46759 | 1.184021 | 1.838109 | 0.866392 | 0.092536 | 0.996809 |
| P2 SD50 | 0.80% | 0.131056 | 0.412552 | 0.912612 | 1.470042 | 0.875322 | 0.073784 | 0.999386 |
| P2 SD75 | 0.09% | 0.137523 | 0.396999 | 0.960102 | 1.511544 | 0.725689 | 0.076043 | 0.998204 |
| P2 DTP | 0.34% | 0.225016 | 0.62126 | 1.088317 | 1.90751 | 0.170985 | 0.094842 | 0.998751 |
| P2 PD75 | 0.44% | 0.188158 | 0.526889 | 1.54967 | 2.357052 | 0.661901 | 0.118621 | 0.993623 |
| P2 PD50 | 0.10% | 0.235114 | 0.766548 | 1.982007 | 3.098933 | 0.736153 | 0.155535 | 0.996681 |
| P2 PD25 | 1.04% | 0.228165 | 0.608883 | 1.517734 | 2.391335 | 0.801823 | 0.120118 | 0.997798 |
| P2 PAX | 0.05% | 0.217951 | 0.61645 | 1.451636 | 2.313864 | 0.771011 | 0.11615 | 0.998719 |

***Zeta Potential***

| pH Test 1 | pH Test 2 | pH Test 3 | pH Average | error |
|---|---|---|---|---|
| 3.00 | 3.07 | 3.01 | 3.03 | 0.09 |
| 5.21 | 5.22 | 4.93 | 5.12 | 0.41 |
| 7.09 | 7.17 | 6.87 | 7.04 | 0.39 |
| 8.94 | 8.87 | 8.86 | 8.89 | 0.11 |
| 11.43 | 11.57 | 11.41 | 11.47 | 0.22 |
| | | | | |
| pH Test 1 | pH Test 2 | pH Test 3 | pH Average | error |
| 3.20 | 3.15 | 2.95 | 3.10 | 0.33 |
| 4.9 | 4.93 | 4.6 | 4.81 | 0.45 |
| 7 | 6.92 | 6.9 | 6.94 | 0.13 |
| 8.95 | 9.12 | 8.84 | 8.97 | 0.35 |
| 11.48 | 11.52 | 11.2 | 11.40 | 0.43 |
| | | | | |
| pH Test 1 | pH Test 2 | pH Test 3 | pH Average | error |
| 3.25 | 3.15 | 2.96 | 3.12 | 0.37 |
| 5.05 | 5.11 | 4.75 | 4.97 | 0.48 |
| 7.4 | 7.35 | 7.06 | 7.27 | 0.46 |
| 9.19 | 9.28 | 9.16 | 9.21 | 0.16 |
| 11.5 | 11.48 | 11.58 | 11.52 | 0.13 |
| | | | | |
| pH Test 1 | pH Test 2 | pH Test 3 | pH Average | error |
| 3.00 | 3.16 | 2.99 | 3.05 | 0.24 |
| 4.19 | 4.28 | 4.2 | 4.22 | 0.12 |
| 7.3 | 7.34 | 6.96 | 7.20 | 0.52 |
| 9 | 9.17 | 8.89 | 9.02 | 0.35 |

| | | | | |
|---|---|---|---|---|
| 11.42 | 11.34 | 11.11 | 11.29 | 0.40 |
| | | | | |
| pH Test 1 | pH Test 2 | pH Test 3 | pH Average | error |
| 3.10 | 3.05 | 2.76 | 2.97 | 0.46 |
| 5.23 | 5.06 | 4.98 | 5.09 | 0.32 |
| 7.18 | 7.11 | 6.89 | 7.06 | 0.38 |
| 8.94 | 8.78 | 8.71 | 8.81 | 0.29 |
| 11.66 | 11.58 | 11.46 | 11.57 | 0.25 |
| | | | | |
| pH Test 1 | pH Test 2 | pH Test 3 | pH Average | error |
| 3.06 | 3.05 | 2.83 | 2.98 | 0.32 |
| 5.01 | 5.04 | 4.74 | 4.93 | 0.41 |
| 7.08 | 7.08 | 6.75 | 6.97 | 0.47 |
| 9.19 | 9.24 | 8.93 | 9.12 | 0.41 |
| 11.61 | 11.74 | 11.54 | 11.63 | 0.25 |
| | | | | |
| pH Test 1 | pH Test 2 | pH Test 3 | pH Average | error |
| 3.09 | 3.02 | 3.10 | 3.07 | 0.11 |
| 5.03 | 5.11 | 4.92 | 5.02 | 0.24 |
| 7.11 | 7.05 | 6.84 | 7.00 | 0.35 |
| 9.34 | 9.32 | 8.91 | 9.19 | 0.60 |
| 11.56 | 11.47 | 11.39 | 11.47 | 0.21 |
| | | | | |
| pH Test 1 | pH Test 2 | pH Test 3 | pH Average | error |
| 2.96 | 2.91 | 2.86 | 2.91 | 0.12 |
| 4.87 | 4.96 | 4.87 | 4.90 | 0.13 |
| 7.11 | 7.04 | 6.94 | 7.03 | 0.21 |
| 8.87 | 8.95 | 8.62 | 8.81 | 0.43 |

| | | | | |
|---|---|---|---|---|
| 11.52 | 11.48 | 11.32 | 11.44 | 0.26 |
| | | | | |
| pH Test 1 | pH Test 2 | pH Test 3 | pH Average | error |
| 2.96 | 2.98 | 2.82 | 2.92 | 0.22 |
| 4.84 | 4.83 | 4.97 | 4.88 | 0.19 |
| 7.23 | 7.31 | 7.02 | 7.19 | 0.37 |
| 9.11 | 9.06 | 9.04 | 9.07 | 0.09 |
| 11.76 | 11.65 | 11.54 | 11.65 | 0.27 |
| | | | | |
| pH Test 1 | pH Test 2 | pH Test 3 | pH Average | error |
| 2.92 | 2.92 | 2.90 | 2.91 | 0.03 |
| 5.12 | 5.15 | 5.01 | 5.09 | 0.18 |
| 7.06 | 7.22 | 7.02 | 7.10 | 0.26 |
| 8.93 | 8.98 | 8.94 | 8.95 | 0.07 |
| 11.55 | 11.39 | 11.3 | 11.41 | 0.31 |
| | | | | |
| pH Test 1 | pH Test 2 | pH Test 3 | pH Average | error |
| 3.03 | 3.00 | 2.77 | 2.93 | 0.35 |
| 5.02 | 5.05 | 4.93 | 5.00 | 0.16 |
| 7.17 | 7.18 | 7.16 | 7.17 | 0.02 |
| 9.13 | 9.14 | 8.91 | 9.06 | 0.32 |
| 11.62 | 11.65 | 11.53 | 11.60 | 0.16 |
| | | | | |
| pH Test 1 | pH Test 2 | pH Test 3 | pH Average | error |
| 2.94 | 3.02 | 2.90 | 2.95 | 0.15 |
| 5.07 | 5.03 | 4.78 | 4.96 | 0.39 |
| 7.22 | 7.14 | 7.06 | 7.14 | 0.20 |
| 9.04 | 9.05 | 9.1 | 9.06 | 0.08 |

| | | | | |
|---|---|---|---|---|
| 11.54 | 11.51 | 11.21 | 11.42 | 0.45 |
| | | | | |
| pH Test 1 | pH Test 2 | pH Test 3 | pH Average | error |
| 3.02 | 2.94 | 2.94 | 2.97 | 0.11 |
| 4.9 | 4.91 | 5.01 | 4.94 | 0.15 |
| 7.02 | 7.05 | 7.03 | 7.03 | 0.04 |
| 9.12 | 9.07 | 9.11 | 9.10 | 0.07 |
| 11.59 | 11.43 | 11.32 | 11.45 | 0.34 |
| | | | | |
| pH Test 1 | pH Test 2 | pH Test 3 | pH Average | error |
| 2.97 | 2.99 | 2.91 | 2.96 | 0.10 |
| 5.18 | 5.24 | 4.89 | 5.10 | 0.46 |
| 6.98 | 6.96 | 6.97 | 6.97 | 0.02 |
| 8.78 | 8.81 | 8.8 | 8.80 | 0.04 |
| 11.62 | 11.61 | 11.69 | 11.64 | 0.11 |
| | | | | |
| pH Test 1 | pH Test 2 | pH Test 3 | pH Average | error |
| 3.15 | 3.14 | 2.88 | 3.06 | 0.38 |
| 4.93 | 4.96 | 4.72 | 4.87 | 0.32 |
| 7.16 | 7.22 | 7.1 | 7.16 | 0.15 |
| 9.25 | 9.23 | 8.88 | 9.12 | 0.52 |
| 11.42 | 11.48 | 11.33 | 11.41 | 0.19 |
| | | | | |
| pH Test 1 | pH Test 2 | pH Test 3 | pH Average | error |
| 3.18 | 3.11 | 2.83 | 3.04 | 0.46 |
| 4.87 | 4.88 | 4.91 | 4.89 | 0.05 |
| 7.12 | 7.22 | 7.03 | 7.12 | 0.24 |
| 8.84 | 8.9 | 8.75 | 8.83 | 0.19 |

| | | | | |
|---|---|---|---|---|
| 11.68 | 11.61 | 11.4 | 11.56 | 0.36 |
| | | | | |
| pH Test 1 | pH Test 2 | pH Test 3 | pH Average | error |
| 3.11 | 3.17 | 3.14 | 3.14 | 0.07 |
| 4.95 | 4.89 | 4.78 | 4.87 | 0.21 |
| 6.94 | 6.95 | 7.02 | 6.97 | 0.11 |
| 8.89 | 8.83 | 8.83 | 8.85 | 0.09 |
| 11.52 | 11.47 | 11.51 | 11.50 | 0.07 |
| | | | | |
| pH Test 1 | pH Test 2 | pH Test 3 | pH Average | error |
| 2.88 | 3.05 | 2.83 | 2.92 | 0.29 |
| 4.95 | 4.92 | 4.68 | 4.85 | 0.37 |
| 7.08 | 7.05 | 6.98 | 7.04 | 0.13 |
| 9.05 | 9.05 | 8.81 | 8.97 | 0.34 |
| 11.55 | 11.62 | 11.62 | 11.60 | 0.10 |
| | | | | |
| pH Test 1 | pH Test 2 | pH Test 3 | pH Average | error |
| 2.96 | 3.02 | 2.87 | 2.95 | 0.19 |
| 5.03 | 5.02 | 5.1 | 5.05 | 0.11 |
| 6.9 | 7.04 | 6.88 | 6.94 | 0.22 |
| 9.03 | 9.05 | 9.04 | 9.04 | 0.02 |
| 11.55 | 11.48 | 11.5 | 11.51 | 0.09 |
| | | | | |
| pH Test 1 | pH Test 2 | pH Test 3 | pH Average | error |
| 3.10 | 3.17 | 3.06 | 3.11 | 0.14 |
| 5.13 | 5.18 | 5 | 5.10 | 0.23 |
| 7.05 | 7.05 | 6.77 | 6.96 | 0.40 |
| 9.13 | 9.02 | 8.94 | 9.03 | 0.24 |

| | | | | |
|---|---|---|---|---|
| 11.56 | 11.58 | 11.43 | 11.52 | 0.20 |

| Pyrite 1 Result 1 | Pyrite 1 Result 2 | Pyrite 1 Result 3 | Pyrite 1 Average | error |
|---|---|---|---|---|
| 20.09 | 20.16 | 17.44 | 19.23 | 0.90 |
| 17.5 | 16.77 | 14.09 | 16.12 | 1.04 |
| 6.99 | 6.42 | 3.21 | 5.54 | 1.18 |
| -12.59 | -12.07 | -12.18 | -12.28 | 0.16 |
| -26.91 | -26.08 | -26.87 | -26.62 | 0.27 |
| | | | | |
| Pyrite 2 Result 1 | Pyrite 2 Result 2 | Pyrite 2 Result 3 | Pyrite 2 Average | error |
| 11.96 | 13.16 | 11.51 | 12.21 | 0.49 |
| 11.49 | 10.21 | 8.87 | 10.19 | 0.76 |
| -2.38 | -1.14 | -3.5 | -2.34 | 0.68 |
| -16.56 | -16.3 | -19.4 | -17.42 | 0.99 |
| -30.4 | -30.24 | -32.5 | -31.05 | 0.73 |
| | | | | |
| P1 SIBX Result 1 | P1 SIBX Result 2 | P1 SIBX Result 3 | P1 SIBX Average | error |
| 9.2 | 8.79 | 5.26 | 7.75 | 1.25 |
| 8.28 | 8.53 | 8.87 | 8.56 | 0.17 |
| -13.65 | -13.8 | -17.5 | -14.98 | 1.26 |
| -21.18 | -22.31 | -21.97 | -21.82 | 0.33 |
| -33.43 | -34.47 | -34.43 | -34.11 | 0.34 |
| | | | | |
| P2 SIBX Result 1 | P2 SIBX Result 2 | P2 SIBX Result 3 | P2 SIBX Average | error |
| 6.17 | 6.08 | 6.53 | 6.26 | 0.14 |
| 4.66 | 5.12 | 3.6 | 4.46 | 0.45 |
| -17.37 | -16.55 | -19.03 | -17.65 | 0.73 |

| | | | | |
|---|---|---|---|---|
| -27.38 | -27.8 | -28.46 | -27.88 | 0.31 |
| -38.11 | -36.99 | -38.6 | -37.90 | 0.48 |
| | | | | |
| P1 SD25 Result 1 | P1 SD25 Result 2 | P1 SD25 Result 3 | P1 SD25 Average | error |
| 11.05 | 10.26 | 8.62 | 9.98 | 0.72 |
| 9.23 | 8.7 | 6.88 | 8.27 | 0.71 |
| -11.46 | -11.8 | -12.11 | -11.79 | 0.19 |
| -11.23 | -11.85 | -14.27 | -12.45 | 0.93 |
| -37.06 | -35.77 | -38.07 | -36.97 | 0.67 |
| | | | | |
| P2 SD25 Result 1 | P2 SD25 Result 2 | P2 SD25 Result 3 | P2 SD25 Average | error |
| 6.73 | 7.07 | 4.22 | 6.01 | 0.90 |
| 4 | 4.15 | 3.94 | 4.03 | 0.06 |
| -14.55 | -14.45 | -15.39 | -14.80 | 0.30 |
| -24.67 | -23.23 | -25.23 | -24.38 | 0.60 |
| -35.69 | -36.11 | -36.95 | -36.25 | 0.37 |
| | | | | |
| P1 SD50 Result 1 | P1 SD50 Result 2 | P1 SD50 Result 3 | P1 SD50 Average | error |
| 4.46 | 4.93 | 3.01 | 4.13 | 0.58 |
| 7.76 | 7.56 | 5.5 | 6.94 | 0.72 |
| -4.11 | -4.18 | -5.24 | -4.51 | 0.37 |
| -17.57 | -17.49 | -19.51 | -18.19 | 0.66 |
| -29.67 | -31.48 | -32.15 | -31.10 | 0.74 |
| | | | | |
| P2 SD50 Result 1 | P2 SD50 Result 2 | P2 SD50 Result 3 | P2 SD50 Average | error |
| -1.65 | -2.07 | -3.21 | -2.31 | 0.47 |
| 1 | 0.57 | -1.88 | -0.10 | 0.90 |
| -11.99 | -10.79 | -13.67 | -12.15 | 0.84 |

| | | | | |
|---|---|---|---|---|
| -22.7 | -21.23 | -23.78 | -22.57 | 0.74 |
| -35.16 | -34.77 | -36.24 | -35.39 | 0.44 |
| | | | | |
| P1 SD75 Result 1 | P1 SD75 Result 2 | P1 SD75 Result 3 | P1 SD75 Average | error |
| 14.01 | 13.75 | 11.08 | 12.95 | 0.94 |
| 11.97 | 10.8 | 11.07 | 11.28 | 0.35 |
| 3.16 | 1.55 | 0.67 | 1.79 | 0.73 |
| -16.33 | -17.15 | -16.5 | -16.66 | 0.25 |
| -31.72 | -33.46 | -34.33 | -33.17 | 0.77 |
| | | | | |
| P2 SD75 Result 1 | P2 SD75 Result 2 | P2 SD75 Result 3 | P2 SD75 Average | error |
| 7.86 | 7.11 | 4.27 | 6.41 | 1.09 |
| 6.1 | 5.22 | 3.7 | 5.01 | 0.70 |
| -5.83 | -6.25 | -5.92 | -6.00 | 0.13 |
| -19.76 | -21.47 | -22.55 | -21.26 | 0.81 |
| -34.47 | -35.96 | -36.55 | -35.66 | 0.62 |
| | | | | |
| P1 DTP Result 1 | P1 DTP Result 2 | P1 DTP Result 3 | P1 DTP Average | error |
| 19.33 | 20.42 | 19.39 | 19.71 | 0.35 |
| 16.55 | 16.29 | 13.32 | 15.39 | 1.04 |
| 5.96 | 5.64 | 6.58 | 6.06 | 0.28 |
| -14.88 | -13.37 | -15.58 | -14.61 | 0.65 |
| -34.2 | -33.15 | -33.81 | -33.72 | 0.31 |
| | | | | |
| P2 DTP Result 1 | P2 DTP Result 2 | P2 DTP Result 3 | P2 DTP Average | error |
| 13.91 | 13.6 | 10.32 | 12.61 | 1.15 |
| 8.75 | 9.07 | 8.21 | 8.68 | 0.25 |
| -1.41 | -0.67 | -0.73 | -0.94 | 0.24 |

| | | | | |
|---|---|---|---|---|
| -20.82 | -19.87 | -21.86 | -20.85 | 0.57 |
| -37.74 | -37.84 | -40.88 | -38.82 | 1.03 |
| | | | | |
| P1 PD75 Result 1 | P1 PD75 Result 2 | P1 PD75 Result 3 | P1 PD75 Average | error |
| 8.79 | 9.34 | 8.12 | 8.75 | 0.35 |
| 9.74 | 9.86 | 9.74 | 9.78 | 0.04 |
| 0.83 | 1.1 | -1.52 | 0.14 | 0.83 |
| -18.17 | -17.28 | -19.83 | -18.43 | 0.75 |
| -34.07 | -33.5 | -33.72 | -33.76 | 0.17 |
| | | | | |
| P2 PD75 Result 1 | P2 PD75 Result 2 | P2 PD75 Result 3 | P2 PD75 Average | error |
| 3.02 | 4.24 | 3.05 | 3.44 | 0.40 |
| 6.12 | 6.33 | 4.96 | 5.80 | 0.43 |
| -7.12 | -6.89 | -7.17 | -7.06 | 0.09 |
| -25.27 | -23.8 | -26.09 | -25.05 | 0.67 |
| -38.98 | -37.39 | -39.15 | -38.51 | 0.56 |
| | | | | |
| P1 PD50 Result 1 | P1 PD50 Result 2 | P1 PD50 Result 3 | P1 PD50 Average | error |
| -1.37 | -0.38 | -1.13 | -0.96 | 0.30 |
| 6.62 | 7.91 | 5.97 | 6.83 | 0.57 |
| -2.41 | -3.9 | -4.79 | -3.70 | 0.69 |
| -21.18 | -20.52 | -23.01 | -21.57 | 0.74 |
| -31.47 | -31.47 | -34.8 | -32.58 | 1.11 |
| | | | | |
| P2 PD50 Result 1 | P2 PD50 Result 2 | P2 PD50 Result 3 | P2 PD50 Average | error |
| -7.82 | -7.01 | -9.2 | -8.01 | 0.64 |
| 0.89 | 0.3 | -0.14 | 0.35 | 0.30 |
| -11.66 | -11.43 | -12.97 | -12.02 | 0.48 |

| | | | | |
|---|---|---|---|---|
| -27.55 | -26.1 | -28.16 | -27.27 | 0.61 |
| -36.82 | -37.23 | -36.68 | -36.91 | 0.17 |
| | | | | |
| P1 PD25 Result 1 | P1 PD25 Result 2 | P1 PD25 Result 3 | P1 PD25 Average | error |
| 7.53 | 6.53 | 6.31 | 6.79 | 0.38 |
| 10.74 | 11.56 | 10.58 | 10.96 | 0.30 |
| -7.96 | -7.43 | -11.21 | -8.87 | 1.18 |
| -16.79 | -15.53 | -18.32 | -16.88 | 0.81 |
| -30.03 | -28.94 | -31.51 | -30.16 | 0.74 |
| | | | | |
| P2 PD25 Result 1 | P2 PD25 Result 2 | P2 PD25 Result 3 | P2 PD25 Average | error |
| -3.2 | -1.9 | -4.23 | -3.11 | 0.67 |
| 2.66 | 1.8 | -0.96 | 1.17 | 1.09 |
| -18.38 | -16.85 | -18.89 | -18.04 | 0.61 |
| -25.69 | -24.94 | -26.5 | -25.71 | 0.45 |
| -39.32 | -38.88 | -40.87 | -39.69 | 0.60 |
| | | | | |
| P1 PAX Result 1 | P1 PAX Result 2 | P1 PAX Result 3 | P1 PAX Average | error |
| 10.54 | 10.34 | 6.63 | 9.17 | 1.27 |
| 6.79 | 7.54 | 7.43 | 7.25 | 0.23 |
| -9.47 | -9.67 | -12.87 | -10.67 | 1.10 |
| -17.04 | -17.43 | -18.43 | -17.63 | 0.41 |
| -29.7 | -28.24 | -30.26 | -29.40 | 0.60 |
| | | | | |
| P2 PAX Result 1 | P2 PAX Result 2 | P2 PAX Result 3 | P2 PAX Average | error |
| 6.55 | 5.35 | 4.38 | 5.43 | 0.63 |
| 3.13 | 4.08 | 0.56 | 2.59 | 1.05 |
| -17.6 | -18.56 | -18.86 | -18.34 | 0.38 |

| | | | | |
|---|---|---|---|---|
| -18.78 | -19.6 | -22.4 | -20.26 | 1.10 |
| -34.56 | -34.42 | -34.37 | -34.45 | 0.06 |